FROM DESIGN TO SYNTHESIS AND FROM STRUCTURE TO FUNCTION: HELICAL POLYMERS

A THESIS SUBMITTED TO
THE GRADUATE SCHOOL OF NATURAL AND APPLIED SCIENCES
OF
MIDDLE EAST TECHNICAL UNIVERSITY

BY

GİZEM ÇALIŞGAN ÜNAY

IN PARTIAL FULFILLMENT OF THE REQUIREMENTS
FOR
THE DEGREE OF DOCTOR OF PHILOSOPHY
IN
CHEMISTRY

JULY 2022

Approval of the thesis:

FROM DESIGN TO SYNTHESIS AND FROM STRUCTURE TO FUNCTION: HELICAL POLYMERS

submitted by **Gizem Çalışgan Ünay** in partial fulfillment of the requirements for the degree of **Doctor of Philosophy** i**n Chemistry, Middle East Technical University** by,

Prof. Dr. Halil Kalıpçılar

Dean, Graduate School of **Natural and Applied Sciences** _____

Prof. Dr. Özdemir Doğan

Head of the Department, **Chemistry** _____

Prof. Dr. Akın Akdağ

Supervisor, **Chemistry, METU** _____

Examining Committee Members:

Prof. Dr. Özdemir Doğan

Chemistry, METU _____

Prof. Dr. Akın Akdağ

Chemistry, METU _____

Assoc. Prof. Dr. Serhan Türkyılmaz

Chemistry, METU _____

Assoc. Prof. Dr. Bilge Baytekin

Chemistry, İ.D. Bilkent University _____

Assoc. Prof. Dr. Yunus Emre Türkmen

Chemistry, İ.D. Bilkent University _____

Date: 01.07.2022

I hereby declare that all information in this document has been obtained and presented in accordance with academic rules and ethical conduct. I also declare that, as required by these rules and conduct, I have fully cited and referenced all material and results that are not original to this work.

Name Last name : Gizem Çalışgan Ünay

Signature :

ABSTRACT

FROM DESIGN TO SYNTHESIS AND FROM STRUCTURE TO FUNCTION: HELICAL POLYMERS

Çalışgan Ünay, Gizem
Doctor of Philosophy, Chemistry
Supervisor : Prof. Dr. Akın Akdağ

July 2022, 235 pages

The helical structure is one of the most distinguished motifs encountered at various scales in nature, from subatomic to galactic scale. In the cosmos, as the size reaches a macro level, functionality increases, and the structures become more ordered. In such systems, helicity is commonly observed and plays a crucial role in functionality. With this in mind, helicity at a molecular level is also found intriguing. To form helical structures, small chiral building blocks arrange themselves accordingly with the help of external factors such as solvation. Inspired by these features, novel chiral polymers with modified tartaric acid moiety in the backbone have been designed in this thesis study. For further characterization of the ordered structures, possibly formed by intramolecular interactions and solvent effect, chromophoric units, either squaraine or diaminoterephthalate, were introduced to the polymer backbone during the condensation polymerization. Besides the polymeric level studies, both enantiomeric forms of small chiral squaraine dye-containing compounds were developed and characterized. Furthermore, other than chiral counterparts, three novel squaraine dyes were synthesized. Studies on optical properties, chirality induction, and solvent effects have been carried out using these various-sized compounds.

After the synthesis and characterization, small chiral squaraine dye-containing compounds were subjected to aggregation studies in different solvent mixtures. CD activity was observed in the same sense for the aggregates of both *D* and *L*-modified alanine dyes. From these results, it was found that the aggregation starts from core squaraine units, and the aggregates of both enantiomers arrange themselves in the most stable form by the same sense positioning. The results were supported by theoretical calculations.

In the case of chiral squaraine-containing polymers, the results obtained from CD spectroscopy showed that the helical assemblies were formed during aggregation studies, and the sense of helicity could be controlled by the chirality of the tartaric acid unit.

The diaminoterephthale (DAT) containing polymers showed CD activity in single solvents because of their chiroptical features. For the further investigation of DAT chromophores, a model monomer was synthesized and characterized. The results obtained from optical studies of model monomer were consistent with the polymers. It was also found that storage conditions affected the behavior of the DATs in solutions. Theoretical calculations revealed that the H-bonding is essential in their arrangement in solution.

The details of synthetic, spectroscopic, chromatographic, and theoretical studies were covered in the following parts of the dissertation.

Keywords: Tartaric Acid, Helical Structures, CD Spectroscopy, Aggregation, Squaraines and Diaminoterephthalate Chromophores

ÖZ

TASARIMDAN SENTEZE VE YAPIDAN FONKSİYONA: HELİKAL POLİMERLER

Çalışgan Ünay, Gizem
Doktora, Kimya
Tez Yöneticisi: Prof. Dr. Akın Akdağ

Temmuz 2022, 235 sayfa

Heliks yapıları, atomaltı boyuttan galaktik boyuta kadar doğada çeşitli ölçeklerde karşılaşılan en seçkin motiflerden biridir. Evrende boyut makro düzeye ulaştıkça işlevsellik artar ve yapılar daha düzenli hale gelir. Bu tür sistemlerde sarmallık yaygın olarak oluşur ve işlevsellikte çok önemli bir rol oynar. Küçük kiral yapı taşları helisel yapılar oluşturmak için çözünme gibi dış etkenlerin yardımıyla kendilerini düzenlerler. Bu özelliklerden esinlenerek, omurgasında modifiye edilmiş tartarik asit bileşiğine sahip yeni kiral polimerler tasarlanmıştır.Muhtemel molekül içi etkileşimler ve çözücü etkisi ile oluşturulan düzenli yapıların karakterizasyonu için, kondenzasyon polimerizasyonu sırasında polimer omurgasına skuarain veya diaminotereftalat gibi kromoforik birimler eklenmiştir. Polimerik seviye çalışmalarının yanı sıra, küçük kiral skuarain boya içeren bileşiklerin her iki enantiyomerik formu geliştirilmiş ve karakterize edilmiştir. Ayrıca, kiral muadilleri dışında, üç yeni squarain boyası sentezlenmştir. Çeşitli büyüklükteki bu bileşikler kullanılarak optik özellikler, kiralite indüksiyonu ve solvent etkileri üzerine çalışmalar yapılmıştır.

Sentez ve karakterizasyon çalışmalarının ardından, küçük kiral squarain boya içeren bileşikler, farklı çözücü karışımlarında agregasyon çalışmalarına tabi tutulmuştur.

Yapılan çalışmalarda, hem *D* hem de *L* modifiye alanin boyalarının agregatlarının aynı yönde CD aktivitesine sahip olduğu gözlemlenmiştir. Bu sonuçlardan agregasyonun çekirdek kare birimlerden başladığı ve her iki enantiyomerin agregatlarının aynı yöne doğu konumlandırmasıyla kendilerini en kararlı biçimde düzenledikleri ortaya konmuştur. Sonuçlar teorik hesaplamalarla desteklenmiştir.

Kiral squarain içeren polimerler kısmında, CD spektroskopisinden elde edilen sonuçlar, sarmal yapıların agregasyon çalışmaları sırasında oluştuğunu ve sarmallık yönünün tartarik asit biriminin kiralitesi ile kontrol edilebileceğini göstermiştir.

Diaminotereftalat (DAT) içeren polimerler, kayroptik özelliklerinden dolayı tekli çözücülerde CD aktivitesi göstermiştir. DAT kromoforların özelliklerinin daha ayrıntılı araştırılması için model monomer sentezlenmiş ve karakterize edilmiştir. Model monomerin optik çalışmalarından elde edilen sonuçlar polimerlerle tutarlı sonuçlar vermiştir. Ayrıca, saklama koşullarının çözücü içindeki DAT'ların davranışını etkilediği görülmüştür. Teorik hesaplamalar, H-bağının çözeltideki düzenlemelerinde esas olduğunu ortaya koymuştur.

Sentetik, spektroskopik, kromatografik ve teorik çalışmaların detayları tezin ilerleyen bölümlerinde ele alınmıştır.

Anahtar Kelimeler:Tartarik Asit, Heliks Yapılar, CD Spektroskopisi, Aggregasyon, Skuarain ve Diaminotereftalat Kromoforları

To caffeine, taurine, and nicotine

ACKNOWLEDGMENTS

My PhD journey would not have been possible without the support of my professor, family and friends. First and foremost, I would like to express my deepest appreciation to my advisor, Prof. Dr. Akın Akdağ, whose sincerity and encouragement I will never forget. His immense knowledge and plentiful experience have encouraged me in all the time of my academic research.

I would like to thank advisory commitee members Assoc. Prof. Dr. Serhan Türkyılmaz, Assoc. Prof. Dr. Bilge Baytekin for their time and criticism.

Besides my advisor and thesis advisory commitee members, I would like to thank the committee members Prof.Dr. Özdemir Doğan, and Assoc. Prof. Dr. Yunus Emre Türkmen their invaluable comments, and assistance in shaping the final draft of this study.

I am also thankful to Berçin Verda Asya and Bulem Çakmak for their help during the synthesis process.

I would like to thank Oğuzhan Karakurt in Prof. Dr. Ali Çırpan's group for GPC measurements.

I would like to thank TÜBİTAK 118Z710 for financial support.

I would like to extend my sincere thanks to AARG group members for their friendship, conversation, and harmonious working environment. There are so many unforgettable memories that we shared. Nothing would be easier without their support.

Special thanks to my friends and comrades Perihan Öztürk Düzenli, Bengi Şentürk, Berçin Verda Asya, Ece Ayça Erdoğan and Ege Hoşgör for the debates, dinners, help and friendship. We have faced with a lot of difficulties and overcome all of them together throughout the years.

Many thanks to my second brother Oğuzhan Albayrak for his moral support, phone calls, coffee talks and being there whenever I needed a friend.

I would like to extend my sincere thanks to my new friend Özlem Yazır Aksakallı for listening, offering me advice, and supporting me over the past year.

I could not have undertaken this journey without the support of my family. I always knew that they believed in me and wanted the best for me. Words cannot express my gratitude to my family for guiding me to learn, to be happy, and to know and understand myself.

Last but not least, I owe thanks to a very special person, my beloved life partner, Hakan for his continued and unfailing love, support and understanding during my pursuit of PhD journey that made the completion of the dissertation possible.

TABLE OF CONTENTS

LIST OF TABLES

TABLES

LIST OF FIGURES

FIGURES

LIST OF SCHEMES

SCHEMES

LIST OF ABBREVIATIONS

ABBREVIATIONS

GPC	Gel Permeation Chromatography
FTIR	Fourier Transform Infrared
NMR	Nuclear Magnetic Resonance
HRMS	High Resolution Mass Spectroscopy
DCC	Dicyclohexyl carbodiimide
DCM	Dichloromethane
ACN	Acetonitrile
DMSO	Dimethylsulfoxide
DMF	Dimethylformamide
DME	1,2-Dimethoxy ethane
DMP	2,2 Dimethoxy propane
EDC	1-Ethyl-3-(3-dimethylaminopropyl)carbodiimide
MeOH	Methanol
EtOH	Ethanol
BuOH	Butanol
HOBt	1-Hydroxybenzotriazole
DAT	Diaminoterephthalate

CHAPTER 1

INTRODUCTION

The Universe is asymmetric, and I am persuaded that life, as it is known to us, is a direct result of the asymmetry of the Universe or of its indirect consequences. The Universe is asymmetric.

Louis Pasteur

1.1 Chirality and Origin of Life

The term chirality describes the fact that some substances have pairs of molecules in the sense of non-superimposable mirror image counterparts. Louis Pasteur achieved the discovery of this fact in 1858. He observed that one set of ammonium tartrate molecules rotated polarized light clockwise while the other rotated counterclockwise to the same extent.[1] The sets of two molecules were the optical isomers of each other and were called dissymmetric by Pasteur. The term 'chiral' was coined by Lord Kelvin in 1894 and took part in the terminology of Chemistry in 1962.[2] Since then; chirality has become core to chemistry, biology, and physics.

Chirality plays a crucial role in the evolution of life. Almost all essential biomolecules are homochiral.[3] Although there are various theories and hypotheses[4–7]concerning origin of homochirality on Earth, the handedness of biomolecules is still a mystery. Some of them are summarized below: [8]

1. *The "Sterile" and the Left-Handed Neutrino*

   "Sterile neutrinos" are the name of neutrinos with right-handed spin, and their non-existence was proven in 2016. [9] According to studies, only subatomic particles having left-handed decay exist in the Universe.[10,11] Thus, it may affect the occurrence of handedness in the Universe and the primordial protoplanets.

2. *The Panspermia Hypothesis*

   Panspermia Hypothesis proposes that life originated elsewhere in the Universe, not on Earth. For instance, it was known that some of the complex organic compounds such as proteogenic L-aminoacids arrived on Earth by meteorites. In other words, asteroids or comets may be the building blocks of terrestrial life.[12]

3. *The Primordial Soup Hypothesis*

   The Primordial Soup Hypothesis (Oparin-Haldane Model) suggests that at the beginning of the Earth's evolution, a mixture of carbon-based chemicals in the sea, also called as primordial soup, provided the proper conditions for the formation of organic compounds, and the complexity of the compounds increased gradually. As a result, fundamental biomolecules such as carbohydrates and proteins emerged. The major dilemma of this idea is the delicacy of the crucial biomolecules, such as DNA, RNA, nucleic acids, and proteins, in water and known as "the water paradox". Scientists proposed that another crucial compound for synthesizing prebiotic precursors like amino acids, formamide, could solve this problem. It could provide a suitable microenvironment for chemical reactions.[13–15]

4. *Parity Violation in Weak Interactions—Energy Difference in Enantiomers*

   The theory of Parity Violation in Weak Interactions has a remarkable contribution to the explanation of chirality. According to experimental findings, during the processes associated with weak interactions, such as the interaction of enantiomers-electrons, enantiomers-nucleons, and so on, it was observed that the energy of the mirror images was not the same. In other words, these interactions make one of the enantiomers more stable.[16,17] Energy difference between enantiomers could explain the emergence of homochirality on Earth.

5. *Enantiomeric Excess as a Catalyst of Homochirality on Earth*[18–20]

   In general, life on Earth is defined as homochiral, yet biomolecules on the planet are composed of compounds having high enantiomeric excess, not purely homochiral. The high enantiomeric excess in the biosphere could be originated from the formation of homochiral biomolecules in the presence of a small amount of enantioenriched (formed by autocatalysis or originated from extraterrestrial sources) molecules such as amino acid or sugar.[21] As a result, enantiomeric excess might be the biomarker of homochiral life.

6. *Chirality and Photochemistry*

   According to the hypothesis, interstellar or circumstellar circularly polarized light might cause the initial symmetry breaking. When a racemic mixture of organic compounds is exposed to UV circularly polarized light (UVCPL), the amount of one enantiomer may increase due to the photolysis of the other one. As stated in the previous studies, a neutron star can generate UVCPL as synchrotron radiation, as well as Mie scattering of light from interstellar clouds by aligned interstellar grains. The interaction of UVCPL with organic matter on or near the surface of a primordial planet might bring about the formation of enantiomeric excesses.[22]

1.1.1 Chirality Concept

Life on Earth has evolved by favoring one kind of enantiomer. Thereby, while proteins are mainly composed of *L*-aminoacids, D-sugars are one of the building blocks of DNA and RNA. Moreover, chirality can be seen at various levels, from subatomic to galactic scale (Figure 1.1).[23]

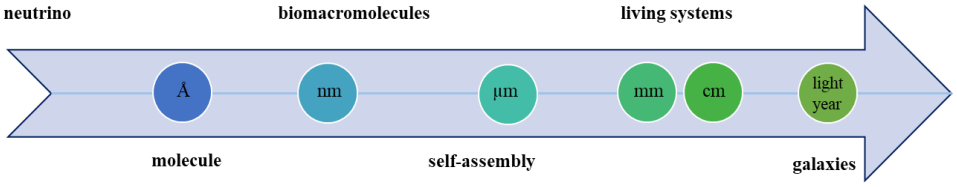

Figure 1. 1 Chirality scale in the Universe

1.1.1.1 Molecular and Supramolecular Chirality

Molecular and supramolecular level chirality is essential to construct the chiral structure at higher levels. It is well known that molecular chirality is at the core of drug design and functional molecules. For instance, the *L*-form of artificial sweetener aspartame has a sweet taste, but *D*-form is tasteless.[24] While the smell of *R*-carvone is like spearmint, *S*-carvone smells like caraway.[25] The chelation therapy and the treatment of rheumatoid arthritis are carried out with *D*-penicillamine, but the *L*-form is toxic since it inhibits the pyridoxine activity, an essential vitamin B_6.[26] Besides, more research has been conducted in recent years related to supramolecular chirality due to its importance in biological systems.

As mentioned in the previous chapter, chirality is a spatial arrangement of an object or a molecule, and if they could not be superimposed with the mirror images, they are called chiral. To explain further, the absence of a symmetry element of second-order (σ, i, S_n) makes a molecule chiral.[27] From a chemistry point of view, molecular chirality can be described in three classes:[28]

Point chirality: If sp^3 hybridized carbon atom is attached to four different types of atoms or groups of atoms, it has point chirality, and is called as asymmetric carbon (Figure 1.2.a).

Planar chirality: If a molecule lacks an asymmetric carbon but has two non-coplanar rings connected dissymmetrically, it has a planar chirality. These molecules have restricted rotation about the chemical bond. (Figure 1.2.b).

Axial chirality: If a molecule does not have a chiral center but an axis about which the attached atoms or groups are kept in a spatial arrangement that cannot be superimposed on its mirror image, it has an axial chirality. (Figure 1.2.c).

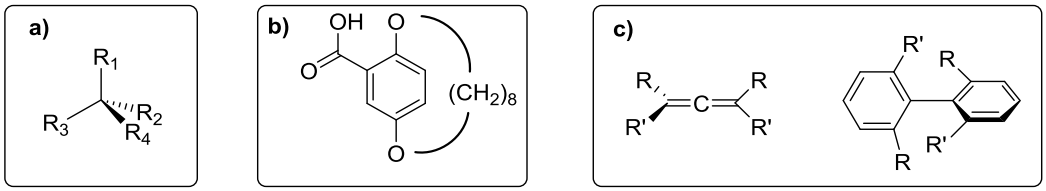

Figure 1. 2. Examples of a) point chirality, b) planar chirality, c) axial chirality

Besides, supramolecular chirality can be thought of as chirality at the supramolecular level and arises due to molecular self-assembly. There are various ways to obtain supramolecular chirality—using chiral components, combining chiral and achiral molecules, or just achiral molecules. In all cases, assemblies of these molecular components determine the manner of supramolecular systems. One of the main parameters that cause the emergence of supramolecular chirality is intermolecular noncovalent interactions. As a result, the formation of self-assemblies in biological systems provides crucial functionalities such as transferring and storing genetic information.[29]

1.2 Helicity or Helical Chirality

Helical chirality can be thought of as a subset of axial chirality. In this case, molecules show screw-like assemblies along the chirality axis, such as in the case of helicenes (Figure 1.3.a). Helicity is often encountered in biomolecules. The typical

examples of helical chirality are the backbone of RNA and DNA (Figure 1.3.b and 1.3.c).[30]

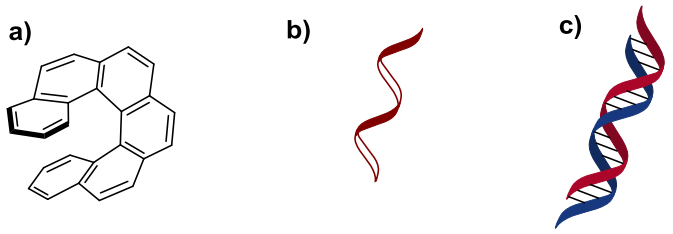

Figure 1. 3. The helical structure of a) helicene, b) α-helix of protein, c) ds DNA

1.2.1 Helical Polymers

In nature, as the molecular size increases, its functionality increases, and the structures become more ordered. Proteins, genes, DNA, and RNA are the most striking examples of these macromolecules. In such systems, helicity is a commonly formed structure in the polymer's backbone and provides a crucial role in their biological activities.[30,31] Inspired by biology, helicity has become an attractive subject for scientists working on synthetic polymers due to their broad applications and features described in the following section.

The history of synthetic helical polymer is based on the structural discoveries of natural polymers. Nakano and Okamoto summarized the cornerstones of the historical developments, shown in Table 1.1.[32]

Table 1.1 The historical developments of synthetic helical polymers

1937	α-Amylose (Hanes [Freudenberg 1939])
1951	Polypeptide (α-helix) (Pauling)
1953	DNA (Franklin, Watson, Crick)
1955	Isotactic polypropylene (Natta)
1956	Poly(γ-benzyl-Lglutamate) (Doty)
1960	Isotactic poly(3-methyl-1-pentene) (Pino)
1969	Poly((+)-1-phenylethyl isocyanide) (Millich)
1970	Poly(isocyanate) (Goodman)
1974	Poly(*t*-butyl isocyanide) (Drenth, Nolte)
1974	Polyacetylene derivatives (Ciardelli [Sinionescu,Percec 1977; Grubbs 1991; Yashima, Okamoto 1995])
1979	Poly(triphenylmetyl methacrylate) (Okamoto, Yuki)
1980	Polychloral (Vogl [Ute, Hatada,Vogl 1991]
1984	Poly(α-isobutyl-L-aspartate) (Subirana [Yuki 1978])
1987	Helicates (Lehn)
1988	Poly(alkyl isocyanate) with isotopic chirality (the uniform chiral field concept) (Green)
1994	Polysilane (Fujiki, Möller [Matyjaszewski 1992])
1995	Induced helix of poly(phenylacetylene) derivatives (Yashima, Okamoto)
1995	Oligoarylene (Lehn)
1996	β- Peptide oligomers (Seebach, Gellman)
1997	Oligoaryleneethynylene (Moore)

As discussed in the previous section, helical structures are chiral, and to get resolved helical polymers, synthesis must be done to select one sense, or helicity is induced by external factors. Additionally, even if the polymer does not have a

configurationally well-defined chiral group in the backbone or side chain, it may still be optically active.[32]

1.2.2 Static and Dynamic Helical Polymers

The valuable studies performed by Nolte[33], Okamoto[34], and Green[35] have been a guide to classifying artificial helical polymers as static and dynamic helical polymers according to their helix inversion barrier. The helix inversion barrier is significantly higher for the static helical polymers than those of the dynamic ones. Moreover, while static helical polymers are stable at room temperature, dynamic helical polymers have a dynamic nature, and helix reversals can move along the polymer's backbone (Figure 1.4).

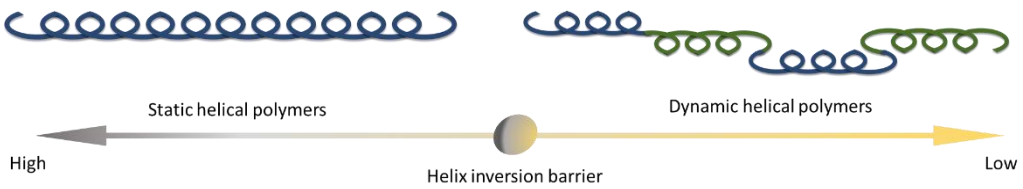

Figure 1. 4. Static and dynamic helical polymers in terms of their helix inversion barriers

Poly(triphenylmethyl methacrylate),[34] poly(t-butyl isocyanide),[33] and polychloral,[36] belong to the class of static helical polymers. (Figure 1.5) These polymers can be synthesized with an excess of one sense by using a chiral monomer as well as bulky achiral monomers with the help of an optically active catalyst or initiator. Polymerization reaction occurs under kinetic control, and obtained polymers can maintain their conformation in a solution. This feature provides the separation of both enantiomeric forms of helices by chiral column chromatography.[32]

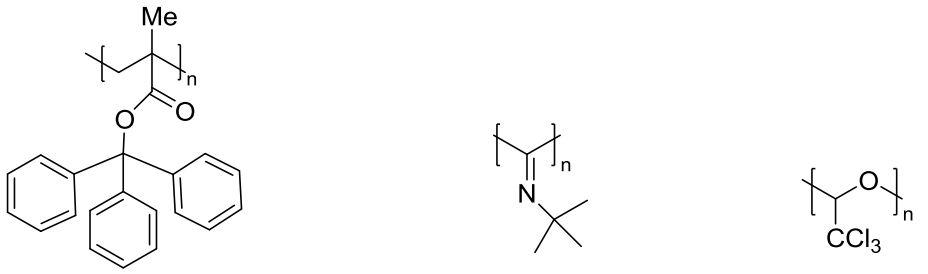

Figure 1. 5. Examples of static helical polymers

On the other hand, since the helix inversion barrier is low for dynamic helical polymers, such as polyisocyanates[37] and polysilanes,[38] they cannot be separated using chiral column chromatography (Figure 1.6). These polymers have energetically unfavoured helical reversal at certain points, and the equal mixture of left and right-handed helical segments can be inverted at ambient temperature.[39] The addition of a small amount of chiral bias to the copolymer produces a helical polymer with a large helix-sense excess under thermodynamic control. These chiral amplification methods were first experienced for dynamic polyisocyanates by Green et al. and named as "sergeants and soldiers(S&S)"[35] effect and "majority rule (MR)",[40] respectively. These phenomena opened the doors of new research areas in polymer and supramolecular chemistry.[41]

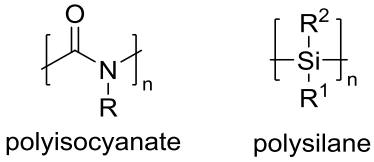

Figure 1. 6. Structures of polyisocyanate and polysilane

Besides, it was observed that some of the helical polymers such as poly(quinoxaline-2,3-diyl)s, polyguanidines, and most of the poly(mono- and di-substituted acetylene)s and poly(phenyl isocyanide)s show characteristics of both static and dynamic helical polymers. (Figure 1.7) [42–45] The features of these polymers depend on the difference in the chiral or achiral substituents in the monomers. With this

property, the helix inversion barrier can be controlled, and static or dynamic helical polymers having the same backbone structures can be synthesized by adjusting the substituents. [46]

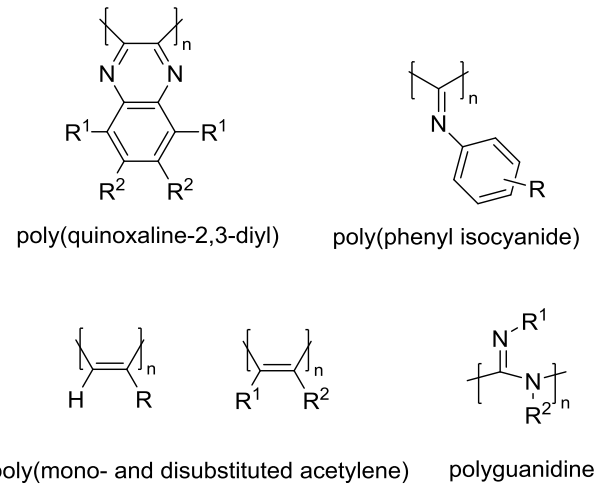

Figure 1. 7. Polymers show both static and dynamic helical polymers features

Nature has utilized the helical structures to attain crucial complex functions such as data storage, soft tissue support, light-harvesting, ion conduction, and chiral switching.[47–50] Inspired by nature, scientists have been challenged by reproducing these features and synthesizing helical polymers due to their prominent optical activities.[51–58] They have diverse applications such as chiral recognition,[59] enantioselective crystallization,[60,61] enantioselective release,[62,63], and asymmetric catalysis.[64–66]

In 2011, Yashima et al. synthesized novel optically active poly(phenyl isocyanide)s bearing achiral benzanilide pendant groups to utilize the chiral recognition property of helical polymers. They took advantage of helicity induction and memory strategy by noncovalent interactions. The synthesized helical polymers were used as a chiral stationary phase and immobilized to 3-aminopropyl-silanized silica gel via chemical bonding or coated on the silica gel. Their chiral recognition abilities and enantiomeric separation features by HPLC were investigated and obtained promising results. It was also shown that using helical polymers with macromolecular helicity

memory could be a good strategy for preparing novel chiral stationary phase for particular racemates. With this way, required functional groups, chiral or achiral, could be inserted to the pendant groups. Moreover, the preferred helical structure could be maintained. The synthesis and working mechanism of the corresponding study were summarized in Figure 1.8. The polymers were obtained by ‘‘helicity induction and memory strategy’’. To induce helicity, (*S*)- and (*R*)-phenylglycinol were used and modified using aniline and its derivatives with a long alkyl chain and an ester group at the para position. After characterization studies, helical polyisocyanides immobilize onto a (3-aminopropyl)-silanized silica gel. [67]

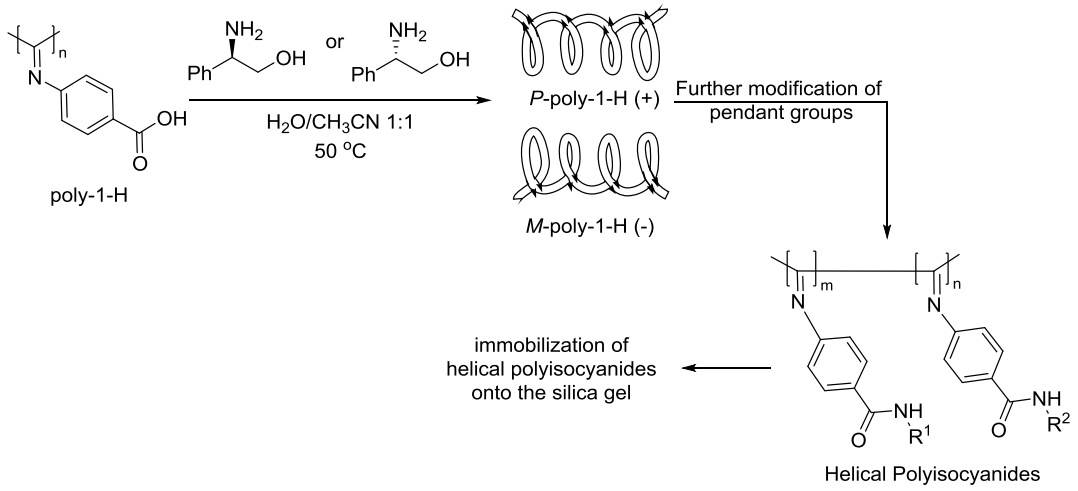

Scheme 1. 1. Synthesis of optically active poly(phenyl isocyanide)s bearing achiral benzanilide pendant groups to utilize the chiral recognition property of helical polymers.

In 2016, Wu et al. made use of the enantioselective crystallization property of the helical polymers by the controlled synthesis of hybrid silica nanoparticles modified with helical poly(phenyl isocyanide)s.[60] An *L*- or *D*-alanine was preferred as a pendant group with a long alkyl chain. As a result, optically active, left-handed helical polyisocyanide grafted onto the silica nanoparticles was obtained. It was shown that these optically active nanoparticles could provide enantioselective crystallization of racemic compounds. They reported that the enantiomeric excess (*ee*) of the induced crystals of Boc-alanine could be up to 95% (Figure 1.9).

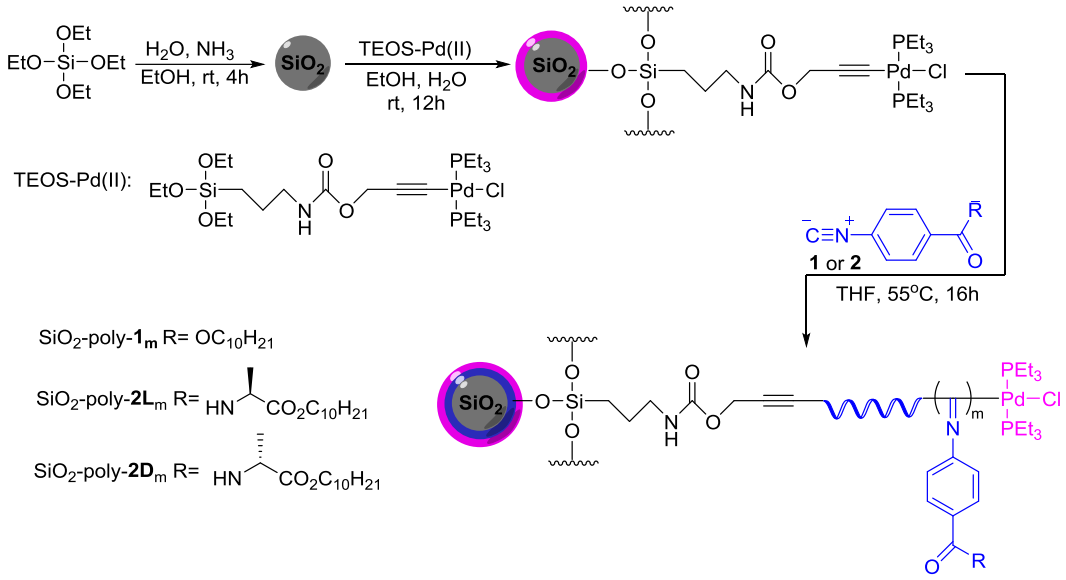

Scheme 1. 2. Synthesis of optically active, left-handed helical polyisocyanide grafted onto the silica nanoparticles.

In 2018, Deng and Liang conducted a study to investigate the enantioselectivity of helical polymers in a chiral release applications. In this study, polylactide bearing polymerizable alkynyl groups were synthesized, and the obtained compound was copolymerized with optically active alkylnyl monomer with the suspension polymerization method. Terminal hydroxy groups in polyactide acted as an emulsifier and provided a porous structure to the final product. The final porous particles were utilized to load optically active drug naproxen to perform enantioselective release studies. Releasing studies with naproxen-loaded chiral particles were performed in two modes: single enantiomer release and racemate release. Single enantiomer release showed a significant difference in the releasing time of a particular enantiomer. Although racemates did not differ with respect to releasing time, there was a significant difference in enantiomeric excess. As a result of the studies, this work showed that the enantioselectivity of chiral materials could be modified by combining other chiral components (Figure 1.10).[62]

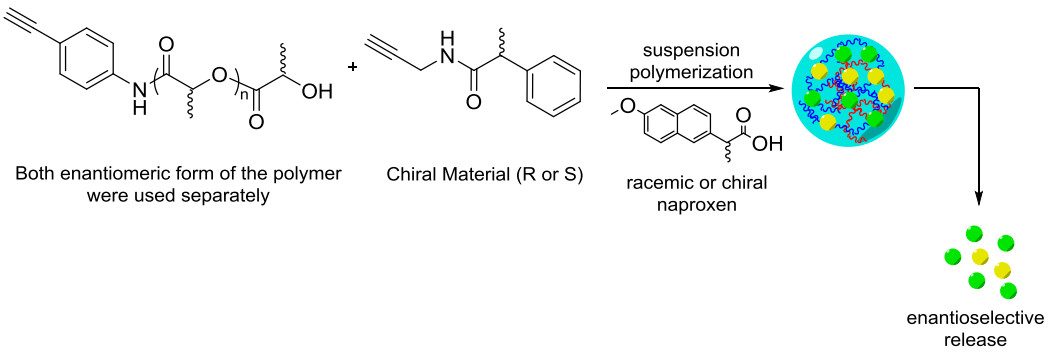

Scheme 1. 3. Synthesis of polylactide bearing polymerizable alkynyl groups and the copolymerization with optically active alkylnyl monomer with the suspension polymerization method and process for enantioselective release

In another study conducted by Deng et al. in 2012, helical polymers were used as asymmetric catalysts. They synthesized a novel helical copolymer and showed it could catalyze asymmetric aldol reaction. In addition, they also found that the helical structure in the backbone was essential for catalyzing the reaction (Scheme 1.4).[65]

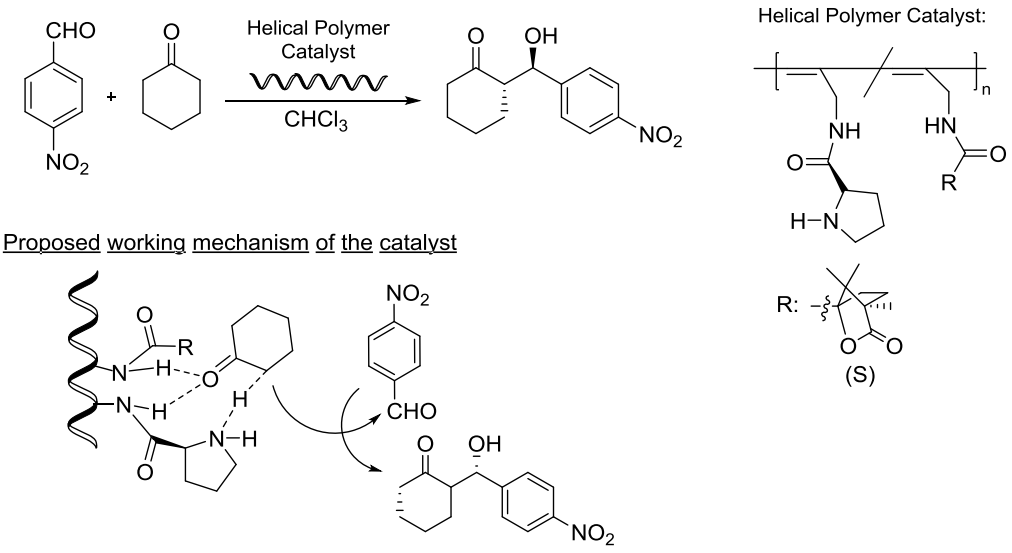

Scheme 1. 4 Use of helical polymers in Aldol reaction of cyclohexanone with nitrobenzaldehyde as a chiral catalyst.

1.2.3 Helical Structure Determination

In recent years, interest in helical polymer synthesis has increased due to the above-mentioned outstanding properties and various application areas. The most challenging part of the characterization of helical polymers is the determination of their handedness (right- or left-handed). Structure determination of helical polymers is essential to understanding the mechanism of helix formation, the relationship between helix and function, and developing specialized polymers. Figure 1.8 shows methods utilized for structural analysis of helical polymers.[68]

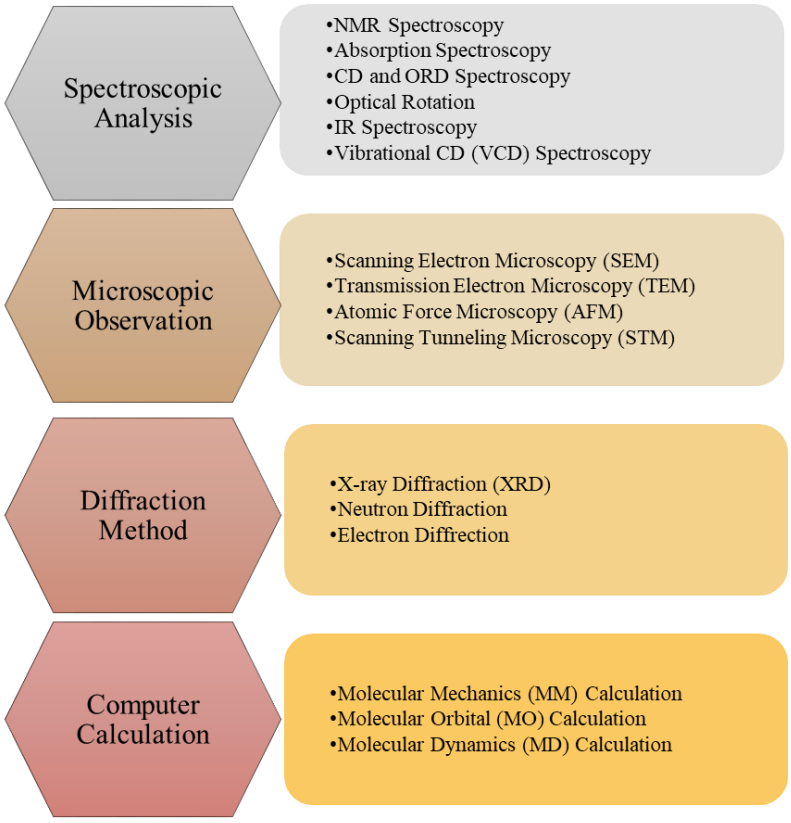

Figure 1.8. Methods utilized for structural analysis of helical polymers

NMR, IR, and absorption spectroscopy are the methods used primarily in the characterization of the helical polymer, as in the case of the determination of the structure of organic compounds. XRD, neutron diffraction, and electron diffraction

methods are advantageous for getting information about ordered polymer structures, especially in the solid-state. Among them, XRD is widely used to determine the helical structures of polymers. Nevertheless, with limited diffractions and difficulty in obtaining proper crystals from polymers, it is hard to determine the exact helical structure of polymers. Scanning electron microscopy (SEM) and transmission electron microscope (TEM) are mainly used to elucidate the structures of self-assembled supramolecular aggregates made up of small molecules or oligomers. However, due to poor resolution, it is hard to characterize the helical structures exactly. Among microscopic observation methods, scanning tunneling microscopy (STM) and Atomic Force Microscopy give the most noticeable results and have been extensively used. Theoretical calculation methods such as molecular mechanics (MM), molecular orbital (MO), and molecular dynamics (MD) are used as a complement to other methods for the prediction of helical structures and their dynamic behaviors.[68]

The method that gives one of the most explicit information about helix formation with helical sense is circular dichroism (CD) and/ or optical rotation. As mentioned above, CD spectroscopy has many advantages compared to other methods such as crystallography, electron microscopy, and NMR spectroscopy. For instance, it can be performed in both solution and solid-state with proper equipment. Furthermore, the changes in helical structure can be detected with respect to changing parameters such as temperature and pH.[69]

1.2.3.1 Circular Dichroism (CD)

The various types of interactions between radiation and molecules have been utilized to shed light on the structures of molecules. UV-Vis, IR, and NMR spectroscopy methods are crucial for the structural determination of compounds, and each of them gives unique information about the structures. Moreover, it is well-known that polarized light interacts with chiral molecules in a specific way. After the discovery of rotatory dispersion of quartz, optical rotation measurements with sodium D-line

(588.9950 and 589.5924 nm) have been widely used by organic chemists.[70] For instance, amino acids in biological systems are mainly L (Levo rotary) optical isomers that rotate plane-polarized light to the left. Similarly, sugars mostly in D (Dextro rotary) form and rotate plane-polarized light to the right. Optical rotation dispersion (ORD) and circular dichroism (CD) measurements are utilized to explain the effects of molecules on polarized light.[70] Before going into the detail of these techniques and applications, it is essential first to understand the properties of light.

1.2.3.1.1 Properties of Light

Light is electromagnetic radiation that consists of two main components, electric and magnetic fields, that are perpendicular to each other (Figure 1.9). The periodic change of electric and magnetic fields produces the electromagnetic spectrum having different wavelengths. The term wavelength expresses the distance that light travels in one oscillation, and the unit of wavelength is nanometer (nm).

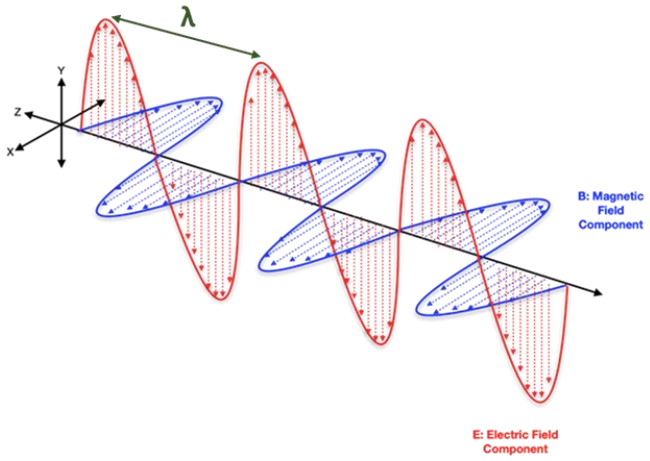

Figure 1. 9. The components of electromagnetic radiation

Another term, frequency, is the number of waves that pass a point in a unit time and are measured in terms of Hertz (Hz). Electromagnetic radiation is defined by either wavelength or frequency. In order of decreasing wavelength (or increasing frequency), electromagnetic waves are named as follows: radio waves, microwaves,

infrared radiation, visible light, ultraviolet radiation, X-rays, and gamma rays (Figure 1.10).[71]

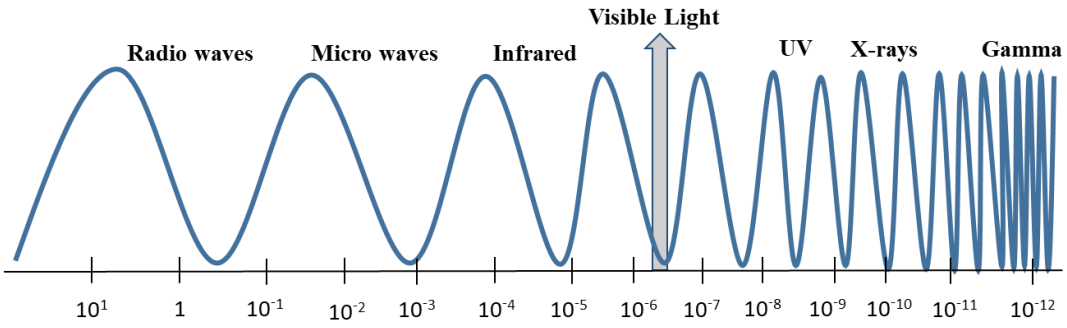

Figure 1. 10 Classification of electromagnetic waves in terms of frequency (Hz)

Typical light sources such as sunlight, halogen lighting, LED spotlights, and incandescent bulbs, produce unpolarized light, consisting of different wavelengths of magnetic radiation, while monochromatic light contains only one narrow range of wavelength. To obtain a desirable monochromatic light wavelength, a monochromator is essential.[72] Regardless of whether it is monochromatic or polychromatic, light oscillates in different planes. If light oscillates in a single plane, like in the case of lasers, it is called plane-polarized or linearly polarized light.[73,74] The discovery of birefringence in crystals by Erasmus Bartholinus and its subsequent interpretation by Christian Huygens around the year 1670 is considered the cornerstone of studies in the field of polarized light.[75] Plane polarized or linearly polarized light can be considered as the electric field of the light limited to a single plane along the direction of propagation. It consists of two components with equal amplitude, and they are perpendicular to each other. There is no phase difference between these components (Figure 1.11).[73,74]

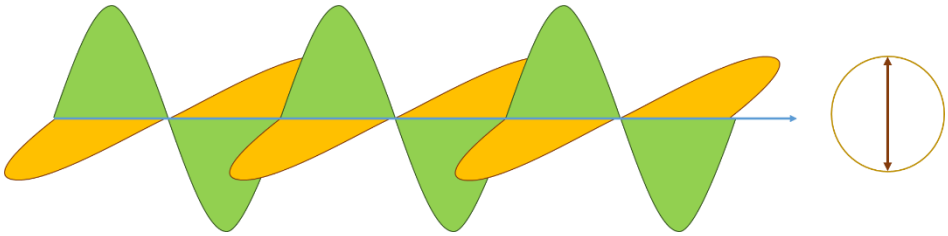

Figure 1.11. The components of plane polarized light

In the case of circularly polarized light, there is a difference of $\pi/2$ between these components. As a result of phase difference electric field has circular rotation along the direction of propagation. It is called left- or right-handed circularly polarized light according to the direction of rotation (Figure 1.12).[74]

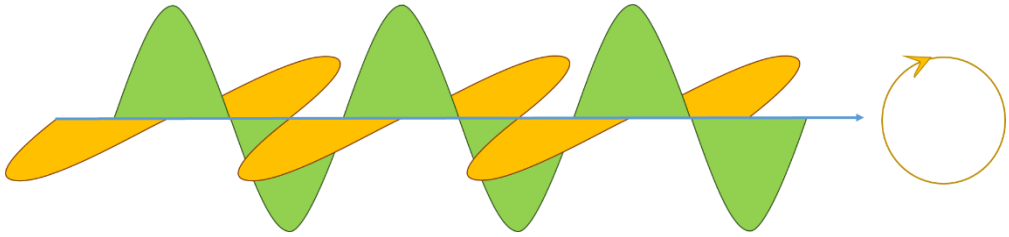

Figure 1. 12. Circularly polarized light

The representation below depicts electric field components of unpolarized, linearly or plane-polarized and circularly polarized light. In all three cases, light moves along the y axis, and the direction of the arrow shows the direction of the electric field. Unpolarized light spreads in all directions, while polarized light only in the z direction. Circularly polarized light could have a direction of rotation either clockwise or counterclockwise (Figure 1.13).

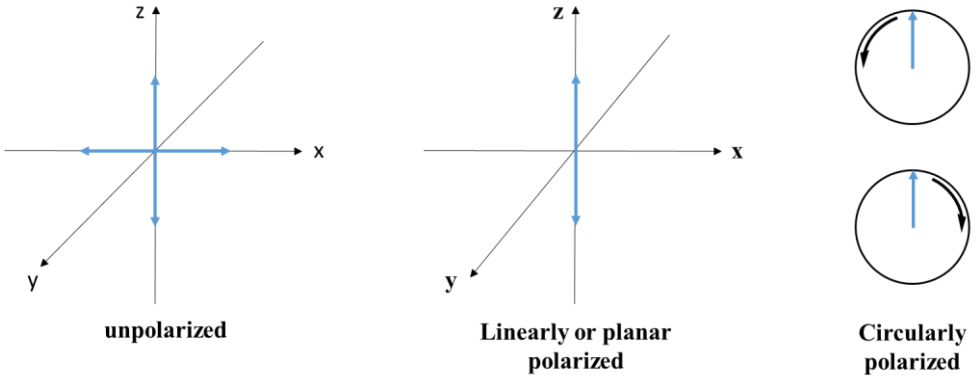

Figure 1. 13. Electric field components and direction of unpolarized, linearly or plane-polarized, and circularly polarized light.

If left-handed and right-handed circularly polarized light has the same amplitudes, the combination of these two produces linearly polarized light. Besides, when the two linear components of light have different amplitudes and/ or a phase difference is not $\pi/2$, the electric field of light produces an elliptically polarized light (Figure 1.14).[76]

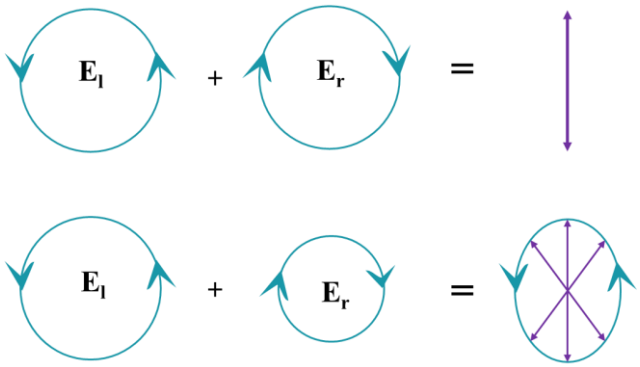

Figure 1. 14. Linearly and elliptically polarized light

1.2.3.1.2 Physical Basics of Plane Polarized Light[74]

1.2.3.1.2.1 Electric Field Vector

The approach of electromagnetic waves is derived from nonzero solutions of Maxwell's equations in a vacuum which represents the absence of electric charges in

the following equations.[77] In these equations, E is the electric field of an electromagnetic wave that travels in the direction of z in Euclidean coordinates (x, y, z). the speed of light is denoted with c. The trigonometric notation of E:

$$E(t, z) = E(0, 0) \cos(\omega t - kz - \phi) \quad (1)$$

where ω is the angular frequency, t is the time, k= ω/c is the absolute value of the wave vector, and ϕ is an arbitrary phase. Since the electric field vector is perpendicular to the z-axis, E(t, z) can be separated into x and y components. To make the equation simple, the location is regarded as 0 (z=0) means that the location of E(t) is in the xy plane. The x and y components of the electric field are

$$E_x(t) = E_x(0) \cos(\omega t - \phi_1) \quad (2)$$

$$E_y(t) = E_y(0) \cos(\omega t - \phi_2)$$

ϕ_1 and ϕ_2 are a priori arbitrary phases. The angle between E(t) and the positive x-axis is the polarization angle, regarded as a counter-clockwise direction with χ. The polarization of the wave is shown by the relative values of $E_x(0)$, $E_y(0)$, ϕ_1, and ϕ_2.[78]

Linear Polarization

In the case of $\phi_1 = \phi_2$, specifically used here as $\phi_1 = \phi_2 = 0$ in order not to lose generality;

$$E_x(t) = E_x(0) \cos(\omega t) \quad (3)$$

$$E_y(t) = E_y(0) \cos(\omega t)$$

From these equations, it can be seen that the orientation of electric field E relies only on the magnitudes of $E_x(0)$ and $E_y(0)$ and is independent of time. The polarization angle χ is constant with $\chi \in [0, \pi]$. The plane of polarization is the plane wherein the wave is located. It is given by the polarization angle χ. It has an orientation but does not have a direction. As a result, the location of linear polarization in the xy plane is not a vector.[78]

Circular Polarization

In case of a relative $\phi_1 = \phi_2 \pm \pi/2$, specifically used here as $\phi_1 = \phi_2 = 0$ in order not to lose generality $E_x(0) = E_y(0)$;

$E_x(t) = E_x(0) \cos(\omega t)$ (4)

$E_y(t) = \pm E_y(0) \sin(\omega t)$

With the angular frequency ω, the electric field vector has circular motion in the xy plane. Hence, the radiation becomes circularly polarized. The sign of $E_y(t)$ defines the sense of the motion of E, and it is derived from the relative phase. The counter-clockwise motion has a positive sign called right-handed circular (RHC) polarization, and the clockwise direction has a negative sign and is referred to as left-handed circular (LHC) polarization.[78]

1.2.3.1.3 Optical Rotary Dispersion (ORD)

As mentioned above, optical rotation can be thought of as the rotation of linearly polarized light by an optically active molecule. The term optical rotary dispersion (ORD) defines the wavelength dependence of the optical rotation. The extent of rotation of white light varies according to the wavelength. As the wavelength increases, the amount of rotation per unit of distance decreases. The measurement of optical rotation is performed by using monochromatic plane-polarized light.[79]

As illustrated in Figure 1.15, when linearly polarized light along the y-axis passes through the optically active compound, the phase difference occurs between the circularly-polarized components, and the difference is denoted as α. When the rotation is to the left, it is called Levo (L) or (-); when the rotation occurs to the right, it is called Dextro (D) or (+).[80]

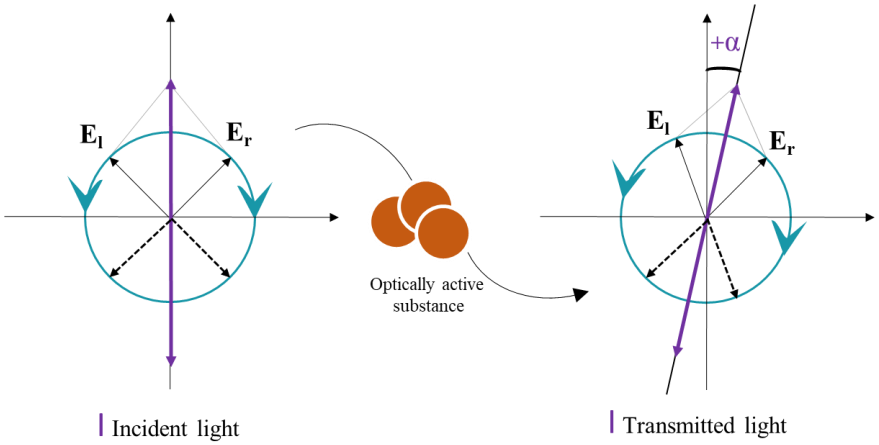

Figure 1. 15. Principle of optical rotation

Nowadays, the CD has started to be preferred over ORD due to its advantages. In ORD, all rotary contributions from UV and visible regions are only represented in the visible region. However, the CD shows the bands in UV and visible regions separately, revealing structural details.[81]

1.2.3.1.4 Circular Dichroism Spectroscopy

The circular dichroism (CD) phenomenon arises when optically active substances absorb the left and right circularly polarized light to a different extent, and transmitted light becomes elliptically polarized.[82]

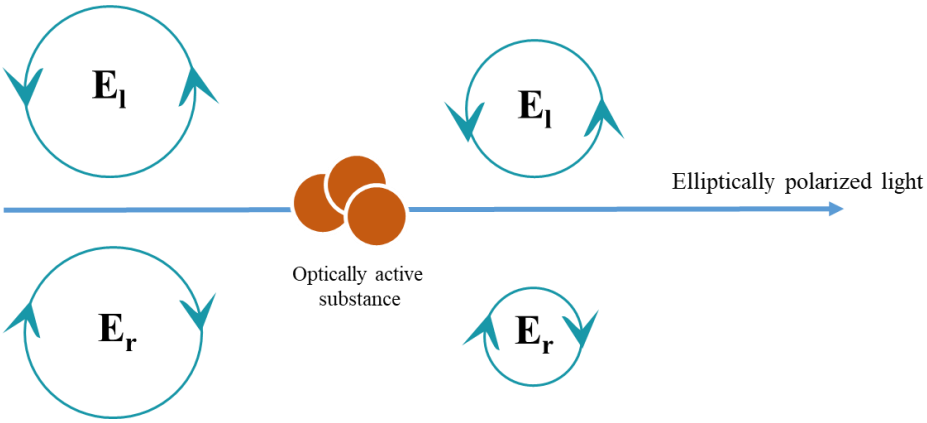

Figure 1.16. Elliptically polarized light

The difference between the absorbance of the substance for right and left circularly polarized light is the direct measurement of circular polarization.[82]

$\Delta A = A_L - A_R$ (5)

Based on the Beer-Lambert Law: $A = \varepsilon * b * c$ where b is pathlength, c=molar concentration; ε_L and ε_R are the molar extinction coefficients for LCP and RCP light $\Delta\varepsilon$ is molar circular dichroism. Then the equation becomes

$\Delta\varepsilon = \varepsilon_l$ and ε_r (6)

The spectroscopic technique that uses the phenomenon explained above is referred to as circular dichroism (CD) spectroscopy. This technique is mainly utilized to examine chiral molecules of all types and sizes and measure the CD of compounds over a range of wavelengths.[83] In Figure 1.16 working principle is summarized.

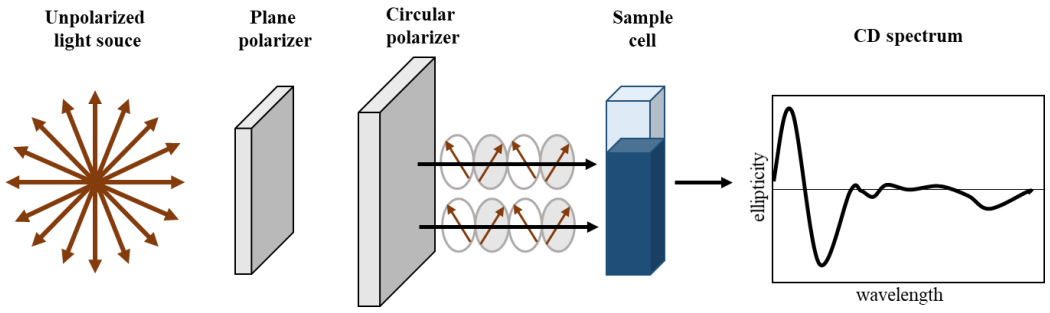

Figure 1.17. Working principle of circular dichroism spectroscopy

CD spectroscopy is mainly facilitated for biological molecules and macromolecules. Structural, kinetic, and thermodynamic information can be obtained from this technique.[84] It has been utilized in the field of biological molecules for over 50 years to determine secondary structures, interactions in solution, and folding. CD spectroscopy has also been used in various research areas related to optically active compounds in recent years. It provides a valuable output about the self-assembly of the supramolecules. Helical structures formed during the assembly processes can be examined by CD spectroscopy.[83]

From the working principle point of view, CD spectroscopy is similar to UV-Vis absorption spectroscopy. Since CD is based on absorption changes, the contribution of the chromophores in the conventional absorption spectrum is almost the same in the case of the CD spectrum. The only difference is that to detect CD signal, chromophore must be inherently chiral or in the optically active (asymmetric) environment.[85,86]

1.2.4 Chromophore Functionalized Helical Polymers

In recent years, polymers functionalized with chromophores have become one of the hotspots for scientists due to their potential properties and applications.[87,88] The design and preparation of organic optical absorbing materials have been extensively studied since they have solution processability, and their chemical and physical properties can be modified by changing the molecular design. Furthermore,

introducing chirality to these polymers provides more sophisticated properties such as non-linear[89] or circularly polarized luminescence[90] to the materials.

The conjugated dyes that meet these expectations include phthalocyanine, polymethine cyanine, squaraine, diamino terephthalates, radical dyes, azo, and their derivatives.[91] The properties of squaraine and diamino terephthalate chromophores were examined in detail in the following parts.

1.2.4.1 Squaraines

Squaraines are a branch of the polymethine dye family, a few examples of which are shown below (Figure 1.17). Polymethines are classified with respect to two heteroatoms attached by an odd number of repeating methane units = CH – which forms conjugated systems. According to the heteroatoms, they can be cationic, anionic, zwitterionic, or neutral.[92] Cyanines belong to the cationic polymethine class, and heteroatoms are amine and iminium groups. These heteroatoms are generally included in a ring system, but there are also examples of one nitrogen-containing cyanine called hemicyanines. Oxonols are anionic cyanines and terminate with oxygen atoms. The examples of neutral cyanines are merocyanines, and they have one oxygen and one nitrogen at each end of the polymethine unit. Due to the strong dipole moment in the structure, they have a distinct zwitterionic character.[92,93]

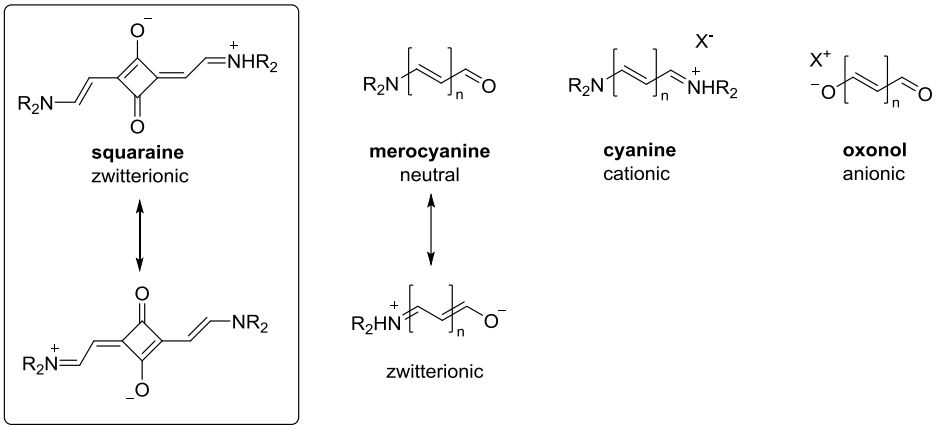

Figure 1. 18. Classification of polymethine dyes

Squaraines or squarylium cyanines with donor-acceptor-donor (D-A-D) are obtained from the condensation reaction between squaric acid (3,4-dihydroxy-1,2-dioxocyclobut-3-ene) and electron-donating aromatic (e.g., *N*,*N* dimethylaniline) (Scheme 1.5) or heterocyclic (e.g., 2-methyl-benzothiazole) (Scheme 1.6) methylene bases. The framework of squaraines is similar to cyanine dyes and leads to effective electron delocalization. Squarylium cyanines exhibit a complete zwitterionic character, and they are neutral overall.[92]

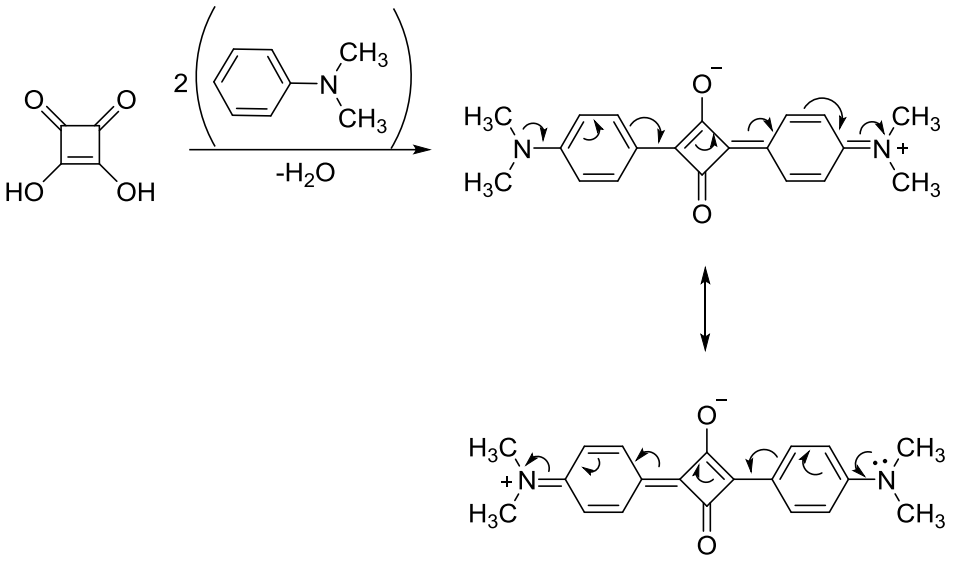

Scheme 1.5. Aromatic Squarylium Cyanine Dye

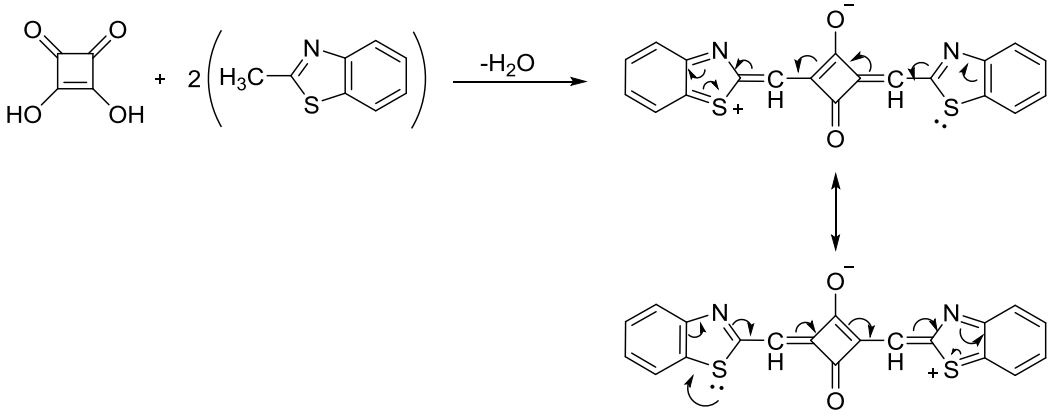

Scheme 1. 6. Heterocyclic Squarylium Cyanine Dye

The history of squaraine dyes goes back to the mid-1900s. In 1965, Triebs and Jacob stated that the reaction between squaric acid and pyrrole (**s1** and **ps1**) or phloroglucinol (**s2**) formed a red-violet solid. They also synthesized the polymeric form of the pyrrole containing squaraine dyes. This was the first report about the synthesis of squaraine dyes (Figure 1.19).[94]

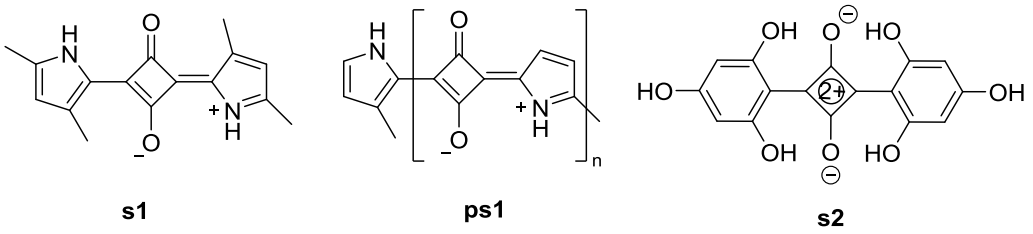

Figure 1. 19. Structures of first squaraines reported by Treibs and Jacob

In 1968, Treibs and Jacob published their work on this new condensation reaction mechanism. In this study, they designed a series of experiments that provided to obtain a possible intermediate of the condensation reaction, that is, the compound formed with the addition of just one nucleophile to the squaric acid. With the isolation of the intermediate so-called semi-squaraine, they revealed the formation mechanism of squaraine and proposed a method for synthesizing unsymmetrical squaraine dyes. Moreover, by comparing the IR spectra concerning the vibrations of the central core unit of products, they conducted a guiding study on understanding which product is formed. Both semisquaraines and 3,4 disubstitution products had IR signals at ~ 1770 cm^{-1} and ~ 1720 cm^{-1} relating to the cyclobutenone groups. On the other hand, the IR signal at ~ 1615 cm^{-1} emerged in the spectra of 1-3 disubstitution products which proved the delocalization of the electrons on the chromophore.[94,95] In 1980, 1,3 disubstituted squaric acid derivatives having delocalized bonds were called ‘squaraines’ by Schmidt. The name ‘squaraine’ was derived from the *squa*ric acid and beta*ine* character of the dyes.[96]

Squaraine dyes usually have planar structures, and in the case of two identical electron donor moieties, they are centrosymmetric.[97] One of the most distinctive properties of the squaraine dyes is the sharp and intense absorption and emission in

between the red visible to the near-IR region and their molar absorption coefficients are high ($\varepsilon > 10^5$ L mol^{-1} cm^{-1}).[98,99] Moreover, absorption and emission wavelength can be tuned in the range of 550 to 850 nm by modifying the structures of electron donor groups. In literature, aromatic and heterocyclic groups such as *N*,*N*-dialkylanilines, phenols, pyrroles, indoles, benzothiazoles, and quinolones were used as electron-donating groups to adjust the optical properties of the corresponding squaraine dyes.[91] These properties make the squaraine dyes outstanding candidates for the potential applications in photovoltaics, photodynamic therapy, conducting devices, non-linear optics, and bio labeling.[97,100–108] Besides, squaraine dyes have been utilized to detect various ions, including Ca^{2+}, Mg^{2+}, Hg^{2+}, Fe^{3+}, Cu^{2+}, Pd^{2+}.[109–114] Moreover, as explained in the following parts, the aggregation feature has been applied in many areas (Figure 1.20).[115]

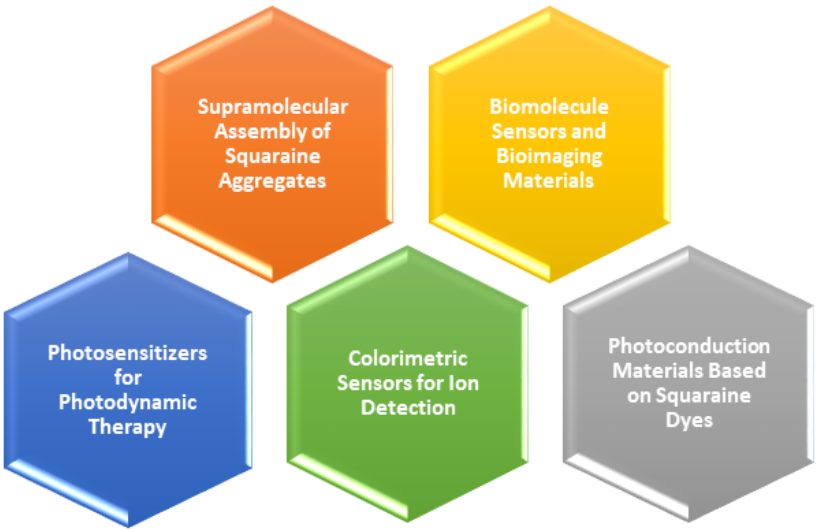

Figure 1. 20. Potential applications of squaraine dyes

The first synthesis of squaraine dyes were accomplished in the presence of acetic anhydride as a solvent. After a year, Sprenger and Ziegenbein also synthesized squaraine dyes using a different procedure. They used a mixture of benzene and 1-butanol as a solvent, and two equivalents of aromatic nucleophiles and one equivalent of squaric acid were condensed under the azeotropic distillation of water by the Dean-Stark trap.[116] Later, this method became a classical procedure for

synthesizing symmetrical squaraine dyes. Now, instead of benzene, toluene is used due to health safety concerns.

The reaction mechanism proposed by Sprenger and Ziegenbein under these conditions is shown in Scheme 1.7.[117] Firstly, the activated form of monobutyl squarate is formed upon water removal. Nucleophile attacks vinylogous ester in 4-position, and butanol leaves the molecule. This results in the formation of semi-squaraine acid, containing formal ketone and vinylogous carboxylic acid parts. The second nucleophile attacks the formal ketone due to the higher reactivity after the elimination of water from the compound, symmetrical squaraine dye forms.

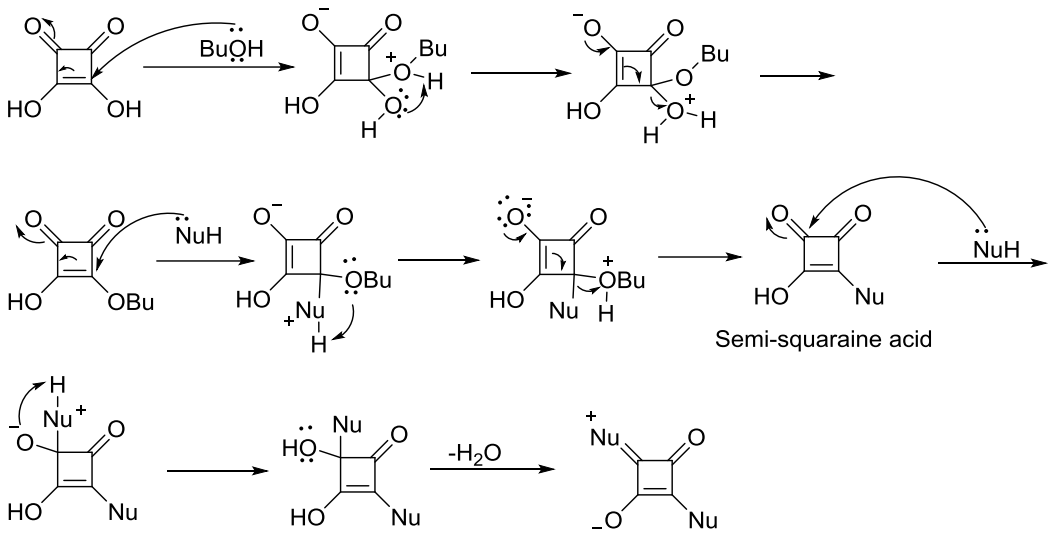

Scheme 1. 7. Symmetrical squaraine formation mechanism

As explained above, symmetrical squaraines can simply be obtained by condensing two equivalents of the identical nucleophile with squaric acid. In case of unsymmetrical dye, more steps are needed. A more target structure-oriented approach has been developed to get the desired compound. Firstly, squaric acid is converted into more activated forms, either squarate (ethyl or butyl ester) or acid chloride.[118] The critical step for the unsymmetrical squaraine synthesis is the formation of semi-squaraine.[96] In this step, one equivalent nucleophile is condensed with activated squaraine, similar to the symmetrical squaraine synthesis. As a result,

semi-squaraine ester or semi-squaraine chloride is obtained depending on the form of activated squaraine. The second nucleophile can not be directly condensed with these semi-squaraines. Before condensation, they have to be hydrolyzed in the presence of acid or base. After converting them into semi-squaraine acid, second nucleophile can be added to the structure by water removal, and asymmetric squaraine dye is formed.

Apart from these methods, several other procedures include the squaraine and semisquaraine synthesis.[119,120] In this context, the most commonly used methods are mentioned (Scheme 1.8).

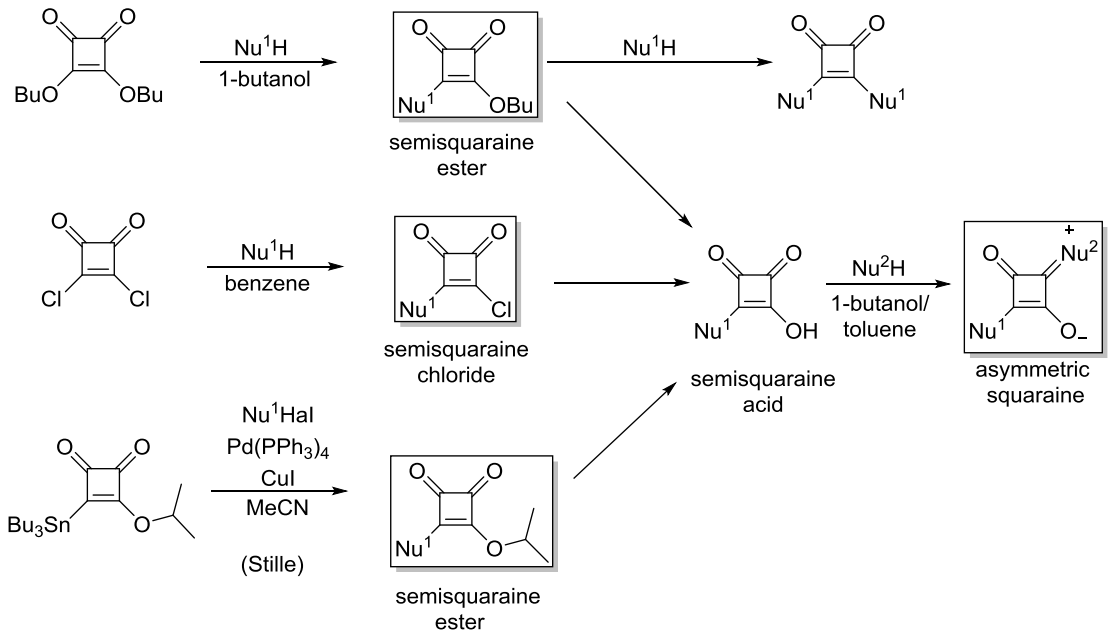

Scheme 1. 8. Synthesis methods of asymmetric squaraines

1.2.4.1.1 Supramolecular Assembly of Squaraine Aggregates

Similar to other organic dyes, squaraines are also able to form supramolecular assemblies. Van der Waals forces, hydrogen bonding, electrostatic forces, hydrophilic and hydrophobic interactions, π – π stacking are the non-covalent interactions that provide the formation of multiple ordered subunits, self-assembly.[121,122] In this point of view, because of the strong π–π stacking interactions

due to their rigid and planar zwitterionic structures, squaraine dyes tend to form aggregates. Squaraine aggregates have unique and useful properties that differ from those of monomers.[115,123–126] The absorption band is blue or red-shifted depending on the aggregation type compared to the monomeric form. In J-aggregates, the absorption band shifts to the longer wavelength (bathochromic shift, red-shift) with increased sharpness, providing a higher absorption coefficient. In contrast to J aggregates, H-aggregates show shorter wavelength shifts (hypsochromic shift, blue-shift). When the aggregation between dye molecules takes place in parallel with a plane to plane stacking, dye molecules form H-aggregate while a head-to-tail stacking observed molecular assemblies are in the form of J-aggregates (Figure 1.21).[127–135]

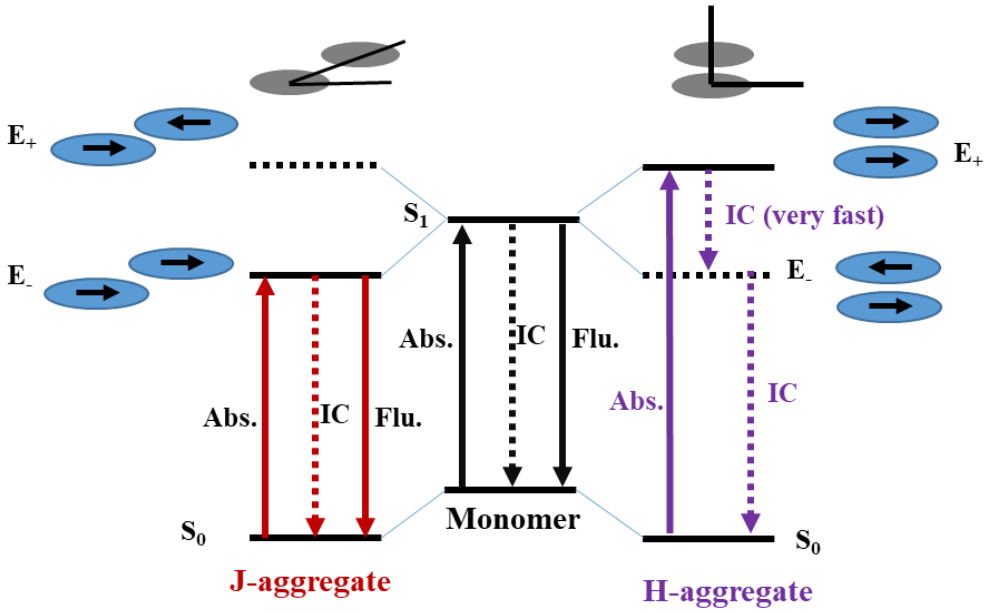

Figure 1. 21. Formation mechanism of J and H-aggregate[131]

According to Kasha's exciton model, the optical properties of the H- and J-aggregates differ from each other.[135] The coupling between the transition dipole moments causes to coincide with the long molecular axis. The coupling between the transition dipole moments of the adjacent molecules that coincide with the long

molecular axis causes the formation of excited states of the monomers. As a result, each degenerate excited state pair of monomers comes together to form excitonic states in the dimer structure. The excitonic states split into two energy levels. On one level, transition moments of the two molecules are parallel, and on another level, transition moments are antiparallel (Figure 1.21).

In most cases, the H-aggregates are nonfluorescent since the lower exciton state has antiparallel transition dipole moments, and the transition from a ground state to that state is forbidden. The point to be noted here is that although the higher exciton energy having parallel transition dipole moments is occupied by the direct absorption process, rapid internal conversion occurs, and electrons populate the lower exciton state. On the other hand, J aggregates are frequently formed fluorescent self-assemblies.[131] Both H-and J aggregates of squaraine dyes have been frequently studied in recent years, and it is encountered in both symmetric and asymmetric dyes.[128,133,134]

As mentioned in previous chapters, chirality is one of the guiding factors directing the self-assembly mechanism. Although there are numerous studies investigating the optical properties of squaraine dyes, research based on the chiral group-containing derivatives is just emerging.

In 2006, Rabe and Hecht et al. synthesized a chiral squaraine dye by using modified *L*-proline as a chiral moiety with a two-step, one-pot reaction procedure and investigated the aggregation behavior of squaraine dye **SQC-1** (Scheme 1.9).[136] It was shown that the emergence of J-aggregate in acetonitrile solution with increasing water portion. Aggregation of the **SQC-1** was proven by the red-shifted absorption band in the UV-Vis spectrum, and the strong negative Cotton effect at the red-shifted absorption band position in the corresponding circular dichroism (CD) spectra.

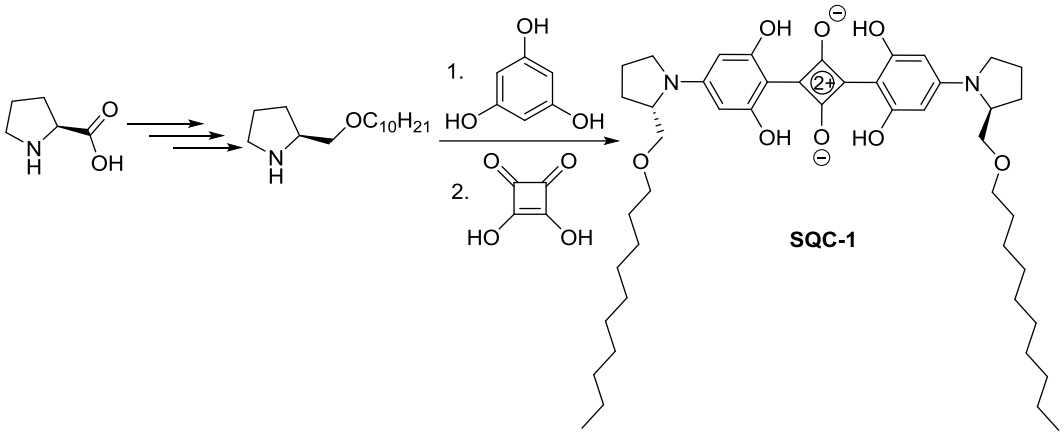

Scheme 1. 9. Synthesis of chiral squaraine **SQC-1**

Later on, **SQC-1** was utilized in organic photodiodes to take advantage of aggregation behavior in solution and thin films. This study uncovered that homochiral proline groups were acting as a structure-directing unit, and with these groups, molecular chirality was transferred to a supramolecular level, which is necessary for thin-film device application.[137]

1.2.4.2 Diaminoterephthalates (DAT)

Diaminoterephthalates (DAT) can be defined as stable chromophores with a relatively simple structure. They have strong fluorescence with high quantum yields and are resistant to photobleaching.[138–140] The synthesis of the dialkyl 2,5-diaminoterephthalate was first carried out and published by von Baeyer in 1886.[141] Although the distinctive properties have been known for almost 150 years, the studies related to DAT are limited compared to other chromophores in literature.

For the synthesis of DATs, dialkyl succinates are generally used as starting materials, and in the presence of a base, Claisen condensation product, oxo esters, are observed. The reaction of oxo esters with ammonia or primary amines (aliphatic or aromatic)[142] yields bis enamines which are more stable than the diimine tautomer due to the H-bonding. These compounds generally are light yellow. Target DATs are obtained in

deep orange to red with the oxidation step. Oxidation can be carried out either in the presence of bromine, iodine, or simply atmospheric oxygen.[143] The proposed mechanism for the formation of DATs was shown in Scheme 1.10.

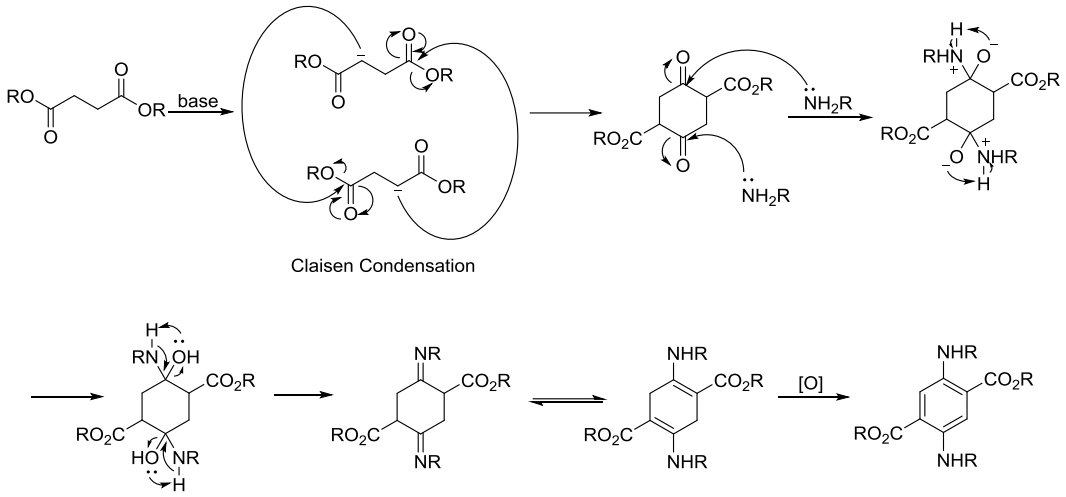

Scheme 1. 10. Proposed reaction mechanism for the formation of DATs

As seen from the structure, DAT chromophores can be orthogonally functionalized, which provides the adjustment of the structural properties of the compounds. Because of that, DATs have potential applications in various areas. In literature, there are examples that DATs are used as fluorescent scaffolds, hydrogen peroxide sensors, turn-on probes for thiols, alkynyl probes for click reactions, and so on.[144–148] Moreover, the studies investigating their properties in solid-state, metal complexes, and silica hybrid materials can be found in the literature.[143]

Besides, few examples in the literature cover the synthesis of a polymer having DAT in the backbone. In 1975 Moore et al. synthesized polyamine ester using diethyl 2,5-bis(benzylamino-3,6-dihydroterephthalate) and benzylic diamines, and the polymer was oxidized to get the final product (Scheme 1.11).[149]

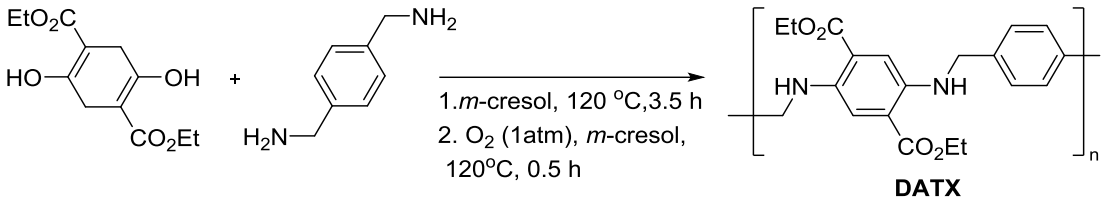

Scheme 1. 11. Synthesis of **DATX** polymer

In 2017 Yokoyama et al. prepared a ladder-type polymer using benzoxazine derivative, which could be thought of as the activated form of DAT as an anhydride. To overcome the solubility problem, long alkyl chains (n-octyl) were introduced to the structure as substituents R^2 (Scheme 1.12).[150]

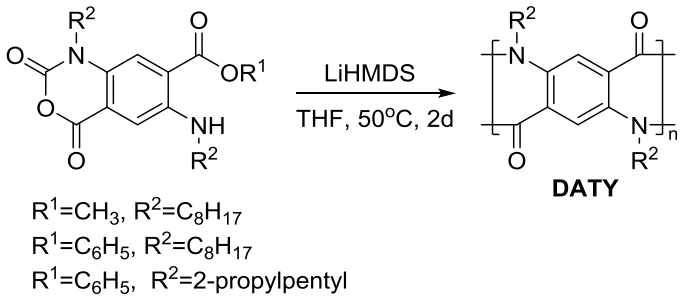

Scheme 1.12. Preparation of ladder-type polymer **DATY**

The reaction between *N*-methylanthranilic acid methyl ester and N-methylisatoic anhydride in the presence of a strong base (lithium hexamethyldisilazide (LiHMDS) was studied as a model reaction for ladder polymerization. The proposed reaction mechanism was shown in Scheme 1.13.

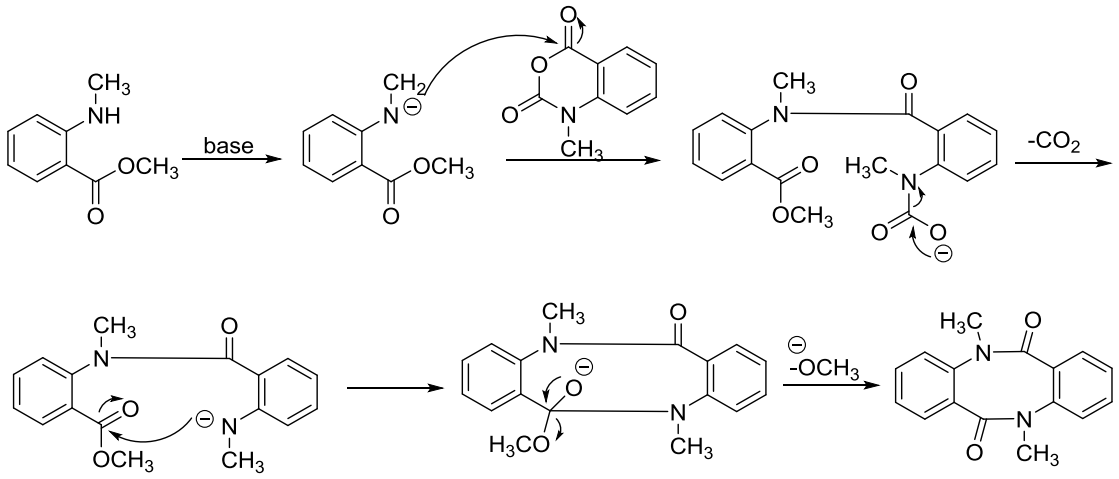

Scheme 1. 13. Mechanism of model reaction suggested to ladder polymerization

In 2019, Shimizu et al. synthesized Poly(terephthalate)s having blue emission in the solid-state. In this study, to achieve blue emission, amino groups in DAT were replaced by less electron-donating groups, alkoxy groups. As a result of polymerization reaction with itself or terephthaloyl chloride, a blue emissive polymer in solid-state was obtained.[151] The corresponding reaction was shown in Scheme 1.14

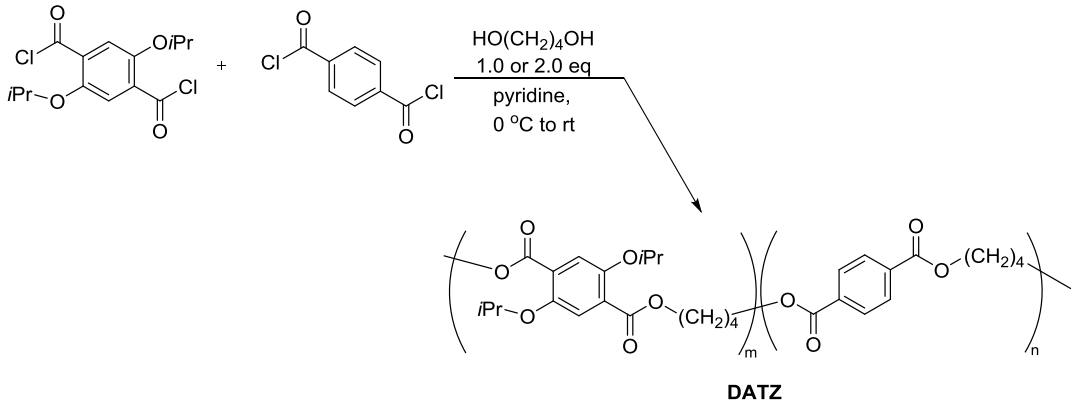

Scheme 1. 14. (Poly)terephthalates having blue emission in the solid-state

CHAPTER 2

AIM OF THE STUDY

Helicity is one of the most common motifs encountered in nature, as stated in the introduction part of this thesis. Grasping it from a chemistry point of view would allow one to develop such sophisticated motifs for a given purpose. According to the literature survey summarized earlier, helicity is generally induced in polymers through side chains. These polymers mostly have a dynamic helical conformation, and the main chain may not orient itself in the desired conformational configuration. The use of a chiral backbone for obtaining helical polymers is mainly ubiquitous in nature, while such synthetic polymers are rare.

Unlike the lack of studies using a chiral backbone for synthetic helical polymers, we have recently synthesized helical polymers using chiral monomers in the backbone. We proposed that the main chain take the helical conformational configuration, which could be controlled by intramolecular hydrogen bonding as well as the chiral backbone units. Tartaric acid-derived monomers were found to be promising candidates for chiral backbone forming monomers. As inferred from computational studies, tartaric acid should be protected as acetonide to force rigidity to the backbone. The protected tartaric acid-derived amines were polymerized with p-phenylenediisocyanate to get helical polyureas.[152] Scanning electron microscopy (SEM) was used to visualize the helix formation in solid state (Fig. 2.1). We could not facilitate CD spectroscopy for this study due to the lack of solubility. Further elaborations were done with computational methods.

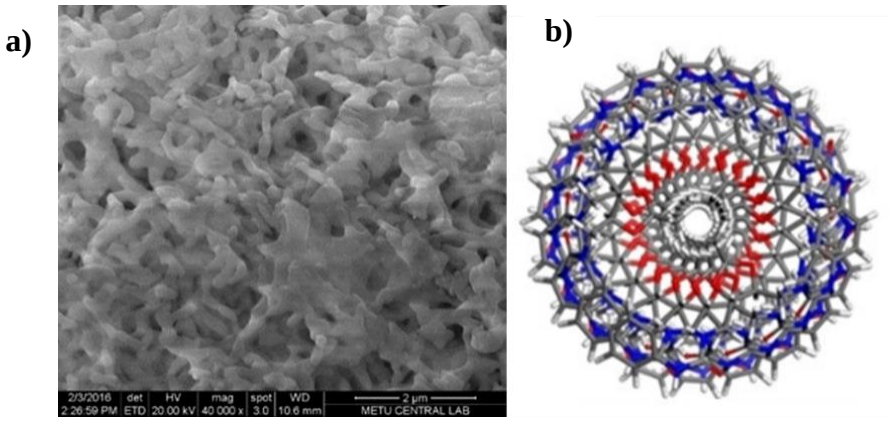

Figure 2.1 **a)** SEM image and **b)** 3D representation of helix formation of tartaric acid derived helical polyurea[152]

With the lessons learned from previous studies, it was decided to follow a new strategy. The new strategy should include synthesis of soluble and easy-to-characterize polymers. Toward this goal, tartaric acid derived monomers will be used in the backbone for inducing chirality to the polymer. Squaraine and diaminoteraphthalate dyes will be employed for their absorption spectrum in the visible region to characterize polymers with corresponding optical spectroscopic techniques. Overall, the synthesis of polymers derived from tartaric acid-dye monomers will be executed as depicted in Figure 2.2. Their photophysical features will be investigated. The information about the helicity of the such compounds will be extracted using circular dichroism spectroscopy.

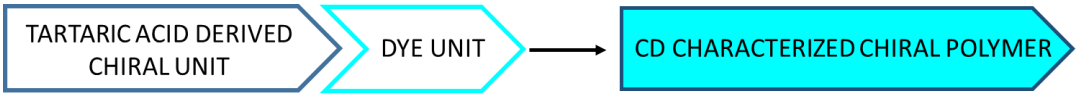

Figure 2. 2. Synthetic route of designed polymers

CHAPTER 3

RESULTS AND DISCUSSION

3.1 Polymer Design

Four polymers were designed to meet our expectations mentioned in the aim of the study part. Tartaric acid was chosen to be a backbone of a chiral polymer since it brought about the formation of a helix in one sense in the previous study performed in our laboratory.[152] In this case, both enantiomeric forms of tartaric acid were introduced to the backbone of the polymers separately. As a chromophore unit, squaraine was utilized in three of these polymers. The remaining two polymers were designed by inserting diamino terephthalate moiety as a chromophore. The structures of the corresponding polymers are shown in Figure 3.1.

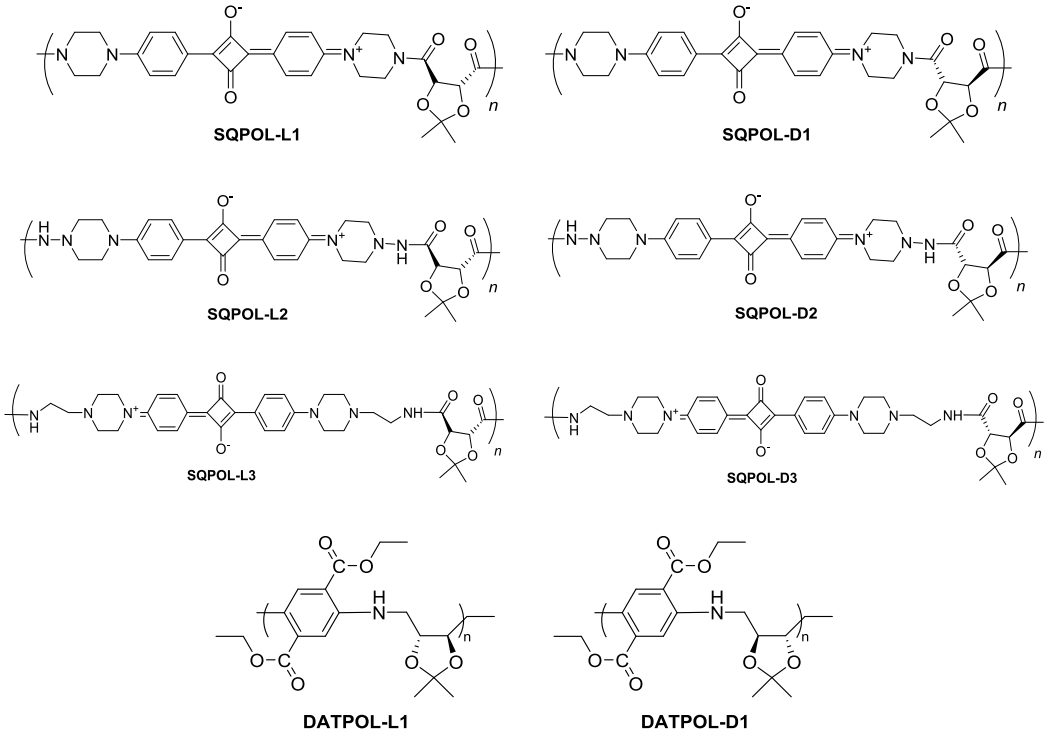

Figure 3.1. The structures of designed polymers

The synthesis design of the squaraine-based helical polymers is based on three sub-units: aryl diamine as a linker and a part of the chromophore to obtain squaraine moiety, squaric acid as the main component of squaraine dye, modified tartaric acid as a chiral and bifunctional monomeric unit for condensation polymerization. In this context, two methods have been proposed. The synthesis of **SQPOL-L1** was shown below as a representation of the reaction pathways. The same synthesis routes were planned for other squaraine containing polymers (**SQPOL-L2 (D2)** and **SQPOL-L3 (D3))** (Scheme 3.1).

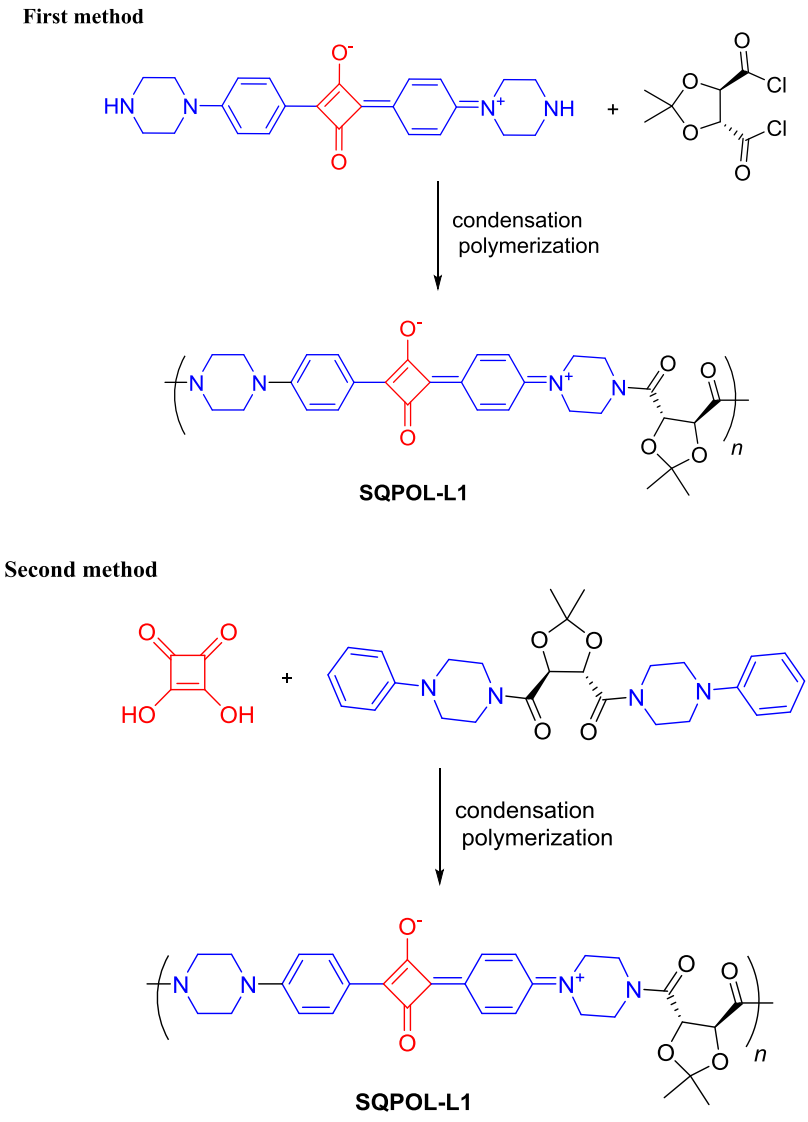

Scheme 3.1. Proposed synthesis methods for squaraine based polymers.

Similarly, the synthetic pathway of the diamino terephthalate polymer is rooted in modified tartaric acid as a chiral unit and diethyl succinyl succinate as a starting material of the chromophore (Scheme 3.2).

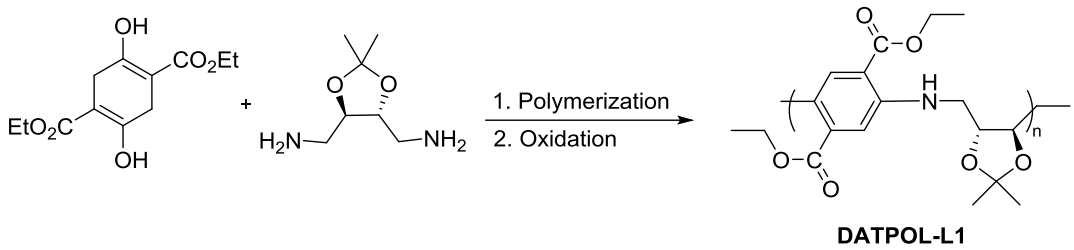

Scheme 3.2. Proposed synthesis method for diamino terephthalate based polymers.

The dye used in the synthesis should have some essential properties:

- ✓ It must be planar, so the conformation of the polymer is only affected by the chiral unit
- ✓ It can be modified for polymerization
- ✓ Tendency to form aggregate to assist the formation of chiral assemblies

Among the limited options, squaraine dyes would meet our primary expectations. Besides, as explained in previous chapters, squaraines have further advantages as a chromophore.[153] Similarly, 2,5-diaminoterephtalates meet the above-mentioned criteria. Before starting the synthesis of target polymers, it was decided to be proficient with the squaraines by examining fundamental properties experimentally.

3.2 Squaraines

3.2.1 Effect of the nucleophile and reaction conditions on squaraine synthesis

In general, the synthesis of symmetric squaraine dyes takes place between two equivalents of nucleophiles and one equivalent of squaric acid. It is worth noting

that, in the case of using arylamines as nucleophiles, the structure of the product changes depending on the class of arylamine (1º, 2º, or 3º) and reaction conditions.[154]

Within the framework of this information, for the efficient synthesis of 1,2-squaramide isomer, conversion of squaric acid to the ester is essential. The reaction of squarate diester with either primary or secondary amine yields 1,2 disubstituted squaramide under basic and mild conditions.[155]

With this information, first, squaric acid was converted to ethyl ester with azeotropic water removal. The corresponding ester was treated with aniline in the presence of triethylamine (TEA) and EtOH, the preferred solvent for this reaction, at room temperature. (Scheme 3.3) **S-2** was obtained as a white solid, and its absorption band was around 325 nm in DCM ($1.3x10^{-4}$ M), as declared in the literature (Figure 3.2).[156–158]

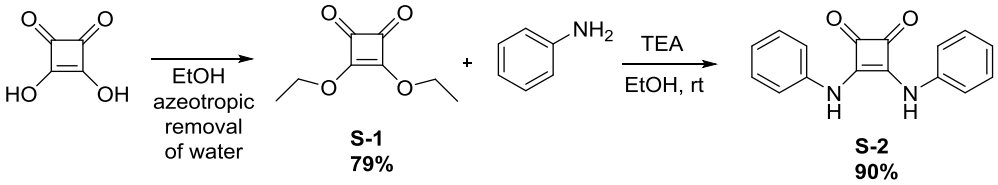

Scheme 3.3. Synthesis of **S-2**

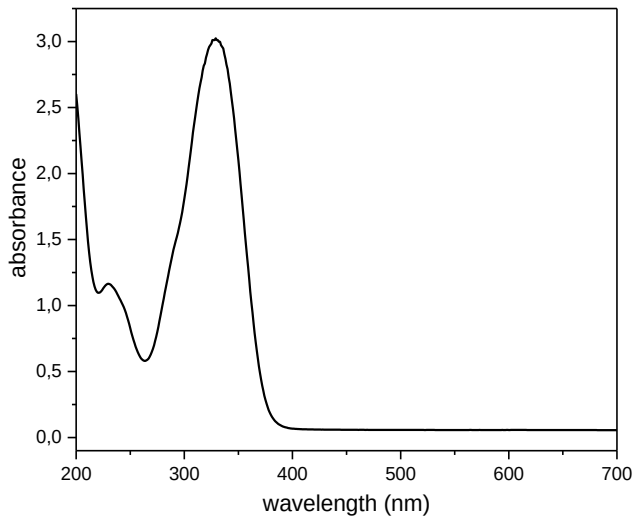

Figure 3.2. UV-Vis spectrum of **S-2** in DCM

The synthesis of 1,3-disubstituted symmetric squaraine with arylamine as a nucleophile has two possible products when the reaction mixture is heated and water is removed azeotropically (Figure 3.3).[159]

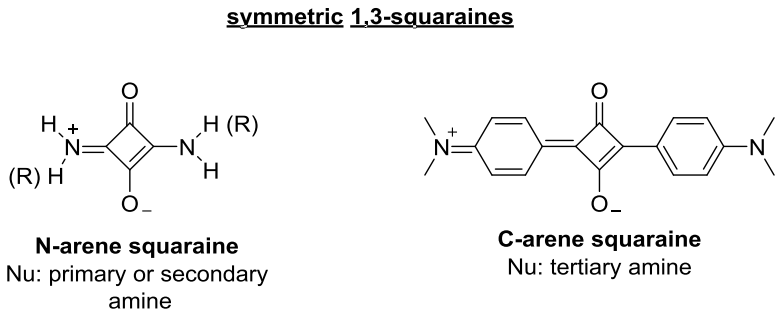

Figure 3.3. N-arene and C-arene squaraines

At this point, we synthesized the simplest member of the 1,3 *N*-arene squaraine family using aniline. As stated in the literature, primary amine reacted with amine functionality in the form of 1,3 squaraine (Scheme 3.4).

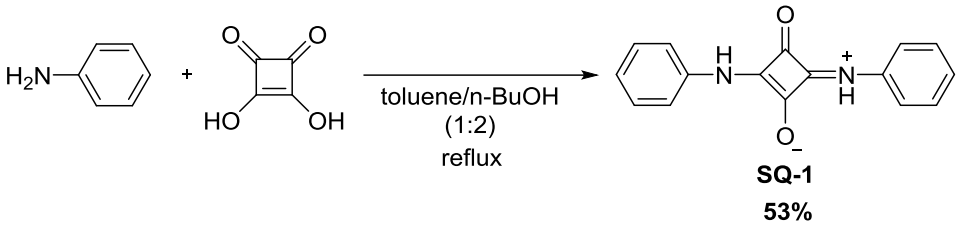

Scheme 3.4. Synthesis of **SQ-1**

The product obtained after removing water azeotropically was in the form of yellow crystals. UV-Vis measurement of **SQ-1** in DCM ($M=4.8x10^{-4}$) showed that the absorption peak appeared at around 400 nm, which is consistent with the literature (Figure 3.4).[160,161]

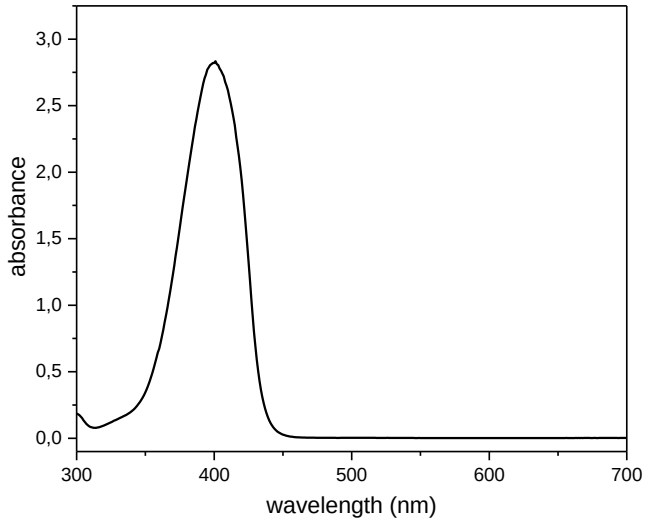

Figure 3.4. UV-Vis spectrum of **SQ-1** in DCM

The most common synthesis method was applied to get a typical near-IR absorbing symmetrical squaraine dye as the following experiment. The condensation of tertiary aromatic amines (*N*, *N*-dimethyl aniline) with squaric acid in the n-BuOH/toluene solvent mixture method was utilized to obtain the compound **SQ-2** (Scheme 3.5).[155]

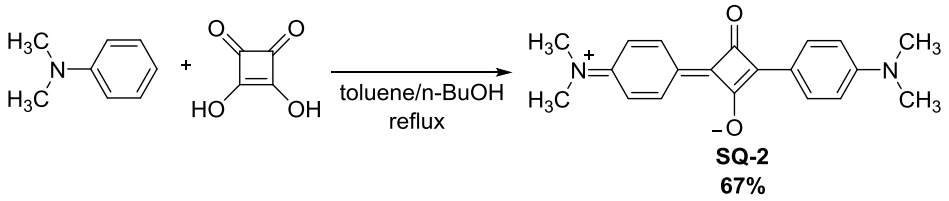

Scheme 3.5. Synthesis of **SQ-2**

Similar to the previous procedures, water was removed azeotropically. After overnight reflux, **SQ-2** was separated from the reaction medium by crystallization in diethyl ether and obtained as blue solids. Due to the low solubility, the compound could not be characterized by NMR spectroscopy. Instead, UV-Vis and fluorescence spectroscopy were used, showing that **SQ-2** has characteristic excitation and emission peaks of squaraine dyes around 630 and 660 nm in DCM (1.2×10^{-4} M for UV-Vis, 1.2×10^{-5} M for fluorescence) respectively (Figure 3.5). We concluded that C-arene type squaraine was formed under these conditions.

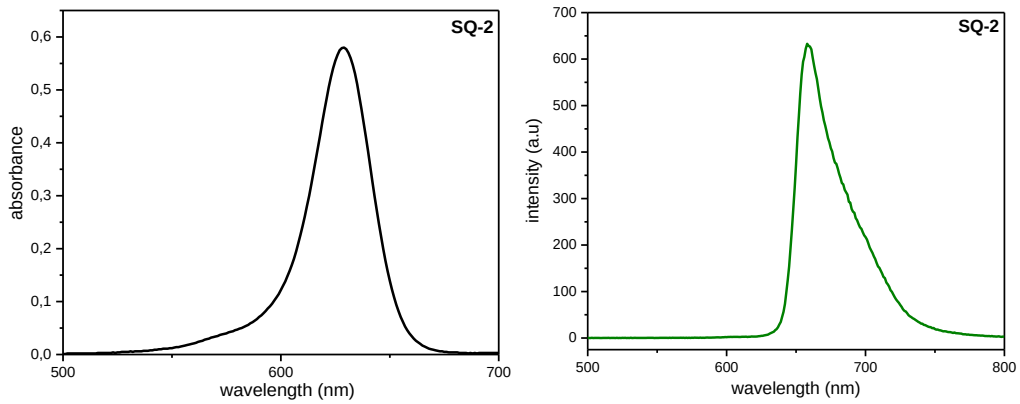

Figure 3.5. UV-Vis and Fluorescence Spectra of **SQ-2** in DCM

This result led us to synthesize a soluble squaraine dye to gain further experience with the characterization and properties of squaraine. For this purpose, **SQ-3** was synthesized by the synthetic route given in Scheme 3.6. To increase the electron density on the aromatic ring and make the structure more rigid, 5-(dibutylamino)benzene-1,3-diol was synthesized. Squaric acid was directly added to the reaction mixture without any purification of the intermediate product. Water was removed azeotropically during the progress, and **SQ-3** was obtained as metallic green crystals (Scheme 3.6).

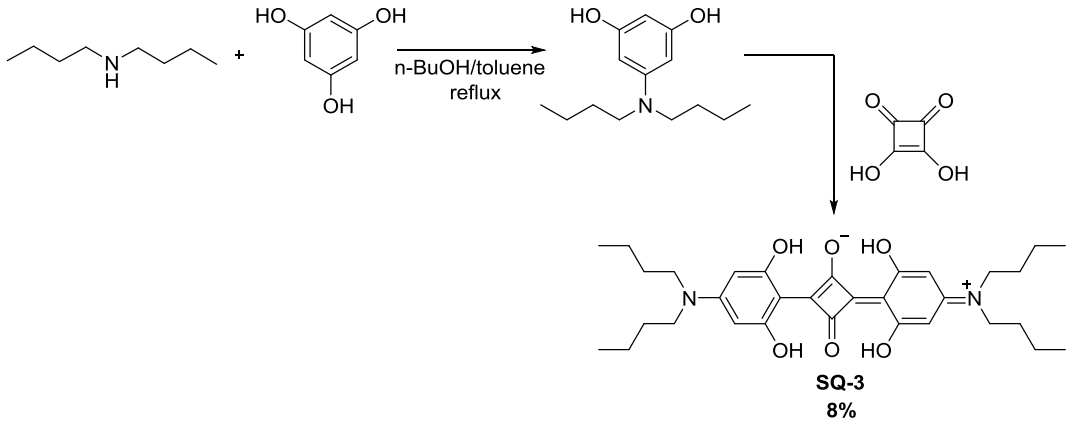

Scheme 3.6. Synthesis of **SQ-3**

Unlike dimethyl aniline-derived **SQ-2** dye, the solubility of **SQ-3** was sufficient enough for characterization with NMR spectroscopy (Figure 3.6). In the region

between 1-4 ppm peaks of butyl groups were detected. The peak at 5.8 ppm belonged to aromatic protons. It appeared at the high field due to the electron-donating groups on the rings. The peak observed at 11 ppm was the –OH protons

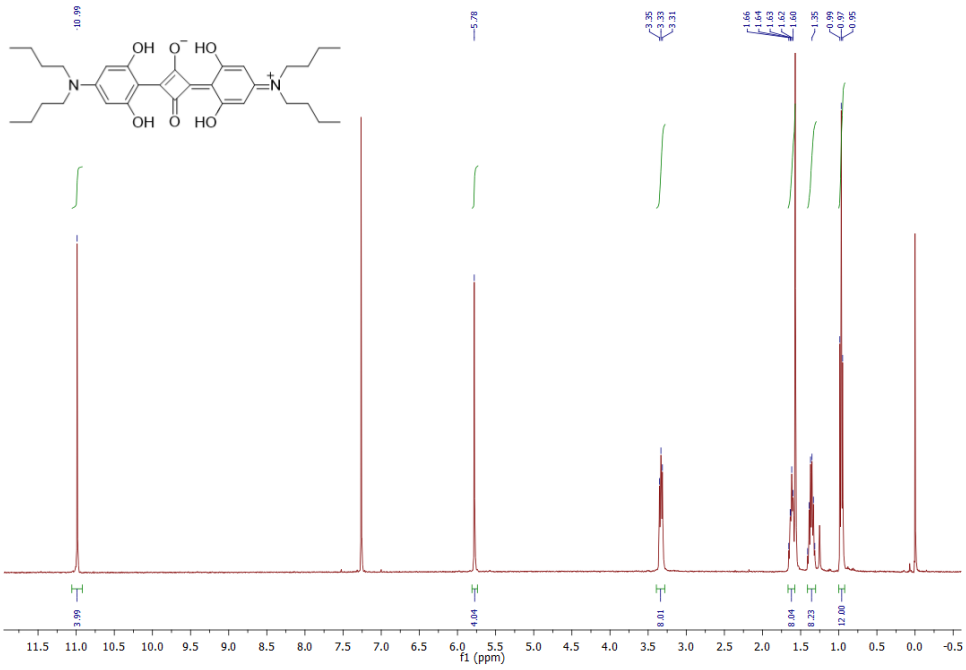

Figure 3.6. ^{1}H NMR Spectrum of **SQ-3**

As shown in Figure 3.7, **SQ-3** had an absorption of around 648 nm and an emission of approximately 675 nm in DCM ($3.28x10^{-5}$). When the results were compared with **SQ-2**, it was revealed that hydroxyl groups on the benzene ring caused the red-shift in both absorption and emission bands.

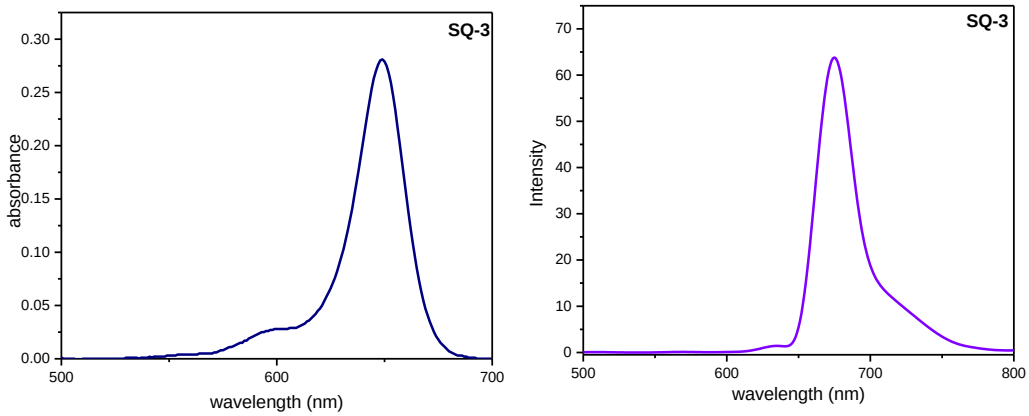

Figure 3.7. UV-Vis and Fluorescence Spectra of **SQ-3**

3.2.2 Studies on Squaraine Dye Monomer Proposed in the First Method

In this section, we focused on the synthesis of squaraine dye monomers, included in the first proposed method for obtaining **SQPOL**s. As an arylamine moiety, phenyl piperazine and its hydroxyl derivatives were utilized.

Firstly to check the effect of reaction conditions and the use of secondary amine, 1-phenyl piperazine was treated with squaric acid in the presence of n-BuOH/toluene mixture under reflux conditions with azeotropic water removal. After reaction completion, compound **SQ-4** was obtained as a white solid (Scheme 3.7). The IR results (-C=O peaks around 1600 and 1621 cm^{-1}) showed that using secondary amine as a nucleophile under these conditions resulted in the formation of 1,3 *N*-arene squaraines (Figure 3.8).

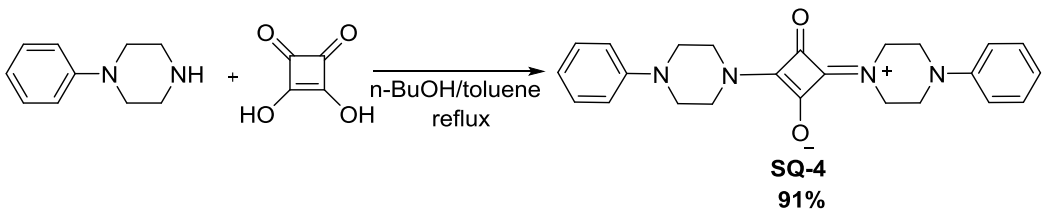

Scheme 3.7. Synthesis of **SQ-4**

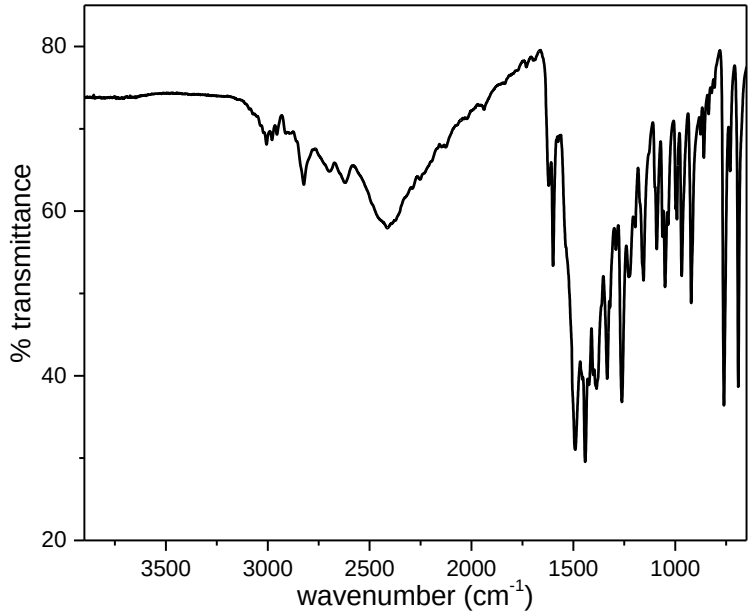

Figure 3.8. IR spectrum of **SQ-4**

It is worth noting that a couple of methods (based on Buchwald-Hartwig coupling) have been tried to synthesize 1-phenyl piperazine (Scheme 3.8).[162,163] Methyl piperazine was chosen as the starting material to optimize the reaction conditions. Only one of them yielded the target product **P-1** with a low yield (~15%) among the methods applied (Scheme 3.9).[164] This result led us to use commercially available phenyl piperazine.

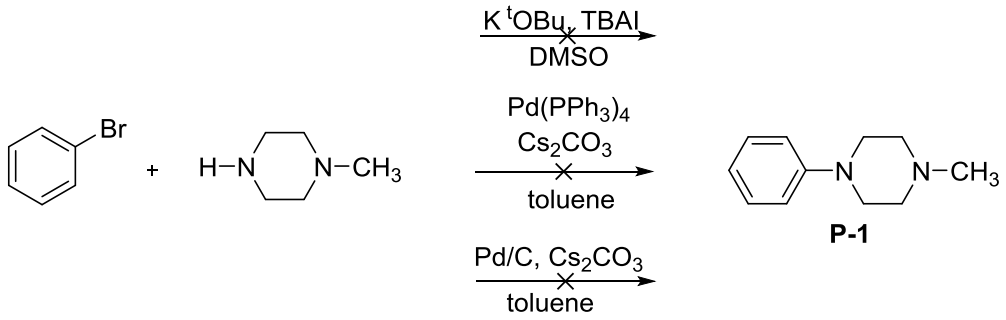

Scheme 3.8. Synthesis attempts of **P-1**

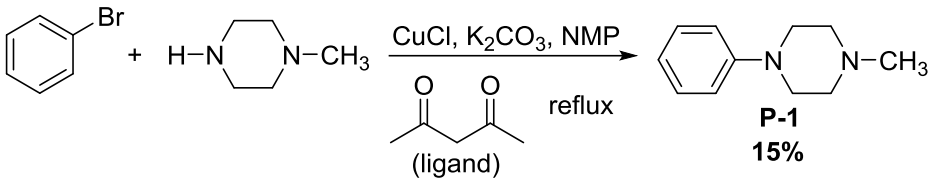

Scheme 3.9. Synthesis of **P-1**

As stated in the literature,[155] these results proved that to obtain 1,3 C-arene type squaraine dye, conversion of 1-phenylpiperazine to its tertiary form is essential. This reaction was necessary to observe if amide formation would occur during polymer synthesis. To accomplish acetylation of phenyl piperazine, acetic anhydride was treated with 1-phenyl piperazine. With **P-2** in hand, it was reacted with squaric acid in toluene buthanol solvent mixture under Dean-Stark to yield **SQ-5** (Scheme 3.10).

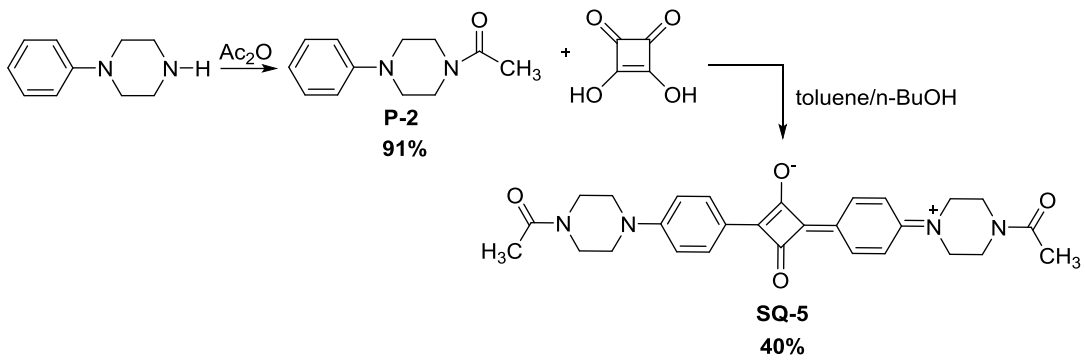

Scheme 3.10. Synthesis of **SQ-5**

UV-Vis and fluorescence spectra in Figure 3.9 proved the formation of conventional squaraine dye by the absorption around 625 nm and emission peak around 650 nm in DCM ($2.3x10^{-5}$M). The elemental composition of **SQ-5** was further confirmed with HRMS.

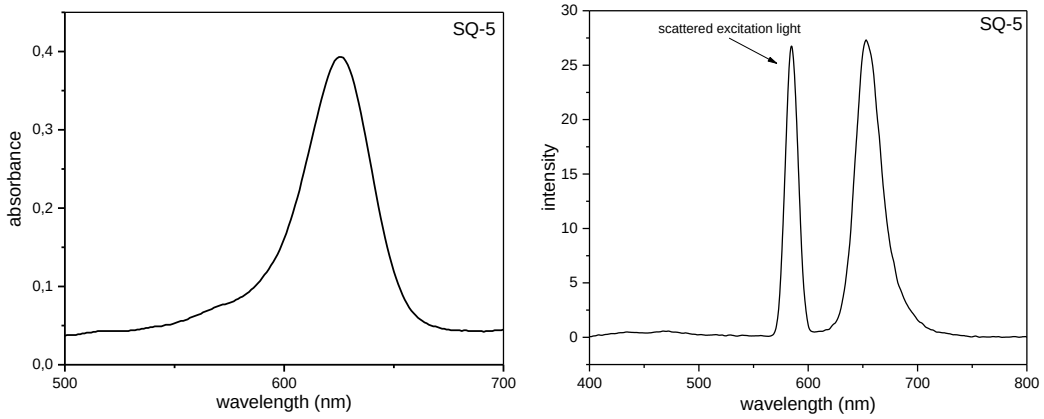

Figure 3.9. UV-Vis and Fluorescence Spectra of **SQ-5** in DCM

These results also clarified the details of the first method and polymer synthesis steps. Accordingly, the proposed synthetic pathway was shown in Scheme 3.11 to achieve compound **SQ-6,** one of the target squaraine dye monomers. To convert secondary amine in phenyl piperazine into a tertiary amine, it was protected with $(Boc)_2O$. Then, the compound **P-3** was treated with squaric acid and obtained as blue solids.

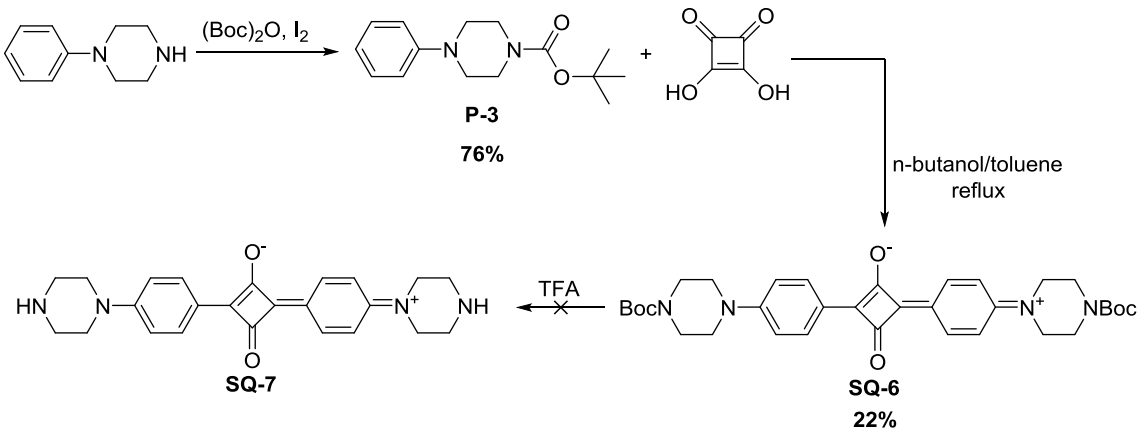

Scheme 3.11. Synthesis of **SQ-6**

Since the solubility of **SQ-6** was low, it was characterized by UV-V

is spectroscopy. The compound has a characteristic squaraine absorption peak of around 600 nm in DCM. (Figure 3.10) Furthermore, HRMS results were also consistent with the theoretical elemental composition.

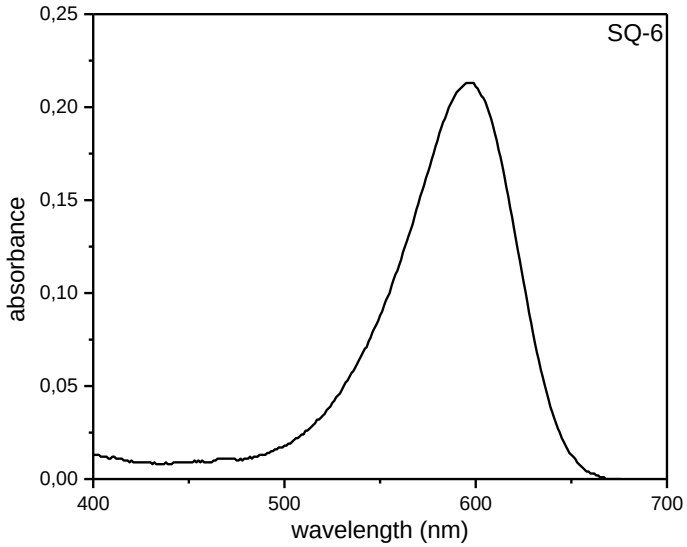

Figure 3.10. UV-Vis Spectrum of **SQ-6**

As a final step, deprotection was performed with trifluoroacetic acid (TFA) to prepare the functional groups in the compound **SQ-6** available for polymerization. The deprotection reaction results were unsatisfactory due to the zwitterionic character of squaraine dyes. After adding TFA, the compound's color turned from blue to red. This was the visual indication of the structural change of the squaraine dye core. The characterization attempts also showed the disintegration of the dye.

Apart from these, various squaraine dye syntheses have been studied, but the expected results from these dyes, whose chemical structures are shown below, could not be obtained (Figure 3.11). Except for the **SQ-A**, the tertiary amines utilized as a starting material of squaraine synthesis were prepared successfully, unlike corresponding squaraine dyes.

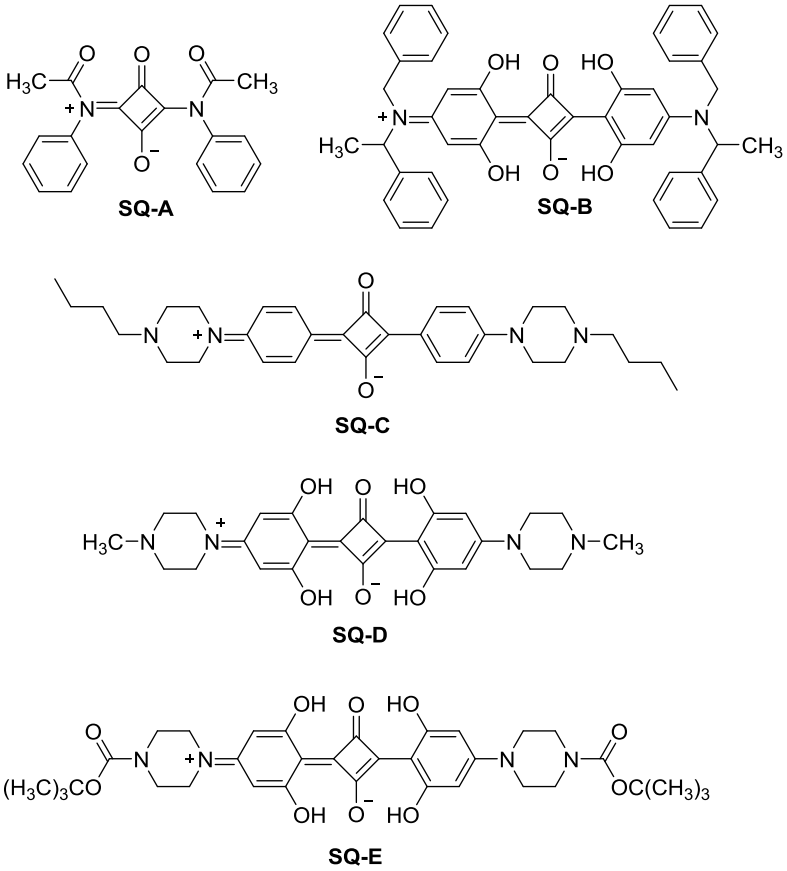

Figure 3.11. Squaraine dyes attempted yet failed to be synthesized

3.3 Chiral Squaraine Dyes

Further studies, including squaraine dyes, were carried out to prepare them by integrating the chiral unit. The synthesis of chiral squaraine dyes is the critical part of this study since;

- It was expected to have properties similar to chiral squaraine polymers
- It was thought that handling and characterization would be easier than the corresponding polymers.

Although numerous studies have investigated the optical properties of squaraine dyes, research based on the chiral group-containing derivatives is just emerging.[136,165] The studies on chiroptical applications of chiral squaraine dyes are

in high demand to understand such red-emitting dyes.[137,166,167] In this part of our study, we aimed to synthesize and investigate the optical properties of chiral squaraine dyes. Additionally, the effect of chiral units on aggregation was sought.

To experience the chiral squaraine dyes, we started with the synthesis of proline-bearing squaraine. As stated in the introduction, the most common and recent chiral squaraine dyes were synthesized using proline as a chiral moiety.[137,165] Inspired by these studies, we designed a pathway to synthesize **L-CSPID** shown in Scheme 3.12.

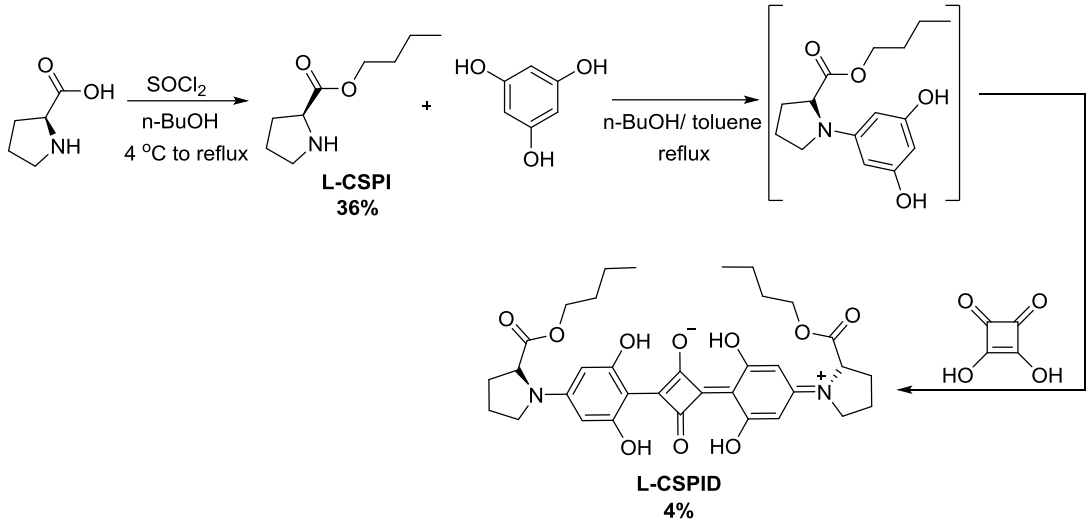

Scheme 3.12. Synthesis of chiral squaraine **L-CSPID**

Compound **L-CSPID** was obtained as a blue solid as in the case of other C-arene squaraines. NMR spectroscopy could not be used to characterize the compound due to the low solubility. For this reason, UV-Vis spectroscopy was utilized, and the obtained result, absorption at 600 nm in DCM, was consistent with the literature (Figure 3.12)

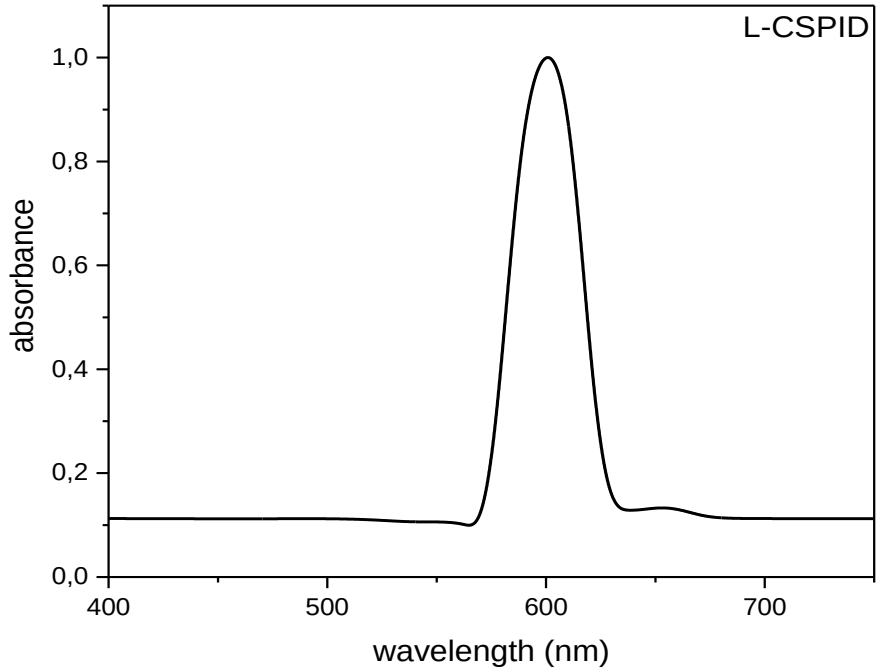

Figure 3.12. UV-Vis Spectrum of **L-CSPID** in DCM

The solubility problem was solved in literature by introducing the long alkyl chains to the structure. Moreover, it has been stated that longer alkyl chains (-$C_{10}H_{21}$) contribute to one-sense directional aggregation, especially in mixed solvent systems (dissolved/not dissolved type). Although **L-CSPID** had a shorter alkyl chain, the aggregation potential was promising even in a non-mixed solvent, as shown in the CD spectrum. (Figure 3.13) The CD activity around 600 nm also showed that chirality could be induced through the squaraine dye. Soluble chiral group bearing squarine dyes showed no chiroptical activity in their fully solvated state.[165]

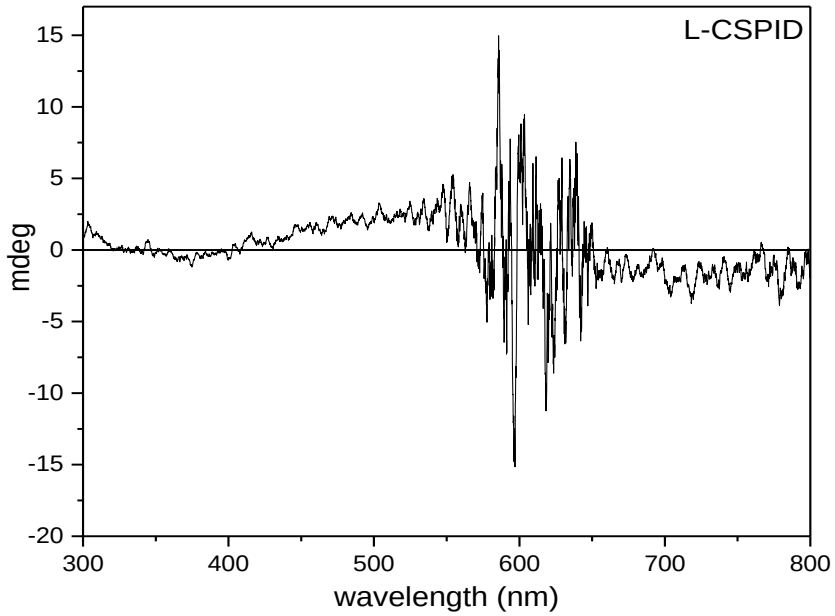

Figure 3.13. CD spectrum of **L-CSPID** in DCM

After getting promising results from this attempt, we turned our attention to the synthesis of the novel chiral squaraine dye. For this purpose, we designed squaraine dyes with enantiomerically pure alanine and phenylalanine derivatives. Furthermore, we also aimed to investigate the effect of chirality on aggregation behavior. The homochiral alanine and phenylalanine moiety were considered aggregation directing units for the squaraine assembly. The synthesis started with derivatization at the amino group on alanine and phenylalanine with phthalic anhydride. Phthalic anhydride was chosen for its planarity and limited conformational space. In aggregation studies, this was thought to be crucial for more ordered aggregation. With compound **LCSA-1** in hand, they were coupled with 1-phenyl piperazine to get compound **LCSA-2**.

In literature, coupling reactions are widely used to obtain amide functionality.[168,169] Before going into details of the synthetic pathway, it should be mentioned basic properties of coupling reactions. In coupling reactions, the first step is the activation of the carboxyl moiety. During the second step, the nucleophile (amino group) attacks the activated carboxylic acid (Scheme 3.13).

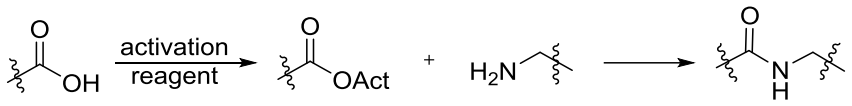

Scheme 3.13. General presentation of coupling reactions

There are various activation reagents in the literature since none of them can be used in every coupling reaction. The structures of the most common ones are shown in Figure 3.14.a.[169,170] In the case of enantiopure starting materials, additives such as HOBt, HOAt, and DMAP are utilized to enhance the reactivity, accelerate the reaction and suppress the racemization (Figure 3.14.b).[171–173]

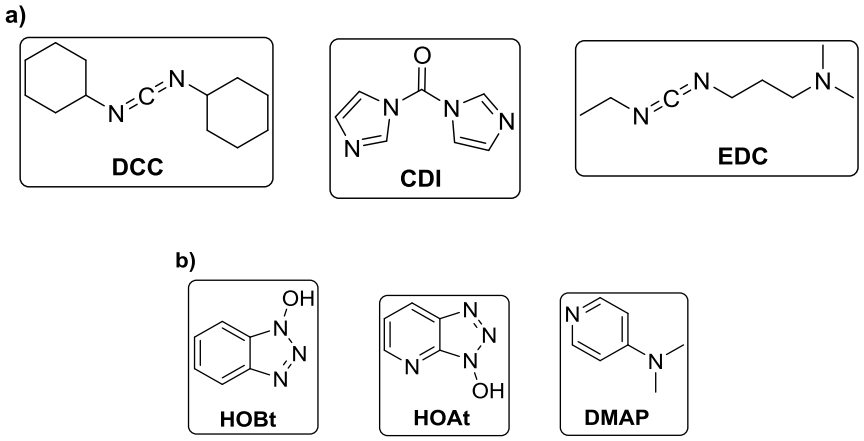

Figure 3.14. Structures of **a)** activation reagent and **b)** additives utilized in coupling reactions

Among the coupling conditions found in the literature, we decided to start with EDC/ HOBt pair due to its feasibility. As an amine moiety, we preferred 1-phenyl piperazine since piperazine units in the chair conformation, the substituents at 1 and 4 positions are equatorial, making the compound pseudo planar. Due to the straight nature of piperazine, this was not expected to affect the aggregation behavior of the dyes. Moreover, it is an advantageous candidate for squaraine condensation reaction. The piperazine unit activates the phenyl ring with its electron donor ability for further reactions. Amino acid bonded to phenyl piperazines **LCSA-2** were treated with squaric acid in a 50-50 toluene-butanol mixture under a Dean-Stark condenser. This reaction successfully yielded squaraine dyes as green-blue solids after

recrystallization from methanol. The synthesis protocol and the yields of the reactions were summarized in Scheme 3.14.

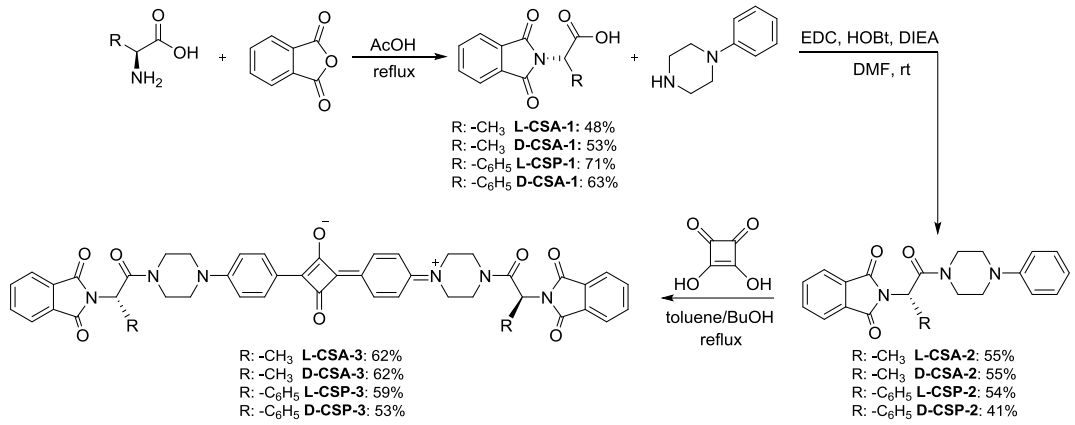

Scheme 3.14. Synthesis of the alanine and phenyl alanine derived squaraine dyes

^{1}H NMR of these compounds showed two chemically equivalent protons in the aromatic region for alanine derivatives **L-CSA-3**, **D-CSA-3, L-CSP-3,** and **D-CSP-3**. This result indicated that the phenyl group reacted with squaric acid from the para position of the phenyl piperazine. Moreover, the dyes were characterized with UV-Vis spectroscopy. UV-vis spectra of such squaraine dyes have a characteristic absorption peak at around 600 nm.[174] The UV-Vis spectra of **L-CSA-3** and **L-CSP-3** in chloroform showed absorption at about 610 nm, as shown in Figure 3.15. Both D and L forms of the dyes had identical UV-Vis spectra. This showed that the side chains did not affect the absorption behavior of these dyes.

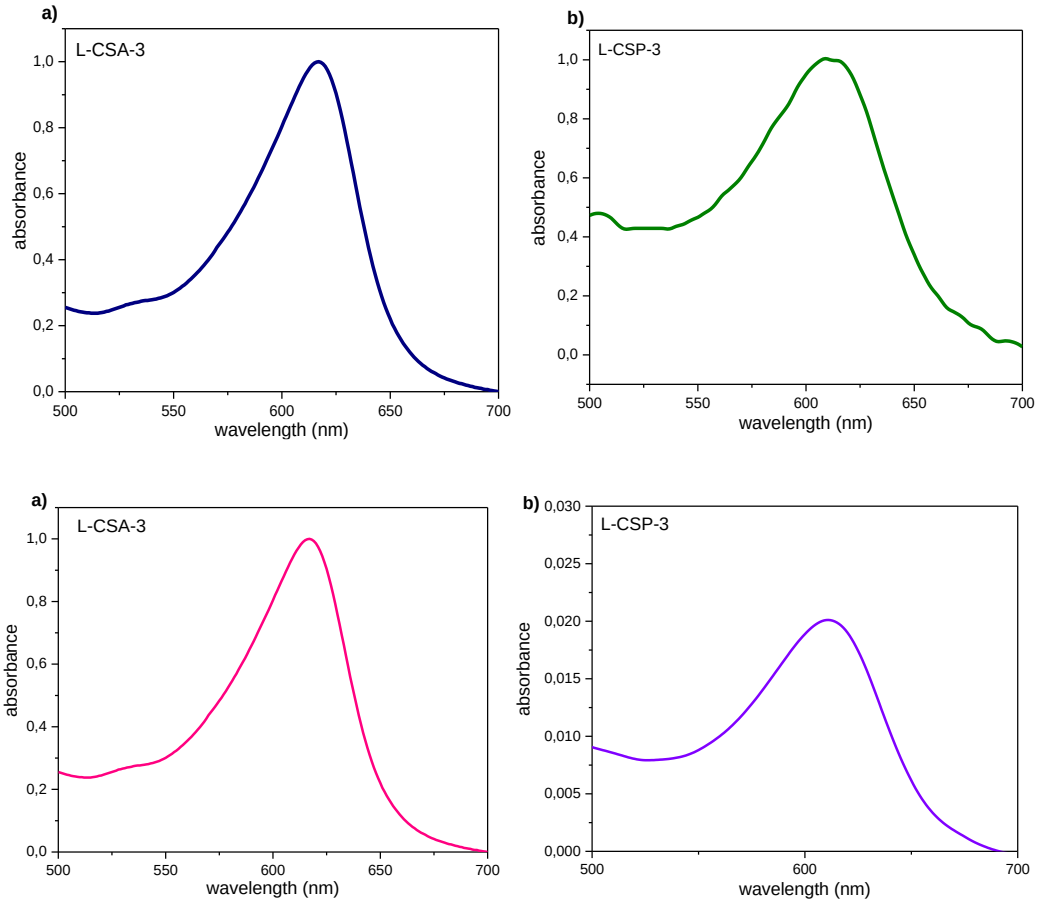

Figure 3. 15 Normalized UV-Vis spectrum of **a) L-CSA-3** ($5x10^{-5}$ M) and **b) L-CSP-3.** UV-Vis spectrum of **c) L-CSA-3 d) L-CSP-3.** The concentrations are $5x10^{-5}$ M in chloroform.

It is worth noting that the same concentrations of **L-CSA-3** and **L-CSP-3** in chloroform show that the **L-CSP-3** has significantly lower solubility as seen in unnormalized UV-Vis spectra, Even though phenyl alanine-derived squaraine dyes **L-CSP-3,** and **D-CSP-3** were characterized successfully, their solubilities were not sufficient enough to pursue further studies. The aggregation studies were performed for alanine-derived squaraine dyes.

UV-Vis spectra of alanine-derived squaraine dyes **L-CSA-3** and **L-CSP-3** were recorded in chloroform, THF, and acetonitrile (Figure 3.16). Although we attempted to measure UV-Vis spectra in hexanes, we could not observe any absorption peak in the UV-Vis spectrum, indicating that these dyes do not dissolve in hexanes. The

absorption value was lower in THF and acetonitrile than in chloroform for the same concentrations. This indicates that these squaraine dyes were not well solvated in THF and acetonitrile. In addition, the UV-Vis spectrum in chloroform was less broadened than the spectra in THF and acetonitrile. Furthermore, the UV-Vis spectra in chloroform show bathochromic shift compared to the spectra in THF and acetonitrile (ACN: 604 nm, THF:609 nm, chloroform: 617 nm).

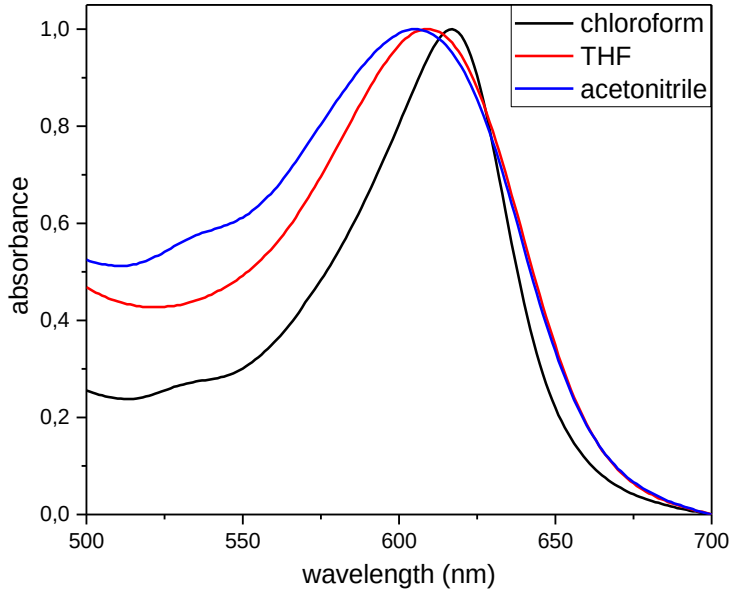

Figure 3. 16 Normalized UV-Vis spectra of **L-CSA-3** ($5x10^{-5}$ M) in chloroform, THF, and acetonitrile.

Fluorescence studies were performed on alanine-derived squaraine dyes **L-CSA-3, D-CSA-3, L-CSP-3** and **D-CSP-3.** The excitation and emission spectra of **L-CSA-3** and **L-CSP-3** showed Stokes shift with 13 nm and 18 nm, respectively, showing the rigid nature of these squaraine dyes (Figure 3.17).

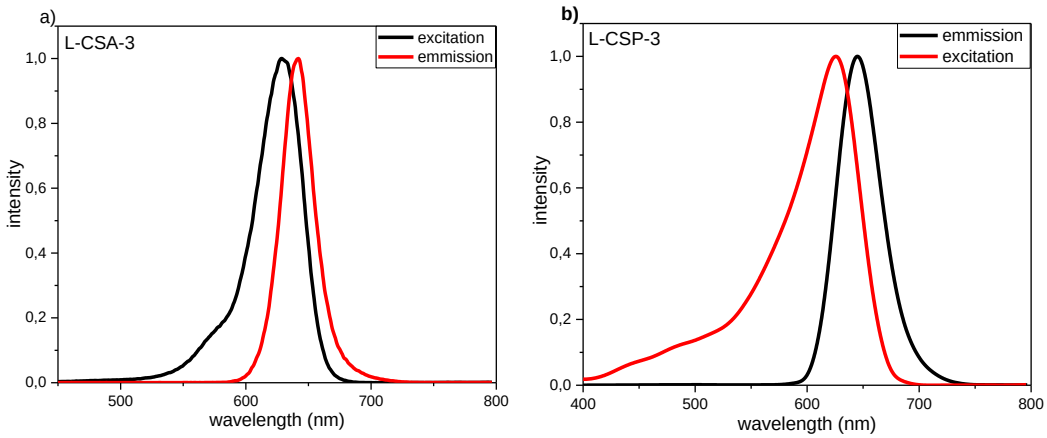

Figure 3.17. Normalized excitation-emission spectra of **a) L-CSA-3** and **b) L-CSP-3.** The concentrations are 1,24x10^{-5} M in chloroform.

When the excitation and emission spectra of L-CSA-3 were measured, the spectra in THF and acetonitrile differed from compounds in chloroform, as seen in Figure 3.18. In THF and acetonitrile, both excitation and emission bands red-shifted compared to the spectra in chloroform. Dielectric constants of THF and chloroform are close to each other and lower than acetonitrile. This suggests that acetonitrile and THF interact with the dye molecules and is further inferred from the stoke shifts that increased with increasing polarity (Chloroform 12 nm, THF 15 nm, and acetonitrile 19 nm).

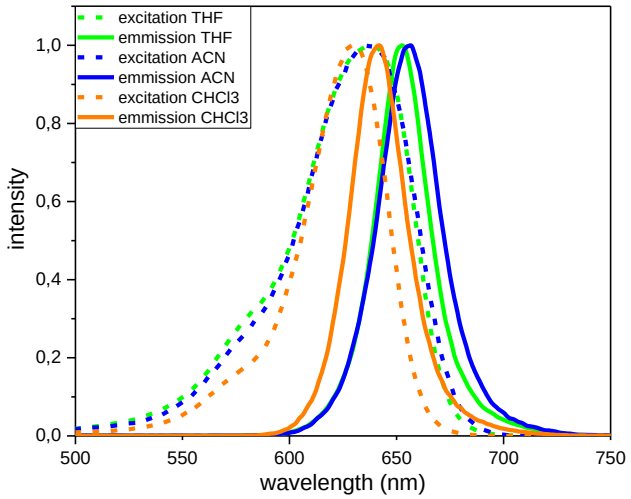

Figure 3.18. Normalized excitation-emission spectra of **L-CSA-3** dissolved in THF, ACN, and $CHCl_3$. Concentrations are 10^{-5} M.

Initial aggregation studies were performed in chloroform by increasing the amount of acetonitrile. Acetonitrile was a poor solvent for the dyes. Compound **L-CSA-3** and **D-CSA-3** were dissolved in chloroform to have a *ca.* 10^{-5} M solution. Then, UV-Vis spectra were recorded by increasing the acetonitrile content. Up to 33% acetonitrile content, there was a slight red shift (*ca.* 3 nm) (Figure 3.19.a). With the increasing content of acetonitrile, the absorption value decreased in UV-Vis spectra (Figure 3.19.b).

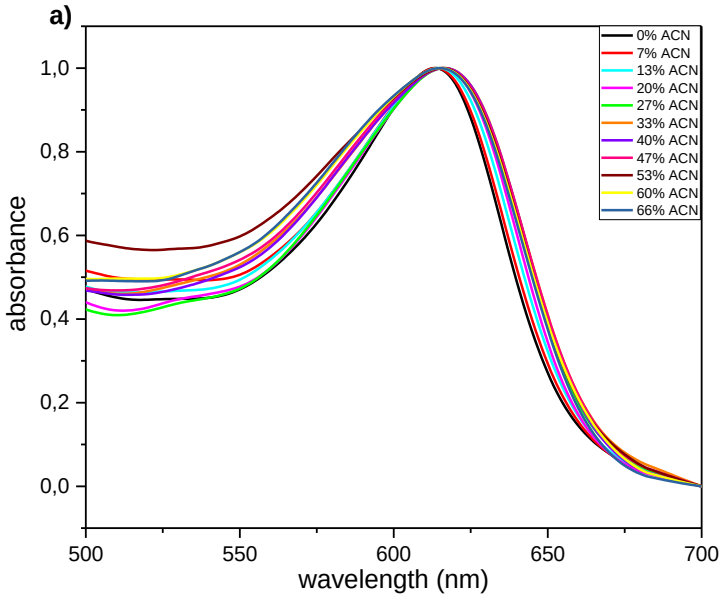

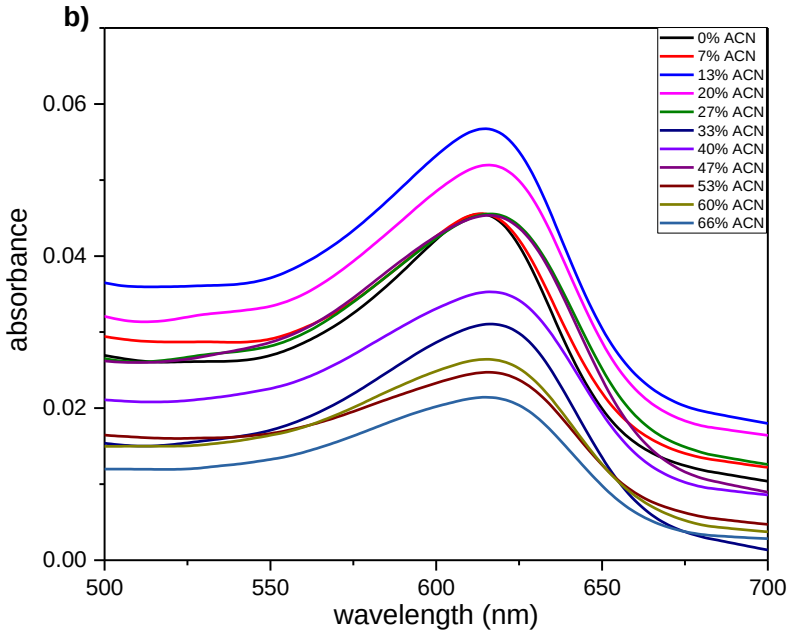

Figure 3. 19. **a)** Normalized UV/Vis spectra **b)** UV/Vis spectra of **L-CSA-3** dissolved in acetonitrile-chloroform solvent mixtures with varying ACN volume percentages as indicated in the graphs. The concentration was kept constant at $0.83x10^{-5}$ M.

Furthermore, it was observed that compounds were not stable in the solutions; the compounds decomposed right after measuring the UV-Vis spectra, which was obvious even with naked eyes (color changes from blue to colorless). Kinetic studies were carried out to determine whether the substance had a significant decomposition during the measurement period. **L-CSA-3** did not show decomposition during 300 sec in ACN and $CHCl_3$ separately.

CD studies in chloroform acetonitrile solvent mixture were also investigated. It was found that there was no CD activity in the region *ca*. 600 nm in any varied solvent mixture. This shows that the side chain chirality is not inducing a CD activity on the dye. However, we expected the chirality on side groups to direct the aggregation to get chiral aggregates. This, in turn, would lead to a CD activity. The lack of CD signal in any solvent mixture suggested that one should use two different solvents with one dissolves the compound, and the other does not entirely dissolve the dye.

Although the compounds **L-CSA-3** and **D-CSA-3** have low solubility in acetonitrile, they dissolve to some extent. The dyes do not dissolve in water. With this in mind, the dyes were dissolved in acetonitrile, and water was added sequentially to get aggregates. UV-Vis spectra of these were recorded. The measurement should be done immediately as the compound decolorized when waited for more than 5 minutes. As the water content increased, the absorption decreased. When the spectra normalized (Figure 3.20), it was observed that there was a 10 nm bathochromic shift as the water content increased to 33 %. This shift was more than the one observed in the chloroform/acetonitrile solvent system. This suggests that the aggregation formation is more induced in the acetonitrile/water mixture than in the chloroform/acetonitrile mixture.

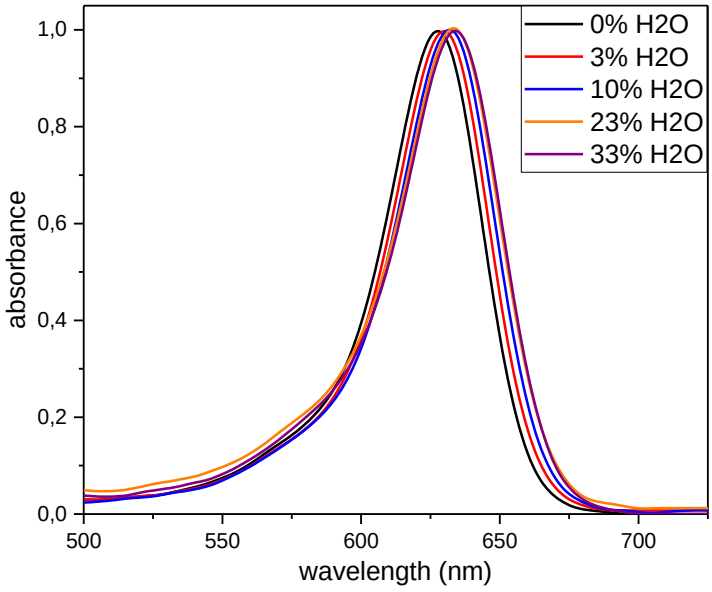

Figure 3. 20. Normalized UV/Vis spectra of **L-CSA-3** dissolved in water-acetonitrile solvent mixtures with varying H_2O volume percentages as indicated in the graph. The concentration was kept constant at $0.83x10^{-5}$ M.

The fluorescence aggregation studies showed that as the water content increased in acetonitrile, the fluorescence intensity decreased when excited at 637 nm. With increasing the water content, a new fluorescence band appeared at 633 nm. At 66% water content, this band is the largest on the spectrum. This results showed that aggregates do not have aggregation induced fluorescence. Further, the new

aggregates have high energy emission which may be due to H-aggregate formation (Figure 3.21).

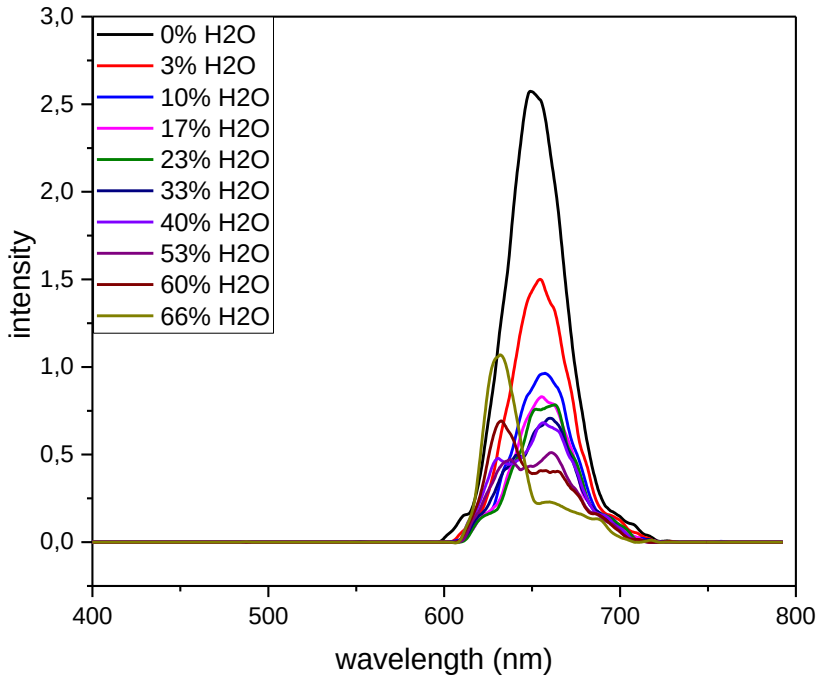

Figure 3.21. Fluorescence spectra of **L-CSA-3** dissolved in water-acetonitrile solvent mixtures with varying H_2O volume percentages, as indicated in the graph. The concentration was kept constant at $0.83x10^{-5}$ M.

The CD measurements for the acetonitrile/water mixture were recorded by varying the water content. In acetonitrile, CD spectra of **L-CSA-3** and **D-CSA-3** showed weak CD signals beyond 500 nm with opposite signs (Figure 3.23 a). These signals were broad in that they spanned from 500 to 800 nm. With this in mind, the CD measurements of varied water content were carried out for both **L-CSA-3** and **D-CSA-3**. As the water content increased, a positive CD signal at 576 nm for **L-CSA-3** was observed (Figure 3.22.a). Similarly, a positive CD signal was observed for **D-CSA-3** (Figure 3.22.b). As the water content increases, both D and L form chiral aggregates in the same direction. The trend of being in the same direction is most evident at 66% water content (Figure 3.23.b)

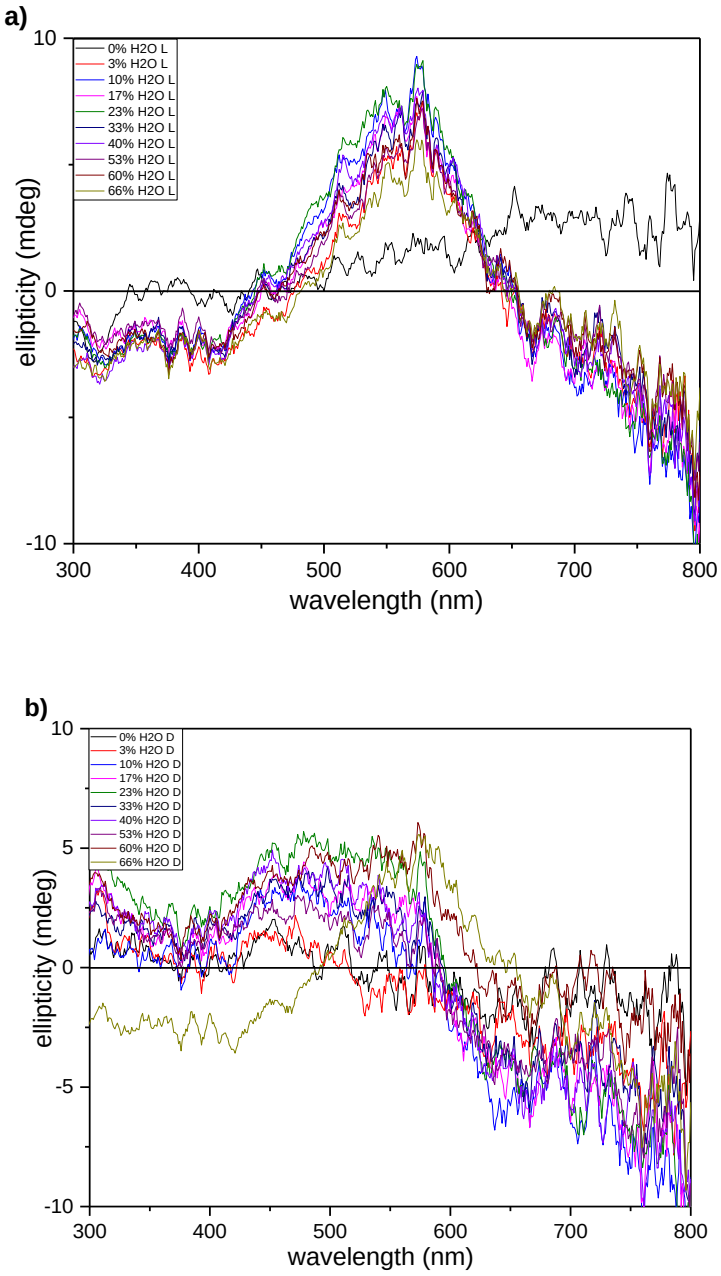

Figure 3.22. CD spectra of **a) L-CSA-3** and **b) D-CSA-3** dissolved in water-acetonitrile solvent mixtures with water varying volume percentages as indicated in the graphs. The concentration of **3A-L** and **3A-D** were kept constant at 0.83×10^{-5} M.

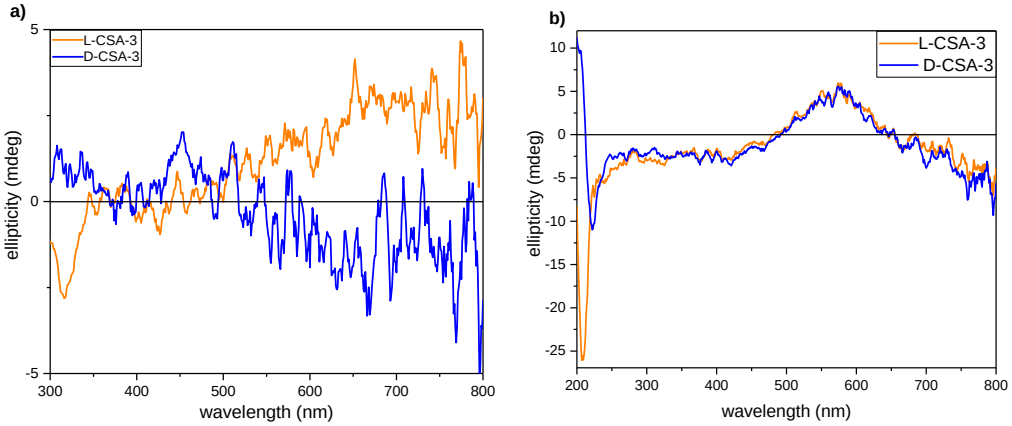

Figure 3.23. CD spectra of **a) L-CSA-3** and **D-CSA-3** dissolved in **a)** acetonitrile and **b)** water-acetonitrile solvent mixtures with 66% H_2O content. The concentrations of the solutions having water were $0.83x10^{-5}$

A powdered X-ray study was performed for both D- and L-forms to prove CD observation further. With this method, we hope to see the directional behavior of the aggregates in solid form. The results showed that both **L-CSA-3** and **D-CSA-3** have exactly the same X-ray diffraction pattern in their solid-state (Figure 3.24). Further powder X-ray spectra revealed that the compounds have crystalline units.

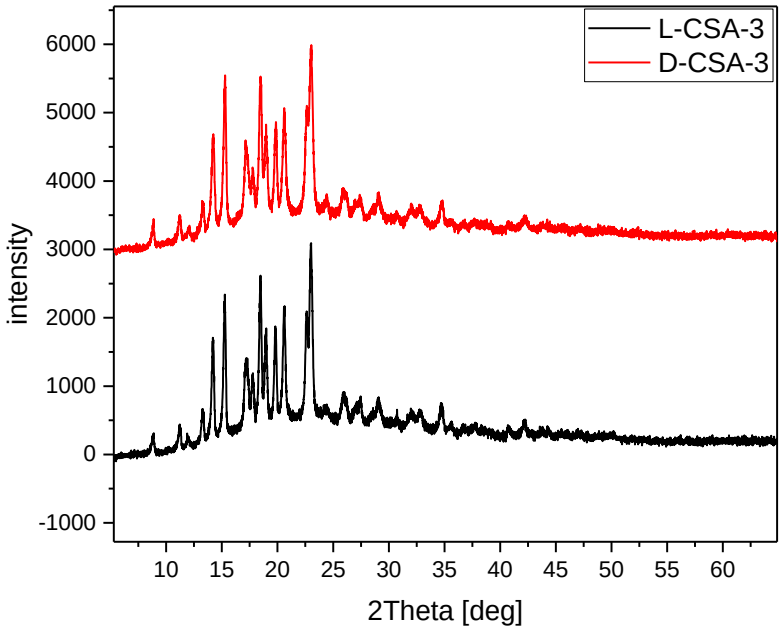

Figure 3.24. X-ray diffraction graph of **L-CSA-3** and **D-CSA-3**

The dye aggregation occurs by forming chiral aggregates whose chirality was induced by the protected amino acids. Even though protected amino acids induce chirality to aggregates, they are not effective in directing the chirality of aggregates in opposite directions. Furthermore, it is suggested that the aggregation starts from the core of the dye. If one wants to direct the aggregation in the opposite senses, one should introduce a chiral moiety on which aggregation emerges. Related studies made use of long alkyl chains in this regard.[165]

3.3.1 Calculations

Geometries of alanine derivatized squaraine dyes in *D* and *L* configurations were optimized at B3LYP hybrid functional with 6-31+g(d) basis set. Left-handed (1) and right-handed (2) seeds of the aggregated complexes based on the *D* and *L* molecular configurations were prepared for two-layer, three-layer, and five-layer structures. Geometries were optimized at PM7 semiempirical method that showed successful results for intermolecular interactions between molecules with a high number of atoms. Intermolecular interaction energies were determined for two-layer aggregated complexes and the interaction between the middle molecule with top and bottom molecular layers. Intermolecular interaction types and total energies were compared for five-layer aggregated complexes to elucidate the origins of the experimentally observed phenomenon.

Computational Results

Interaction energies were calculated for the two-layer and three-layer aggregated complexes for four different isomer and helical directions named as D1 and D2, L1, and L2 corresponding to the left and right-handed structures.

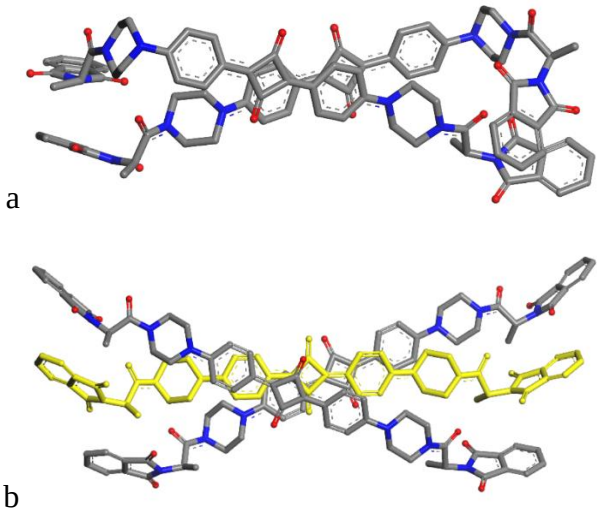

Figure 3.25. Binary and ternary interaction for D isomer of the alanine derivatized squaraine dyes with left-handed helical structures (D1).

Interaction energies showed that both for D and L isomers, right-handed isomers have more attractive interactions compared to the left-handed helical structures (Table 3.1).

Table 3.1. Binary and ternary interaction between the two and three-layer aggregates of the alanine derivatized squaraine dyes.

Structure	**Binary Interaction kcal/mol**	**Ternary Interaction kcal/mol**
D1	-58.42	-84.84
D2	-61.68	-100.79
L1	-52.33	-74.56
L2	-53.58	-96.78

To elucidate the origin of this helical direction preference, five-layer structures were optimized, and their total energies were compared. We found that right-handed D2 and L2 isomer aggregations have lower energies than left-handed ones (Figure 3.26).

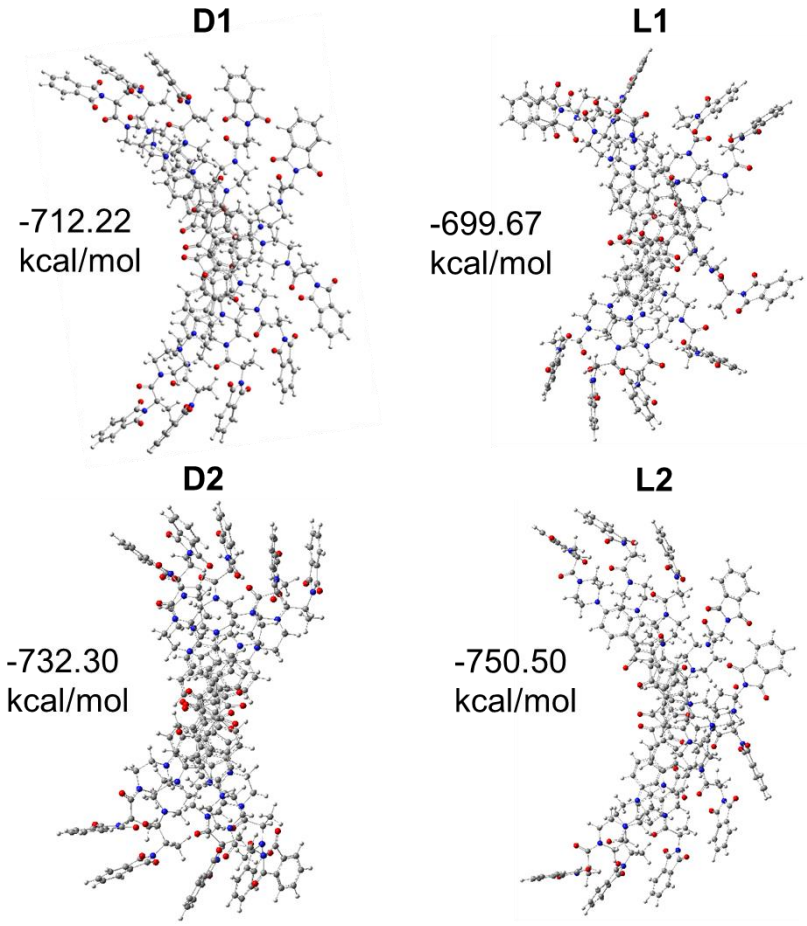

Figure 3.26. Structure and total energy D and L isomers of the alanine derivatized squaraine dyes in two different directions.

Shifted-packing of squaraine centers with 15-30˚ of rotation per layer and 3.30-3.45 Å interlayer distance were determined for all central parts as given for D2 in Figure 3.27.

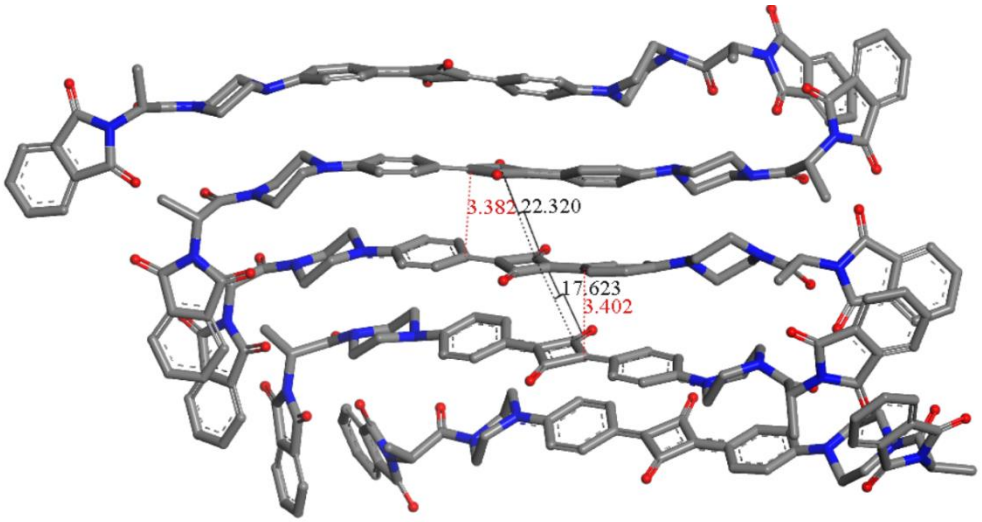

Alternative structure

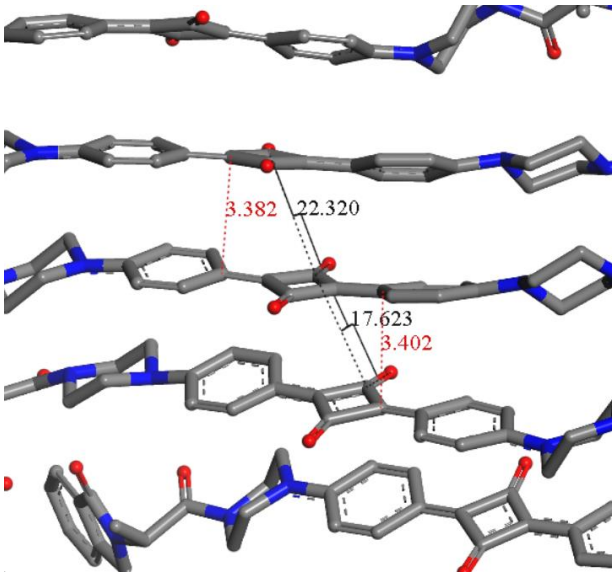

Figure 3. 27. Torsional angle between carbony groups of subsequent squarines and interlayer distance (red) for the 5 layer aggregate of the D2 configuration.

We observed significant packing differences and intermolecular interactions for the pendant groups. The interactions are mainly based on the carbonyl oxygens with methyl hydrogens and piperazine hydrogens that accommodate partially positive charges on them (Figure 3.28).

a)

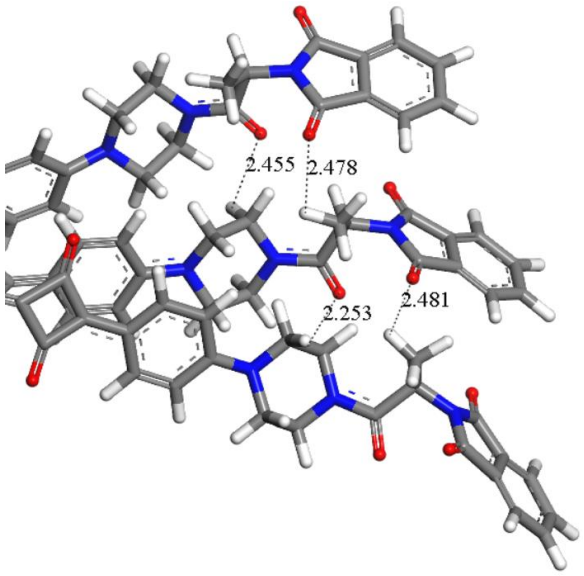

b)

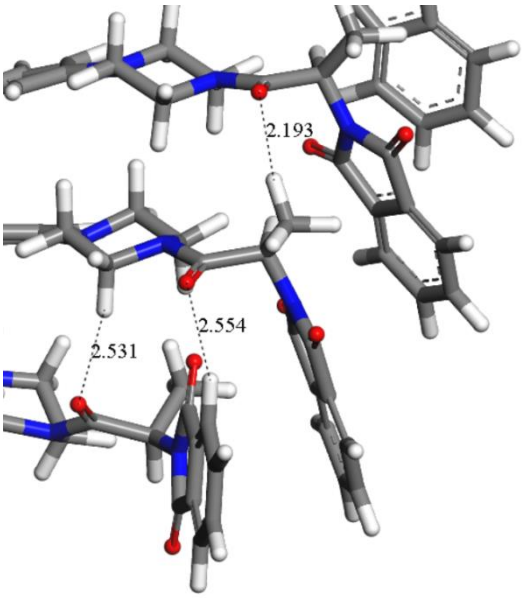

c)

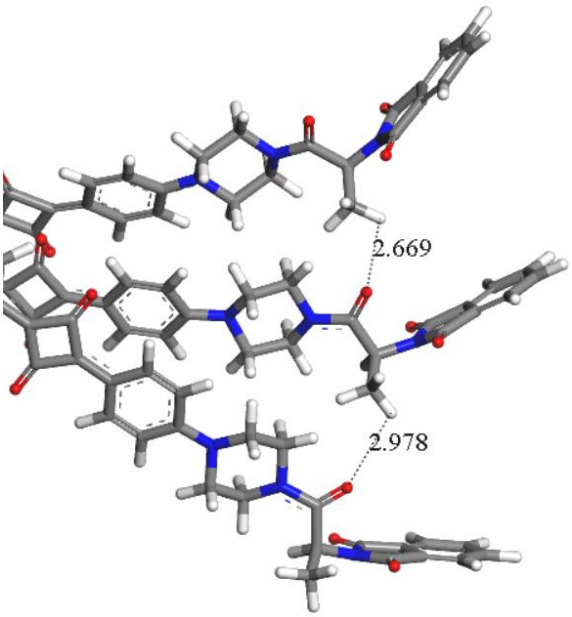

d)

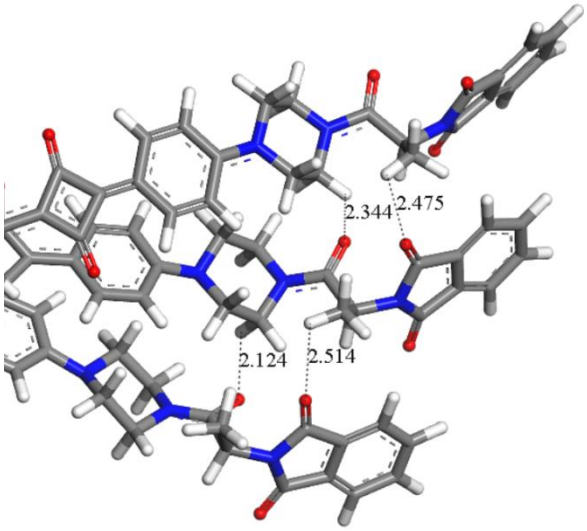

Figure 3. 28. Intermolecular interactions between geometry optimized structures of the *D* and *L* isomer in two different directions a) D1 and b) D2, L isomer in two different directions c) L1 and d) L2.

It was interesting to observe same right handed helical direction preference for both D2 and L2. Our semiempirical calculations presents that, although D2 and L2 have similar right handed helical conformation, the pendant groups have different

directions that provide same molecular interactions for right handed structures that is more attractive than the interactions provided by left handed helical structures (Figure 5). As a result of this alteration in the pendant group packing direction, same helical direction is preferred for both D and L isomers.

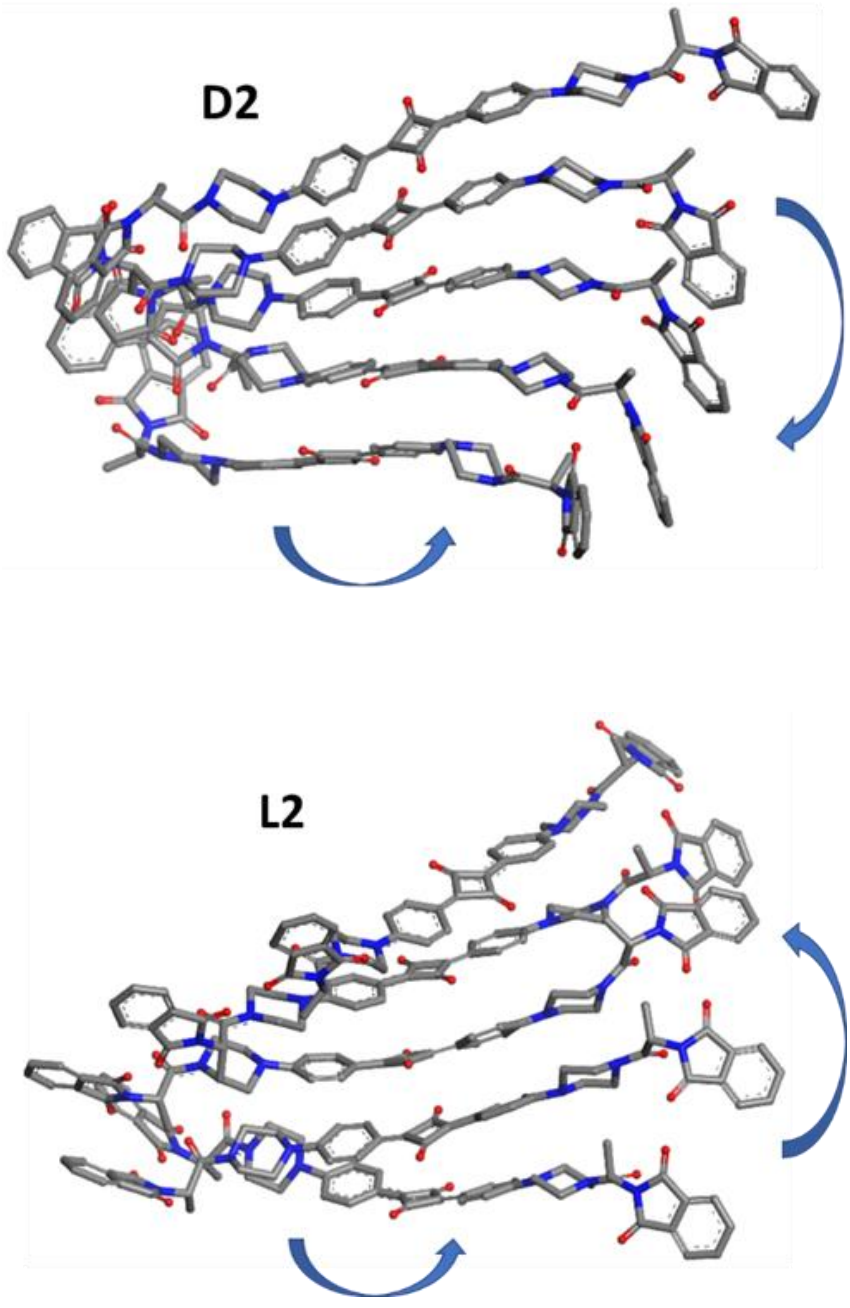

Figure 3.29. Low energy helical directions (right handed) for the *D* and *L* isomers with the different direction of side group.

3.3.2 Conclusion

In this section, fifteen squaraine dyes were attempted to be synthesized. Ten of them were successfully obtained and characterized. Among the ten, seven are novel, and their further characterization was completed with HRMS. The biggest problem encountered in this part of the study is the product's low solubility and susceptibility to nucleophilic attacks. Moreover, two novel enantiomeric pairs of squaraine dyes were synthesized by incorporating enantiomerically pure amino acids, alanine, and phenyl alanine, to induce chirality. Phenyl alanine-derived compounds were found to be having lower solubilities than the alanine-derived dyes. Solvent-dependent chiroptical properties were observed for alanine derivatives. Further studies on aggregation of these dyes revealed that chiral aggregates are formed in the same sense inferred from CD studies. These results concluded that side-chain aggregation is not prevailing over the dye aggregation. Therefore, enantiomeric dyes aggregate in the same direction. It was also supported by the theoretical calculations.

3.4 Squaraine Polymers

In light of these studies, we embark on the synthesis of the polymers. As mentioned at the beginning of this chapter, two methods were proposed to synthesize target polymers.

3.4.1 Studies on SQPOL-L1 and SQPOL-D1

3.4.1.1 Method 1

The first method included the formation of squaraine dye as a monomer and polymerizing it with modified enantiopure chiral tartaric acid (Scheme 3.15, red frame). The studies on the squaraine monomer suggested that (Scheme 3.15, green frame) the modification of tartaric acid would make it suitable for polymerization.

Scheme 3.15 shows the synthetic pathway belonging to the modified tartaric acid monomer in the blue frame.

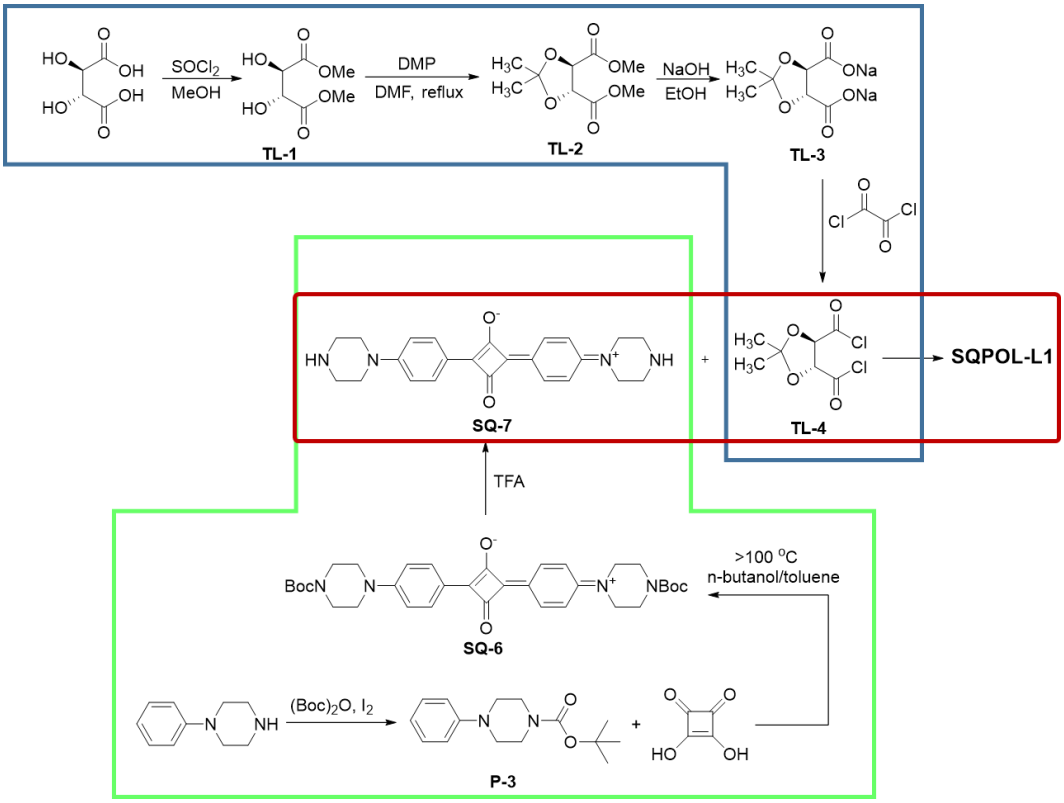

Scheme 3.15. Synthetic pathway of **SQPOL-L1**

The steps shown above were followed to convert carboxylic acid moiety into acyl chloride. Except for the last one, the yields of each step were sufficient, and the compounds were pure enough to use in the next step. Yields and characterization information were given in the experimental part. It is worth mentioning that the synthesis of compound **TL-4** was grueling since it was susceptible to moisture, and purification was tedious. Although chlorination was performed for both oxalyl chloride and thionyl chloride, the results were not reproducible.

According to the outputs during the synthesis attempts using the first method, it was seen that this method is not feasible for polymer synthesis due to the following reasons:

1. The low solubility of squaraine monomers
2. During deprotection of tertiary amine, decomposition of **SQ-6**
3. Low yield and troublesome synthesis of **TL-4**

3.4.1.2 Method 2

Because of the above-mentioned reasons, we moved to Method 2 to synthesize the target polymers. In this method, a synthetic pathway in which the squaraine moiety is formed during condensation polymerization was planned. In this case, squaric acid becomes one monomer, and the structure of other monomers for each polymer is shown below (Figure 3.30).

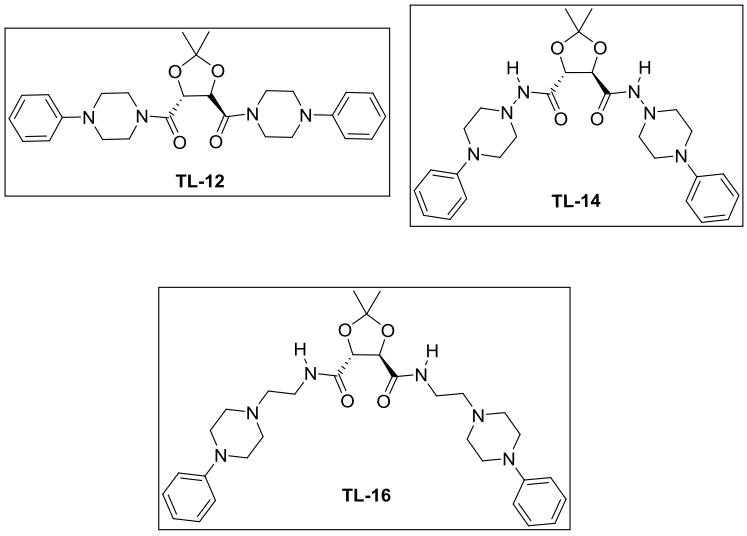

Figure 3.30. Structures of monomers designed to use in method 2

In the synthesis of these monomers, amide bond formation was the critical step (Scheme 3.16). For this purpose, we focused on two sub-methods to get **TL-12**. The results obtained from the synthesis of **TL-12** could be used to synthesize **TL-14** and **TL-16**. Method **(A)** covered the conversion of a carboxylic acid moiety into a good leaving group, preferably ester, and treating the resulting compound with an amine group. In this case, tartaric acid was converted to methyl ester, then protected with 2,2-dimethoxy propane with the proposed procedure in the literature.[175] Ester

functionality in compound **TL-2** was tried to be converted into amide in the presence of 1-phenylpiperazine with proper reaction conditions. However, monomer **TL-12** could not be synthesized with this method.

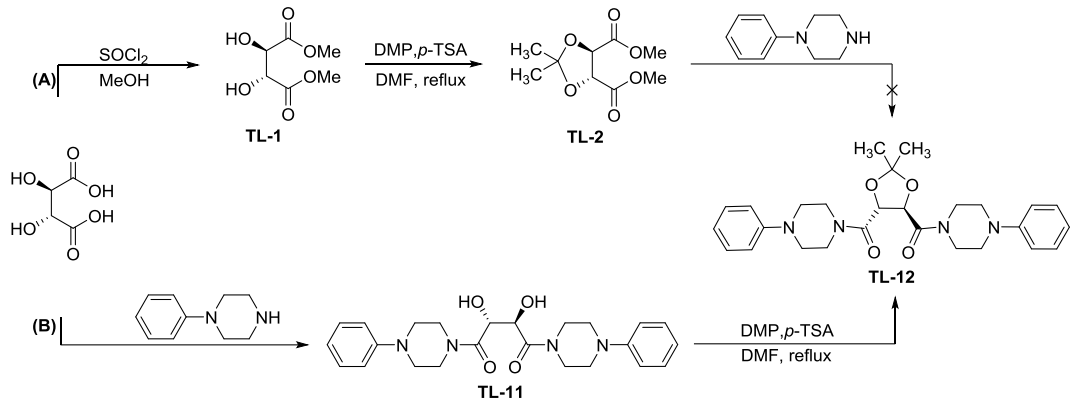

Scheme 3.16. Proposed synthesis methods for monomer **TL-12**

Alternatively, coupling reactions were proposed. We facilitated various coupling reaction conditions besides the EDC coupling applied in the previous part. According to the results summarized in Table 3.1, the target compound **TL-12** was obtained only in EDC coupling conditions with a sufficient yield. Before polymerization, diol moiety in **TL-12** was protected with 2,2 dimethoxy propane in DMF as the last step of the monomer synthesis (Scheme 3.17).

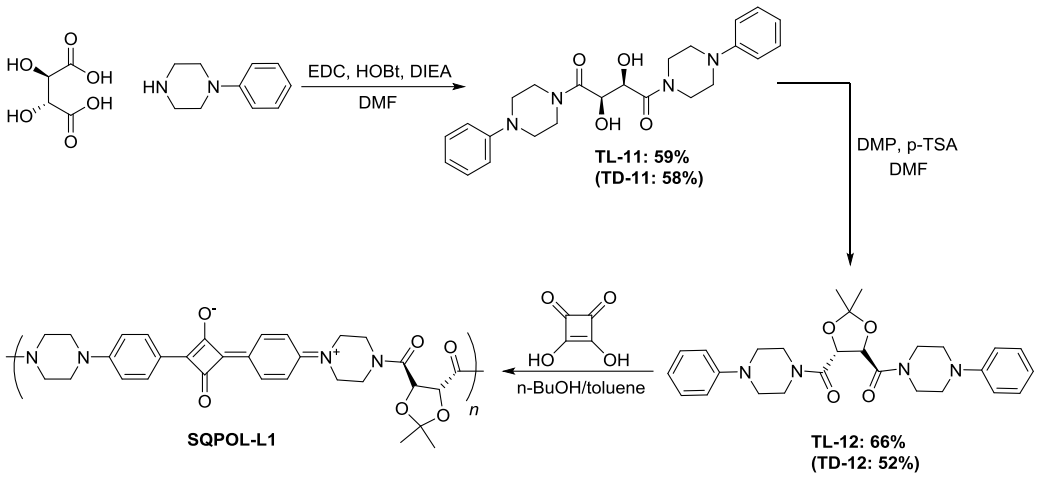

Scheme 3.17. Synthesis of **SQPOL-L1**

Table 3.2. Coupling reaction conditions facilitated to synthesize **TL-11**

Reagent	Solvent	Temperature	Result
N, N'-dicyclohexylcarbodiimide (**DCC**)	DCM	rt	X
N, N'-dicyclohexylcarbodiimide (**DCC**), HOBt	DCM	rt	X
1,1'-Carbonyldiimidazole (**CDI**), 1,8-Diazabicyclo [5.4.0] undec-7-ene (**DBU**)	THF	80 °C	X
1-Ethyl-3- (3-dimethylaminopropyl) carbodiimide (**EDC**), HOBt, Hünig's base (**DIEA**)	DMF	rt	✓

Tartaric acid bonded to 1-phenyl piperazines **TL-12** was treated with squaric acid in a 50:50 toluene butanol mixture under a Dean-Stark condenser. This reaction yielded polysquaraine successfully. Polymer **SQPOL-L1** was purified by crystallization from methanol. The reaction steps mentioned above were summarized in **Scheme 3.17**. D enantiomer of the polymer **SQPOL-D1** was also synthesized by the following same steps.

Two chemically equivalent protons in the aromatic region were obtained in ^{1}H NMR of the polymers **SQPOL-L1** and **SQPOL-D1** (Figure 3.31). This shows that the reaction occurred between the para-position of the phenyl group and squaric acid. Besides, the peak around 190 ppm in ^{13}C NMR belongs to the four-membered carbonyl carbon of the squaraine moiety, another indication of polymer formation.

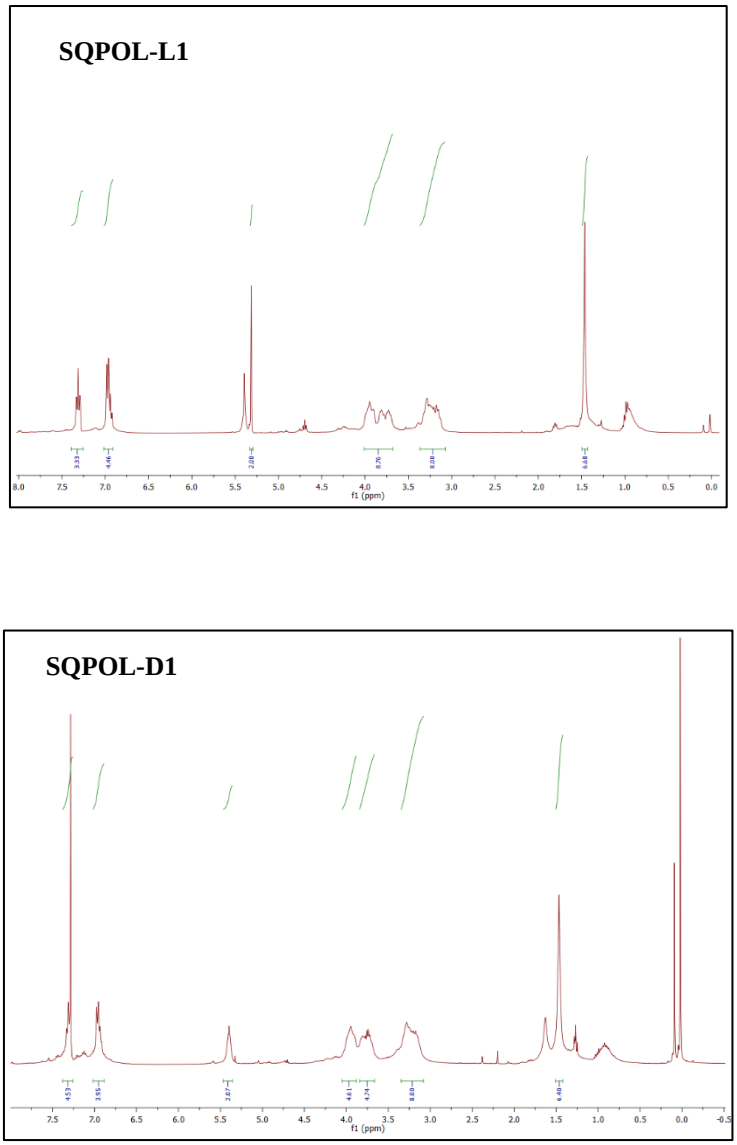

Figure 3.31. 1H NMR spectrum of **SQPOL-L1** and **SQPOL-D1**

The molecular weight measurements of these polymers were done by GPC calibrated for polystyrene. It was found that, for *D* and *L* form M_n= 5.8 kDa, M_w= 7.2 kDa and PDI 1.23, M_n= 3.1 kDa, M_w= 3.6 kDa and PDI 1.17 respectively. It should be noted that these values could deviate since GPC was calibrated for polystyrene.[176]

Further characterization of the polymers was done with UV-Vis spectroscopy, and at around 600 nm, the characteristic absorption peak of the squaraine dyes was

observed in all three solvents (THF, $CHCl_3$, and acetonitrile).[174] A 5 nm blue-shift was detected in $CHCl_3$ with respect to acetonitrile and THF (Figure 3.32). A reverse trend was observed for monomeric chiral squaraine dyes. In THF and acetonitrile, the monomeric dyes showed absorbance blue-shifted compared to chloroform by more than 10 nm. These results indicate that THF and acetonitrile interact less with squaraine units in polymers than chiral squaraine dye molecules. Moreover, polymers showed absorbance by 5 nm apart from each other in chloroform while in THF and acetonitrile, around 20 nm. This is a strong indication that structures are not in monomeric form.[177]

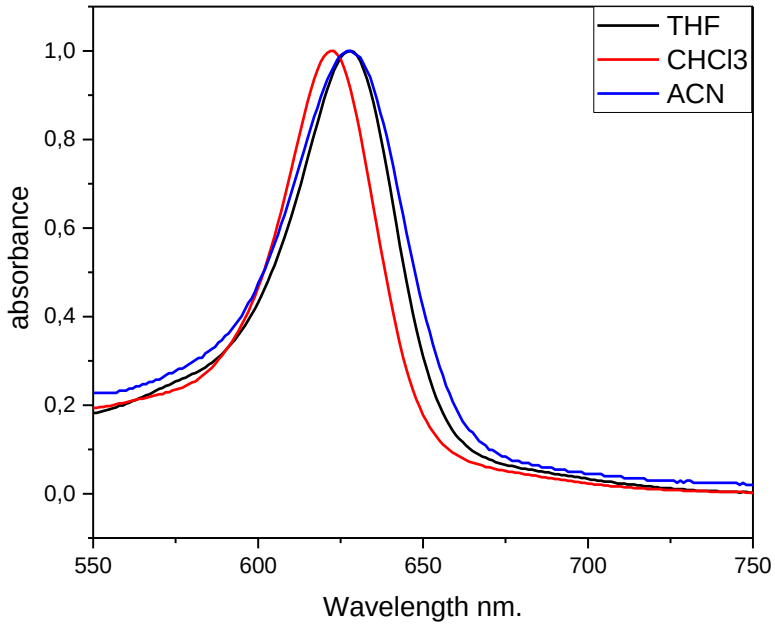

Figure 3.32. UV Solvent Screening of **SQPOL-D1.** Concentrations are $4.8x10^{-5}$ M.

Excitation-emission spectra of both enantiomeric forms of the polymer **SQPOL-D1** and **SQPOL-L1** were recorded in THF, $CHCl_3$, and acetonitrile (Figure 3.33). In THF and acetonitrile, both excitation and emission bands red-shifted compared to the spectra in chloroform, as observed in the absorption spectra. Besides, Stoke shifts in all three solvents were detected around 14 nm. The emission bandwidth in THF and acetonitrile is more broadened than in chloroform by almost 10 nm. This proposed that the polymers interact with THF and acetonitrile. It was, indeed,

apparent that these compounds decomposed faster in acetonitrile and THF than in chloroform. Therefore, one needs to check the absorbance and fluorescence wavelengths (λ_{max}) rather than the intensity when studying these compounds.

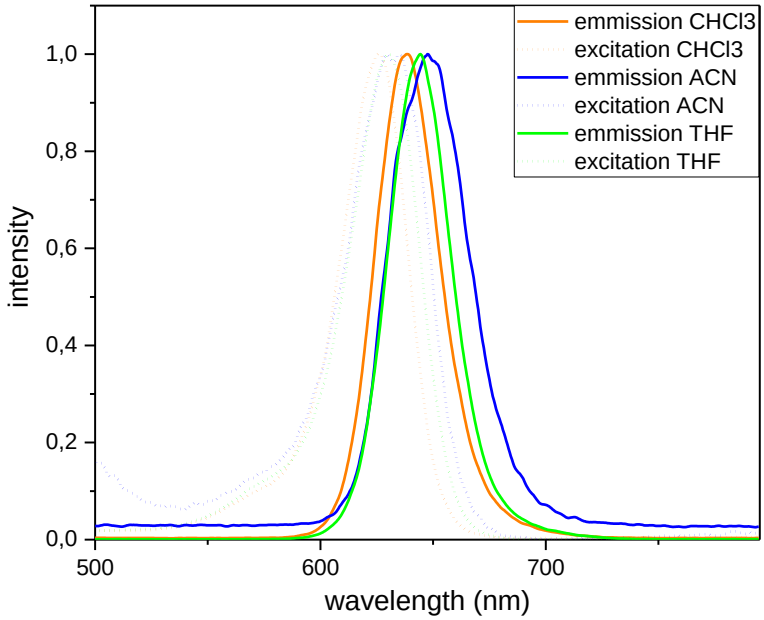

Figure 3.33. Normalized Fluorescence Solvent Screening of **SQPOL-D1.** Concentrations are 4.8×10^{-5} M.

These polymers are known to precipitate in methanol. Therefore, the compounds were dissolved in THF, and methanol was added gradually to get aggregates. As the methanol amount increased in the solvent mixture, the UV-Vis spectra were recorded (Figures 3.34.a and 3.34.b). It was seen that the absorbance decreased as the methanol portion increased. This was probably due to the solubility decrease in the solvent mixture. Moreover, the normalized UV-Vis spectra showed a slight red-shift of the absorbance band as the methanol portion increased. The results suggested aggregation for these compounds (Figure 3.34.b). These compounds are found to be delicate to study. After adding methanol, within 10 minutes, the compounds started to decompose. This was apparent with the disappearance of the absorbance band around 630 nm over 10 minutes.

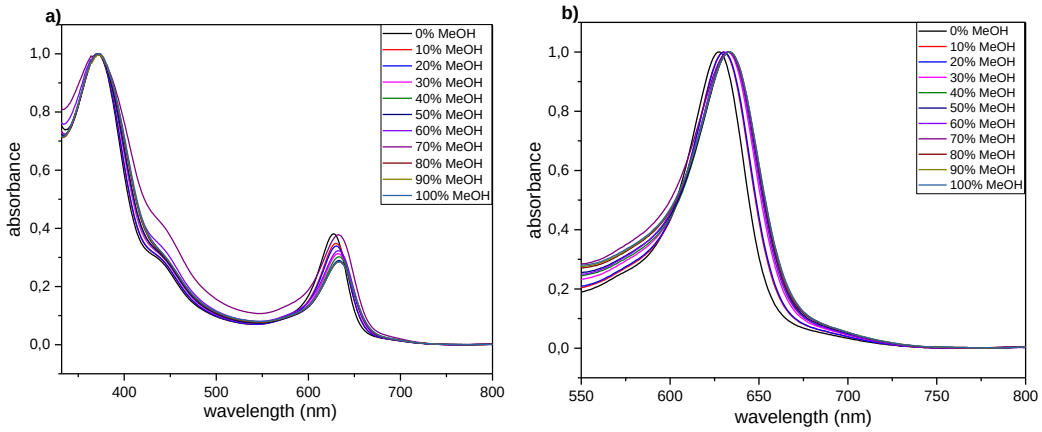

Figure 3.34. **a)** Unnormalized **b)** Normalized UV-Vis titration experiment of **SQPOL-D1.** Concentrations are $6x10^{-4}$ M.

With the aggregation studies monitored with UV-Vis spectra in hand, CD spectroscopic measurements were performed similar to UV-Vis studies. It was found that these compounds do not have a CD activity in THF. As the methanol portion increased, the CD absorption band appeared on the spectra around 600 nm (Figure 3.35.a and 3.35.b) for both enantiomers. The corresponding absorption band became more pronounced when the methanol portion increased to 60%. This result showed that the aggregation formed from these were chiral aggregates (Figure 3.35c and d) and should have a helical nature. For D and L forms of the polymer showed opposite CD signals due to their opposite sense helical aggregates.

In the case of the studies covering alanine-derived chiral squaraine, we did not observe opposite CD signals for enantiomeric forms. On the contrary, squaraine dyes aggregated; we observed helical aggregates in the same screw sense. This was attributed to the steric of the side chain. In this part, which covers chiral polymers of squaraine dye, we have observed CD signals in the opposite sense as aggregation occurred, which further supports our proposal.[177]

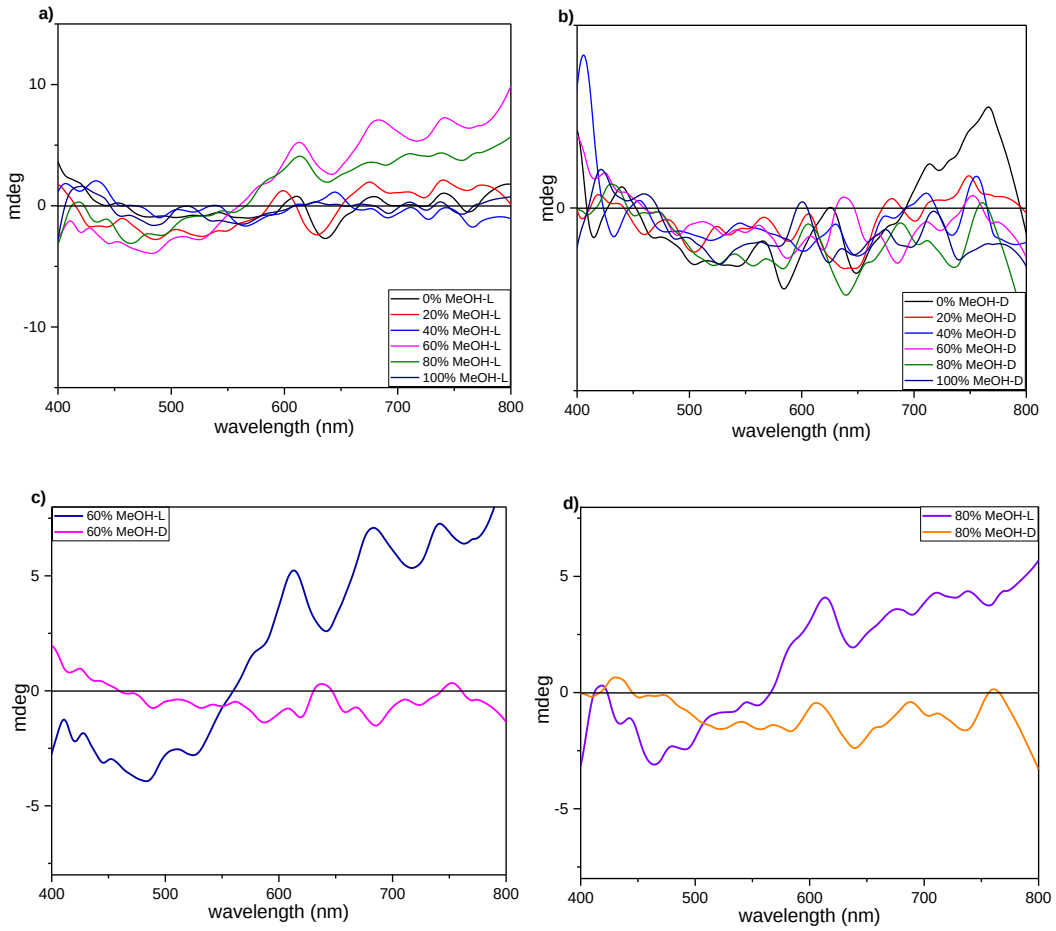

Figure 3.35. Smoothened CD titration experiment of **a) SQPOL-L1** and **b) SQPOL-D1** solvent mixtures with varying ACN volume percentages indicated in the graphs. The concentration was kept constant at $6x10^{-4}$ M **c)** 60% MeOH-THF solvent system **d)** 80% MeOH-THF solvent system.

3.4.2 Studies on SQPOL-L2 and SQPOL-D2

With this information in hand, we moved to the synthesis of polymer **SQPOL-L2.** The synthetic protocol was applied to achieve the target monomer **TL-14** is shown below. 1-Phenyl piperazine was treated with $NaNO_2$ in the presence of acid. This reaction was pH-sensitive, and during the course of the reaction, pH must be kept at 5-6 by adding dilute acid. Then the compound **P-5** was exposed to reduction with two methods. The first one, including Zn as a reducing agent, generated the desired product, but the yield was low (~35%) (Scheme 3.18).

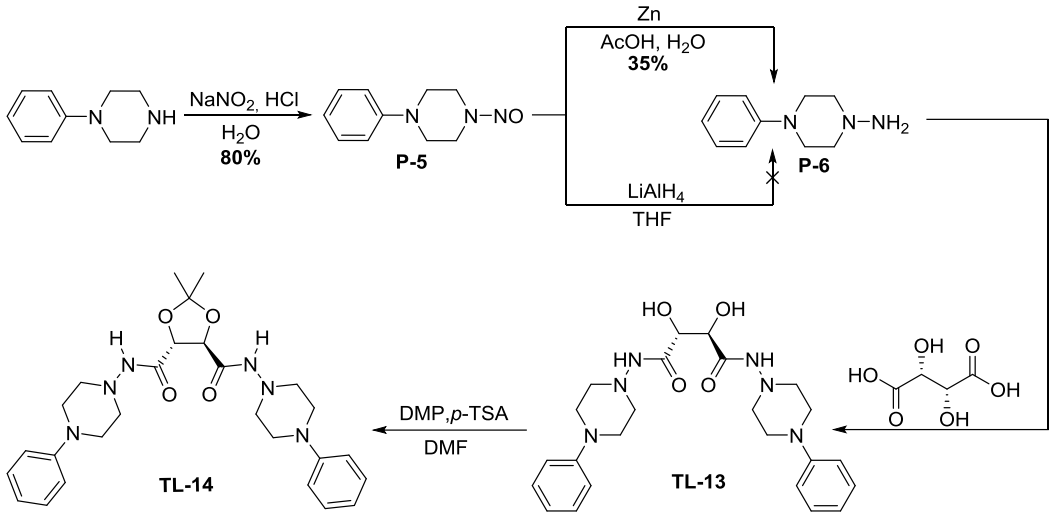

Scheme 3.18. Synthesis of monomer **TL-14**

With the compound **P-6** in hand, coupling reactions with different reagents and conditions are summarized in Table 3.3. were applied. In these studies, we mainly focused on the EDC/HOBt conditions because of promising results obtained in the synthesis of monomer **TL-12** and **TD-12.** However, we could get the desired compound **TL-13** with none of these coupling methods.

Table 3.3. Coupling reaction conditions utilized for the synthesis of **TL-13**

Method	Reagent	Solvent	Temperature	Result
1	**(EDC)**, HOBt, DIEA	DMF	rt	**X**
2	**(EDC)**, HOBt	DMF	rt	**X**
3	**(EDC.HCl)**, HOBt	DMF	rt	**X**
4	**(EDC)**, HOBt	DCM	rt	**X**
6	**(EDC.HCl)**, HOBt	ACN	0 ^{o}C to rt	**X**
5	**(DCC)**, HOBt	DCM	0 ^{o}C to rt	**X**

Since the proposed methods did not work out for this compound, we found an alternative one. Instead of using compound **P-6** directly, it was decided to form it during the cyclization reaction. The proposed synthetic protocol is shown in Scheme 3.19.

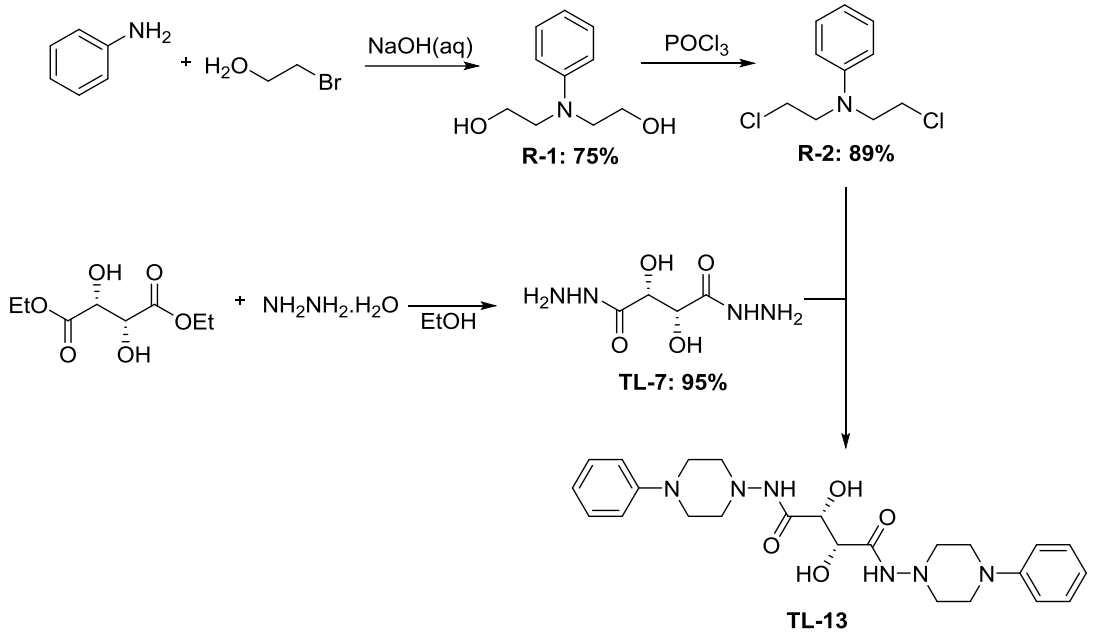

Scheme 3.19. Alternative proposed synthetic pathway for **TL-13** synthesis

Compound **R-1**, **R-2,** and **TL-7** were synthesized with sufficient yields. Before moving to the last step, cyclization reaction conditions were tested with **R-2** and ethanolamine (Scheme 3.20). After getting promising results from this reaction, the same conditions were applied to the reaction between **TL-7** and **R-2**. However, **TL-13** could not be synthesized by this method (Scheme 3.21).

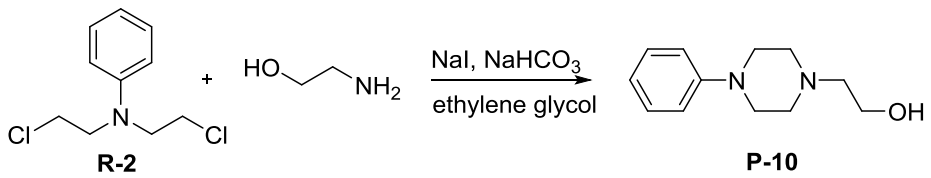

Scheme 3.20. Synthesis of **P-10**

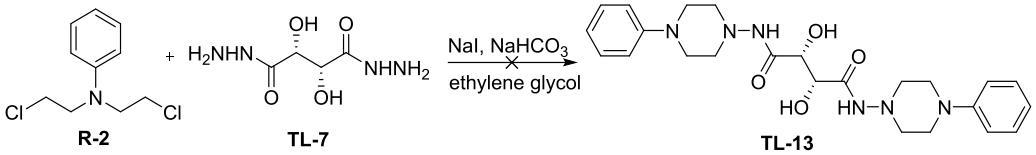

Scheme 3.21. Attempt to synthesize **TL-13** with an alternative method

The same strategy was performed between **R-2** and protected tartaric acid dihydrazide **TL-8** in the presence of Na_2CO_3 and KI shown in Scheme 3.22. In this case, compound **TL-14** was synthesized, but the yield was not sufficient. Moreover, the compound could not be synthesized again, although many times were tried. The ^{1}H NMR spectrum of the compound **TL-14** synthesized once, was shown in Figure 3.36.

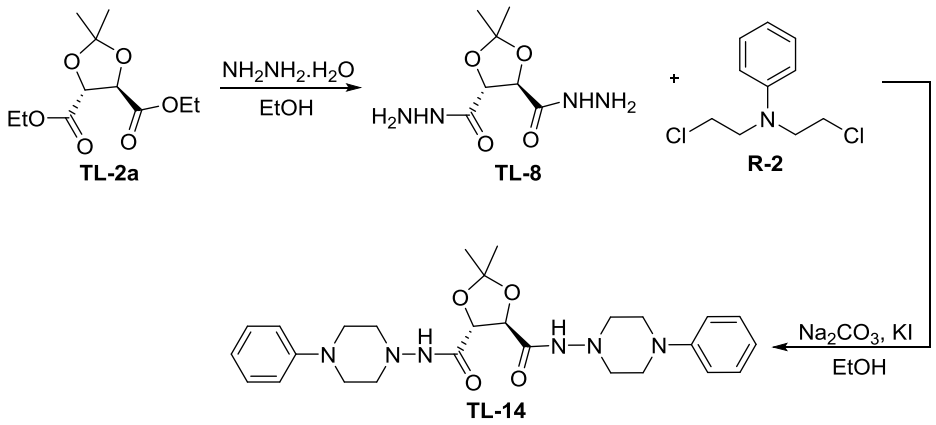

Scheme 3.22. Synthesis of monomer **TL-14**

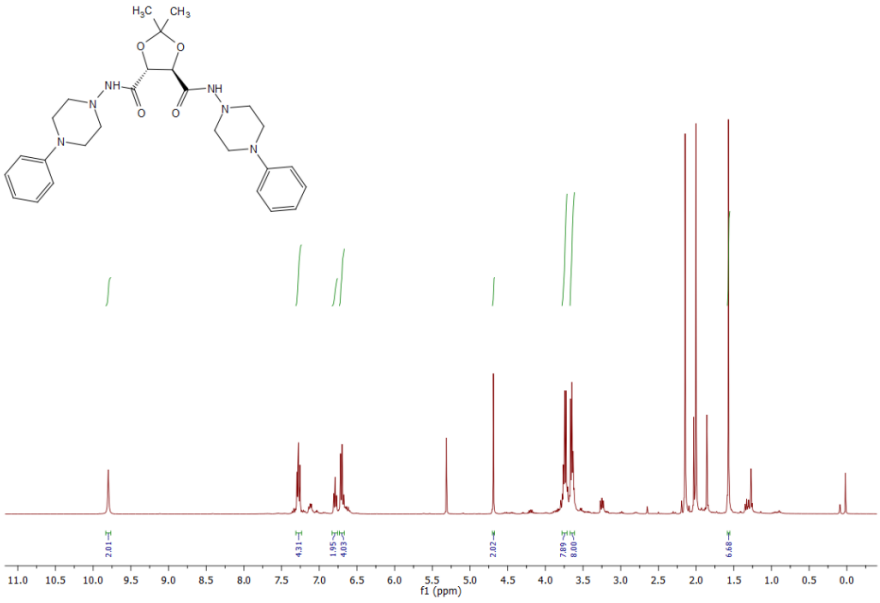

Figure 3.36. ^{1}H NMR spectrum of **TL-14**

Although many different methods have been employed more than once, and most of them have been tried more than once, polymer synthesis could not be performed because the target monomer **TL-14** could not be synthesized. Although it was synthesized, we could not reproduce this compound.

3.4.3 Studies on SQPOL-L3 and SQPOL-D3

In parallel with the studies on the synthesis of polymer **SQPOL-L2**, synthesis studies of polymer **SQPOL-L3** have also been started. The synthetic protocol put into action during the synthesis of **TL-12** and **TL-14** was applied to get monomer **TL-16.** (Scheme 3.23).

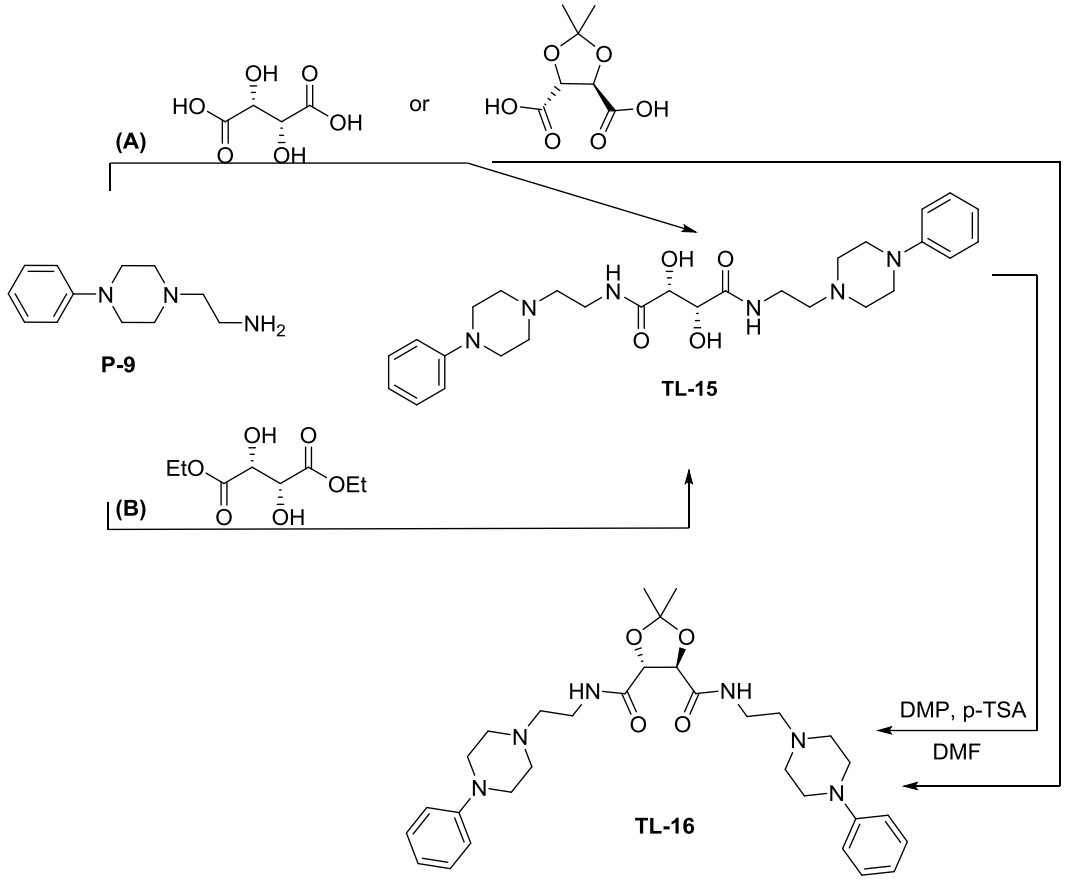

Scheme 3.23. The synthesis scheme of **TL-16**

Starting material for these reactions was not commercially available, so the compound **P-9** was prepared before starting these syntheses. Compound **P-8** was obtained starting from 1-phenyl piperazine and reacted with N-(2-bromoethyl)phthalimide in the presence of K_2CO_3 and KI. The yellow solids were exposed to deprotection reaction by hydrazine monohydrate and yielded compound **P-9.**

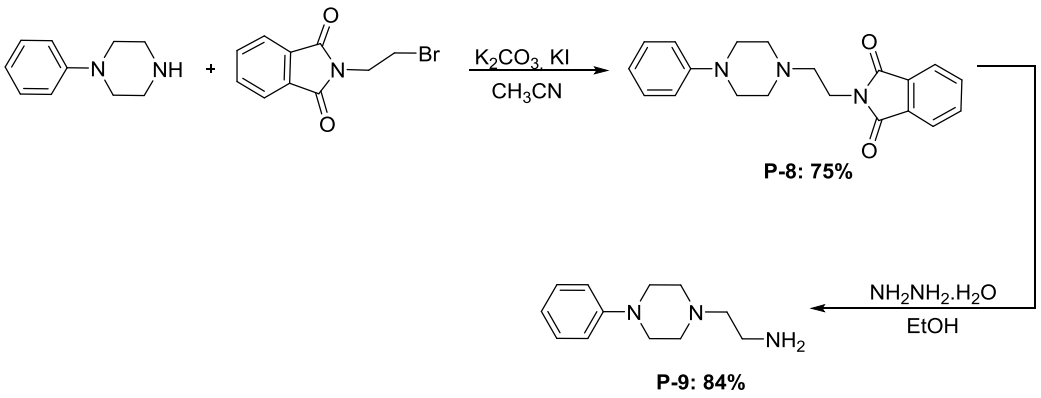

Scheme 3.24. Synthesis of **P-9**

After the synthesis of the **P-9** Method **(A)** and **(B)** were applied separately. As seen in the reaction scheme, method **(A)** included the coupling reactions. In this case, EDC/ HOBt coupling reaction could not give satisfactory results. To make carboxyl moiety in tartaric acid more available to nucleophilic attack by changing its spatial arrangement, we decided to protect diol moiety and then convert it into the corresponding carboxylic acid. In previous parts, the synthesis of **TL-3** was explained. It was treated with aqueous HCl to get **TL-5,** and the resulting compound was subjected to a coupling reaction (Scheme 3.25). The monomer **TL-16** was obtained after burdensome flash column chromatography. Unfortunately, the yield was so low that only characterization could be done with the obtained substance.

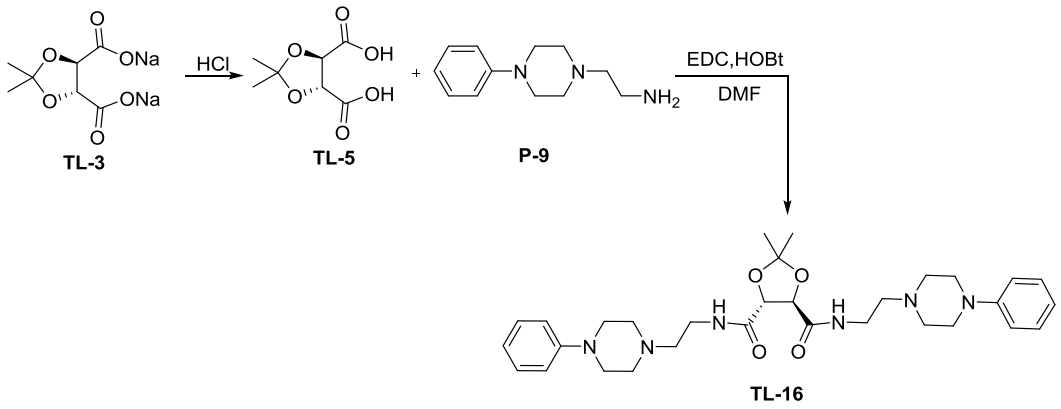

Scheme 3.25. Synthesis of monomer **TL-16**

Then we moved to the method **(B)** and applied various reaction conditions summarized in Table 3.4. Only the condition shown in the last row of Table 3.4

yielded the desired compound, but the yield was again low and could not be purified properly.

Table 3.4. Reaction conditions applied in Method (B)

Method (B)			
Solvent	**Temperature/ time**	**Reagent**	**Result**
THF	66°C reflux /overnight	-	×
EtOH	79°C reflux/ overnight	-	×
EtOH	150°C, 6 bar /1 day	-	×
-	Room Temperature/ 4 days	-	✓ (low yield)

To increase the reaction yield, method **(C)** (including protected tartaric acid ethyl ester **TL-3a** and **P-9**) was proposed. These two compounds were reacted with each other in the presence of NaCN and EtOH, and the target compound was obtained after flash column chromatography. Again purification part was time-consuming, and the yield was not satisfactory. As a final method, we utilized method **(D)** that we are familiar with from the synthesis of monomer **TL-14,** and we got promising results. Again although **TL-16** was synthesized, the yield was insufficient.

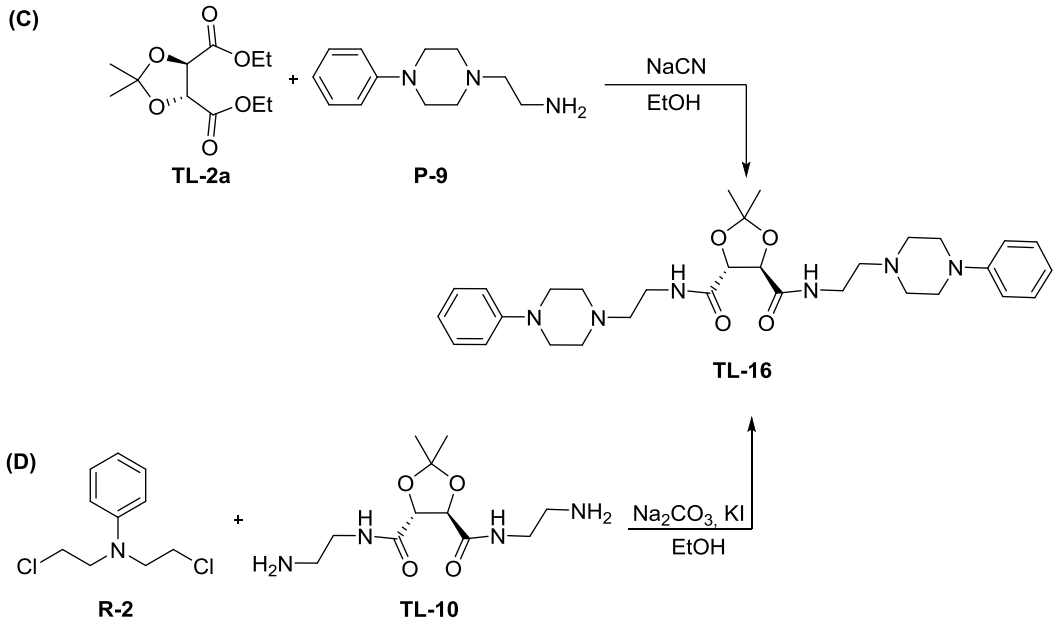

Scheme 3.26. Proposed synthesis methods for **TL-16**

The biggest challenge we faced with all the methods was the purification of the substance. Moreover, after purification with flash column chromatography, none of the methods resulted in more than 7% yield. As a result, although the target monomer **TL-16** was synthesized, the amount obtained was not sufficient for the polymerization reaction.

When we examine the obtained results in terms of the differences in the chemical structures of the monomers, it was seen that the coupling reactions with the secondary amine-derived **TL-11** and **TD-11** were successful. On the other hand, primary amine, hydrazine, and hydrazide moiety could not give coupling reactions with tartaric acid. The reason could be the low nucleophilicity of the primary amine, hydrazine, and hydrazide compared to secondary amines.

In the studies conducted by Herbert Mayr,[178,179] scaled various electrophiles and nucleophiles according to their reactivity. The tables built by Mayr are based on the formula shown below:

$$\log k_{20^{o}C} = s_N(N+E) \qquad (7)$$

E = electrophilicity parameter; N = nucleophilicity parameter s_N = nucleophile-specific sensitivity parameter (N and s_N are solvent-dependent). N is determined by using a reference electrophile bis(4-methoxyphenyl)carbenium ion, and E was assigned 0 for this compound. N values of functional groups that we also have in our polymers were indicated in Figure 3.37.

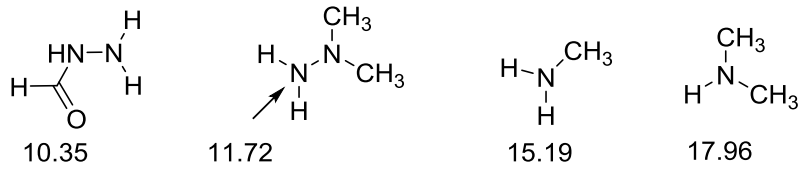

Figure 3.37. Nucleophilicity parameters (N) of selected hydrazide, hydrazine primary, and secondary amine

The results that we obtained from experiments are consistent with the N values of each functional group these values. When we think through equation (7), logarithmically increasing differences emerge between the reaction rates. It also means that reaction with secondary amines proceeds faster than the others. It can also be associated with the low yield and long reaction period of the synthesis of **TL16**. Though the mechanism of the synthetic pathways utilized to synthesize **TL-14** and **TL-16** still needs to be elucidated.

3.4.4 Conclusion

In this part, three different enantiomeric pairs of chiral squaraine polymers were designed and attempted to be synthesized. To obtain the monomers of **SQPOL-L2 (D2)** and **SQPOL-L3 (D3),** namely **TL-14 (TD-14)** and **TL-16 (TD-16),** were tried to be synthesized with several methods. Among these methods, three of them gave the target compounds in yield sufficient for only characterization. Because of this reason, the polymers **SQPOL-L2 (D2)** and **SQPOL-L3 (D3)** could not be synthesized.

On the contrary, **SQPOL-L1** and **SQPOL-D1** were synthesized and characterized successfully. The chirality of these polymers was introduced through tartaric acid. Even though these dyes are shown to be prone to decomposition in protic solvents, we were able to study the aggregation of these polymeric chiral dyes in the THF/methanol solvent system. Our studies with CD spectroscopy showed that these dyes formed helical assemblies. The sense of helicity is controlled by the point chirality introduced to the polymers with tartaric acid units. Furthermore, the large chiral groups attached to the squaraine dyes affect the squaraine dyes' helicity in their aggregated form.

3.5 Diaminoterephthalate (DAT) Polymers

In the final part, we designed two novel polymers with a more stable chromophore by keeping the idea of backbone chirality in the polymer chain with a tartaric acid-derived chiral monomer. It was seen that 2,5-diaminoterephthalate (DAT) chromophores are suitable candidates to meet our expectations. As mentioned in the introduction part, diaminoterephthalates are stable with a simple structure. These compounds have absorption spectra in the visible region and strong fluorescent emissions with high quantum yields.[138–140] DAT chromophores can be orthogonally functionalized, which provides the adjustment of the structural properties of the compounds. The structures of polymers designed in the light of this information are shown in Figure 3.38.

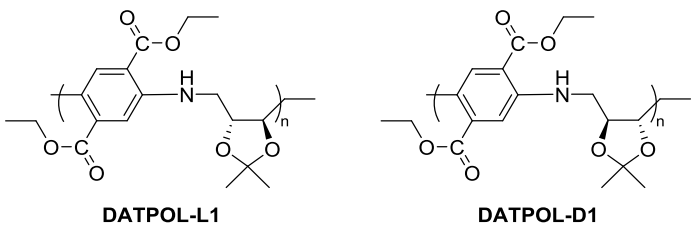

Figure 3. 38. The structures of **DAT** polymers

3.5.1 Synthesis of Dye Monomer S-4 and Model Dye S-6

Before attempting the polymerization reaction, DAT dye **S-6** was synthesized as a model monomer to compare the results obtained from polymers. For this purpose, firstly, monomeric dye **S-4** was synthesized. Diethyl ester of succinyl succinate (**S-4)** was synthesized through condensation of diethyl succinate, as depicted in **Scheme 3.27**. Succinic acid was treated with thionyl chloride in EtOH to obtain diethyl succinate. By employing Claisen condensation on **S-3**, compound **S-4** was in hand with 42% yield as a light yellow solid. Then, monomer **S-4** was treated with methyl amine in the presence of MeOH. After the completion of the reaction, methanol was removed, and the resulting compound **S-5** was directly exposed to an oxidation reaction employing bromine and sodium carbonate to get the target compound **S-6**.

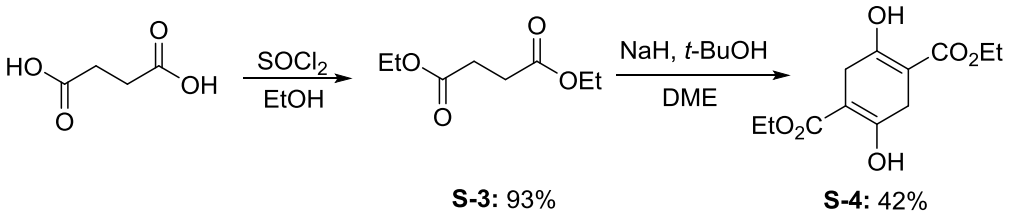

Scheme 3.27. Synthesis of monomer **S-4**

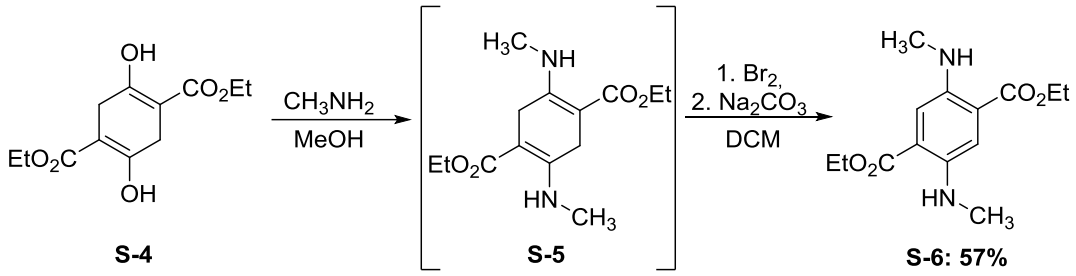

Scheme 3.28. Synthesis of model dye **S-6**

Further studies of model dye **S-6** include UV-Vis and geometry optimization at the level of B3LYP/6-31G(d) theory as implemented in Gaussian 09.[180] Compound **S-6**

was dissolved in the following solvents (chloroform, acetonitrile, methanol, and tetrahydrofuran) with the same concentrations (Figure 3.39). It was observed that in chloroform, the absorption maximum blue-shifted significantly (90 nm). The absorption maximum was also blue-shifted in methanol by 12 nm compared to in THF and acetonitrile. These results suggested that the hydrogen bonding capability of the solvent plays a role in the UV-Vis absorption properties of the compound **S-6**. Although solvents do not participate in any kind of hydrogen bonding, in chloroform, solvents interact with compound **S-6** by playing a role by either the H-bond donor or acceptor in the other three solvents. Methanol can act as both an H-bond donor and acceptor. THF and acetonitrile can act as H-bond acceptors. H-bond acceptors interact with N-H moieties in the molecule, which results in longer wavelength absorption, while H-bond donors interact with the carbonyl oxygen, bringing the absorption maximum to higher energy.

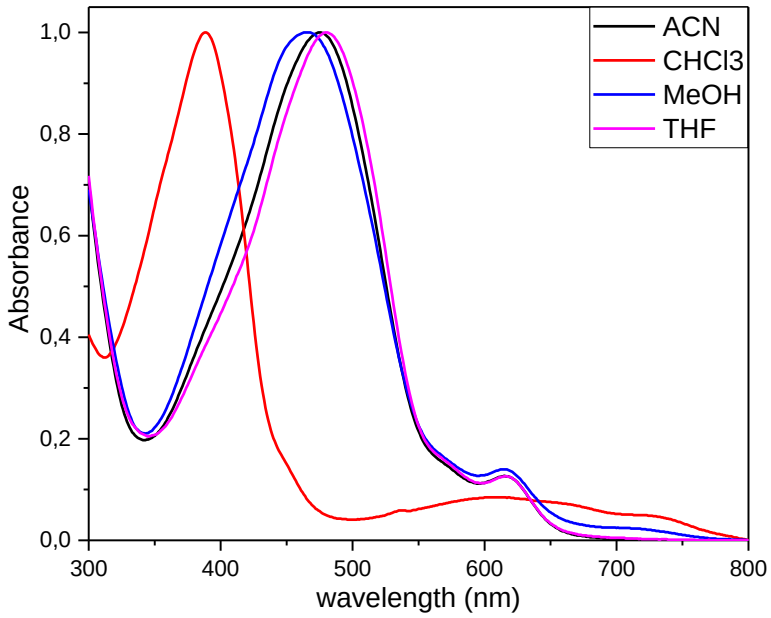

Figure 3. 39. UV-Vis Spectrum of **S-6** (M=1.78x10^{-3})

To model the above-mentioned results, compound **S-6** was geometry optimized at the level of B3LYP/6-31G(d) theory as implemented in Gaussian 09.[180] Initially, two

geometries were optimized (Figure 3.40); 1) the ester oxygen pointing to the N-H (**TPA**), and 2) the carbonyl oxygen of the ester pointing to the N-H (**TPB**). It was found that **TPB** is lower in energy than **TPA** by 7.03 kcal/mol. With these results, two explicit methanol molecules were included in the geometry optimization **TPB_M**. For **TPB_M**, N-H forms H-bond with methanol oxygen; meanwhile, O-H of methanol forms H-bond with the carbonyl oxygen of the esters.

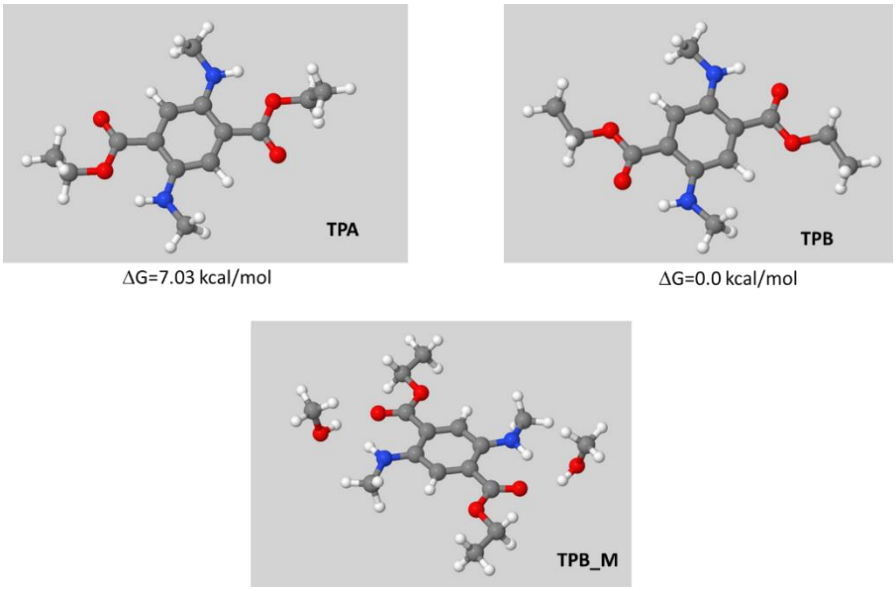

Figure 3. 40. B3LYP/6-31G(d) optimized structures of **TPA**, **TPB**, and **TPB_M**

Vertical excitations were calculated for the optimized structures given above. The results are summarized in Table 3.5. It shows that the conformation shifts the first excitation state, which corresponds to the HOMO-LUMO transition. The orientation of the N-H and carbonyl group in **TPB** toward each other leads to the first excitation with 435 nm, while 410 nm excitation was calculated in **TPA**. H-bond acceptor and donor ability of methanol red shifted the first calculated excitation. It is due to the change in electron density of the chromophore **S-6,** which is affected significantly by its H-bond donating property from N-H. These results were in accordance with the experimental observations qualitatively.

Table 3.5. Vertical excitation calculations of **TPA**, **TPB**, and **TPB_M** (f: oscillator strength)

Excitation	TPA	TPB	TPB_M
1	410.9 nm (f=0.1441)	435.5 nm (f=0.1589)	483.5 nm (f=0.1404)
2	244.9 nm (f=0.1353)	251.1 nm (f=0.0000)	269.7 nm (f=0.0003)
3	241.4 nm (f=0.0002)	245.6 nm (f=0.0003)	250.3 nm (f=0.0050)
4	241.3 nm (f=0.0074)	244.7 nm (f=0.1194)	248.6 nm (f=0.0956)
5	235.8 nm (f=0.0003)	232.4 nm (f=0.0000)	246.5 nm (f=0.0025)

When the solutions of model monomer **S-6** were kept at 4 ^{o}C for one month, UV-Vis spectra of the compound in MeOH did not change, while chloroform solution showed the absorption maxima red-shifted compared to the freshly prepared solution (Figure 3.41). To solve this puzzle, the stored chloroform solution was heated at 70 ^{o}C for 10 minutes and sonicated for two minutes. λ_{max} at 400 nm had a significant increase in the UV-Vis spectrum of the resulting solution. This suggests that the stored solutions in chloroform self-assembled through intermolecular hydrogen bonds; by heating and sonicating, these assemblies were broken.

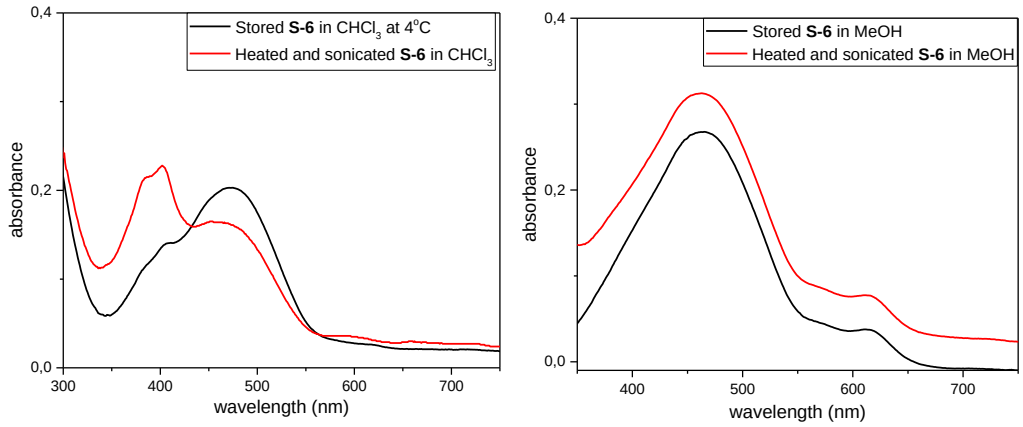

Figure 3.41. UV-Vis Spectra of stored and, heated and sonicated **S-6** solutions in $CHCl_3$ and MeOH M=1.78x10^{-4}

3.5.2 DATPOL-L and DATPOL-D

3.5.2.1 Synthesis of the Polymers

The synthesis of diamine **TL-6** and **TD-6** started from corresponding tartaric acid (Scheme 3.27). The enantiopure tartaric acid was converted to dimethyl ester, **TL-1** (**TD-1)**, through Fischer esterification via in situ formation of HCl with the action of thionyl chloride in methanol. The diol group on compound **TL-1 (TD-1)** was treated with 2,2-dimethoxypropane to get acetonide **TL-2** (**TD-2)** in good yield. The compound **TL-2 (TD-2)** and ammonia in methanol were placed in a stainless steel vessel at -40 °C. Then, the vessel was sealed and heated to 50 °C for 6 hours to get compound **TL-5 (TD-5)**. The amide was subjected to a reduction reaction with $LiAlH_4$ to get target diamines in a Soxhlet apparatus.[181] Conventional mix-stir reduction did not yield the amine. Therefore, the amide was placed in Soxhlet thimble, and $LiAlH_4$ was suspended in THF. After 6 hours of heating at 66 °C, compound **TL-6 (TD-6)** was in hand in more than 60 % yield.

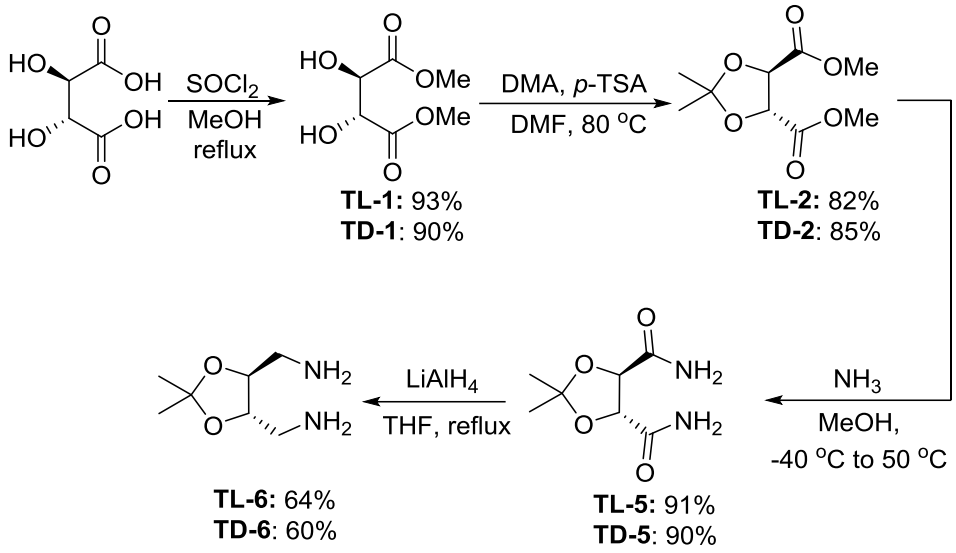

Scheme 3.29. Synthesis of modified tartaric acid monomers **TL-6** and **TD-6**

With the starting materials **TL-6 (TD-6)** and **S-4** in hand, they were treated with each other in ethanol in the presence of a catalytic amount of HCl to get a prepolymer. The reaction did not proceed in the absence of HCl. The enamines were aromatized with bromine in the presence of sodium carbonate to yield **DATPOL-L** and **DATPOL-D**.

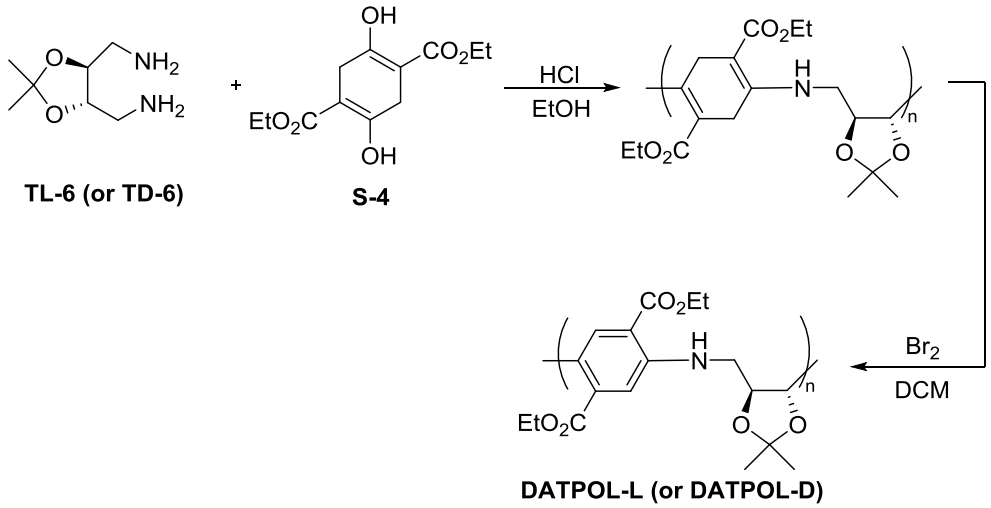

Scheme 3.30. Reaction scheme of **DATPOL-L** and **DATPOL-D**

3.5.2.2 Characterization of the Polymers

^{1}H NMR spectra of **DATPOL** polymers showed aromatic protons around 7.2 ppm. The peaks for the aliphatic region are complex as expected for polymers. Even though ^{1}H and ^{13}C NMR spectra of **DATPOL-L** and **DATPOL-D** are similar, they show minor differences (Figure 3.42 and 3.43). These differences are expected because the number of repeating units is not the same. GPC (calibrated for polystyrene) results showed that the molecular weight distributions for **DATPOL-L** and **DATPOL-D** showed M_w as 1.319 kDa and 1.861 kDa, respectively.

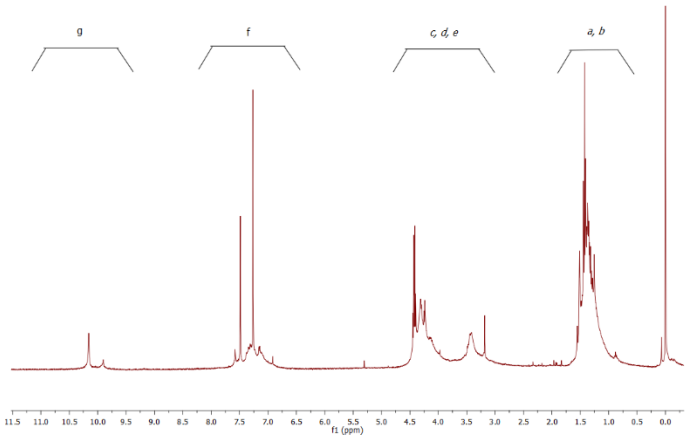

Figure 3.42. ^{1}H NMR Spectrum of **DATPOL-L**

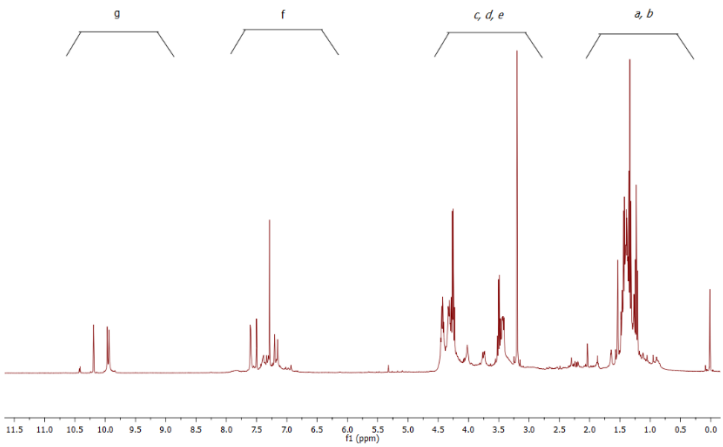

Figure 3.43. ^{1}H NMR Spectrum of **DATPOL-D**

3.5.2.3 Optical Studies of the Polymers

UV-Vis spectra of **DATPOL-L** and **DATPOL-D** also showed a similar trend in different solvents. **DATPOL-L** has an absorption 407 nm in chloroform and around 438 nm in THF, MeOH, and ACN (Figure 3.44.a). **DATPOL-D** has an absorption 386 nm in chloroform, 423nm in THF, 445 nm in MeOH, and ACN (Figure 3.44.b). The spectra imply that the large shift in chloroform is due to a lack of solvent-solute interaction, as explained for the reference compound **S-4**.

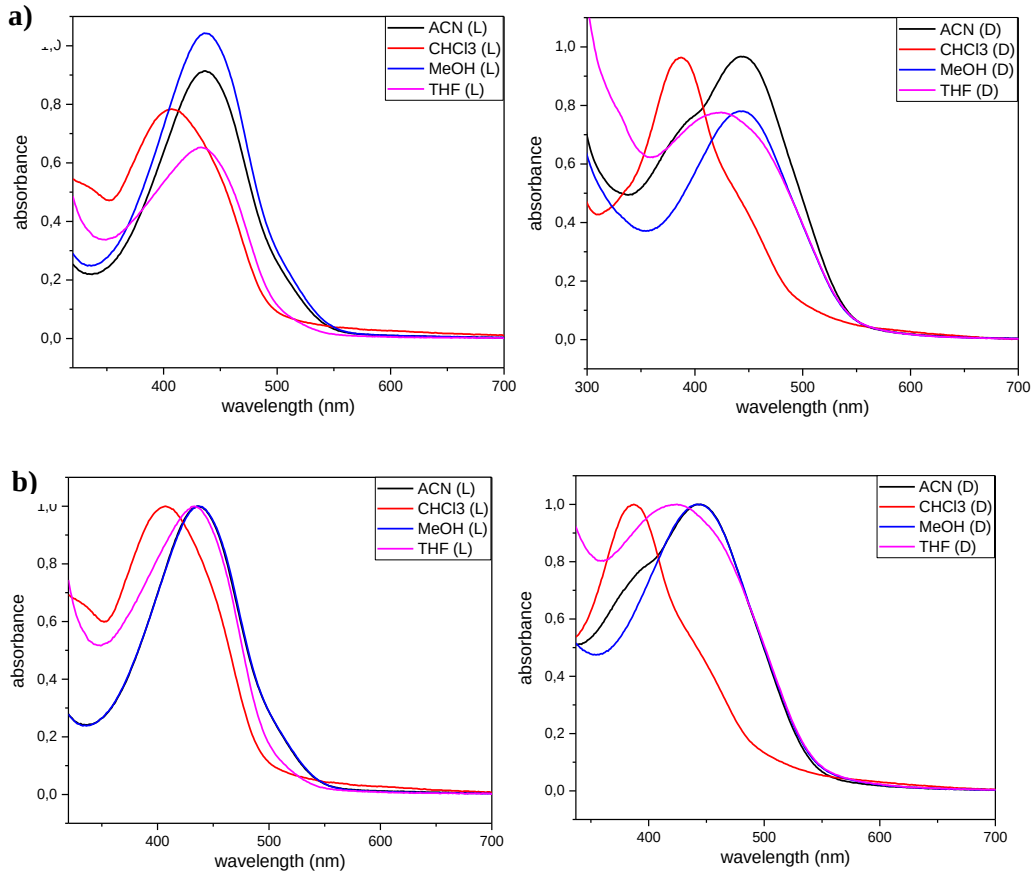

Figure 3. 44 a) UV-Vis spectra b) normalized UV-Vis Spectra of **DATPOL-L** and **DATPOL-D** in different solvents. Concentrations are 2.63×10^{-4} M.

Fluorescence emission spectra in the above-mentioned solvents were recorded by exciting all solutions at 420 nm (Figure 3.45). Both **DALPOL-L** and **DATPOL-D** emitted light at around 450 nm in chloroform. In other solvents, the emission wavelength red-shifted with the decrease in fluorescence intensity. This is probably

due to the well-solvated **DATPOL**s having nonradiative transitions. That is, the H-bonds between solvent and the **DATPOL**s increase the degrees of freedom.

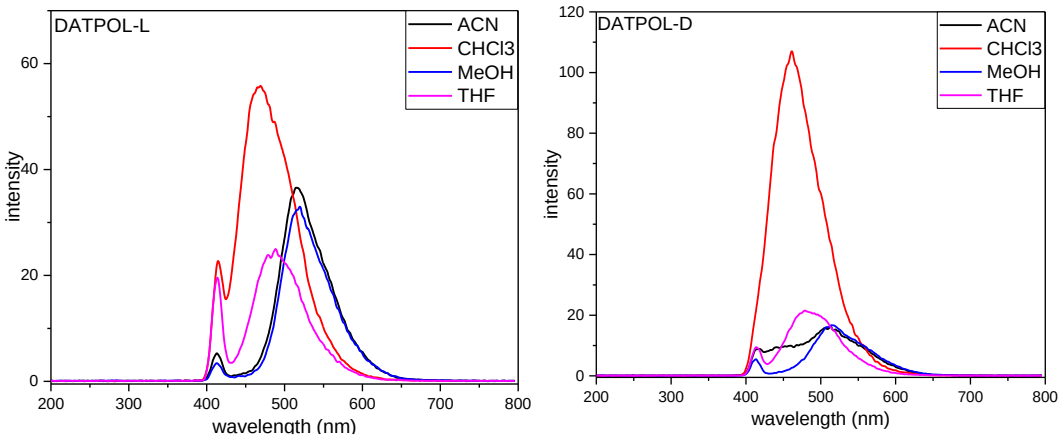

Figure 3.45. Fluorescence emission spectra of **DATPOL-L** and **DATPOL-D** Concentrations are 2.63×10^{-5} M.

CD studies of freshly prepared solutions with a concentration of 2.63×10^{-3} M in chloroform, THF, acetonitrile, and methanol were carried out, and the measurement was performed using 1 mm quartz cuvette. In our first measurements, we observed CD activity in their absorption region for all solutions. *D*- and *L*-polymers have reversed signals with respect to each other (Figure 3.46).

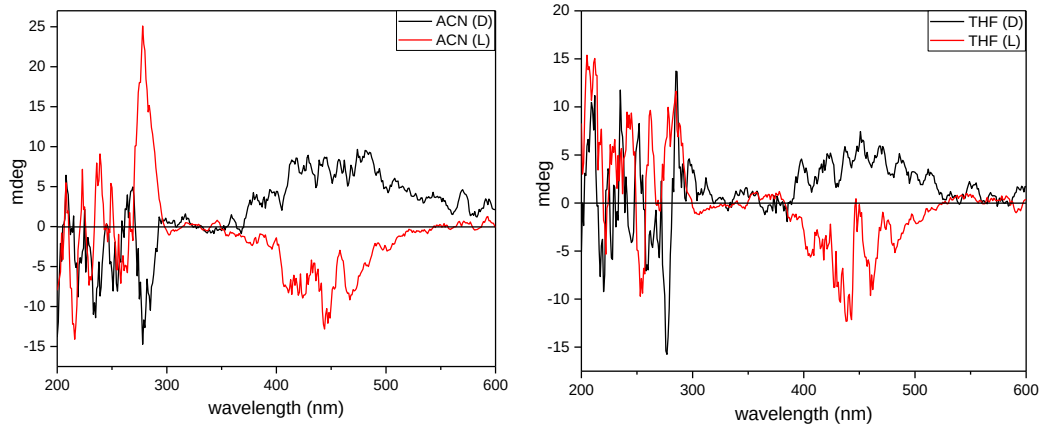

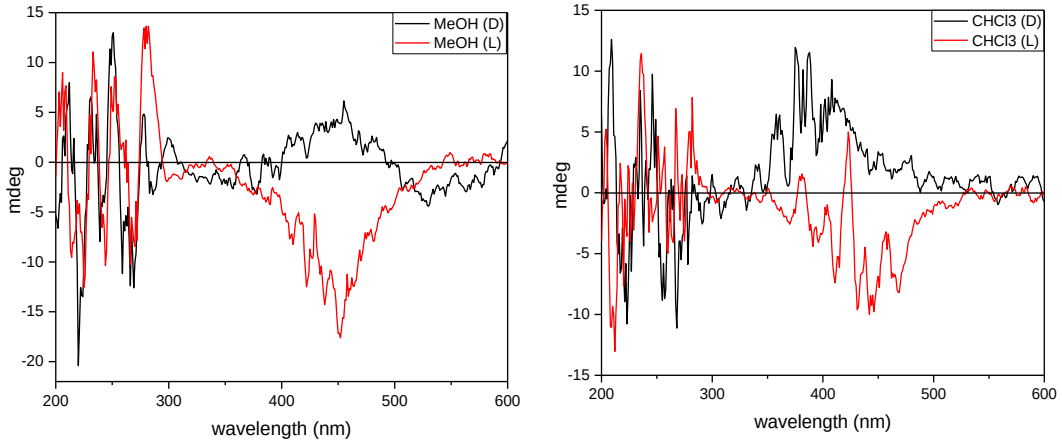

Figure 3.46. CD spectra of **DATPOL-L** and **DATPOL-D** in ACN, THF, MeOH, and $CHCl_3$

When we repeated the CD measurements for the compounds stored as solids for more than 2 weeks, we observed CD signals reversed in their absorption region. However, new red-shifted signals were observed (Figure 3.47). This implies that the segments interacted with each through intramolecular and intermolecular interactions, e.g, H-bond as minute amounts of solvent evaporated. When solids dissolved in solutions, these interactions were not broken despite the fact that we had homogenous solutions. Therefore, these new signals are due to the supramolecular chirality of **DATPOL**s.

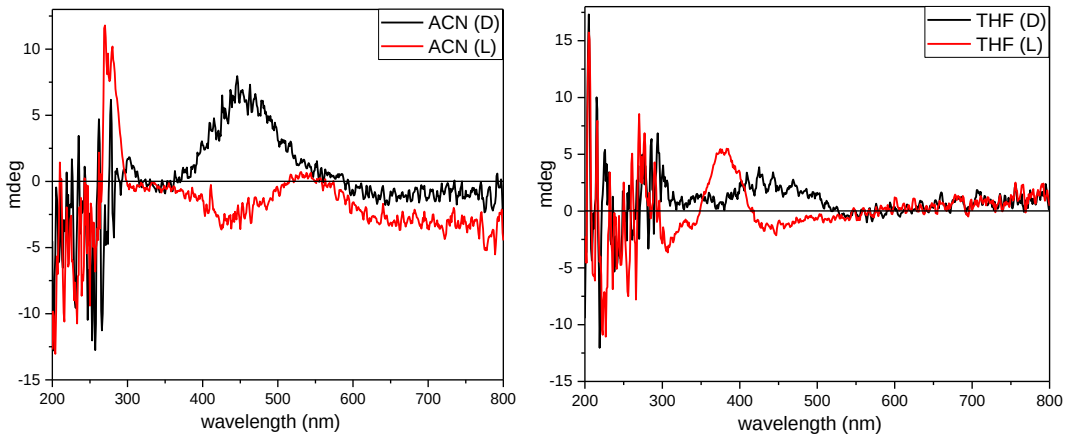

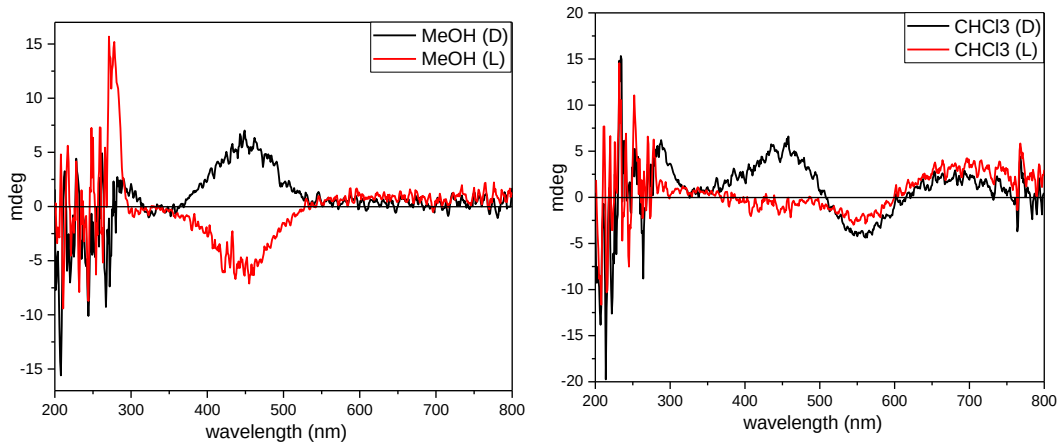

Figure 3.47. Repeated CD measurements of **DATPOL-L** and **DATPOL-D** in ACN, THF, MeOH, and $CHCl_3$ with freshly prepared solutions

Solutions from the second measurements were kept at 4 ^oC for a month. CD measurements were repeated for these solutions (Figure 3.48). In chloroform, a reverse signal in the absorption region was observed while a very pronounced CD signal at the same side around 550 nm appeared. This signal is not due to the chiroptical property of DATs. It is due to the chiral supramolecular assembly. In THF and acetonitrile, these signals were present but not as significant as in chloroform. Such signals are not present in MeOH throughout the studies. It shows H-bond donor and acceptor ability of MeOH restricts the segments forming chiral assemblies. We have observed such a thing for the model monomer **S-6**.

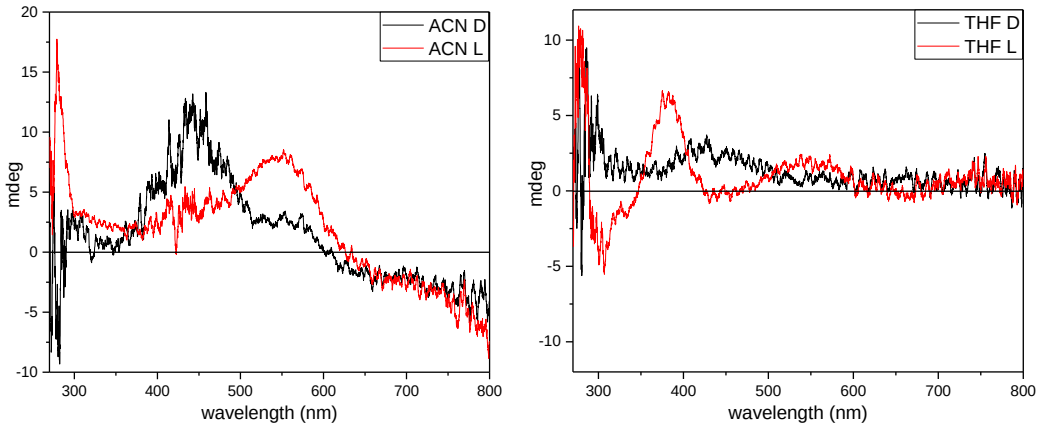

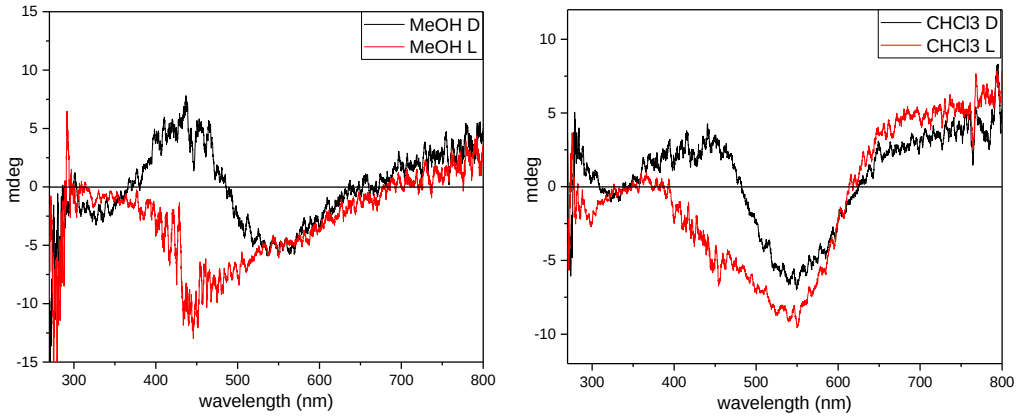

Figure 3.48. CD spectra of awaited solutions of **DATPOL-L** and **DATPOL-D** in ACN, THF, MeOH, and $CHCl_3$

3.5.2.4 Calculations

Due to the large number of atoms and the computational cost, we modeled a segment with four repeating units with PM6 semi-empirical model. For this purpose, a model of L-tartaric acid-derived compound was subjected to optimization at PM6 level. Figure 3.49 shows the optimized structure. From this structure, it was revealed that conformational space was large due to CH-CH_2-NH- rotation. Nevertheless, it was seen that there are helical segments in the polymer. These helical segments could be clockwise or counter-clockwise because of the rotatable bonds.

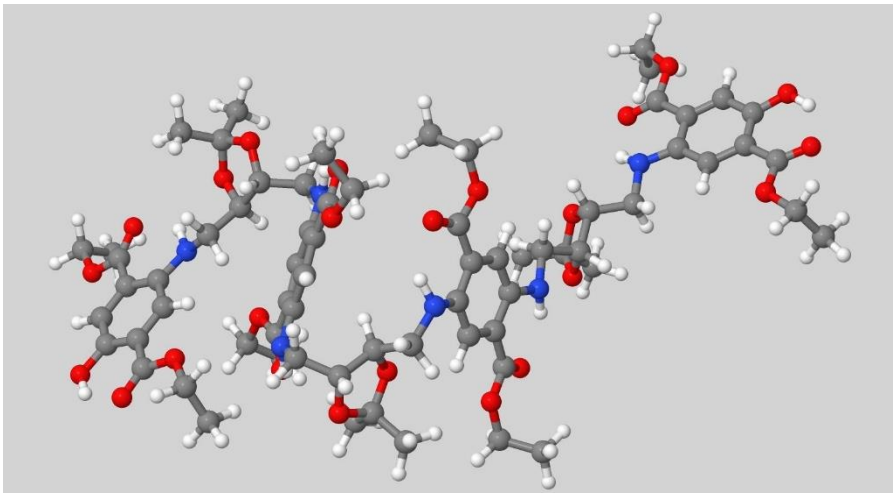

Figure 3.49. Optimized structure of **DATPOL-L**

3.5.3 Conclusion

Diamino terephthalates were shown to be solvatochromic due to their H-bonding property. Further, it was found that chiral amines substituted **DAT**s display chiroptical signals. When **TL-6** and **S-4** were subjected to polymerization, **DATPOL**s were obtained. Depending on the environment and storage conditions, **DATPOL**s were found to be forming chiral assemblies. The assemblies have CD activities that are presumably helical. Calculations showed that DATPOLs have helical segments, which further supports the helical assembly formation.

CHAPTER 4

CONCLUSION

In recent years, studies on artificial chiral polymers have become an attractive field due to their impressive optical activity and functions. In literature, the studies cover the artificial helical polymers, generally consisting of compounds whose helicity is induced through side chains; thus, these polymers mostly have a dynamic nature. Unlike the literature pointed out, we have designed helical polymers having chiral monomers in the backbone to control the main chain conformational configuration by the chiral backbone units. In the light of experience from previous studies, tartaric acid-derived monomers were chosen to form a chiral backbone. Furthermore, squaraine and diaminoterephthalate dyes were introduced to the polymers to make them easily characterized by optical spectroscopic techniques.

In the first part of the dissertation, squaraine dyes were investigated and studied from all perspectives. In this part, six squaraine dyes were successfully obtained and characterized. Among the six, three are novel, and their further characterization was completed with HRMS. Moreover, two novel enantiomeric pairs of squaraine dyes were also synthesized and characterized. Two enantiomerically pure amino acids, alanine and phenyl alanine, were used to induce chirality. Due to the lower solubilities of phenyl alanine-derived squaraine dyes, further studies were performed with alanine-derived squaraines **L-CSA-3** and **D-CSA-3.** From these studies, it was observed that these dyes have solvent-dependent chiroptical properties in their solvated state. Moreover, the aggregation studies revealed that chiral aggregates are formed in the same sense inferred from CD studies. These results concluded that side-chain aggregation is not prevailing over dye aggregation. Therefore, enantiomeric dyes aggregate in the same direction. It was also supported by the theoretical calculations.

In the second part, squaraine-containing chiral polymers, **SQPOL-L1,** and **SQPOL-D1** were synthesized with the help of the experience gained from the first part. Even though these dyes are prone to decomposition in protic solvents, the aggregation studies of these polymeric chiral dyes in the binary solvent system were accomplished. The studies with CD spectroscopy revealed that these dyes formed helical assemblies. The sense of helicity is controlled by the point chirality introduced to the polymers with tartaric acid units. Furthermore, the large chiral groups attached to the squaraine dyes affect the squaraine dyes' helicity in their aggregated form. Although studies were carried out on the synthesis of two more polymers with both enantiomeric forms of tartaric acid in this section, polymerization reactions could not be performed because monomers were obtained with low yields.

In the last part, diaminoterephthalate (**DAT**) was used as a chromophore in the backbone of tartaric acid-derived polymers **DATPOL-L** and **DATPOL-D**. Unlike the results obtained from previous parts, DAT polymers have CD activity in a single solvent due to their chiroptical properties. In this part, monomeric DAT **S-6** was synthesized as a model compound to compare the spectroscopic studies of polymers. It was found that DATs were shown to be solvatochromic due to their H-bonding ability. UV-Vis spectra of both model compound **S-6** and polymers have red-shifted absorption bands in the solvents having H-bonding properties with respect to chloroform. Theoretical calculations supported the results. Furthermore, storage conditions affected the behavior of the DATs in solutions. According to CD spectra, depending on the environment and storage conditions, **DATPOL**s were found to be forming chiral assemblies. Calculations showed that DATPOLs have helical segments, further supporting the helical assembly formation.

CHAPTER 5

EXPERIMENTAL

5.1 General Information

All starting materials and solvents, except ethyl acetate, and hexane, were purchased from Sigma Aldrich and were used without further purifications. Solvents used for Flash Chromatography were distilled prior to use (EtOAc and Hexane over $CaCl_2$). The reactions were monitored by thin-layer chromatography (TLC) (Merck Silica Gel 60 F254) and visualized by UV light at 254 nm.

Structural evaluation of the synthesized compounds was accomplished with the instruments stated below:

^{1}H and ^{13}C nuclear magnetic resonance spectra of the compounds were recorded in deuterated solvents with Bruker Avance III Ultrashield 400 Hz NMR spectrometer. The chemical shifts were stated in parts per million (ppm) with tetramethylsilane (TMS) as an internal reference. Spin multiplicities were indicated as s (singlet), d (doublet), dd (doublet of doublet), t (triplet), tt (triplet of triplet), m (multiplet), and coupling constants (J) were reported as in Hz (Hertz). ^{1}H NMR, ^{13}C NMR, and other NMR techniques spectra of compounds were given in Appendix A. NMR spectra were processed with MestReNova program. Infrared (IR) spectra were recorded with Thermo Scientific Nicolet iS10 ATR-IR spectrometer. Signal locations were reported in reciprocal centimeters (cm^{-1}). The IR spectra of the compounds synthesized are given in Appendix B. UV-Vis measurements were recorded with Shimadzu UV-2450 spectrophotometer. Spectroscopic measurements were carried out in methanol, dichloromethane, tetrahydrofuran, acetonitrile, hexane, and water. High-Resolution Mass Spectra (HRMS) were processed in positive mode on (ES+) using Time of Flight mass analyzer. The high-resolution mass spectra of compounds

synthesized are given in Appendix C. Fluorescence measurements were recorded with Perkin Elmer LS55 spectrofluorometer. CD measurements were recorded with Jasco J-1500 CD Spectrometer. XRD measurements were performed by a Rigaku Mini-Flex X-ray powder Diffractometer (XRD) with a radiation source of Cu-Kα line (λ=1,54056 Å) to confirm phase purity. All spectra were processed with OriginPro 2015.

Aggregation Studies:

For L-CSA-3 and D-CSA-3

Stock solutions were prepared for both enantiomeric forms of alanine dyes L-CSA-3 and D-CSA-3 with concentrations 2.50×10^{-5} M by dissolving in good solvent (chloroform or acetonitrile). For each measurement, 1 mL of stock solution was taken into quartz cuvette and diluted with 2 mL good and poor solvent (acetonitrile or water) mixture to get a 0.83×10^{-5} M solution. The poor solvent volume percentage ranges from 3% to 66% with respect to total volume in a quartz cuvette. The cuvette was shaken four times gently, and measurements were performed immediately.

For SQPOL-L1 and SQPOL-D1

Stock solutions were prepared for both enantiomeric forms of alanine dyes **SQPOL-L1** and **SQPOL-D1** with concentrations of 1.79×10^{-3} M by dissolving in a good solvent (THF). For each measurement, 1 mL of stock solution was taken into quartz cuvette and diluted with 2 mL good and poor solvent (MeOH) mixture to get a 5.96×10^{-4} M solution. The poor solvent volume percentage ranges from 10% to 100% with respect to the total volume (2 mL) added in a quartz cuvette containing 1 ml stock solution. The cuvette was shaken four times gently, and measurements were performed immediately.

5.2 Synthesis of dimethyl (2R,3R)-2,3-dihydroxysuccinate[182]

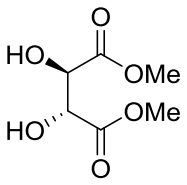

TL-1

To L-tartaric acid (5.00 g, 33.31 mmol) solution in 16 ml methanol, $SOCl_2$ (20.74 g, 174.33 mmol) was added slowly in a water-ice bath. After an hour of stirring, the mixture was heated to reflux temperature for 3 hours to give a pale yellow solution. After cooling down, solvent and excess thionyl chloride were removed under vacuo to yield an oily product. Yield: 5.45 g 93%.

^{1}H NMR ($CDCl_3$): δ 4.50 (s, 2H), 3.80 (s, 6H), 3.11-3.10 (bs, 2 -OH)

5.3 Synthesis of dimethyl (4R,5R)-2,2-dimethyl-1,3-dioxolane-4,5-dicarboxylate[181]

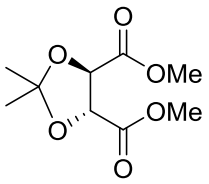

TL-2

To a solution of L-dimethyl tartrate **TL-1** (8.00 g, 44.91 mmol) in 20.00 ml DMF, 2-2 dimethoxy propane (28.71 g, 275.75 mmol) and 0.4 g *p*-TSA were added. The mixture was refluxed overnight and then concentrated under reduced pressure. The resulting residue was treated with a 2% of $NaHCO_3$ solution and extracted with $CHCl_3$. The organic phase was washed with water, dried with Na_2SO_4, filtered, and $CHCl_3$ was removed under reduced pressure. The product was obtained as oily dark brown residue. Yield: 8.01 g, 82%.

^{1}H NMR ($CDCl_3$): δ 4.75 (s, 2H), 3.76 (s, 6H), 1.43 (s, 6H)

5.4 Synthesis of diethyl (4R,5R)-2,2-dimethyl-1,3-dioxolane-4,5-dicarboxylate

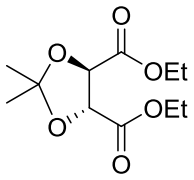

TL-2a

The title compound was synthesized following the procedure described for **TL-2** using L-diethyl tartrate as a starting material. Yield: 90%.

^{1}H NMR (400 MHz, $CDCl_3$) δ 4.76 (s, 2H), 4.27 (q, *J* = 7.1 Hz, 4H), 1.49 (s, 6H), 1.31 (t, *J* = 7.1 Hz, 6H).,

5.5 Synthesis of diethyl (4S,5S)-2,2-dimethyl-1,3-dioxolane-4,5-dicarboxylate

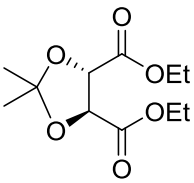

TD-2a

The title compound was synthesized following the procedure described for **TL-2** using D-diethyl tartrate as a starting material of **TD-2a**. Yield: 85%.

5.6 Synthesis of sodium (4R,5R)-2,2-dimethyl-1,3-dioxolane-4,5-dicarboxylate[181]

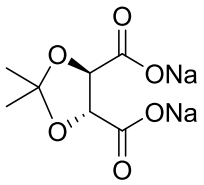

TL-3

Dimethyl tartrate **TL-2** (3,00 gr; 12.18 mmol) was added to a NaOH (1.1 g, 26.80 mmol) solution in EtOH (30 mL) and heated to 70 ºC, while NaOH was dissolved in 5 mL of water and diluted with 25 mL EtOH. The NaOH solution was added to the reaction mixture dropwise. After the addition was completed, the mixture was refluxed for 15 min. The target compound was obtained as a white solid after the removal of EtOH and washed with cold EtOH. Yield: 2.5 g, 88%.

^{1}H NMR (400 MHz, D_2O) δ 4.30 (s, 2H), 1.26 (s, 6H).

5.7 Synthesis of sodium (4S,5S)-2,2-dimethyl-1,3-dioxolane-4,5-dicarboxylate

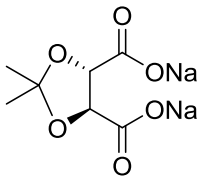

TD-3

The title compound was synthesized following the procedure described for **TL-3** using **TD-2** as a starting material. Yield: 70%.

5.8 Synthesis of (4R,5R)-2,2-dimethyl-1,3-dioxolane-4,5-dicarboxylic acid[181]

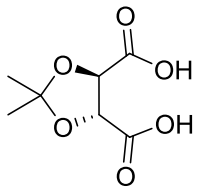

TL-4

Sodium (4R,5R)-2,2-dimethyl-1,3-dioxolane-4,5-dicarboxylate **(TL-3)** (2.34 g, was dissolved in water and cooled in an ice bath.The solution was acidified with 1M HCl until pH≤ 2 and extracted with EtOAc. The organic phase was dried over $MgSO_4$ and filtered off. The solvent was removed under vacuo to obtain the title compound as a white solid. Yield: 1.00 g, 53%.

^{1}H NMR (400 MHz, $CDCl_3$) δ 4.92 (s, 2H), 1.56 (s, 6H).

5.9 Synthesis of (4S,5S)-2,2-dimethyl-1,3-dioxolane-4,5-dicarboxylic acid[181]

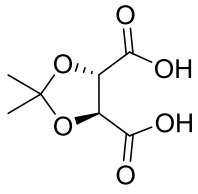

TD-4

The title compound was synthesized following the procedure described for **TL-4** using **TD-3** as a starting material. Yield: 60%.

5.10 Synthesis of (4R,5R)-2,2-dimethyl-1,3-dioxolane-4,5-dicarboxamide[183]

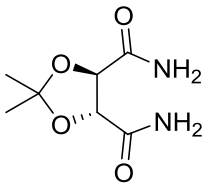

TL-5

Solution of diethyl 2,2-dimethyl-1,3-dioxolane-4,5-dicarboxylate **(TL-2)** (3.1 g, 12.59 mmol) in EtOH (30 mL) was cooled with liquid nitrogen to -40°C and ammonia gas was bubbled through the solution until it was saturated. The resulting solution is directly placed in the high-pressure reactor and heated overnight to 55 ^{o}C. After cooling the resulting medium to room temperature, excess ammonia and ethanol were removed in vacuo to yield brown solids Yield: 2.17 g, 92%.

^{1}H NMR (400 MHz, DMSO) δ 7.49 (s, 2H), 7.42 (s, 2H), 4.43 (s, 2H), 1.39 (s, 6H).

5.11 Synthesis of (4S,5S)-2,2-dimethyl-1,3-dioxolane-4,5-dicarboxamide[183]

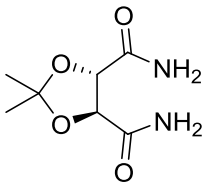

TD-5

The title compound was synthesized following the procedure described for **TL-5** using **TD-2** as a starting material. Yield: 95%.

5.12 Synthesis of ((4R,5R)-2,2-dimethyl-1,3-dioxolane-4,5-diyl)dimethanamine[183]

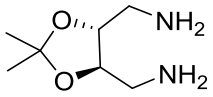

TL-6

To a solution of $LiAlH_4$ (1.3 g, 33.23 mmol, 2.5 eq) in THF, compound **TL-5** (2.5 g, 13.29 mmol, 1 eq) was extracted with a Soxhlet thimble. The resulting mixture was refluxed for 6 hours, followed by stirring at room temperature for 16 hours. Afterward, the reaction was quenched by a minimum amount of water and 15% NaOH solution. The mixture was filtered, and precipitates were washed several times with THF. THF was removed *in vacuo* from combined filtrates to yield the corresponding diamine Yield: 1.1g, 52 %.

^{1}H NMR (DMSO-d$_6$): δ 3.69-3.63 (m,2H), 2.75-2.65 (m, 4H), 1.29 (s, 6H)

5.13 Synthesis of ((4S,5S)-2,2-dimethyl-1,3-dioxolane-4,5-diyl)dimethanamine[183]

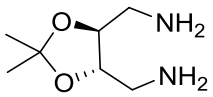

TD-6

The title compound was synthesized following the procedure described for **TL-6** using **TD-5** as a starting material. Yield: 40%.

5.14 Synthesis of (2R,3R)-2,3-dihydroxysuccinohydrazide[184]

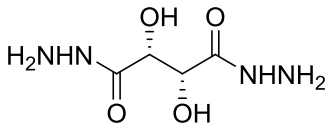

TL-7

To a solution of (+)-diethyl L-tartrate (5 mL, 29.2 mmol) in ethanol (40 mL), Hydrazine monohydrate (3.1 mL, 116.8 mmol) was added, and the mixture was refluxed for 1 h. The precipitate was filtered off, washed with MeOH, Et_2O, and dried to obtain the target compound as a white solid. Yield: 1.65 g, 95%.

^{1}H NMR (400 MHz, DMSO-d_6) δ 8.79 (2H, bs, -NH), 5.37 (2H, d, *J* = 7.3 Hz), 4.25-4.22 (6H, m,-NH_2 and -OH)

5.15 (4R,5R)-2,2-dimethyl-1,3-dioxolane-4,5-dicarbohydrazide

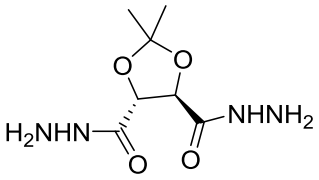

TL-8

Hydrazine monohydrate (1.62 g; 32.5 mmol) was added to a stirred solution of **TL-2a** (2.00 g, 8.12 mmole) in EtOH. The resulting mixture was refluxed for 7h. The removal of the solvent yielded the title compound **TL-8** as a viscous yellow oil. Yield: 1.7 g, 96%.

^{1}H NMR (400 MHz, DMSO-d_6) δ 9.39 (bs, 2H), 4.45 (s, 2H), 3.50 (bs, 4H), 1.38 (s, 6H).

5.16 (4R,5R)-2,2-dimethyl-1,3-dioxolane-4,5-dicarbohydrazide

The title compound was synthesized following the procedure described for **TL-8** using **TD-2a** as a starting material. Yield: 95%.

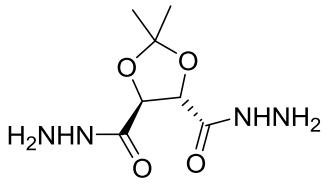

TD-8

5.17 (4R,5R)-N^4,N^5-bis(2-aminoethyl)-2,2-dimethyl-1,3-dioxolane-4,5dicarboxamide[185]

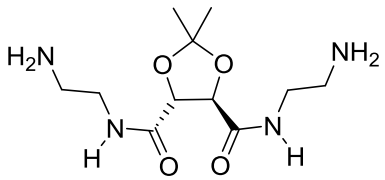

TL-9

Diethyl 2,2-dimethyl-1,3-dioxolane-4,5-dicarboxylate **TL-2a** (1 g, 4.1 mmol) and ethylenediamine (5 mL, 74.9 mmol) were mixed at room temperature in a round bottomed-flask, and the resulting mixture was stirred 2 days at room temperature. Excess ethylenediamine was co-evaporated with methanol and toluene several times *in vacuo* and vacuum-dried for 1 day. Yield: 1 g, 88.9%.

^{1}H NMR (400 MHz, DMSO-d_6) δ 8.05 (t, *J* = 5.3 Hz, 2H), 4.48 (s, 2H), 3.15 – 3.06 (m, 4H), 2.62 – 2.56 (m, 4H), 1.40 (s, 6H).

5.18 (4S,5S)-N^4,N^5-bis(2-aminoethyl)-2,2-dimethyl-1,3-dioxolane-4,5-dicarboxamide

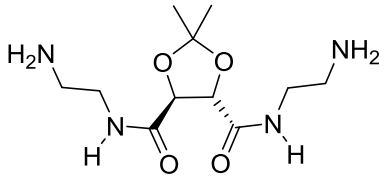

TD-9

The title compound was synthesized following the procedure described for **TL-9** using **TD-2a** as a starting material. The compound was obtained as a white-beige solid. Yield: 85%.

5.19 Synthesis of (2R,3R)-2,3-dihydroxy-1,4-bis(4-phenylpiperazin-1-yl)butane-1,4-dione[186]

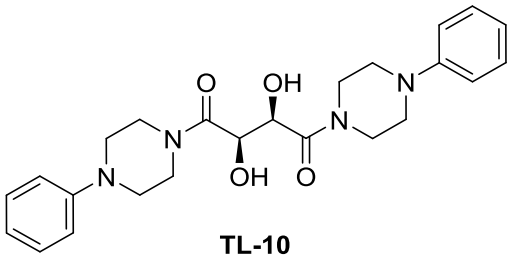

TL-10

To a 100 ml round-bottomed flask containing 1-phenyl piperazine (1.08 g, 6.66 mmol) in DMF (30 mL), EDC.HCl (1.53 g, 8.00 mmol), DIEA (2.8 mL, 16.65 mmol) and HOBt (1.07 g, 8.00 mmole) were added under Argon atmosphere. The resulting solution was stirred at room temperature for 15 min, and L-tartaric acid (0.5 g, 3.33 mmol) was introduced to the solution. The reaction mixture was continued to stir for 16 h at room temperature. DMF was removed under reduced pressure. The resultant residue was purified by extraction using dichloromethane as an organic solvent. The organic phase was washed with $NaHCO_3$ solution (x2), water (x3), and brine and dried over Na_2SO_4. Dichloromethane was removed under reduced pressure.

Obtained yellowish crystals were triturated with EtOH for further purification. The target compound was obtained as white-beige crystals. Yield: 0.86 g, 59%. Rf value in EtOAc: 0.47. Melting point: 158-165 °C.

^{1}H NMR (400 MHz, $CDCl_3$) δ 7.33 – 7.24 (m, 4H), 6.95-6.90 (dd, J = 8.2, 2.8 Hz, 6H), 4.73 (d, J = 5.7 Hz, 2H), 4.29 (d, J = 6.3 Hz, 2H), 3.91-3.71 (m, 8H), 3.30-3.13 (m, 8H).

^{13}C NMR (101 MHz, $CDCl_3$) δ 169.84, 150.81, 129.29, 120.73, 116.79, 70.27, 49.86, 49.37, 45.75, 42.78

IR (cm^{-1}): 3392 (w), 3304 (w), 3037 (w), 2970 (w), 2906 (w), 2819 (w), 1620 (s), 1596 (s), 1489 (m), 1453 (m), 1381 (m), 1318 (m), 1230 (s), 1146 (m), 1075 (m), 1015 (s), 971 (m), 892 (s), 848 (m), 752 (s)

HRMS: (ESI-MS) m/z: $[M+H]^+$ calculated for $C_{24}H_{31}N_4O_4$: 439.2345, found: 439.2345

5.20 Synthesis of (2S,3S)-2,3-dihydroxy-1,4-bis(4-phenylpiperazin-1-yl)butane-1,4-dione

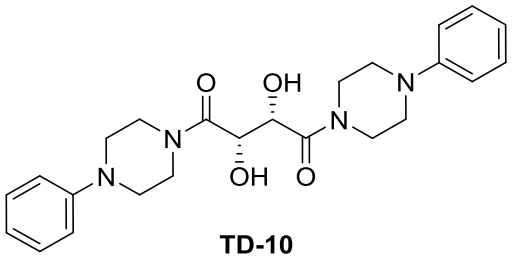

TD-10

The title compound was synthesized following the procedure described for **TL-10** using **D-tartaric acid** as a starting material. The compound was obtained as a white-beige solid. Yield: 0.80 g, 58%.

5.21 Synthesis of ((4R,5R)-2,2-dimethyl-1,3-dioxolane-4,5-diyl)bis((4-phenylpiperazin-1-yl)methanone)

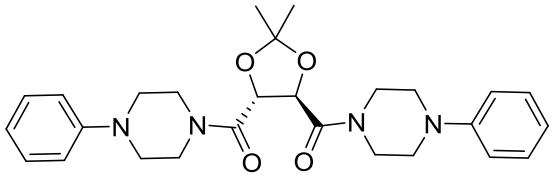

TL-11

To the solution of **TL-10** (0.53g, 1.21 mmol) in DMF (7ml), 2,2 dimethoxypropane (0.5 mL, 3.63 mmol) and a catalytic amount of p-TSA were added. The resulting solution was heated to 100 ^{o}C and stirred at this temperature for 6h. After cooling the mixture to room temperature, dichloromethane was added, and extraction was performed with saturated $NaHCO_3$ solution (x3), water (x3), and brine. The organic phase dried over Na_2SO_4, and dichloromethane was removed under reduced pressure. Column chromatography was applied with the hexane/ethyl acetate solvent system for purification. The target compound was obtained as a white solid. Yield: 0.38 g, 66%. R_f value in 1:1 (EtOAc: Hexane):0.48. Melting point: 128-138 °C.

^{1}H NMR (400 MHz, $CDCl_3$) δ 7.31-7.27 (m, 4H), 6.95-6.89 (m, 6H), 5.38 (s, 2H), 3.98 – 3.86 (m, 4H), 3.81 – 3.66 (m, 4H), 3.30-3.12 (m, 8H), 1.44 (s, 6H).

^{13}C NMR (101 MHz, $CDCl_3$) δ167.07, 150.96, 129.26, 120.53, 116.66, 112.32, 75.36, 49.87, 49.32, 45.57, 42.28, 26.52.

IR (cm^{-1}): 2986 (w), 2906 (w), 2810 (w), 1640(s), 1596 (s), 1500 (m), 1441 (s), 1377 (m), 1230 (s), 1210 (s), 1154 (s), 1015 (s), 876 (m), 760 (s),

HRMS: (ESI-MS) m/z: $[M+H]^+$ calculated for $C_{27}H_{35}N_4O_4$: 479.2658, found: 479.2657

5.22 Synthesis of ((4S,5S)-2,2-dimethyl-1,3-dioxolane-4,5-diyl)bis((4-phenylpiperazin-1-yl)methanone)

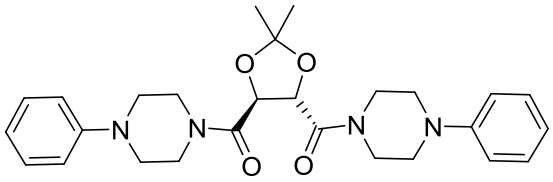

TD-11

The title compound was synthesized following the procedure described for **TL-11** using **TD-10** as a starting material. The compound was obtained as a white-beige solid. Yield: 0.80 g, 58%.

5.23 Synthesis of (4R,5R)-2,2-dimethyl-N^4,N^5-bis(2-(4-phenylpiperazin-1-yl)ethyl)-1,3-dioxolane-4,5-dicarboxamide

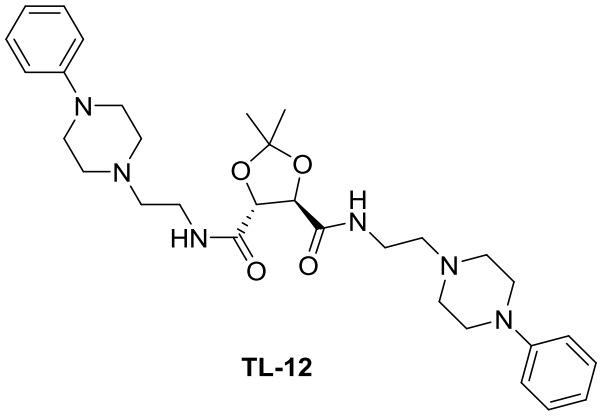

TL-12

5.23.1 Method (A)[186]

To a solution of protected tartaric acid **TL-4** (0.22 g, 1.17 mmol) in DMF (15 mL), EDC (0.5 mL, 2.8 mmol) and HOBt (0.38 g, 2.8 mmol) were added. After stirring for 1 hour at room temperature under Ar atmosphere, 2-(4-phenylpiperazin-1-

yl)ethan-1-amine (0.48 g, 2. 34 mmol) was added to the reaction mixture and stirred overnight at room temperature. Extraction was performed with $NaHCO_3$(aq) and DCM. Combined organic layers are dried over Na_2SO_4, and DCM is removed under vacuo. The resulting product was further purified with column chromatography, and the desired product was collected in 1:15 MeOH/EtOAc. Yield: 0.03 g, 3%.

^{1}H NMR (400 MHz, $CDCl_3$) δ 7.36-7.32 (m, 2H), 7.31 – 7.25 (m, 4H), 6.95 (d, *J* = 7.9 Hz, 4H), 6.89 (t, *J* = 7.3 Hz, 2H), 4.65 (s, 2H), 3.55 – 3.40 (m, 4H), 3.26 – 3.18 (m, 8H), 2.70 – 2.63 (m, 8H), 2.62 – 2.57 (m, *J* = 6.0, 2.9 Hz, 4H), 1.51 (s, 6H).

5.23.2 Method (B)

L-diethyl tartrate (0.22 mL,1.06 mmol) was added to a round-bottomed flask containing compound **P-9** (0.46 g; 2.24 mmol). The reaction mixture was stirred at room temperature for 4 days. The reaction was monitored by TLC. To the mixture 15 mL ethanol was added, and the white solids formed filtrated. Yield: 0.05 g, 7%. The raw ^{1}H NMR data of this compound is shown in Appendix A.

5.23.3 Method (C)[187]

2-(4-phenylpiperazin-1-yl)ethan-1-amine (**P-9)** (0.4 g, 1.95 mmol) and NaCN (0.01 g, 0.2 mmol) were added to a solution of protected diethyl tartrate **TL-2a** (0.24 g, 0.98 mmol) in EtOH (20 mL). The resulting mixture was refluxed for 20 hours. EtOH was removed under vacuo, and the crude product was purified by column chromatography. (All compound was used for NMR analyses).

^{1}H NMR (400 MHz, $CDCl_3$) δ 7.39 – 7.34 (m, 2H), 7.32 – 7.26 (m, 4H), 6.95 (m, 4H), 6.88 (m, 2H), 4.65 (s, 2H), 3.52 – 3.40 (m, 4H), 3.21 (m, 8H), 2.72 – 2.63 (m, 8H), 2.61 – 2.55 (m, *J* = 2.1 Hz, 4H), 1.50 (s, 6H).

5.23.4 Method (D)[188]

To a solution of N4,N5-bis(2-aminoethyl)-2,2-dimethyl-1,3-dioxolane-4,5-dicarboxamide **TL-9** (0.5 g, 1.8 mmol) in EtOH (15 mL), Na_2CO_3 (1.14 g, 10.8 mmol), KI (0.54 g, 3.6 mmol) and N,N-bis(2-chloroethyl)aniline (0.78 g, 3.6 mmol) were added. The resulting mixture refluxed overnight under Ar atmosphere. After cooling down to room temperature, white precipitates were filtered off, and EtOH was removed under vacuo. Extraction was performed by adding DCM and water to the residue. The organic phase was dried over anhydrous Na_2SO_4, and the solvent was removed under vacuo. For further purification, column chromatography was performed. (Solvent system: 1:15 MeOH/EtOAc) To remove the remaining impurities, the compound was dissolved in Et_2O, and white precipitates were filtered off. The filtrate was concentrated under vacuo to yield white solids as the desired compound. Yield: 0.05 g, 7%

^{1}H NMR (400 MHz, $CDCl_3$) δ 7.37 (t, *J* = 5.3 Hz, 2H), 7.29 (t, 6H), 6.95 (d, 5H), 6.89 (t, 2H), 4.64 (s, 2H), 3.51 – 3.46 (m, 4H), 3.24 – 3.19 (m, 8H), 2.79 – 2.75 (m, 2H), 2.71 – 2.66 (m, 8H), 2.63 – 2.60 (m, 3H), 1.51 (s, 6H).

HRMS: (ESI-MS) m/z: $[M+H]^+$ calculated for $C_{31}H_{45}N_6O_4^+$ 565.3502, found 565.3503

5.24 Synthesis of (4S,5S)-2,2-dimethyl-N^4,N^5-bis(2-(4-phenylpiperazin-1-yl)ethyl)-1,3-dioxolane-4,5-dicarboxamide

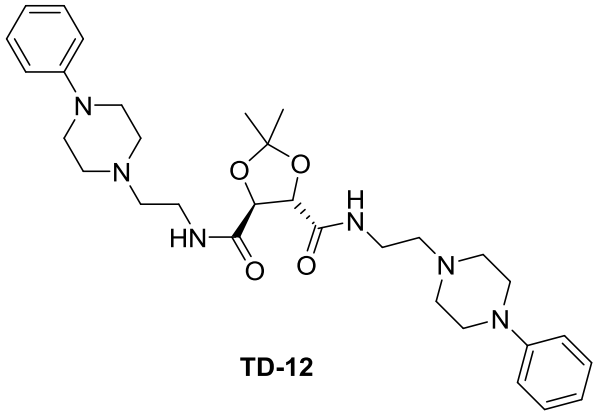

TD-12

The title compound was synthesized following the procedure in **Method (D)** described for **TL-12** using **TD-9** as a starting material. The compound was obtained as a white-beige solid. Yield: 0.04 g, 7%.

5.25 Synthesis of (4R,5R)-2,2-dimethyl-N4,N5-bis(4-phenylpiperazin-1-yl)-1,3-dioxolane-4,5-dicarboxamide[188]

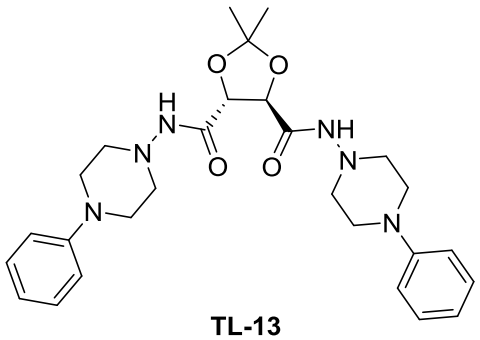

TL-13

To a solution of **TL-8** in EtOH, Na_2CO_3 (3.83g, 36.18 mmol), KI (1.8 g, 12.06 mmol), and N, N-bis(2-chloroethyl)aniline **(R2)** were added. The resulting mixture was stirred under reflux overnight. After cooling down to room temperature, white precipitates were filtered off, and the filtrate was concentrated under reduced pressure. For purification, extraction was performed with DCM. Yield: < 2%.

^{1}H NMR (400 MHz, $CDCl_3$) δ 9.80 (s, 2H), 7.31 – 7.23 (m, 4H), 6.79 (t, *J* = 7.3 Hz, 2H), 6.73 – 6.67 (m, 4H), 4.69 (s, 2H), 3.78 – 3.71 (m, 8H), 3.67 – 3.61 (m, 8H), 1.57 (s, 6H).

5.26 Synthesis of 1-methyl-4-phenylpiperazine[164]

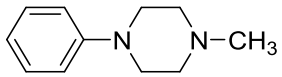

P-1

To a round bottomed-flask K_2CO_3 (7.26 g; 52.5 mmol), CuCl (0.25 g; 2.5 mmol), and N-methyl-2-pyrrolidone (NMP) (15 mL) were added, and the flask was flushed with N_2. After the addition of bromobenzene (5.2 mL; 50 mmol), N-methyl piperazine (6.7 mL; 60 mmol), and acetylacetone (0.64 mL; 6.25 mmol; as a ligand), the reaction mixture was heated to 130^{o}C and refluxed for 16 h under N_2 atmosphere. After reaction completion, extraction was performed with 1N Na_2CO_3 solution and DCM. The organic phase was dried over Mg_2SO_4, filtered, and the solvent was removed under reduced pressure. Yield: 0.61 g, 6%.

^{1}H NMR (400 MHz, $CDCl_3$) δ 7.30 (t, *J* = 8.0 Hz, 2H), 6.97 (d, *J* = 8.5 Hz, 2H), 6.89 (t, *J* = 7.3 Hz, 1H), 3.29 – 3.20 (m, 4H), 2.65 – 2.55 (m, 4H), 2.38 (s, 3H).

5.27 Synthesis of 1-(4-phenylpiperazin-1-yl)ethan-1-one[189]

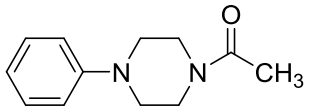

P-2

To a round-bottomed flask 1-phenyl piperazine (2.00 g; 12.33 mmol) was added and dissolved in 50 mL DCM. To the stirring solution, acetic anhydride (2.38 ml; 26.76 mmol), pyridine (0.7 g; 13.56 mmol), and catalytic amount of 4-(dimethylamino) pyridine) were added. The resulting mixture was stirred at room temperature for 24

h. After reaction completion (checked by TLC monitoring), the reaction mixture was washed with saturated $NaHCO_3$ solution (3x, 100 mL). The organic phase was dried over Na2SO4, and the solvent was evaporated under reduced pressure to get the target compound as a white solid. Yield: 2.3 g, 91%.

^{1}H NMR (400 MHz, $CDCl_3$) δ 7.20 (dd, *J* = 8.7, 7.3 Hz, 2H), 6.92 – 6.75 (m, 3H), 3.74 – 3.62 (m, 2H), 3.58 – 3.47 (m, 2H), 3.18 – 2.96 (m, 4H), 2.05 (s, 3H).

5.28 Synthesis of tert-butyl 4-phenylpiperazine-1-carboxylate[190]

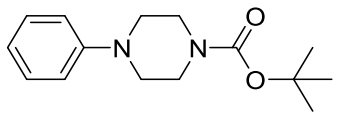

P-3

To a stirred mixture of 1-phenyl piperazine (2.00 g; 13.33 mmol) and di-tert butyl dicarbonate (2.69 g, 12.33 mmol) catalytic amount of I_2 was added under solvent-free conditions at room temperature. After 45 min. stirring, Et_2O was added to the reaction mixture, and it was washed with $Na_2S_2O_3$ (5% ~10 mL) to quench excess iodine. To the resulting solution saturated $NaHCO_3$ solution was added, and extraction was performed. The organic phase was dried over Na_2SO_4, and the solvent was evaporated under reduced pressure to get the target compound as a white solid. Yield: 2.67 g, 76%.

^{1}H NMR (400 MHz, $CDCl_3$) δ 7.32-7.26 (m, 2H), 6.97-6,91 (m, 1H), 3.63-3.58 (m, 4H), 3.17-3.12 (m, 4H), 1.51 (s, 9H).

^{13}C NMR (101 MHz, $CDCl_3$) δ 154.75, 153.83, 129.22, 120.35, 116.68, 79.91, 49.47, 28.44.

5.29 Synthesis of 1-butyl-4-phenylpiperazine

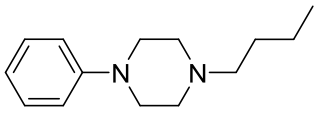

P-4

Phenyl piperazine (1.00 g; 6.16 mmol), bromobutane (0.80; 6.78 mmol), and K_2CO_3 (2.55 g, 18.48 mmol) in acetonitrile was refluxed for 15h. After cooling down to room temperature, solids were filtered, and the filtrate part was concentrated under reduced pressure. Yield: 1.1 g, 52%.

^{1}H NMR (400 MHz, $CDCl_3$) δ 7.25 (t, *J* = 8.0 Hz, 2H), 6.92 (d, *J* = 8.5 Hz, 2H), 6.84 (t, *J* = 7.3 Hz, 1H), 3.23 – 3.16 (m, 4H), 2.72 – 2.52 (m, 4H), 2.37 (dd, *J* = 8.8, 6.7 Hz, 2H), 1.58 – 1.46 (m, 2H), 1.43 – 1.25 (m, 2H), 0.93 (t, *J* = 7.3 Hz, 3H).

5.30 Synthesis of 1-nitroso-4-phenylpiperazine[191,192]

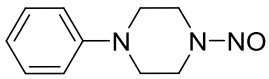

P-5

To a mixture of 1-phenylpiperazine (10.8 g; 66.57 mmol) in 200 mL water, 1N HCl was added dropwise until the pH was 5-6. A solution of $NaNO_2$ in 15 mL water was added over a period of 10 minutes, keeping the pH 5-6 by adding 15% HCl to the center of the stirring reaction flask. The resulting solution was stirred at room temperature for 1h and then kept in the fridge for an additional 1h. Yellowish solids were filtered and recrystallized in Et_2O and petroleum ether. Yield: 10.17g, 80%.

^{1}H NMR (400 MHz, $CDCl_3$) δ 7.35-7.31 (m, 2H), 7.00-6.96 (m, 3H), 4.46-4.44 (m, 2H), 4.03-4.00 (m, 2H), 3.46-3.44 (m, 2H), 3.23, 3.20 (m, 2H).

5.31 Synthesis of 4-phenylpiperazin-1-amine[191,192]

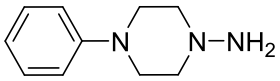

P-6

To the solution of 1-nitroso, 4-phenylpiperazine (2.13 g; 11.13 mmol) in 30 mL acetic acid, 5 mL of water, and 5 mL of concentrated HCl were added and while stirring Zn dust (4.00 g; 61.18 mmol) was added slowly. The reaction was stirred at room temperature until all nitroso moiety was reduced to amine, checked by TLC monitoring. (If necessary, the reaction mixture could be heated to 50 ^{o}C for 3 h). after reaction completion, solvents were removed under reduced pressure, and the remaining part was basified with a 4M NaOH solution. Solids formed during this period were filtered. The filtrate part was extracted with DCM, and the organic phase was dried over Na_2SO_4 and filtered. The resulting brown residue was crystallized DCM by keeping the solution in the fridge. Yield: 0.64 g 35%.

^{1}H NMR (400 MHz, DMSO) δ 9.29 (2H bs), 7.28-7.24 (m 2H), 7.00-6.98 (m 2H), 6.87-6.84 (m 2H), 3.37-3.35 (m 2H), 3.21-3.18 (m 2H).

5.32 Synthesis of tert-butyl piperazine-1-carboxylate[193]

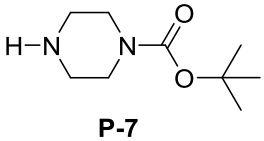

P-7

To a mixture of piperazine (5 g; 58.05 mmol), triethylamine (13 ml; 87.08 mmol) in methanol (50 mL), di-tert-butyl dicarbonate was added slowly (5.1 g; 23.22 mmol) and continued stirring at room temperature until the starting material was consumed. After the resulting reaction mixture was concentrated under reduced pressure, EtOAc was added, and the solids were filtered off. The filtrate was washed with water (x3),

dried over Na_2SO_4, and EtOAc was evaporated under reduced pressure to give the title compound as a colorless oil. Yield: 4 g, 92%.

^{1}H NMR (400 MHz, $CDCl_3$) δ 3.39 (m, 4H), 2.92 – 2.70 (m, 4H), 1.46 (s, 9H).

5.33 Synthesis of 2-(2-(4-phenylpiperazin-1-yl)ethyl)isoindoline-1,3-dione[194]

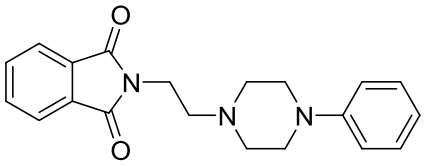

P-8

To a solution of (2-bromoethyl)phtalimide (6.26 g; 24.66 mmol) in acetonitrile, phenyl piperazine (4.00 g; 24.66 mmol), K_2CO_3 (6.82 g; 49.32 mmol), and potassium iodide (1.64 g; 9.86 mmol) was added. The resulting mixture was refluxed for 48 h, and acetonitrile was removed under reduced pressure. Water was added to the remaining yellow solids, washed with water, and dissolved in DCM. Extraction was performed by adding water, and the organic phase was dried over Na_2SO_4. The solvent was removed under vacuo, and the title compound was obtained as a yellow solid. Yield: 6.17 g, 75%.

^{1}H NMR (400 MHz, $CDCl_3$): δ 7.88-7.85 (m, 2H), 7.75-7.72 (m, 2H), 7.25 (d, 2H), 6.92 (d, 2H), 6.85 (t, 1H), 3.89 (t, 2H), 3.16 (t, 4H), 2.71 (m, 6H).

5.34 Synthesis of 2-(4-phenylpiperazin-1-yl)ethan-1-amine[194]

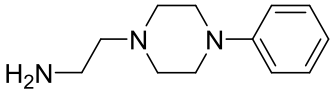

P-9

Hydrazine monohydrate was added to a solution of 2-(2-(4-phenylpiperazin-1-yl)ethyl)isoindoline-1,3-dione (1.07 g; 3.18 mmol), and the resulting mixture was refluxed for 4 h. Formed white solids were filtered off and washed with water to get a yellow oily product. Yield: 0.55 g, %84.

^{1}H NMR (400 MHz, $CDCl_3$): δ 7.30-7.26 (m, 2H), 7.01-6.93 (m, 2H), 6.92-6.84 (m, 1H), 3.22 (t, 4H), 2.86 (m, 2H), 2.64 (m, 4H), 2.51 (m, 2H), 1.96 (bs, 4H).

5.35 Synthesis of 2-(4-phenylpiperazin-1-yl)ethan-1-ol[195]

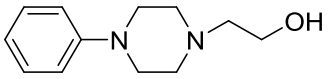

P-10

N,N-Bis(2-chloroethyl)aniline **(R-2)** (0.50 g, 2.30 mmol), $NaHCO_3$ (0.58 g; 6.90 mmol) and NaI (0.70 g; 4.2 mmol) were added to a solution of the ethanolamine (0.30 g; 4.60 mmol) in ethylene glycol (20 mL). The reaction mixture was heated to 110 ^oC for 1.5 h. Then the solution was cooled to room temperature, and water was added to the mixture. The resulting residue was taken in CH_2Cl_2 and washed with water repeatedly to remove ethylene glycol. The organic layer was dried over Mg_2SO_4, and the solvent was removed. Yield: 0.32 g, 27%.

^{1}H NMR (400 MHz, $CDCl_3$) δ 7.33 – 7.26 (m, 2H), 7.01 – 6.94 (m, 2H), 6.89 (t, *J* = 7.3 Hz, 1H), 3.71 – 3.66 (m, 2H), 3.29 – 3.21 (m, 4H), 2.76 – 2.68 (m, 4H), 2.66 – 2.61 (m, 2H).

5.36 Synthesis of 5-(4-methylpiperazin-1-yl)benzene-1,3-diol[196]

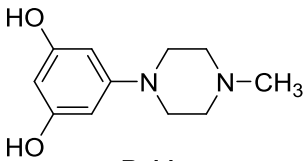

P-11

Phloroglucinol (1.00 g; 7.93 mmol) and 1-methyl piperazine (0.95 g, 9.52 mmol) were added into a round-bottomed flask containing a mixture of 1:3 (20 ml:60 ml) n-butanol:toluene. The solution was refluxed overnight under Dean-Stark to get rid of water from the reaction mixture. Excess solvents were removed under vacuo. For purification, basic extraction was performed first with $CHCl_3$ and a 1 M of $NaHCO_3$ solution until no more bubble was formed. 1M HCl solution was added dropwise to the aqueous phase until crystallization started. The resulting mixture was stood in the fridge overnight for completion of crystallization. Solids were filtered and washed with EtOH to get the target compound as pinkish crystals. Yield 0.88 g, 20%.

^{1}H NMR (400 MHz, DMSO) δ 8.95 (s, 2H), 5.78-5.75 (m, 2H), 5.71-5.68 (m, 1H), 3.02-2.95 (m, 4H), 2.42-2.35 (m, 4H), 2.19 (s, 3H).

5.37 Synthesis of 2,2'-(phenylazanediyl)bis(ethan-1-ol)[197]

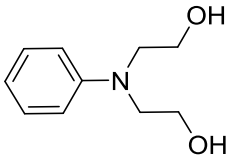

R-1

To a two-necked round-bottomed flask, distilled aniline (2.55 g, 27.38 mmol) and 2-bromohydrine (8.55 g, 68.45 mmol) were added and heated to reflux. During this period, 10% NaOH (25 mL) was slowly added, and the resulting solution was refluxed for 4 h. After the reaction completion (checked by TLC monitoring), the solution was cooled to room temperature, and extraction was performed with water and ethyl acetate. Then the organic layer was washed with brine and dried over Na_2SO_4. The solvent was removed under reduced pressure, and the compound was obtained as a yellowish solid. Yield: 3.75 g; 75%.

^{1}H NMR (400 MHz, $CDCl_3$) δ 7.30 – 7.22 (m, 2H), 6.80 – 6.69 (m, 3H), 3.93 – 3.85 (m, 4H), 3.65 – 3.58 (m, 4H), 3.43 (bs, 2H).

5.38 Synthesis of N, N-bis(2-chloroethyl)aniline[198]

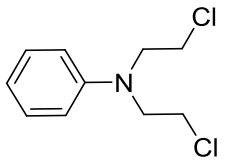

R-2

2,2'-(phenylazanediyl)bis(ethan-1-ol) (3.0 g, 16.55 mmol) was slowly added into a previously cooled with an ice bath round-bottomed flask containing phosphorus oxychloride (3.5 mL). After the addition was completed, the reaction mixture was heated at 110 °C for 1 h, then cooled to room temperature. The solution was poured into ethyl acetate (50 mL), organic part was repeatedly washed with water and dried over anhydrous Mg_2SO_4 to give the target compound as a dark greenish-brown viscous oil. Yield: 3.2 g; 89%.

^{1}H NMR (400 MHz, $CDCl_3$) δ 7.35 (t, J = 8.0 Hz, 2H), 6.88 (t, *J* = 7.3 Hz, 1H), 6.81 (d, *J* = 8.3 Hz, 2H), 3.81 – 3.75 (m, 4H), 3.69 (m, 4H).

5.39 Synthesis of 3,4-diethoxycyclobut-3-ene-1,2-dione

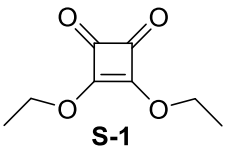

S-1

Squaric acid (2.5 g, 22 mmol) was suspended in ethanol (50 mL) and stirred under reflux for 20 h. The reaction mixture was cooled, and the solvent was removed in vacuo. The white solid was dissolved again in ethanol and brought to reflux for 30 min. This step was repeated three times to obtain full conversion of squaric acid into diethyl squarate. Yield: 3.50 g, 79%.

^{1}H NMR (400 MHz, DMSO) δ 4.65 (q, *J* = 7.1 Hz, 4H), 1.37 (t, *J* = 7.1 Hz, 6H).

5.40 Synthesis of 3,4-Bis(phenylamino)cyclobut-3-ene-1,2-dione[157]

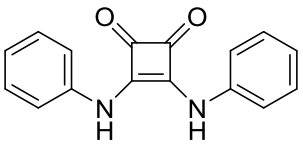

S-2

Aniline (1.73 g, 18.52 mmol) was added to a solution of diethyl squarate **S-1** (1.5 g, 8.81 mmol) and triethylamine (3.57 g, 35.24 mmol) in ethanol. The mixture was stirred at room temperature for 18 hours. Then the reaction mixture was filtered, and the precipitate was washed with diethyl ether and hexane, giving the desired squaramide. Yield:2.1 g, 90%.

^{1}H NMR (400 MHz, DMSO-d6) δ 9.91 (s, 2H, -NH) 7.50 (m, 4H), 7.39 (m, 4H), 7.09 (m, 2H)

5.41 Synthesis of 3-oxo-2-(phenylamino)-4-(phenyliminio)cyclobut-1-en-1-olate[160]

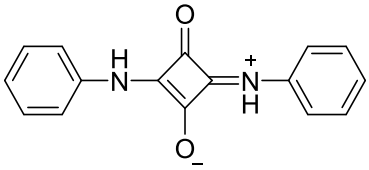

SQ-1

Squaric acid (0.29 g, 2.5 mmol) was heated under reflux in a mixture of 1-butanol and toluene (40 mL: 20 mL), and water was distilled off azeotropically using a Dean-Stark trap. After 1 h, aniline (0.47, 5.00 mmol) was added in one portion, and the reaction mixture refluxed overnight. The purple suspension having yellowish solids was then cooled to room temperature, and the crystals were filtrated and washed with toluene. The target compound was obtained as yellow crystals. Yield: 0.35 g, 53%.
^{1}H NMR (DMSO-d6), δ (ppm): 7.14 (m, 2H); 7.40 (m, 4H); 7.81 (m, 4H); 11.42 (bs, 2H, -NH).

5.42 Synthesis of 2-(4-(dimethylamino)phenyl)-4-(4-(dimethyliminio)cyclohexa-2,5-dien-1-ylidene)-3-oxocyclobut-1-en-1-olate[97,199–201]

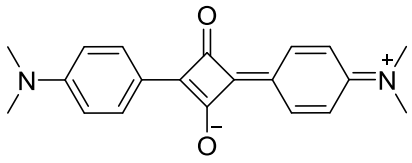

SQ-2

Squaric acid (1.00 g; 8.77 mmol) and N,N-dimethyl aniline (2.13 g; 17.53 mmol) were added into a round-bottomed flask containing a mixture of 1:1 (50 ml:50 ml) toluene:n-butanol. The solution was refluxed overnight under Dean-Stark to remove water from the reaction mixture. Excess toluene and butanol were removed under vacuo. The resulting residue was crystallized in Et_2O and filtrated to obtain the target compound as a blue solid. Yield: 1.88 g, 67%.

Due to the low solubility of the compound, NMR spectroscopy could not be applied. Characterization was done with UV-Vis and fluorescence spectroscopy, shown in Figure 3.5.

5.43 Synthesis of 2,4-bis(4-(dibutylamino)-2,6-dihydroxyphenyl)cyclobuta-1,3-diene-1,3-bis(olate)[97,199–201]

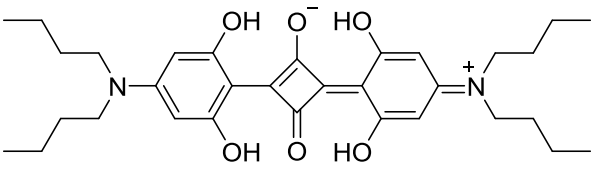

SQ-3

The solution of dibutyl amine (3 mL; 17.45 mmol) and phloroglucinol (2.00 g; 15.86 mmol) in a 3:1 (60ml: 20 ml) toluene:n-butanol solvent mixture was refluxed under Dean-Stark apparatus to remove water overnight. During reflux, the color of the reaction solution turned purple. After cooling it to room temperature, the solvent

ratio was adjusted to 1:1 by adding n-butanol and squaric acid (0.9 g; 7.93 mmol). The resulting solution continued to reflux under the Dean-Stark apparatus for an additional 16 h. Solvents were removed, and the residue was washed with EtOH. The target compound was obtained as metallic green crystals. Yield: 0.32 g, 8%.

^{1}H NMR (400 MHz, $CDCl_3$) δ 10.99 (s, 4H), 5.78 (s, 4H), 3.38 – 3.29 (m, 8H), 1.67 – 1.58 (m, 8H), 1.67 – 1.59 (m, 8H), 1.36 (dq, *J* = 14.7, 7.4 Hz, 8H), 0.97 (t, *J* = 7.3 Hz, 12H)

5.44 Synthesis of 2-(4-(cyclohexa-2,5-dien-1-yl)piperazin-1-yl)-3-oxo-4-(4-phenylpiperazin-1-ium-1-ylidene)cyclobut-1-en-1-olate[97,199–201]

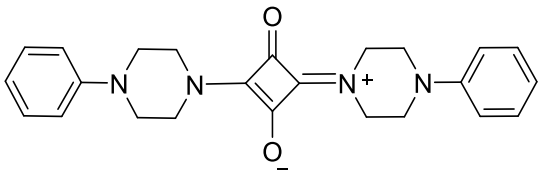

SQ-4

The solution of 1-phenyl piperazine (1.00 g; 6.16 mmol) and squaric acid (0.35 g; 3.08 mmol) in a 1:1 (60ml: 60 ml) toluene:n-butanol solvent mixture was refluxed under Dean-Stark apparatus to remove water for 16 h. Solvents were evaporated under reduced pressure. The remaining residue was crystallized in MeOH, and the target compound was obtained as a light yellow solid. Yield: 1,13 g, 91%.

^{1}H NMR (400 MHz, DMSO) δ 7.25-7.21 (m, 4H), 6.97-6.93 (m, 4H), 6.84-6.79 (m, 2H), 3.22-3.17 (m, 8H), 3.08-3.03 (m, 8H).

5.45 Synthesis of 4-(4-(4-acetylpiperazin-1-ium-1-ylidene)cyclohexa-2,5-dien-1-ylidene)-2-(4-(4-acetylpiperazin-1-yl)phenyl)-3-oxocyclobut-1-en-1-olate[97,199–201]

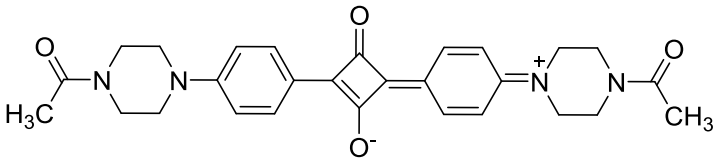

SQ-5

The solution 1-(4-phenylpiperazin-1-yl)ethan-1-one (2.3 g; 11.26 mmol) and squaric acid (0.64 g; 5.63 mmol) in 1:1 (60ml: 60 ml) toluene:n-butanol solvent mixture was refluxed under Dean-Stark apparatus to remove water for 16 h. Solvents were evaporated under reduced pressure. The remaining residue was crystallized in MeOH to obtain a blue solid. Yield: 1.1 g, 40%.

Due to the low solubility of the compound, NMR spectroscopy could not be applied. Characterization was done with UV-Vis and fluorescence spectroscopy, shown in Figure 3.9.

HRMS: (ESI-MS) m/z: $[M+H]^+$ calculated for $C_{28}H_{30}N_4O_4$ 487.2345, found: 487.2349

5.46 Synthesis of 4-(4-(4-(tert-butoxycarbonyl)piperazin-1-ium-1-ylidene)cyclohexa-2,5-dien-1-ylidene)-2-(4-(4-(tert butoxycarbonyl)piperazin-1-yl)phenyl)-3-oxocyclobut-1-en-1-olate[97,199–201]

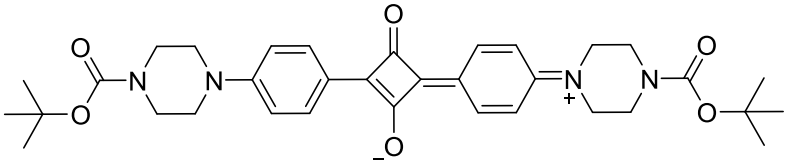

SQ-6

The solution tert-butyl 4-phenylpiperazine-1-carboxylate (2.00 g; 7.62 mmol) and squaric acid (0.43 g; 3.81 mmol) in 1:1 (60ml: 60 ml) toluene:n-butanol solvent mixture was refluxed under Dean-Stark apparatus to remove water for 16 h. Solvents were evaporated under reduced pressure. The remaining residue was crystallized in MeOH to obtain a blue solid. Yield: 0.51 g, 22%.

Characterization was done with UV-Vis and fluorescence spectroscopy, shown in Figure 3.10.

HRMS: (ESI-MS) m/z: $[M+H]^+$ calculated for $C_{34}H_{42}N_4O_6$ 603.3183, found: 601.3026

5.47 Synthesis of butyl L-prolinate[202]

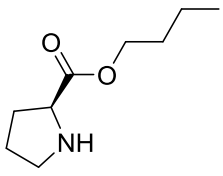

L-CSPI

L-proline (4.00 g, 34.74 mmol) was dissolved in n-BuOH (50 mL) and cooled down in an ice bath. $SOCl_2$ (7.44 g, 62.53 mmol) was added dropwise to the resulting solution and heated to 80 ^oC. It was stirred at this temperature overnight, and excess

volatiles was removed under vacuo and obtained as a salt form of the target compound. It was converted into an organic form by treating $NaHCO_3$ solution and extracted with DCM. Yield: 2,15 g, 36%. (Due to the difficulty in removal of butanol, NMR has butanol peaks. It is shown in Appendix A).

5.48 Synthesis of (E)-2-(2,6-dihydroxy-4-((R)-2-(propoxycarbonyl)pyrrolidin-1-yl)phenyl)-4-((E)-2,6-dihydroxy-4-((S)-2-(propoxycarbonyl)pyrrolidin-1-ium-1-ylidene)cyclohexa-2,5-dien-1-ylidene)-3-oxocyclobut-1-en-1-olate[137]

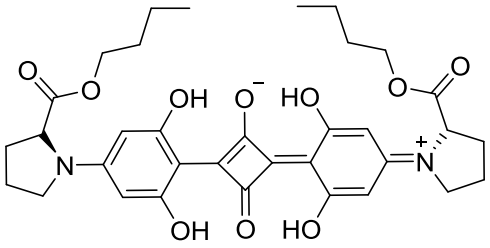

L-CSPID

The solution of phloroglucinol (0.46 g; 3.64 mmol) and (S)-butyl pyrrolidine-2-carboxylate (0.63 g; 3.68 mmol) in a 3:1 (90ml: 30 ml) toluene:n-butanol solvent mixture was refluxed under Dean-Stark apparatus to remove water overnight. After cooling it to room temperature, the solvent ratio was adjusted to 1:1 by adding n-butanol and squaric acid (0.21 g; 1.81 mmol). The resulting solution continued to reflux under the Dean-Stark apparatus for an additional 16 h. Solvents were removed, and the residue was washed with MeOH. The target compound was obtained as dark blue solids. Yield: 0,04 g, 4%.

HRMS: (ESI-MS) m/z: $[M+H]^+$ calculated for $C_{34}H_{40}N_2O_{10}$ 637.2761, found: 637.2762

5.49 Synthesis of (S)-2-(1,3-dioxoisoindolin-2-yl)propanoic acid[203]

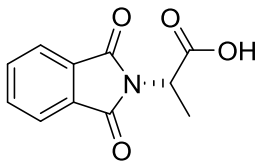

L-CSA-1

To a 100 ml round bottomed flask, L-alanine (2.00 g; 22.45 mmol) and phthalic anhydride (3.325 g; 22.45 mmol were added and dissolved in acetic acid (30 ml). The reaction mixture was refluxed overnight. Excess acetic acid was removed under vacuo. To the resulting residue, water (50 ml) was added and stirred at room temperature for 1h. White solid formed during this period were filtrated and dried. Yield: 2.36 g, 48%.

^{1}H NMR (400 MHz, $CDCl_3$) δ 10.93 (bs, 1H), 7.80 – 7.76 (m, 2H), 7.68 – 7.63 (m, 2H), 4.97 (q, *J* = 7.4 Hz, 1H), 1.67 (d, *J* = 7.4 Hz, 3H)

5.50 Synthesis of (R)-2-(1,3-dioxoisoindolin-2-yl)propanoic acid

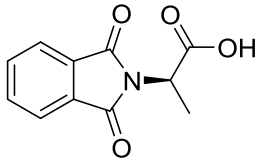

D-CSA-1

The title compound was synthesized following the procedure described for **L-CSA-1** using D-alanine as a stating material. Compound was obtained as white solids. Yield: 2,60 g, 53%.

The NMR data are in accordance with **L-CSA-1.**

5.51 Synthesis of (S)-2-(1,3-dioxoisoindolin-2-yl)-3-phenylpropanoic acid

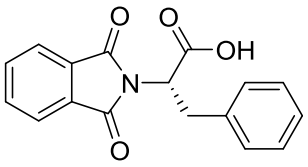

L-CSP-1

The title compound was synthesized following the procedure described for **L-CSA-1** using L-phenyl alanine (0.5 g; 3.00 mmol), phthalic anhydride (0,45 g; 3,00 mmol) and acetic acid (15 ml). Compound was obtained as white solid. Yield: 0.63 g, 71%.

^{1}H NMR (400 MHz, $CDCl_3$) δ 9.48 (bs, 1H), 7.77 (m, 2H), 7.73 – 7.65 (m, 2H), 7.23 – 7.09 (m, 5H), 5.23 (t, *J* = 8.3 Hz, 1H), 3.60 (s, 1H), 3.58 (s, 1H).

5.52 Synthesis of (R)-2-(1,3-dioxoisoindolin-2-yl)-3-phenylpropanoic acid

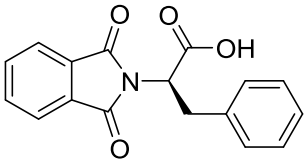

D-CSP-1

The title compound was synthesized following the procedure described for **L-CSA-1** using D-phenyl alanine. The compound was obtained as white solids. Yield: 0,56 g 63%.

The NMR data are in accordance with **L-CSP-1.**

5.53 Synthesis of (S)-2-(1-oxo-1-(4-phenylpiperazin-1-yl)propan-2-yl)isoindoline-1,3-dione

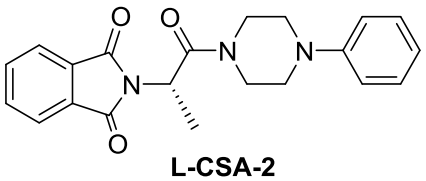

L-CSA-2

To the mixture of phenylpiperazine (0.7 ml; 4.57 mmol), **L-CSA-1** (1.00 g; 4.57 mmol) and HOBt (0.74 g; 5.48 mmol) in DMF (20 mL); EDC (0.85 g; 5.48 mmol) and *N*,*N*-diisopropylethyl amine (3.2 ml; 18.28 mmol) were added and stirred at room temperature overnight under Ar atmosphere. After cooling to rt, DMF was removed under reduced pressure. Remaining mixture was extracted with DCM, and the organic phase was washed with sodium bicarbonate solution 2 times and brine successively. Organic phase was dried over sodium sulfate and DCM was removed under vacuo to obtain crude product. For further purification crude product was recrystallized with EtOH and target compound was obtained as a white-beige solid. Yield: 0,93 g 55%.

^{1}H NMR (400 MHz, $CDCl_3$) δ 7.81 – 7.75 (m, 2H), 7.69 – 7.64 (m, 2H), 7.21-7.17 (m, 2H), 6.84-6.80 (m, 3H), 5.11 (q, *J* = 7.2 Hz, 1H), 3.80-3.65 (m, 2H), 3.55-3.45 (m, 2H), 3.15-3.00 (m, 4H), 1.66 (d, *J* = 7.2 Hz, 3H).

^{13}C NMR (101 MHz, $CDCl_3$) δ 167.67, 167.61, 150.75, 134.26, 131.68, 129.24, 123.55, 120.60, 116.52, 65.86, 49.68, 49.24, 45.44, 42.48, 15.27.

IR (cm^{-1}): 2928 (w), 2838 (w), 2157 (m), 2026(w), 1967 (w), 1778 (m), 1715 (s), 1647 (s), 1606 (m), 1507 (m), 1471 (m), 1381 (s), 1227 (s), 1151 (s), 1056 (s), 1020 (s), 912 (m), 880 (s), 763 (s), 723 (s), 682 (s)

HRMS: (ESI-MS) m/z: $[M+H]^+$ calculated for $C_{21}H_{21}N_3O_3$ 364.1661, found: 364.1669

5.54 Synthesis of (R)-2-(1-oxo-1-(4-phenylpiperazin-1-yl)propan-2-yl)isoindoline-1,3-dione

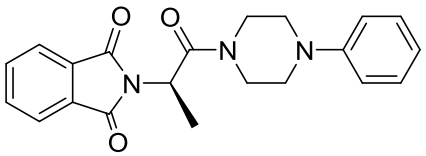

D-CSA-2

The title compound was synthesized following the procedure described for **L-CSA-2** using **D-CSA-1** as a starting material. Compound was obtained as white-beige solid. Yield: 0.92 g, 55%.

The NMR and IR data are in accordance with **L-CSA-2.**

5.55 Synthesis of (S)-2-(1-oxo-3-phenyl-1-(4-phenylpiperazin-1-yl)propan-2-yl)isoindoline-1,3-dione

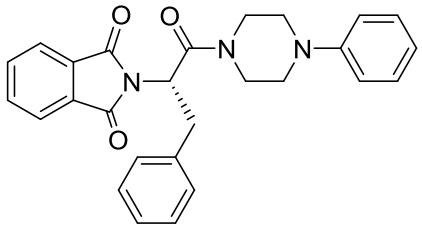

L-CSP-2

To the mixture of phenylpiperazine (0.33 ml; 2.15 mmol), **L-CSP-1** (0.63 g; 2.15 mmol) and HOBt (0.35 g; 2.58 mmol) in DMF (20 mL), EDC (0.4 g; 2,58 mmol) and *N,N*-diisopropylethyl amine (1.50 ml; 8.60 mmol) were added and stirred at room temperature overnight under Ar atmosphere. After cooling to rt, DMF was removed under reduced pressure. Remaining mixture was extracted with DCM, and the organic phase was washed with sodium bicarbonate solution 2 times and brine successively. Organic phase was dried over sodium sulfate and DCM was removed under vacuo to obtain crude product. For further purification crude product was

recrystallized with EtOH and target compound was obtained as a white-beige solid. Yield: 0,52 g 54%.

^{1}H NMR (400 MHz, $CDCl_3$) δ 7.86 – 7.76 (m, 2H), 7.75 – 7.68 (m, 2H), 7.34 – 7.14 (m, 8H), 6.94 – 6.83 (m, 2H), 5.32 (dd, *J* = 9.8, 6.0 Hz, 1H), 3.85-3.78 (m, 2H) 3.65 (dd, *J* =14.2, 9.8 Hz, 2H), 3.57-3.48 (m, 2H), 3.21-2.91 (m, 4H).

^{13}C NMR (101 MHz, $CDCl_3$) δ 167.56, 166.71, 160.85, 150.66, 136.89, 134.12, 131.27, 129.09, 128.49, 126.86, 123.43, 120.43, 116.48, 52.34, 49.42, 49.13, 45.25, 42.30, 35.10.

IR (cm^{-1}): 3059 (w), 3027 (w), 2933 (w), 2820 (w), 2153 (w), 2031 (w), 1977 (w), 1774 (w), 1719 (s), 1643 (s), 1598 (m), 1498 (m), 1435 (m), 1390 (s), 1323 (m), 1281 (m), 1223 (s), 1147 (m), 1088 (m), 1029 (m), 984 (m), 867 (m), 758 (s), 718 (s), 686 (s)

HRMS: (ESI-MS) m/z: $[M+H]^+$ calculated for $C_{27}H_{25}N_3O_3$ 440.1929, found: 440.1974

5.56 Synthesis of (R)-2-(1-oxo-3-phenyl-1-(4-phenylpiperazin-1-yl)propan-2-yl)isoindoline-1,3-dione

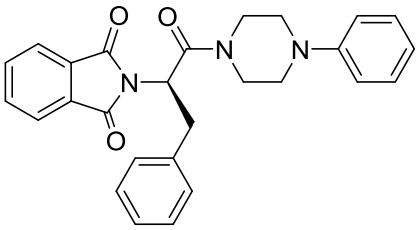

D-CSP-2

The title compound was synthesized following the procedure described for **L-CSP-2** using **D-CSP-1** as a starting material. Compound was obtained as white-beige solid. Yield: 0.92 g, 55%.

The NMR and IR data are in accordance with **L-CSP-2**

5.57 Synthesis of 4-(4-(4-((S)-2-(1,3-dioxoisoindolin-2-yl)propanoyl)piperazin-1-ium-1-ylidene)cyclohexa-2,5-dien-1-ylidene)-2-(4-(4-((S)-2-(1,3-dioxoisoindolin-2-yl)propanoyl)piperazin-1-yl)phenyl)-3-oxocyclobut-1-en-1-olate[97,199–201]

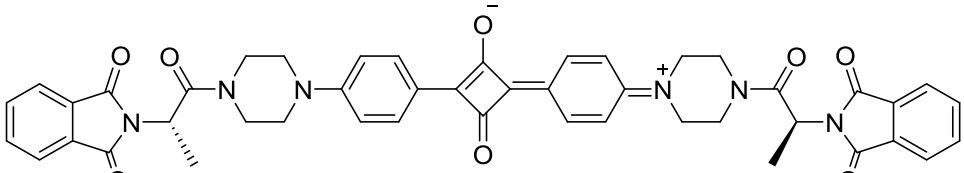

L-CSA-3

A two necked round bottomed flask, filled with toluene/ n-butanol (1:1, 70 ml) solvent mixture, was fitted with Dean-Stark apparatus and heated to reflux. Once the Dean-Stark apparatus fully filled and emptied, squaric acid (0.05 gr; 0.4 mmol) was added and continued to reflux for half an hour. After that, **L-CSA-2** (0.30 gr; 0.80 mmol) was added to the flask and refluxed for 20 h. During this period, the color of the solution turned to green and it was getting darker. After 20 h heating and stirring, excess solvents were removed under reduced pressure. To the resulting residue, MeOH was added to crystallize target squaraine dye as a dark green-blue solid. Yield: 0.2 g, 62%.

^{1}H NMR (400 MHz, $CDCl_3$) δ 7.83 – 7.76 (m, 4H), 7.70 – 7.63 (m, 4H), 7.21-7.17 (m, 5H), 6.84-6.80 (m, 5H), 5.11 (q, *J* = 7.2 Hz, 2H), 3.79-3.65 (m, 4H), 3.54-3.42 (m, 4H), 3.10-3.05 (m, 8H), 1.66 (d, *J* = 7.2 Hz, 6H).

^{13}C NMR (101 MHz, $CDCl_3$) δ 191.53, 182.83, 167.52, 150.45, 134.14, 131.54, 129.12, 123.41, 120.63, 116.56, 49.65, 49.19, 46.67, 45.26, 42.26, 15.54.

IR (cm^{-1}): 2938 (w), 2829 (w), 2166 (w), 2035 (w), 1963 (w), 1774 (w), 1715 (s), 1647 (s), 1503 (m), 1471 (m), 1430 (m), 1372 (s), 1237 (s), 1155 (m), 1061 (m), 1011 (m), 912 (m), 875 (m), 763 (m), 723 (s), 668 (m)

HRMS: (ESI-MS) m/z: $[M+H]^+$ calculated for $C_{46}H_{40}N_6O_8$ 803.2829, found: 803.2830

5.58 Synthesis of 4-(4-(4-((R)-2-(1,3-dioxoisoindolin-2-yl)-3-phenylpropanoyl)piperazin-1-ium-1-ylidene)cyclohexa-2,5-dien-1-ylidene)-2-(4-(4-((R)-2-(1,3-dioxoisoindolin-2-yl)-3-phenylpropanoyl)piperazin-1-yl)phenyl)-3-oxocyclobut-1-en-1-olate

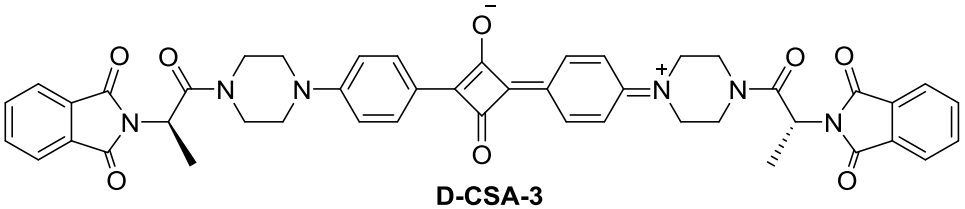

D-CSA-3

The title compound was synthesized following the procedure described for **L-CSA-3** using **D-CSA-2** as a starting material. Compound was obtained as a dark green-blue solid. Yield: 0.92 g, 55%.

The NMR and IR data are in accordance with **L-CSA-3.**

5.59 Synthesis of 4-(4-(4-((S)-2-(1,3-dioxoisoindolin-2-yl)-3-phenylpropanoyl)piperazin-1-ium-1-ylidene)cyclohexa-2,5-dien-1-ylidene)-2-(4-(4-((S)-2-(1,3-dioxoisoindolin-2-yl)-3-phenylpropanoyl)piperazin-1-yl)phenyl)-3-oxocyclobut-1-en-1-olate

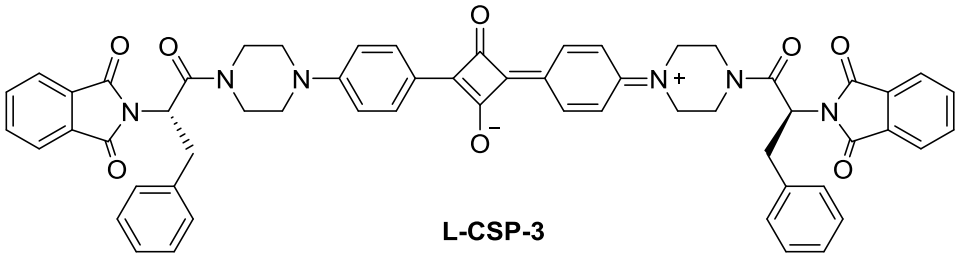

L-CSP-3

The title compound was synthesized following the procedure described for **L-CSA-3** using **L-CSP-2** (0.52 g; 1.17 mmol) and squaric acid (0.067 g; 0.59 mmol). The target squaraine dye was obtained as a green solid. Yield: 0.32 g, 59%.

^{1}H NMR (400 MHz, $CDCl_3$) δ 7.84-7.76 (m, 4H), 7.74-7.66 (m, 4H), 7.31 – 7.12 (m, 14H), 6.92 – 6.82 (m, 4H), 5.32 (dd, *J* = 9.7, 6.1 Hz, 2H), 3.87 – 3.73 (m, 4H), 3.69 – 3.57 (m, 4H), 3.54-3.49 (m, 4H), 3.18 – 2.94 (m, 8H).

^{13}C NMR (101 MHz, $CDCl_3$) δ 167.68, 166.96, 149.94, 136.94, 134.28, 131.36, 129.36, 129.21, 128.62, 127.12, 123.55, 121.39, 116.96, 52.38, 50.01, 49.69, 45.31, 42.26, 35.15.

IR (cm^{-1}): 2965 (w), 2919 (w), 2847 (w), 2166 (w), 2044 (w), 1977 (w), 1774 (w), 1710 (s), 1660 (m), 1588 (m), 1515 (w), 1440 (m), 1377 (s), 1281 (w), 1223 (s), 1192 (s), 1092 (m), 1029 (m), 885 (w), 758 (w), 727 (s), 699 (s)

HRMS: (ESI-MS) m/z: $[M+H]^+$ calculated for $C_{58}H_{48}N_6O_8$ 957.3612, found: 957.3612

5.60 4-(4-(4-((R)-2-(1,3-dioxoisoindolin-2-yl)-3-phenylpropanoyl)piperazin-1-ium-1-ylidene)cyclohexa-2,5-dien-1-ylidene)-2-(4-(4-((R)-2-(1,3-dioxoisoindolin-2-yl)-3-phenylpropanoyl)piperazin-1-yl)phenyl)-3-oxocyclobut-1-en-1-olate

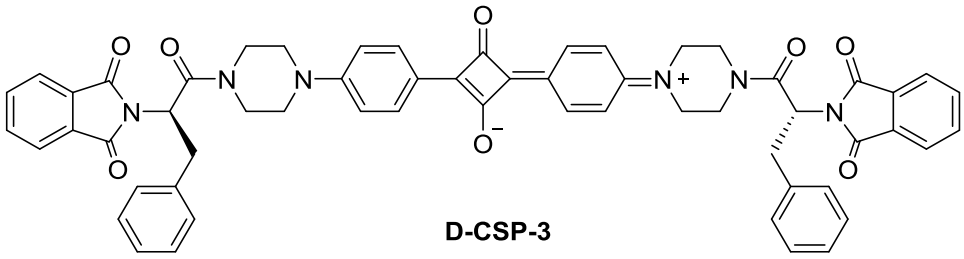

D-CSP-3

The title compound was synthesized following the procedure described for **L-CSA-3** using **D-CSP-2** (0.2 g; 0.45 mmol), and squaric acid (0.025 g; 0.23 mmol) as starting materials. The target squaraine dye was obtained as a green solid. Yield: 0.12 g, 53%.

The NMR and IR data are in accordance with **L-CSP-3.**

5.61 Synthesis of SQPOL-L[97,199–201]

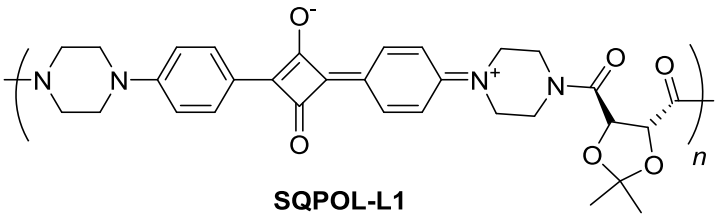

SQPOL-L1

A two-necked round-bottomed flask, filled with toluene/ n-butanol (1:1, 50 ml) solvent mixture, was fitted with Dean-Stark apparatus and heated to reflux. Once the Dean-Stark apparatus was fully filled and emptied, squaric acid (0.1 gr; 0.88 mmol) was added and continued to reflux for half an hour. After that, **TL-2** (0.21 gr; 0.44 mmol) was added to the flask and refluxed for 20 h. During this period, the color of the solution turned green, and it was getting darker. After 20 h heating and stirring, excess solvents were removed under reduced pressure. To the resulting residue, MeOH was added to crystallize the target polysquaraine as a dark green solid. Yield: 0.15 g. Mn= 3.1 kDa, Mw= 3.6 kDa and PDI 1.17

^{1}H NMR (400 MHz, $CDCl_3$) δ 7.33-7.29 (m, 4H), 6.95 (dd, J = 16.1, 7.9 Hz, 4H), 5.31 (s, 2H), 4.02 – 3.66 (m, 8H), 3.35 – 3.10 (m, 8H), 1.46 (s, 6H).

^{13}C NMR (101 MHz, $CDCl_3$) δ 189.34, 184.27, 167.05, 150.76, 129.38, 120.70, 116.73, 112.32, 75.34, 49.96, 49.41, 45.52, 42.23, 26.50.

IR: 3513 (w), 2957 (w), 2896 (w), 2808 (w), 1726 (m), 1648 (s), 1590 (s), 1520 (m), 1429 (s), 1371 (m), 1218 (s), 1143 (s) 1069 (m), 1016 (s), 864 (m), 754 (m), 693 (m)

5.62 Synthesis of SQPOL-D

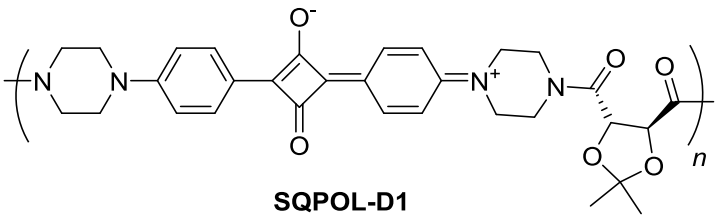

SQPOL-D1

The title compound was synthesized following the procedure described for **SQPOL-L** using **TD-2** as a starting material. The compound was obtained as a dark green solid. Yield: 0.20 g. Mn= 5.8 kDa, Mw= 7.2 kDa and PDI 1.23

The NMR and IR data are in accordance with **SQPOL-L.**

5.63 Synthesis of diethyl succinate

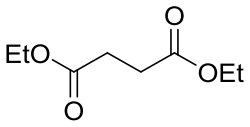

S-3

Succinic acid (20 gr, 169.36 mmol) was dissolved in 150 mL EtOH in two necked round bottomed flask. Thionyl chloride (31 mL) was added dropwise to that mixture in an ice bath. After one hour stirring at room temperature, the solution was refluxed for 3h. the solvent and excess thionyl chloride was removed under vacuo. Yield: 27.5 g, 93%.

^{1}H NMR (400 MHz, $CDCl_3$) δ 4.15 (q, *J* = 7.1 Hz, 4H), 2.62 (s, 4H), 1.26 (t, *J* = 7.1 Hz, 6H).

5.64 Synthesis of diethyl 2,5-dihydroxycyclohexa-1,4-diene-1,4-dicarboxylate[204]

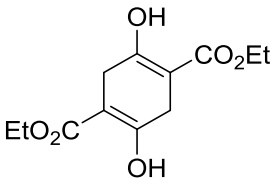

S-4

To a vigorously stirred suspension of NaH (60% dispersion in mineral oil, 2,5 g) in 1,2 dimethoxy ethane, 0.2 g of tert-BuOH was added and the mixture was heated to

60 °C. After gas evolution ceased, diethyl succinate (10 g, 57.41 mmol) was added dropwise. The resulting mixture was stirred for 12 h at 60 °C, than the solution was acidified with 6N H_2SO_4. The precipitate was collected by vacuum filtration , washed with hexane and water. For purification recrystallization with EtOH was applied. The target compound was obtained as a white solid. Yield: 6.2 g, 42%.

^{1}H NMR (400 MHz, $CDCl_3$) δ 12.21 (s, 2H), 4.25 (q, *J* = 7.1 Hz, 4H), 3.18 (s, 4H), 1.32 (t, *J* = 7.1 Hz, 6H).

5.65 Synthesis of diethyl 2,5-bis(methylamino)terephthalate[139]

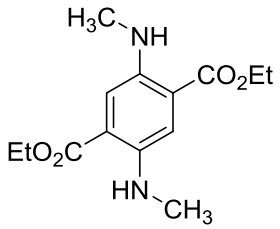

S-6

40% aqueous solution of methylamine (2.42 g, 78.1 mmol) was added to a suspension of **S-4** (2.0 g, 7.81 mmol)in MeOH (25 mL), and the resulting mixture was stirred under reflux for 16h. After cooling to room temperature, the solids in the reaction mixture were filtered and washed with MeOH to afford intermediate product diethyl 2,5-bis(methylamino)cyclohexa-1,4-diene-1,4-dicarboxylate **(S-5)** (0.8 g, 3.12 mmole). The pale pink solids of **S-5** were dissolved in DCM, and Br_2 (0.5 g, 3.12 mmole) was added. After the solution was stirred for 30 min, 20 mL 5% Na_2CO_3 was added, and the resulting mixture was purified by extraction. The organic phase was dried over Na_2SO_4, and DCM was removed under reduced pressure to get the target compound as orange solids. Yield: 0.5 g, 57%.

^{1}H NMR (400 MHz, $CDCl_3$) δ 7.28 (s, 2H), 6.75 (bs, 2H), 4.35 (q, *J* = 13.14 Hz, 4H), 2.89 (s, 6H), 1.40 (t, *J* = 7.1 Hz, 6H).

5.66 Synthesis of DATPOL-L[142]

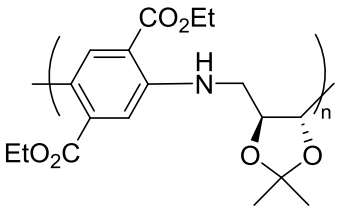

DATPOL-L

Protected L-tartaric acid diamine (0.8 g, 5 mmol) was dissolved in EtOH, and diethyl 2,5-dihydroxycyclohexa-1,4-diene-1,4-dicarboxylate (1.28 g, 5 mmol) was added to the solution. After addition of 1-2 drops of concentrated HCl, obtained light yellow mixture was refluxed for 24 h. O_2 was bubbled through the resulting reaction mixture and EtOH was removed under vacuo. The residue was dissolved in DCM and Br_2 (0.4 g, 2.5 mmol) was added. After stirring 20 min, Br_2 was quenched with Na_2CO_3 (5%, 20 ml). Extraction was performed and organic phase was dried over Na_2SO_4. DCM was removed under vacuo. For further purification solids were washed with Et_2O. The target polymer was obtained as a dark red solid.

NMR spectrum of the compound was explained in Figure 3.42.

IR: 3376 (w), 2986 (m), 2918 (m), 2162 (w), 2034 (w), 1970 (w), 1676 (s), 1517 (s), 1469 (m), 1373 (m), 1301 (m), 1190 (s), 1091 (s), 1054 (m), 1007 (m), 899 (m), 896 (m), 855 (m), 788 (m).

5.67 Synthesis of DATPOL-D

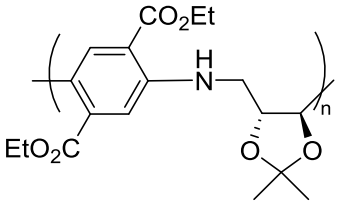

DATPOL-D

The title compound was synthesized following the procedure described for **DATPOL-L** using **TL-6** as a starting material. The compound was obtained as a dark red solid.

NMR spectrum of the compound was explained in Figure 3.43.

IR data are in accordance with **DATPOL-L.**

REFERENCES

(1) Pasteur, O. Recherches Sur Les Propriétés Spécifiques Des Deux Acides Qui Composent l'acide Racémique. *Ann. Chim. Phys.* **1922**, 56–99.

(2) Gal, J. Louis Pasteur, Language, and Molecular Chirality. I. Background and Dissymmetry. *Chirality* **2011**, 1–16. https://doi.org/10.1002/chir.20866.

(3) Inaki, M.; Liu, J.; Matsuno, K. Cell Chirality: Its Origin and Roles in Left–Right Asymmetric Development. *Philos. Trans. R. Soc. B Biol. Sci.* **2016**, *371*, 20150403. https://doi.org/10.1098/rstb.2015.0403.

(4) Podlech, J. Origin of Organic Molecules and Biomolecular Homochirality. *Cell. Mol. Life Sci.* **2001**, *58*, 44–60. https://doi.org/10.1007/PL00000777.

(5) Plasson, R.; Kondepudi, D. K.; Bersini, H.; Commeyras, A.; Asakura, K. Emergence of Homochirality in Far-from-Equilibrium Systems: Mechanisms and Role in Prebiotic Chemistry. *Chirality* **2007**, *19*, 589–600. https://doi.org/10.1002/chir.20440.

(6) Oro, J.; Miller, S. L.; Lazcano, A. The Origin and Early Evolution of Life on Earth. *Annual Review of Earth & Planetary Sciences*. 1990, 317–356. https://doi.org/10.1146/annurev.earth.18.1.317.

(7) Bailey, J.; Chrysostomou, A.; Hough, J. H.; Gledhill, T. M.; McCall, A.; Clark, S.; Ménard, F.; Tamura, M. Circular Polarization in Star- Formation Regions: Implications for Biomolecular Homochirality. *Science*, **1998**, *281* (5377), 672–674. https://doi.org/10.1126/science.281.5377.672.

(8) Devínsky, F. Chirality and the Origin of Life. *Symmetry (Basel).* **2021**, *13*, 2277. https://doi.org/10.3390/sym13122277.

(9) Aartsen, M. G.; Abraham, K.; Ackermann, M.; Adams, J.; Aguilar, J. A.; Ahlers, M.; Ahrens, M.; Altmann, D.; Andeen, K.; Anderson, T.; et al.

Searches for Sterile Neutrinos with the IceCube Detector. *Phys. Rev. Lett.* **2016**, *117*, 071801. https://doi.org/10.1103/PhysRevLett.117.071801.

(10) Drewes, M. The Phenomenology of Right Handed Neutrinos. *Int. J. Mod. Phys. E*. **2013**,1330019. https://doi.org/10.1142/S0218301313300191.

(11) Angle, J.; Aprile, E.; Arneodo, F.; Baudis, L.; Bernstein, A.; Bolozdynya, A.; Coelho, L. C. C.; Dahl, C. E.; Deviveiros, L.; Ferella, A. D.; et al. Limits on Spin-Dependent WIMP-Nucleon Cross Sections from the XENON10 Experiment. *Phys. Rev. Lett.* **2008**, *101*, 091301. https://doi.org/10.1103/PhysRevLett.101.091301.

(12) Cronin, J. R.; Pizzarello, S. Amino Acid Enantiomer Excesses in Meteorites: Origin and Significance. *Adv. Sp. Res.* **1999**, *23*, 293–299. https://doi.org/10.1016/S0273-1177(99)00050-2.

(13) Oparin, A. .; Morgulis, S. *The Origin of Life*, 2nd ed.; Dover Publications: Mineola, NY, USA, 2003.

(14) Bernal, J. D. *The Origin of Life*; World Publishing: Cleveland, USA, 1967.

(15) Shapiro, R. *Origins: A Skeptic's Guide to the Creation of Life on Earth; Bantam New Age*; New York, USA, 1986.

(16) Lee, T. D.; Yang, C. N. Question of Parity Conservation in Weak Interactions. *Phys. Rev.* **1957**, *106*, 1371–1371. https://doi.org/10.1103/PhysRev.106.1371.

(17) Wu, C. S.; Ambler, E.; Hayward, R. W.; Hoppes, D. D.; Hudson, R. P. Experimental Test of Parity Conservation in Beta Decay. *Phys. Rev.* **1957**, *105* , 1413–1415. https://doi.org/10.1103/PhysRev.105.1413.

(18) Nanita, S. C.; Cooks, R. G. Serine Octamers: Cluster Formation, Reactions, and Implications for Biomolecule Homochirality. *Angew. Chem. Int. Ed.* **2006**, 45, 554–569. https://doi.org/10.1002/anie.200501328.

(19) Toxvaerd, S. Homochirality in Bio-Organic Systems and Glyceraldehyde in the Formose Reaction. *J. Biol. Phys.* **2005**, *31*, 599–606. https://doi.org/10.1007/s10867-005-6063-7.

(20) Córdova, A.; Sundén, H.; Xu, Y.; Ibrahem, I.; Zou, W.; Engqvist, M. Sugar-Assisted Kinetic Resolution of Amino Acids and Amplification of Enantiomeric Excess of Organic Molecules. *Chem. - A Eur. J.* **2006**, *12*, 5446–5451. https://doi.org/10.1002/chem.200600526.

(21) Avnir, D. Critical Review of Chirality Indicators of Extraterrestrial Life. *New Astron. Rev.* **2021**, *92*, 101596. https://doi.org/10.1016/j.newar.2020.101596.

(22) Myrgorodska, I.; Meinert, C.; Hoffmann, S. V; Jones, N. C.; Nahon, L.; Meierhenrich, U. J. Light on Chirality: Absolute Asymmetric Formation of Chiral Molecules Relevant in Prebiotic Evolution. *Chempluschem* **2017**, *82*, 74–87. https://doi.org/10.1002/cplu.201600214.

(23) Hegstrom, R.A.; Kondepudi, D. . The Handedness of the Universe. *Sci. Am.* **1990**, *262*, 108–115.

(24) Gal, J. The Discovery of Stereoselectivity at Biological Receptors: Arnaldo Piutti and the Taste of the Asparagine Enantiomers-History and Analysis on the 125th Anniversary. *Chirality* **2012**, *24*, 959–976. https://doi.org/10.1002/chir.22071.

(25) Leitereg, T. J.; Guadagni, D. G.; Haris, J.; Mon, T. R.; Teranishi, R. Chemical and Sensory Data Supporting the Difference Between the Odors of the Enantiomeric Carvones. *J. Agr. Food Chem.* **1971**, *19*, 785–787. https://doi.org/10.1021/jf60176a035

(26) Jaffe, I. A.; Altman, K.; Merryman, P. The Antipyridoxine Effect of Penicillamine in Man. *J. Clin. Invest.* **1964**, *43*, 1869–1873. https://doi.org/10.1172/JCI105060.

(27) Cotton, F. A. *Chemical Applications of Group Theory*, 3rd ed.; John Wiley & Sons, Inc.: Canada, 1990.

(28) Liu, M.; Zhang, L.; Wang, T. Supramolecular Chirality in Self-Assembled Systems. *Chem. Rev.* **2015**, *115*, 7304–7397. https://doi.org/10.1021/cr500671p.

(29) Lehn, J.-M. *Supramolecular Chemistry*; Wiley: New York, USA, 1995; Vol. 260. https://doi.org/10.1002/3527607439.

(30) Song, G.; Ren, J. Recognition and Regulation of Unique Nucleic Acid Structures by Small Molecules. *Chem. Commun.* **2010**, *46*, 7283–7294. https://doi.org/10.1039/c0cc01312a.

(31) Voet, D.; Voet, J. G.; Pratt, C. W. *Fundamentals of Biochemistry: Life at the Molecular Level*, 5th ed.; John Wiley & Sons, Inc.: United States of America, 2016.

(32) Nakano, T.; Okamoto, Y. Synthetic Helical Polymers: Conformation and Function. *Chem. Rev.* **2001**, *101*, 4013–4038. https://doi.org/10.1021/cr0000978.

(33) Nolte, R. J. M.; Van Beijnen, A. J. M.; Drenth, W. Chirality in Polyisocyanides. *J. Am. Chem. Soc.* **1974**, *96*, 5932–5933. https://doi.org/10.1021/ja00825a038.

(34) Okamoto, Y.; Suzuki, K.; Ohta, K.; Hatada, K.; Yuki, H. Optically Active Poly(Triphenylmethyl Methacrylate) with One-Handed Helical Conformation. *J. Am. Chem. Soc.* **1979**, *101*, 4763–4765. https://doi.org/10.1021/ja00510a072.

(35) Green, M.; Reidy, M. Macromolecular Stereochemistry: The Out-of-Proportion Influence of Optically Active Comonomers on the Conformational Characteristics of Polyisocyanates. The Sergeants and Soldiers Experiment. *J. Am. Chem. Soc.* **1989**, *111*, 6452–6454.

(36) Corley, L. S.; Vogl, O. Optically Active Polychloral. *Polym. Bull.* **1980**, *3*, 211–217. https://doi.org/10.1007/BF00291959.

(37) Green, M. M.; Peterson, N. C.; Sato, T.; Teramoto, A.; Cook, R.; Lifson, S. A Helical Polymer with a Cooperative Response to Chiral Information. *Science* **1995**, *268*, 1860–1866. https://doi.org/10.1126/science.268.5219.1860.

(38) Fujiki, M. Optically Active Polysilylenes: State-of-the-Art Chiroptical Polymers. *Macromol. Rapid Commun.* **2001**, *22*, 539–563. https://doi.org/10.1002/1521-3927(20010501)22:8<539::AID-MARC539>3.0.CO;2-K.

(39) Green, M. M.; Park, J.; Sato, T.; Teramoto, A.; Lifson, S.; Selinger, R. L. B.; Selinger, J. V. The Macromolecular Route to Chiral Amplification. *Angew. Chem. Int. Ed.* **1999**, *38*, 3138–3154.

(40) Green, M. M.; Garetz, B. A.; Munoz, B.; Chang, H.; Hoke, S.; Cooks, R. G. Majority Rules in the Copolymerization of Mirror Image Isomers. *J. Am. Chem. Soc.* **1995**, *117*, 4181–4182. https://doi.org/10.1021/ja00119a039.

(41) Percec, V.; Xiao, Q. Helical Self-Organizations and Emerging Functions in Architectures, Biological and Synthetic Macromolecules. *Bull. Chem. Soc. Jpn.* **2021**, *94*, 900–928. https://doi.org/10.1246/bcsj.20210015.

(42) Schlitzer, D. S.; Novak, B. M. Trapped Kinetic States, Chiral Amplification and Molecular Chaperoning in Synthetic Polymers: Chiral Induction in Polyguanidines through Ion Pair Interactions. *J. Am. Chem. Soc.* **1998**, *120*, 2196–2197. https://doi.org/10.1021/ja974048x.

(43) Rudick, J. G.; Percec, V. Nanomechanical Function Made Possible by Suppressing Structural Transformations of Polyarylacetylenes. *Macromol. Chem. Phys.* **2008**, *209*, 1759–1768. https://doi.org/10.1002/macp.200800271.

(44) Aoki, T.; Kaneko, T.; Teraguchi, M. Synthesis of Functional π-Conjugated Polymers from Aromatic Acetylenes. *Polymer* **2006**, *47*, 4867–4892. https://doi.org/10.1016/j.polymer.2006.04.047.

(45) Ito, Y.; Kojima, Y.; Murakami, M.; Suginome, M. Racemization and Deracemization of Poly(Quinoxaline-2,3-Diyl)S. *Bull. Chem. Soc. Jpn.* **1997**, *70*, 2801–2806. https://doi.org/10.1246/bcsj.70.2801.

(46) Yashima, E.; Maeda, K.; Furusho, Y. Single- and Double-Stranded Helical Polymers: Synthesis, Structures, and Functions. *Acc. Chem. Res.* **2008**, *41*, 1166–1180. https://doi.org/10.1021/ar800091w.

(47) Jiang, W.; Pacella, M. S.; Vali, H.; Gray, J. J.; McKee, M. D. Chiral Switching in Biomineral Suprastructures Induced by Homochiral L-Amino Acid. *Sci. Adv.* **2018**, *4*, 1–12. https://doi.org/10.1126/sciadv.aas9819.

(48) Church, G. M.; Gao, Y.; Kosuri, S. Next-Generation Digital Information Storage in DNA. *Science* **2012**, 1628. https://doi.org/10.1126/science.1226355.

(49) McDermott, G.; Prince, S. M.; Freer, A. A.; Hawthornthwaite-Lawless, A. M.; Papiz, M. Z.; Cogdell, R. J.; Isaacs, N. W. Crystal Structure of an Integral Membrane Light-Harvesting Complex from Photosynthetic Bacteria. *Nature* **1995**, *374*, 517–521. https://doi.org/10.1038/374517a0.

(50) Lear, J. D.; Wasserman, Z. R.; Degrado, W. F. Synthetic Amphiphilic Peptide Models for Protein Ion Channels. *Science* **1988**, *240*, 1177–1181. https://doi.org/10.1126/science.2453923.

(51) Freire, F.; Quiñoá, E.; Riguera, R. Supramolecular Assemblies from Poly(Phenylacetylene)S. *Chem. Rev.* **2016**, *116*, 1242–1271. https://doi.org/10.1021/acs.chemrev.5b00280.

(52) Zhao, Y.; Abdul Rahim, N. A.; Xia, Y.; Fujiki, M.; Song, B.; Zhang, Z.; Zhang, W.; Zhu, X. Supramolecular Chirality in Achiral Polyfluorene:

Chiral Gelation, Memory of Chirality, and Chiral Sensing Property. *Macromolecules* **2016**, *49*, 3214–3221. https://doi.org/10.1021/acs.macromol.6b00376.

(53) Wang, S.; Chen, J.; Feng, X.; Shi, G.; Zhang, J.; Wan, X. Conformation Shift Switches the Chiral Amplification of Helical Copoly(Phenylacetylene)s from Abnormal to Normal "Sergeants-and-Soldiers" Effect. *Macromolecules* **2017**, *50*, 4610–4615. https://doi.org/10.1021/acs.macromol.7b01028.

(54) Green, M. M.; Park, J. W.; Sato, T.; Teramoto, A.; Lifson, S.; Selinger, R. L. B.; Selinger, J. V. The Macromolecular Route to Chiral Amplification. *Angew. Chem. Int. Ed*. **1999**, 3138–3154. https://doi.org/10.1002/(sici)1521-3773(19991102)38:21<3138::aid-anie3138>3.0.co;2-c.

(55) Aoki, T.; Kaneko, T.; Maruyama, N.; Sumi, A.; Takahashi, M.; Sato, T.; Teraguchi, M. Helix-Sense-Selective Polymerization of Phenylacetylene Having Two Hydroxy Groups Using a Chiral Catalytic System. *J. Am. Chem. Soc.* **2003**, *125*, 6346–6347. https://doi.org/10.1021/ja021233o.

(56) Luo, X.; Deng, J.; Yang, W. Helix-Sense-Selective Polymerization of Achiral Substituted Acetylenes in Chiral Micelles. *Angew. Chem. Int. Ed.* **2011**, *50*, 4909–4912. https://doi.org/10.1002/anie.201006658.

(57) Zhang, C.; Wang, H.; Geng, Q.; Yang, T.; Liu, L.; Sakai, R.; Satoh, T.; Kakuchi, T.; Okamoto, Y. Synthesis of Helical Poly(Phenylacetylene)s with Amide Linkage Bearing l -Phenylalanine and l -Phenylglycine Ethyl Ester Pendants and Their Applications as Chiral Stationary Phases for HPLC. *Macromolecules* **2013**, *46*, 8406–8415. https://doi.org/10.1021/ma4015802.

(58) Xu, Y.; Yang, G.; Xia, H.; Zou, G.; Zhang, Q.; Gao, J. Enantioselective Synthesis of Helical Polydiacetylene by Application of Linearly Polarized Light and Magnetic Field. *Nat. Commun.* **2014**, *5*, 1–6. https://doi.org/10.1038/ncomms6050.

(59) Miyabe, T.; Iida, H.; Ohnishi, A.; Yashima, E. Enantioseparation on Poly(Phenyl Isocyanide)s with Macromolecular Helicity Memory as Chiral Stationary Phases for HPLC. *Chem. Sci.* **2012**, *3*, 863–867. https://doi.org/10.1039/c1sc00708d.

(60) Yang, L.; Tang, Y.; Liu, N.; Liu, C.-H.; Ding, Y.; Wu, Z.-Q. Facile Synthesis of Hybrid Silica Nanoparticles Grafted with Helical Poly(Phenyl Isocyanide)s and Their Enantioselective Crystallization Ability. *Macromolecules* **2016**, *49*, 7692–7702. https://doi.org/10.1021/acs.macromol.6b01870.

(61) Chen, B.; Deng, J.; Yang, W. Hollow Two-Layered Chiral Nanoparticles Consisting of Optically Active Helical Polymer/Silica: Preparation and Application for Enantioselective Crystallization. *Adv. Funct. Mater.* **2011**, *21*, 2345–2350. https://doi.org/10.1002/adfm.201100113.

(62) Liang, J.; Deng, J. Chiral Particles Consisting of Helical Polylactide and Helical Substituted Polyacetylene: Preparation and Synergistic Effects in Enantio-Differentiating Release. *Macromolecules* **2018**, *51*, 4003–4011. https://doi.org/10.1021/acs.macromol.8b00580.

(63) Liang, J.; Wu, Y.; Deng, J. Construction of Molecularly Imprinted Polymer Microspheres by Using Helical Substituted Polyacetylene and Application in Enantio-Differentiating Release and Adsorption. *ACS Appl. Mater. Inter.* **2016**, *8*, 12494–12503. https://doi.org/10.1021/acsami.6b04057.

(64) Megens, R. P.; Roelfes, G. Asymmetric Catalysis with Helical Polymers. *Chem. - A Eur. J.* **2011**, *17*, 8514–8523. https://doi.org/10.1002/chem.201100672.

(65) Zhang, D.; Ren, C.; Yang, W.; Deng, J. Helical Polymer as Mimetic Enzyme Catalyzing Asymmetric Aldol Reaction. *Macromol. Rapid Commun.* **2012**, *33*, 652–657. https://doi.org/10.1002/marc.201100826.

(66) Tang, Z.; Iida, H.; Hu, H. Y.; Yashima, E. Remarkable Enhancement of the

Enantioselectivity of an Organocatalyzed Asymmetric Henry Reaction Assisted by Helical Poly(Phenylacetylene)s Bearing Cinchona Alkaloid Pendants via an Amide Linkage. *ACS Macro Lett.* **2012**, *1*, 261–265. https://doi.org/10.1021/mz200161s.

(67) Miyabe, T.; Iida, H.; Ohnishi, A.; Yashima, E. Enantioseparation on Poly(Phenyl Isocyanide)s with Macromolecular Helicity Memory as Chiral Stationary Phases for HPLC. *Chem. Sci.* **2012**, *3*, 863–867. https://doi.org/10.1039/C1SC00708D.

(68) Yashima, E.; Maeda, K.; Iida, H.; Furusho, Y.; Nagai, K. Helical Polymers : Synthesis , Structures , and Functions. *Chem. Rev.* **2009**, 6102–6211.

(69) Miles, A. J.; Janes, R. W.; Wallace, B. A. Tools and Methods for Circular Dichroism Spectroscopy of Proteins: A Tutorial Review. *Chem. Soc. Rev.* **2021**, *50*, 8400–8413. https://doi.org/10.1039/D0CS00558D.

(70) Djerassi, C. *Optical Rotatory Dispersion: Applications to Organic Chemistry*; McGraw-Hill: New York, NY, USA, 1960.

(71) Maxwell, J. C. A Dynamical Theory of the Electromagnetic Field. *Phil. Trans. R. Soc.* **1865**, *155*, 459–512. https://doi.org/10.1038/119125a0.

(72) Bachmann, L. M.; Miller, W. G. Spectrophotometry. In Contemporary Practice in Clinical Chemistry. *Elsevier* **2020**, 119–133 https://doi.org/10.1016/B978-0-12-815499-1.00007-7.

(73) Kliger, D. S.; Lewis, J. W. *Polarized Light in Optics and Spectroscopy*; Elsevier Science: San Diego, CA, 1990.

(74) Trippe, S. Polarization and Polarimetry: A Review. *J. Korean Astron. Soc.* **2014**, *47*, 15–39. https://doi.org/10.5303/JKAS.2014.47.1.15.

(75) Brosseau, C. *Fundamentals of Polarized Light: A Statistical Optics Approach*; Academic Press: New York, NY, USA, 1998.

(76) Dispersion, O. R.; Dichroism, C. ORD and ECD. *J. Chem. Educ.* **1972**, *51*, A83. https://doi.org/10.1021/ed052pA83

(77) Jackson, J. D. *Classical Electrodynamics*; Wiley, New York, USA, 1998.

(78) Goldstein, D. H. *Polarized Light*, 3rd ed.; Taylor and Francis: United States of America, 2010.

(79) Anderson, J.; Gillen, C.; Wright, J.; Adams, C. S.; Hughes, I. G. Optical Rotation of White Light. *Am. J. Phys.* **2020**, *88*, 247–251. https://doi.org/10.1119/10.0000390.

(80) Eyring, H.; Liu, H.-C.; Caldwell, D. Optical Rotatory Dispersion and Circular Dichroism. *Chem. Rev.* **1968**, *68*, 525–540. https://doi.org/10.1021/cr60255a001.

(81) Fasman, G. D. *Circular Dichroism and the Conformational Analysis of Biomolecules*; Fasman, G. D., Ed.; Springer US: Boston, MA, 1996. https://doi.org/10.1007/978-1-4757-2508-7.

(82) Hammes, G. G. *Spectroscopy for the Biological Sciences*; John Wiley & Sons, Inc.: New Jersey, 2005.

(83) Gottarelli, G.; Lena, S.; Masiero, S.; Pieraccini, S.; Spada, G. P. The Use of Circular Dichroism Spectroscopy for Studying the Chiral Molecular Self-Assembly: An Overview. *Chirality* **2008**, *20*, 471–485. https://doi.org/10.1002/chir.20459.

(84) Johnson, W. C. Secondary Structure of Proteins through Circular Dichroism Spectroscopy. *Ann. Rev. Biophys. Chem.* **1988**, *17*, 145–166.

(85) Martin, S. R.; Schilstra, M. J. Circular Dichroism and Its Application to the Study of Biomolecules. In *Methods in Cell Biology*. **200**8; Vol. 84, 263–293. https://doi.org/10.1016/S0091-679X(07)84010-6.

(86) Greenfield, J. L.; Wade, J.; Brandt, J. R.; Shi, X.; Penfold, T. J.; Fuchter, M.

J. Pathways to Increase the Dissymmetry in the Interaction of Chiral Light and Chiral Molecules. *Chem. Sci.* **2021**, *12*, 8589–8602. https://doi.org/10.1039/D1SC02335G.

(87) Peters, K. C.; Mekala, S.; Gross, R. A.; Singer, K. D. Cooperative Self-Assembly of Helical Exciton-Coupled Biosurfactant-Functionalized Porphyrin Chromophores. *ACS Appl. Bio Mater.* **2019**, *2*, 1703–1713. https://doi.org/10.1021/acsabm.9b00086.

(88) Koeckelberghs, G.; De Groof, L.; Sioncke, S.; Verbiest, T.; Persoons, A.; Samyn, C. Synthesis of Chiral Helical Chromophore-Functionalized Polybinaphthalenes. *Macromol. Rapid Commun.* **2003**, *24*, 413–419. https://doi.org/10.1002/marc.200390058.

(89) Ma, L.; Hu, Q.-S.; Vitharana, D.; Wu, C.; Kwan, C. M. S.; Pu, L. A New Class of Chiral Conjugated Polymers with a Propeller-Like Structure. *Macromolecules* **1997**, *30*, 204–218. https://doi.org/10.1021/ma961192e.

(90) Nishikawa, T.; Nagata, Y.; Suginome, M. Poly(Quinoxaline-2,3-Diyl) as a Multifunctional Chiral Scaffold for Circularly Polarized Luminescent Materials: Color Tuning, Energy Transfer, and Switching of the CPL Handedness. *ACS Macro Lett.* **2017**, 431–435. https://doi.org/10.1021/acsmacrolett.7b00131.

(91) Hu, L.; Yan, Z.; Xu, H. Advances in Synthesis and Application of Near-Infrared Absorbing Squaraine Dyes. *RSC Adv.* **2013**, *3*, 7667. https://doi.org/10.1039/c3ra23048a.

(92) Shindy, H. A. Fundamentals in the Chemistry of Cyanine Dyes: A Review. *Dye. Pigment.* **2017**, *145*, 505–513. https://doi.org/10.1016/j.dyepig.2017.06.029.

(93) Mustroph, H. Oxonol Dyes. *Phys. Sci. Rev.* **2022**, *7*, 37–43. https://doi.org/10.1515/psr-2020-0189.

(94) Treibs, A.; Jacob, K. Cyclotrimethine Dyes Derived from Squaric Acid. *Angew. Chem. Int. Ed.* **1965**, *4*, 694–694. https://doi.org/10.1002/anie.196506941.

(95) Liebermann, H. Über Ester Der Succinylobernsteinsäure Und Ihre Reaktionen Gegen Ammoniak Und Primäre Amine. *Liebigs Ann. Chem.* **1914**, *404*, 272–321. https://doi.org/10.1002/jlac.19144040303.

(96) Schmidt, A. H. Reaktionen von Quadratsäure Und Quadratsäure-Derivaten. *Synthesis* **1980**, *12*, 961–994. https://doi.org/10.1055/s-1980-29291.

(97) Wang, S.; Hall, L.; Diev, V. V.; Haiges, R.; Wei, G.; Xiao, X.; Djurovich, P. I.; Forrest, S. R.; Thompson, M. E. N,N-Di Aryl Anilinosquaraines and Their Application to Organic Photovoltaics. *Chem. Mater.* **2011**, *23*, 4789–4798. https://doi.org/10.1021/cm2020803.

(98) Oswald, B.; Lehmann, F.; Simon, L.; Terpetschnig, E.; Wolfbeis, O. S. Red Laser-Induced Fluorescence Energy Transfer in an Immunosystem. *Anal. Biochem.* **2000**, *280*, 272–277. https://doi.org/10.1006/abio.2000.4553.

(99) Terpetsching, E.; Szmacinski, H.; Lakowicz, J. R. Synthesis, Spectral Properties and Photostabilities of Symmetrical and Unsymmetrical Squarines; a New Class of Flourophores with Long-Wavelength Exiciation and Emmision. *Anal. Chim. Acta* **1993**, *282*, 633–641. https://doi.org/10.1016/0003-2670(93)80128-8.

(100) George Thomas, K.; Thomas, K. J.; Das, S.; George, M. V. A Squaraine-Based near-Infrared Absorbing Sensor for the Selective Detection of Transition and Other Metal Ions in Aqueous Media. *Chem. Commun.* **1997**, *6*, 597–598. https://doi.org/10.1039/a608397h.

(101) Ajayaghosh, A. Chemistry of Squaraine-Derived Materials: Near-IR Dyes, Low Band Gap Systems, and Cation Sensors. *Acc. Chem. Res.* **2005**, *38*, 449–459. https://doi.org/10.1021/ar0401000.

(102) Grande, V.; Shen, C.-A.; Deiana, M.; Dudek, M.; Olesiak-Banska, J.; Matczyszyn, K.; Würthner, F. Selective Parallel G-Quadruplex Recognition by a NIR-to-NIR Two-Photon Squaraine. *Chem. Sci.* **2018**, *9*, 8375–8381. https://doi.org/10.1039/C8SC02882F.

(103) Chen, C.; Marder, S. R.; Cheng, L.-T. Molecular First Hyperpolarizabilities of a New Class of Asymmetric Squaraine Dyes. *J. Chem. Soc. Chem. Commun.* **1994**, *3*, 259. https://doi.org/10.1039/c39940000259.

(104) Law, K. Y. Organic Photoconductive Materials: Recent Trends and Developments. *Chem. Rev.* **1993**, *93*, 449–486. https://doi.org/10.1021/cr00017a020.

(105) Das, S.; Thomas, K. G.; Thomas, K. J.; Kamat, P. V.; George, M. V. Photochemistry of Squaraine Dyes. 8. Photophysical Properties of Crown Ether Squaraine Fluoroionophores and Their Metal Ion Complexes. *J. Phys. Chem.* **1994**, *98*, 9291–9296. https://doi.org/10.1021/j100088a033.

(106) Singh, A. K.; Mele Kavungathodi, M. F.; Nithyanandhan, J. Alkyl-Group-Wrapped Unsymmetrical Squaraine Dyes for Dye-Sensitized Solar Cells: Branched Alkyl Chains Modulate the Aggregation of Dyes and Charge Recombination Processes. *ACS Appl. Mater. Interfaces* **2020**, *12*, 2555–2565. https://doi.org/10.1021/acsami.9b19809.

(107) Della Pelle, A. M.; Homnick, P. J.; Bae, Y.; Lahti, P. M.; Thayumanavan, S. Effect of Substituents on Optical Properties and Charge-Carrier Polarity of Squaraine Dyes. *J. Phys. Chem. C* **2014**, *118*, 1793–1799. https://doi.org/10.1021/jp410362d.

(108) Chen, G.; Sasabe, H.; Igarashi, T.; Hong, Z.; Kido, J. Squaraine Dyes for Organic Photovoltaic Cells. *J. Mater. Chem. A* **2015**, *3*, 14517–14534. https://doi.org/10.1039/C5TA01879J.

(109) Basheer, M. C.; Alex, S.; George Thomas, K.; Suresh, C. H.; Das, S. A Squaraine-Based Chemosensor for Hg2+ and Pb2+. *Tetrahedron* **2006**, *62*,

605–610. https://doi.org/10.1016/j.tet.2005.10.012.

(110) Arunkumar, E.; Chithra, P.; Ajayaghosh, A. A Controlled Supramolecular Approach toward Cation-Specific Chemosensors: Alkaline Earth Metal Ion-Driven Exciton Signaling in Squaraine Tethered Podands. *J. Am. Chem. Soc.* **2004**, *126*, 6590–6598. https://doi.org/10.1021/ja0393776.

(111) Liu, X.; Li, N.; Xu, M.-M.; Jiang, C.; Wang, J.; Song, G.; Wang, Y. Dual Sensing Performance of 1,2-Squaraine for the Colorimetric Detection of Fe^{3+} and Hg^{2+} Ions. *Materials* **2018**, *11*, 1998. https://doi.org/10.3390/ma11101998.

(112) Ahn, H.-Y.; Yao, S.; Wang, X.; Belfield, K. D. Near-Infrared-Emitting Squaraine Dyes with High 2PA Cross-Sections for Multiphoton Fluorescence Imaging. *ACS Appl. Mater. Interfaces* **2012**, *4*, 2847–2854. https://doi.org/10.1021/am300467w.

(113) Arunkumar, E.; Ajayaghosh, A.; Daub, J. Selective Calcium Ion Sensing with a Bichromophoric Squaraine Foldamer. *J. Am. Chem. Soc.* **2005**, *127*, 3156–3164. https://doi.org/10.1021/ja045760e.

(114) Wang, W.; Fu, A.; You, J.; Gao, G.; Lan, J.; Chen, L. Squaraine-Based Colorimetric and Fluorescent Sensors for Cu2+-Specific Detection and Fluorescence Imaging in Living Cells. *Tetrahedron* **2010**, *66*, 3695–3701. https://doi.org/10.1016/j.tet.2010.03.070.

(115) McEwen, J. J.; Wallace, K. J. Squaraine Dyes in Molecular Recognition and Self-Assembly. *Chem. Commun.* **2009**, *42*, 6339. https://doi.org/10.1039/b909572a.

(116) Sprenger, H. -E; Ziegenbein, W. The Cyclobutenediylium Cation, a Novel Chromophore from Squaric Acid. *Angew. Chem Int. Ed.* **1967**, *6*, 553–554. https://doi.org/10.1002/anie.196705531.

(117) Sprenger, H.-E.; Ziegenbein, W. Cyclobutenediylium Dyes. *Angew. Chem.*

Int. Ed. **1968**, *7*, 530–535. https://doi.org/10.1002/anie.196805301.

(118) Keil, D.; Hartmann, H. Synthesis and Characterization of a New Class of Unsymmetrical Squaraine Dyes. *Dye. Pigment.* **2001**, *49*, 161–179. https://doi.org/10.1016/S0143-7208(01)00016-X.

(119) Wendling, L. A.; Koster, S. K.; Murray, J. E.; West, R. Syntheses and Properties of 1,2- and 1,3-Diquinocyclobutanediones. *J. Org. Chem.* **1977**, *42*, 1126–1130.

(120) Yagi, S.; Nakazumi, H. *Heterocyclic Polymethine Dyes* in *Topics in Heterocyclic Chemistry*. *14*, **2008**.

(121) Suzuki, M.; Hanabusa, K. Polymer Organogelators That Make Supramolecular Organogels through Physical Cross-Linking and Self-Assembly. *Chem. Soc. Rev.* **2010**, *39*, 455–463. https://doi.org/10.1039/B910604A.

(122) De Feyter, S.; De Schryver, F. C. Two-Dimensional Supramolecular Self-Assembly Probed by Scanning Tunneling Microscopy. *Chem. Soc. Rev.* **2003**, *32*, 139–150. https://doi.org/10.1039/b206566p.

(123) McKerrow, A. J.; Buncel, E.; Kazmaier, P. M. Aggregation of Squaraine Dyes: Structure–Property Relationships and Solvent Effects. *Can. J. Chem.* **1995**, *73*, 1605–1615. https://doi.org/10.1139/v95-200.

(124) Mayerhöffer, U.; Würthner, F. Cooperative Self-Assembly of Squaraine Dyes. *Chem. Sci.* **2012**, *3*, 1215. https://doi.org/10.1039/c2sc00996j.

(125) Alex, S.; Basheer, M. C.; Arun, K. T.; Ramaiah, D.; Das, S. Aggregation Properties of Heavy Atom Substituted Squaraine Dyes: Evidence for the Formation of J-Type Dimer Aggregates in Aprotic Solvents. *J. Phys. Chem. A* **2007**, *111*, 3226–3230. https://doi.org/10.1021/jp068492a.

(126) Chua, M. H.; Zhou, H.; Lin, T. T.; Wu, J.; Xu, J. Triphenylethylene- and Tetraphenylethylene-Functionalized 1,3-Bis(Pyrrol-2-Yl)Squaraine Dyes:

Synthesis, Aggregation-Caused Quenching to Aggregation-Induced Emission, and Thiol Detection. *ACS Omega* **2018**, *3*, 16424–16435. https://doi.org/10.1021/acsomega.8b02479.

(127) Herz, A. H. Aggregation of Sensitizing Dyes in Solution and Their Adsorption onto Silver Halides. *Adv. Colloid Interface Sci.* **1977**, *8*, 237–298. https://doi.org/10.1016/0001-8686(77)80011-0.

(128) Dimitriev, O. P. Anomalous Aggregation of Squaraine Dyes in Confined Solutions. *J. Mol. Liq.* **2005**, *120*, 131–133. https://doi.org/10.1016/j.molliq.2004.07.053.

(129) Klymchenko, A. S. Emerging Field of Self-Assembled Fluorescent Organic Dye Nanoparticles. *J. Nanosci. Lett.* **2013**, *3*, 1–8.

(130) Hestand, N. J.; Spano, F. C. Expanded Theory of H- and J-Molecular Aggregates: The Effects of Vibronic Coupling and Intermolecular Charge Transfer. *Chem. Rev.* **2018**, *118*, 7069–7163. https://doi.org/10.1021/acs.chemrev.7b00581.

(131) Bayda, M.; Dumoulin, F.; Hug, G. L.; Koput, J.; Gorniak, R.; Wojcik, A. Fluorescent H-Aggregates of an Asymmetrically Substituted Mono-Amino Zn(II) Phthalocyanine. *Dalt. Trans.* **2017**, *46*, 1914–1926. https://doi.org/10.1039/C6DT02651F.

(132) Würthner, F.; Kaiser, T. E.; Saha-Möller, C. R. J-Aggregates: From Serendipitous Discovery to Supramolecular Engineering of Functional Dye Materials. *Angew. Chem. Int. Ed.* **2011**, *50*, 3376–3410. https://doi.org/10.1002/anie.201002307.

(133) Chen, Z.; Lohr, A.; Saha-Möller, C. R.; Würthner, F. Self-Assembled π-Stacks of Functional Dyes in Solution: Structural and Thermodynamic Features. *Chem. Soc. Rev.* **2009**, *38*, 564–584. https://doi.org/10.1039/B809359H.

(134) Dimitriev, O. P.; Dimitriyeva, A. P.; Tolmachev, A. I.; Kurdyukov, V. V. Solvent-Induced Organization of Squaraine Dyes in Solution Capillary Layers and Adsorbed Films. *J. Phys. Chem. B* **2005**, *109*, 4561–4567. https://doi.org/10.1021/jp045097g.

(135) Kasha, M.; Rawls, H. R.; Ashraf El-Bayoumi, M. The Exciton Model in Molecular Spectroscopy. *Pure Appl. Chem.* **1965**, *11*, 371–392. https://doi.org/10.1351/pac196511030371.

(136) Stoll, R. S.; Severin, N.; Rabe, J. P.; Hecht, S. Synthesis of a Novel Chiral Squaraine Dye and Its Unique Aggregation Behavior in Solution and in Self-Assembled Monolayers. *Adv. Mater.* **2006**, *18*, 1271–1275. https://doi.org/10.1002/adma.200502094.

(137) Schulz, M.; Mack, M.; Kolloge, O.; Lützen, A.; Schiek, M. Organic Photodiodes from Homochiral L-Proline Derived Squaraine Compounds with Strong Circular Dichroism. *Phys. Chem. Chem. Phys.* **2017**, *19*, 6996–7008. https://doi.org/10.1039/c7cp00306d.

(138) Shimizu, M.; Fukui, H.; Natakani, M.; Sakaguchi, H. Aggregation-Induced Orange-to-Red Fluorescence of 2,5-Bis(Diarylamino)Terephthalic Acid Dithioesters. *European J. Org. Chem.* **2016**, *36*, 5950–5956. https://doi.org/10.1002/ejoc.201601067.

(139) Tang, B.; Wang, C.; Wang, Y.; Zhang, H. Efficient Red-Emissive Organic Crystals with Amplified Spontaneous Emissions Based on a Single Benzene Framework. *Angew. Chem. Int. Ed.* **2017**, *56*, 12543–12547. https://doi.org/10.1002/anie.201706517.

(140) Shimizu, M.; Asai, Y.; Takeda, Y.; Yamatani, A.; Hiyama, T. Twisting Strategy Applied to N,N-Diorganoquinacridones Leads to Organic Chromophores Exhibiting Efficient Solid-State Fluorescence. *Tetrahedron Lett.* **2011**, *52* (32), 4084–4089. https://doi.org/10.1016/j.tetlet.2011.05.087.

(141) Baeyer, A. Ueber Den Succinylobernsteinsäureäther. *Berichte der Dtsch.*

Chem. Gesellschaft **1886**, *19*, 428–433. https://doi.org/10.1002/cber.188601901105.

(142) Zhang, Y.; Starynowicz, P.; Christoffers, J. Fluorescent Bis(Oligophenylylamino)Terephthalates. *European J. Org. Chem.* **2008**, *2008*, 3488–3495. https://doi.org/10.1002/ejoc.200800211.

(143) Christoffers, J. Diaminoterephthalate Fluorescence Dyes - Versatile Tools for Life Sciences and Materials Science. *European J. Org. Chem.* **2018**, 2366–2377. https://doi.org/10.1002/ejoc.201701447.

(144) Wallisch, M.; Sulmann, S.; Koch, K. W.; Christoffers, J. Bifunctional Diaminoterephthalate Fluorescent Dye as Probe for Cross-Linking Proteins. *Chem. - A Eur. J.* **2017**, *23*, 6535–6543. https://doi.org/10.1002/chem.201700774.

(145) Wache, N.; Schröder, C.; Koch, K.-W.; Christoffers, J. Diaminoterephthalate Turn-On Fluorescence Probes for Thiols-Tagging of Recoverin and Tracking of Its Conformational Change. *ChemBioChem* **2012**, *13*, 993–998. https://doi.org/10.1002/cbic.201200027.

(146) Wache, N.; Scholten, A.; Klüner, T.; Koch, K.-W.; Christoffers, J. Turning On Fluorescence with Thiols - Synthetic and Computational Studies on Diaminoterephthalates and Monitoring the Switch of the Ca^{2+} Sensor Recoverin. *Eur. J. Org. Chem.* **2012**, *2012*, 5712–5722. https://doi.org/10.1002/ejoc.201200879.

(147) Freimuth, L.; Christoffers, J. Bifunctional Diaminoterephthalate Scaffolds as Fluorescence Turn-On Probes for Thiols. *Chem. - A Eur. J.* **2015**, *21*, 8214–8221. https://doi.org/10.1002/chem.201500494.

(148) Pflantz, R.; Christoffers, J. Diaminoterephthalates: Scaffolds for Combinatorial Chemistry. *Chem. - A Eur. J.* **2009**, *15*, 2200–2209. https://doi.org/10.1002/chem.200802151.

(149) Moore, J. A.; Kochanowski, J. E. Poly(Amine Esters) Derived from Diethyl 1,4-Cyclohexanedione-2,5-Dicarboxylate. *Macromolecules* **1975**, *8*, 121–127. https://doi.org/10.1021/ma60044a006.

(150) Yokoyama, A.; Kuramochi, J.; Kiyota, R.; Kishimoto, K.; Takaishi, K.; Yokozawa, T. Polymerization of 2,5-Diaminoterephthalic Acid-Type Monomers for the Synthesis of Polyamides Containing Ladder Unit. *J. Polym. Sci. Part A Polym. Chem.* **2017**, *55*, 2365–2372. https://doi.org/10.1002/pola.28625.

(151) Shimizu, M.; Shigitani, R.; Kinoshita, T.; Sakaguchi, H. (Poly)Terephthalates with Efficient Blue Emission in the Solid State. *Chem. – An Asian J.* **2019**, *14*, 1792–1800. https://doi.org/10.1002/asia.201801619.

(152) Ünay, G. Ç.; Yıldırım, E.; Akdag, A. Chiral Polyurea from Tartaric Acid Derived and Lysine Backbone: A Synthetic and Computational Study. *ChemistrySelect* **2020**, *5*, 13358–13369. https://doi.org/10.1002/slct.202003534.

(153) Beverina, L.; Salice, P. Squaraine Compounds: Tailored Design and Synthesis towards a Variety of Material Science Applications. *European J. Org. Chem.* **2010**, *2010*, 1207–1225. https://doi.org/10.1002/ejoc.200901297.

(154) Beverina, L.; Sassi, M. Twists and Turns Around a Square: The Many Faces of Squaraine Chemistry. *Synlett* **2014**, *25*, 477–490. https://doi.org/10.1055/s-0033-1340482.

(155) Xia, G.; Wang, H. Squaraine Dyes: The Hierarchical Synthesis and Its Application in Optical Detection. *J. Photochem. Photobiol. C Photochem. Rev.* **2017**, *31*, 84–113. https://doi.org/10.1016/j.jphotochemrev.2017.03.001.

(156) Sopeña, S.; Martin, E.; Escudero-Adán, E. C.; Kleij, A. W. Pushing the Limits with Squaramide-Based Organocatalysts in Cyclic Carbonate

Synthesis. *ACS Catal.* **2017**, *7*, 3532–3539. https://doi.org/10.1021/acscatal.7b00475.

(157) Rostami, A.; Colin, A.; Li, X. Y.; Chudzinski, M. G.; Lough, A. J.; Taylor, M. S. N ,N′ -Diarylsquaramides: General, High-Yielding Synthesis and Applications in Colorimetric Anion Sensing. *J. Org. Chem.* **2010**, *75*, 3983–3992. https://doi.org/10.1021/jo100104g.

(158) Fu, N.; Allen, A. D.; Kobayashi, S.; Tidwell, T. T.; Vukovic, S.; Arumugam, S.; Popik, V. V; Mishima, M. Amino Substituted Bisketenes: Generation, Structure, and Reactivity. *J. Org. Chem.* **2007**, *72*, 1951–1956. https://doi.org/10.1021/jo062090h.

(159) Ta, D. D.; Dzyuba, S. V. Squaraine-Based Optical Sensors: Designer Toolbox for Exploring Ionic and Molecular Recognitions. *Chemosensors* **2021**, *9*, 302. https://doi.org/10.3390/chemosensors9110302.

(160) Kabatc, J.; Kostrzewska, K.; Jurek, K.; Dobosz, R.; Orzeł, Ł. 1,3-Bis(Phenylamino)Squaraine – Photophysical and Photochemical Properties. *Dyes Pigments* **2016**, *127*, 179–186. https://doi.org/10.1016/j.dyepig.2015.12.027.

(161) Jurek, K.; Kabatc, J.; Kostrzewska, K. The Synthesis and Spectroscopic Studies of New Aniline-Based Squarylium Dyes. *Dyes Pigments* **2016**, *133*, 273–279. https://doi.org/10.1016/j.dyepig.2016.05.027.

(162) Johnson, C. R.; Ansari, M. I.; Coop, A. Tetrabutylammonium Bromide-Promoted Metal-Free, Efficient, Rapid, and Scalable Synthesis of N-Aryl Amines. *ACS Omega* **2018**, *3*, 10886–10890. https://doi.org/10.1021/acsomega.8b01426.

(163) Wolfe, J. P.; Rennels, R. A.; Buchwald, S. L. Intramolecular Palladium-Catalyzed Aryl Amination and Aryl Amidation. *Tetrahedron* **1996**, *52*, 7525–7546. https://doi.org/10.1016/0040-4020(96)00266-9.

(164) de Lange, B.; Lambers-Verstappen, M.; Schmieder-van de Vondervoort, L.; Sereinig, N.; de Rijk, R.; de Vries, A.; de Vries, J. Aromatic Amination of Aryl Bromides Catalysed by Copper/β-Diketone Catalysts: The Effect of Concentration. *Synlett* **2006**, *2006*, 3105–3109. https://doi.org/10.1055/s-2006-951510.

(165) Schulz, M.; Zablocki, J.; Abdullaeva, O. S.; Brück, S.; Balzer, F.; Lützen, A.; Arteaga, O.; Schiek, M. Giant Intrinsic Circular Dichroism of Prolinol-Derived Squaraine Thin Films. *Nat. Commun.* **2018**, *9*, 1–10. https://doi.org/10.1038/s41467-018-04811-7.

(166) Zablocki, J.; Arteaga, O.; Balzer, F.; Hertel, D.; Holstein, J. J.; Clever, G.; Anhäuser, J.; Puttreddy, R.; Rissanen, K.; Meerholz, K.; et al. Polymorphic Chiral Squaraine Crystallites in Textured Thin Films. *Chirality* **2020**, *32*, 619–631. https://doi.org/10.1002/chir.23213.

(167) Rösch, A. T.; Zhu, Q.; Robben, J.; Tassinari, F.; Meskers, S. C. J.; Naaman, R.; Palmans, A. R. A.; Meijer, E. W. Helicity Control in the Aggregation of Achiral Squaraine Dyes in Solution and Thin Films. *Chem. - A Eur. J.* **2021**, *27*, 298–306. https://doi.org/10.1002/chem.202002695.

(168) Carpino, L. A. Coupling Additive. *J. Am. Chem. Soc.* **1993**, *115*, 4397–4398.

(169) Dunetz, J. R.; Magano, J.; Weisenburger, G. A. Large-Scale Applications of Amide Coupling Reagents for the Synthesis of Pharmaceuticals. *Org. Process Res. Dev.* **2016**, *20*, 140–177. https://doi.org/10.1021/op500305s.

(170) Montalbetti, C. A. G. N.; Falque, V. Amide Bond Formation and Peptide Coupling. *Tetrahedron* **2005**, *61*, 10827–10852. https://doi.org/10.1016/j.tet.2005.08.031.

(171) Carpino, L. A.; Imazumi, H.; Foxman, B. M.; Vela, M. J.; Henklein, P.; El-Faham, A.; Klose, J.; Bienert, M. Comparison of the Effects of 5- and 6-HOAt on Model Peptide Coupling Reactions Relative to the Cases for the 4- and 7-Isomers. *Org. Lett.* **2000**, *2*, 2253–2256.

https://doi.org/10.1021/ol006013z.

(172) Pop, I. E.; Déprez, B. P.; Tartar, A. L. Versatile Acylation of N-Nucleophiles Using a New Polymer-Supported 1-Hydroxybenzotriazole Derivative. *J. Org. Chem.* **1997**, *62*, 2594–2603. https://doi.org/10.1021/jo961761g.

(173) Grondal, C. 4-Dimethylamino-Pyridine (DMAP). *Synlett* **2003**, *10*, 1568–1569.

(174) Khopkar, S.; Shankarling, G. Synthesis, Photophysical Properties and Applications of NIR Absorbing Unsymmetrical Squaraines: A Review. *Dyes Pigments.* **2019**, *170*, 107645. https://doi.org/10.1016/j.dyepig.2019.107645.

(175) de Napoli, L.; Messere, A; Palomba, D.; Piccialli, G.; Piccialli, V.; Evidente, A. Studies toward the Synthesis of Pinolidoxin, a Phytotoxic Nonenolide from the Fungus Ascochyta Pinodes. Determination of the Configuration at the C-7, C-8, and C-9 Chiral Centers and Stereoselective Synthesis of the C(6)-C(18) Fragment. *J. Org. Chem.* **2000**, *65*, 3432–3442. https://doi.org/10.1021/jo991722f.

(176) Rudin, A.; Hoegy, H. L. W. Universal Calibration in GPC. *J. Polym. Sci. Part A; Polym. Chem.* **1972**, *10*, 217–235. https://doi.org/10.1002/pol.1972.150100120.

(177) Ünay, G. Ç.; Akdag, A.; Yıldırım, E. Aggregation Studies of L and D Alanine Derivatized Squarine Dyes. *Manuscript was submitted.* **2022**.

(178) Mayr, H.; Ofial, A. R. Do General Nucleophilicity Scales Exist? *J. Phys. Org. Chem.* **2008**, *21*, 584–595. https://doi.org/10.1002/poc.1325.

(179) Nigst, T. A.; Antipova, A.; Mayr, H. Nucleophilic Reactivities of Hydrazines and Amines: The Futile Search for the α-Effect in Hydrazine Reactivities. *J. Org. Chem.* **2012**, *77*, 8142–8155. https://doi.org/10.1021/jo301497g.

(180) Gaussian 09, Revision A.02, M. J. Frisch, G. W. Trucks, H. B. Schlegel, G. E. Scuseria, M. A. Robb, J. R. Cheeseman, G. Scalmani, V. Barone, B. Mennucci, G. A. Petersson, H. Nakatsuji, M. Caricato, X. Li, H. P. Hratchian, A. F. Izmaylov, J. Bloino, G. Zheng, J. L. Sonnenberg, M. Hada, M. Ehara, K. Toyota, R. Fukuda, J. Hasegawa, M. Ishida, T. Nakajima, Y. Honda, O. Kitao, H. Nakai, T. Vreven, J. A. Montgomery, Jr., J. E. Peralta, F. Ogliaro, M. Bearpark, J. J. Heyd, E. Brothers, K. N. Kudin, V. N. Staroverov, R. Kobayashi, J. Normand, K. Raghavachari, A. Rendell, J. C. Burant, S. S. Iyengar, J. Tomasi, M. Cossi, N. Rega, J. M. Millam, M. Klene, J. E. Knox, J. B. Cross, V. Bakken, C. Adamo, J. Jaramillo, R. Gomperts, R. E. Stratmann, O. Yazyev, A. J. Austin, R. Cammi, C. Pomelli, J. W. Ochterski, R. L. Martin, K. Morokuma, V. G. Zakrzewski, G. A. Voth, P. Salvador, J. J. Dannenberg, S. Dapprich, A. D. Daniels, O. Farkas, J. B. Foresman, J. V. Ortiz, J. Cioslowski, and D. J. Fox, Gaussian, Inc., Wallingford CT, 2009.

(181) Dindaroğlu, M.; Akyol Dinçer, S.; Schmalz, H. G. Synthesis of C2-Symmetric Bisphosphine Ligands from Tartaric Acid, and Their Performance in the Pd-Catalyzed Asymmetric o-Allylation of a Phenol. *European J. Org. Chem.* **2014**, *2014*, 4315–4326. https://doi.org/10.1002/ejoc.201402326.

(182) Kim, B. M.; Bae, S. J.; So, S. M.; Yoo, H. T.; Chang, S. K.; Lee, J. H.; Kang, J. Synthesis of a Chiral Aziridine Derivative as a Versatile Intermediate for HIV Protease Inhibitors. *Org. Lett.* **2001**, *3*, 2349–2351. https://doi.org/ol016147s [pii].

(183) Shainyan, B. A.; Nindakova, L. O.; Ustinov, M. V.; Chipanina, N. N.; Sherstyannikova, L. V. New Chiral Diamines of the Dioxolane Series: (+)-(4S,5S)-2,2-Dimethyl-4,5-Bis(Diphenylaminomethyl)-1,3-Dioxolane and (+)-(4S,5S)-2,2-Dimethyl-4,5-Bis(Methylaminomethyl)-1,3-Dioxolane. *ChemInform* **2003**, *34*, 1802–1805. https://doi.org/10.1002/chin.200326134.

(184) Nour, H. F.; Hourani, N.; Kuhnert, N. Synthesis of Novel Enantiomerically Pure Tetra-Carbohydrazide Cyclophane Macrocycles. *Org. Biomol. Chem.* **2012**, *10*, 4381. https://doi.org/10.1039/c2ob25171j.

(185) Maurer, A.; Zeyher, C.; Amin, B.; Kalbacher, H. A Periodate-Cleavable Linker for Functional Proteomics under Slightly Acidic Conditions: Application for the Analysis of Intracellular Aspartic Proteases. *J. Proteome Res.* **2013**, *12*, 199–207. https://doi.org/10.1021/pr300758c.

(186) Hayashi, Y.; Kinoshita, Y.; Hidaka, K.; Kiso, A.; Uchibori, H.; Kimura, T.; Kiso, Y. Analysis of Amide Bond Formation with an α-Hydroxy-β-Amino Acid Derivative, 3-Amino-2-Hydroxy-4-Phenylbutanoic Acid, as an Acyl Component: Byproduction of Homobislactone. *J. Org. Chem.* **2001**, *66*, 5537–5544. https://doi.org/10.1021/jo010233o.

(187) Lippur, K.; Kanger, T.; Kriis, K.; Kailas, T.; Müürisepp, A.-M.; Pehk, T.; Lopp, M. Synthesis of (2S,2′S)-Bimorpholine N,N′-Quaternary Salts as Chiral Phase Transfer Catalysts. *Tetrahedron: Asymmetry* **2007**, *18*, 137–141. https://doi.org/10.1016/j.tetasy.2007.01.004.

(188) Balasubramanian, V.; Srinivasan, R.; Miskimins, R.; Sykes, A. G. A Simple Aza-Crown Ether Containing an Anthraquinone Fluorophore for the Selective Detection of Mg(II) in Living Cells. *Tetrahedron* **2016**, *72*, 205–209. https://doi.org/10.1016/j.tet.2015.11.033.

(189) Pagano, M.; Castagnolo, D.; Bernardini, M.; Fallacara, A. L.; Laurenzana, I.; Deodato, D.; Kessler, U.; Pilger, B.; Stergiou, L.; Strunze, S.; et al. The Fight against the Influenza A Virus H1N1: Synthesis, Molecular Modeling, and Biological Evaluation of Benzofurazan Derivatives as Viral RNA Polymerase Inhibitors. *ChemMedChem* **2014**, *9*, 129–150. https://doi.org/10.1002/cmdc.201300378.

(190) Varala, R.; Nuvula, S.; Adapa, S. R. Molecular Iodine-Catalyzed Facile Procedure for N -Boc Protection of Amines. *J. Org. Chem.* **2006**, *71*, 8283–

8286. https://doi.org/10.1021/jo0612473.

(191) Loddo, R.; Francesconi, V.; Laurini, E.; Boccardo, S.; Aulic, S.; Fermeglia, M.; Pricl, S.; Tonelli, M. 9-Aminoacridine-Based Agents Impair the Bovine Viral Diarrhea Virus (BVDV) Replication Targeting the RNA-Dependent RNA Polymerase (RdRp). *Bioorg. Med. Chem.* **2018**, *26*, 855–868. https://doi.org/10.1016/j.bmc.2018.01.001.

(192) Prasad, R. N.; Hawkins, L. R.; Tietje, K. Potential Antihypertensive Agents. II. Unsymmetrically 1,4-Disubstituted Piperazines. I. *J. Med. Chem.* **1968**, *11*, 1144–1150. https://doi.org/10.1021/jm00312a009.

(193) Bala, V.; Jangir, S.; Mandalapu, D.; Gupta, S.; Chhonker, Y. S.; Lal, N.; Kushwaha, B.; Chandasana, H.; Krishna, S.; Rawat, K.; et al. Dithiocarbamate–Thiourea Hybrids Useful as Vaginal Microbicides Also Show Reverse Transcriptase Inhibition: Design, Synthesis, Docking and Pharmacokinetic Studies. *Bioorg. Med. Chem. Lett.* **2015**, *25*, 881–886. https://doi.org/10.1016/j.bmcl.2014.12.062.

(194) Hochegger, P.; Faist, J.; Seebacher, W.; Saf, R.; Mäser, P.; Kaiser, M.; Weis, R. Synthesis and Structure-Activity Relationships for New 6-Fluoroquinoline Derivatives with Antiplasmodial Activity. *Bioorg. Med. Chem.* **2019**, *27*, 2052–2065. https://doi.org/10.1016/j.bmc.2019.03.061.

(195) Lazar, S.; Soukri, M.; Leger, J. .; Jarry, C.; Akssira, M.; Chirita, R.; Grig-Alexa, I. .; Finaru, A.; Guillaumet, G. Efficient Synthesis of 2- and 3-Substituted-2,3-Dihydro [1,4]Dioxino[2,3-b]Pyridine Derivatives. *Tetrahedron* **2004**, *60*, 6461–6473. https://doi.org/10.1016/j.tet.2004.06.041.

(196) Plater, M. J.; McKay, M.; Jackson, T. Synthesis of 1,3,5-Tris[4-(Diarylamino)Phenyl]Benzene and 1,3,5-Tris(Diarylamino)Benzene Derivatives. *J. Chem. Soc. Perkin Trans. 1* **2000**, *16*, 2695–2701. https://doi.org/10.1039/b002928i.

(197) Maity, A.; Ghosh, U.; Giri, D.; Mukherjee, D.; Maiti, T. K.; Patra, S. K. A

Water-Soluble BODIPY Based ‘OFF/ON’ Fluorescent Probe for the Detection of Cd 2+ Ions with High Selectivity and Sensitivity. *Dalt. Trans.* **2019**, *48*, 2108–2117. https://doi.org/10.1039/C8DT04016H.

(198) Shen, X.; Liu, H.; Li, Y.; Liu, S. Click-Together Azobenzene Dendrons: Synthesis and Characterization. *Macromolecules* **2008**, *41*, 2421–2425. https://doi.org/10.1021/ma7027566.

(199) Law, K. Y.; Bailey, F. C.; Bluett, L. J. Squaraine Chemistry. on the Anomalous Mass Spectra of Bis(4-Dimethylaminopheny1)Squaraine and Its Derivatives. *Can. J. Chem.* **1985**, *64*, 1607–1619. https://doi.org/10.1139/v86-267.

(200) Yan, Z.; Guang, S.; Xu, H.; Su, X.; Ji, X.; Liu, X. Supramolecular Self-Assembly Structures and Properties of Zwitterionic Squaraine Molecules. *RSC Adv.* **2013**, *3*, 8021. https://doi.org/10.1039/c3ra40690c.

(201) Liu, T.; Liu, X.; Wang, W.; Luo, Z.; Liu, M.; Zou, S.; Sissa, C.; Painelli, A.; Zhang, Y.; Vengris, M.; et al. Systematic Molecular Engineering of a Series of Aniline-Based Squaraine Dyes and Their Structure-Related Properties. *J. Phys. Chem. C* **2018**, *122*, 3994–4008. https://doi.org/10.1021/acs.jpcc.7b11997.

(202) Sferrazza, A.; Triolo, A.; M. Migneco, L.; Caminiti, R. Synthesis and Small and Wide Angle X-Ray Scattering Characterization of L-Proline Based Chiral Ionic Liquids. *Curr. Org. Chem.* **2015**, *19*, 99–104. https://doi.org/10.2174/1385272819666141211221640.

(203) Han, H. W.; Qiu, H. Y.; Hu, C.; Sun, W. X.; Yang, R. W.; Qi, J. L.; Wang, X. M.; Lu, G. H.; Yang, Y. H. Design, Synthesis and Anti-Cancer Activity Evaluation of Podophyllotoxin-Norcantharidin Hybrid Drugs. *Bioorganic Med. Chem. Lett.* **2016**, *26*, 3237–3242. https://doi.org/10.1016/j.bmcl.2016.05.063.

(204) Von Gersdorff, J.; Kirste, B.; Niethammer, D.; Harrer, W.; Kurreck, H. EPR

and ENDOR Investigations of Dynamic Processes in Sterically Overcrowded Phenoxyl-Type Galvinoxyl Radicals. *Magn. Reson. Chem.* **1988**, *26*, 416–424. https://doi.org/10.1002/mrc.1260260513.

APPENDICES

A. NMR Spectra

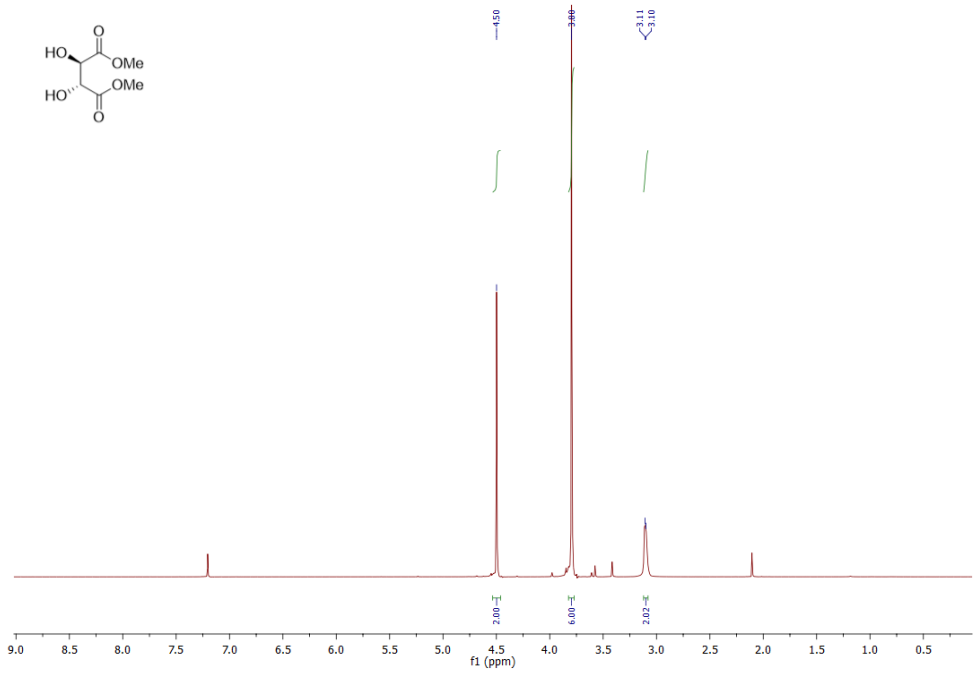

Figure A.1. ^{1}H NMR Spectrum of **TL-1**

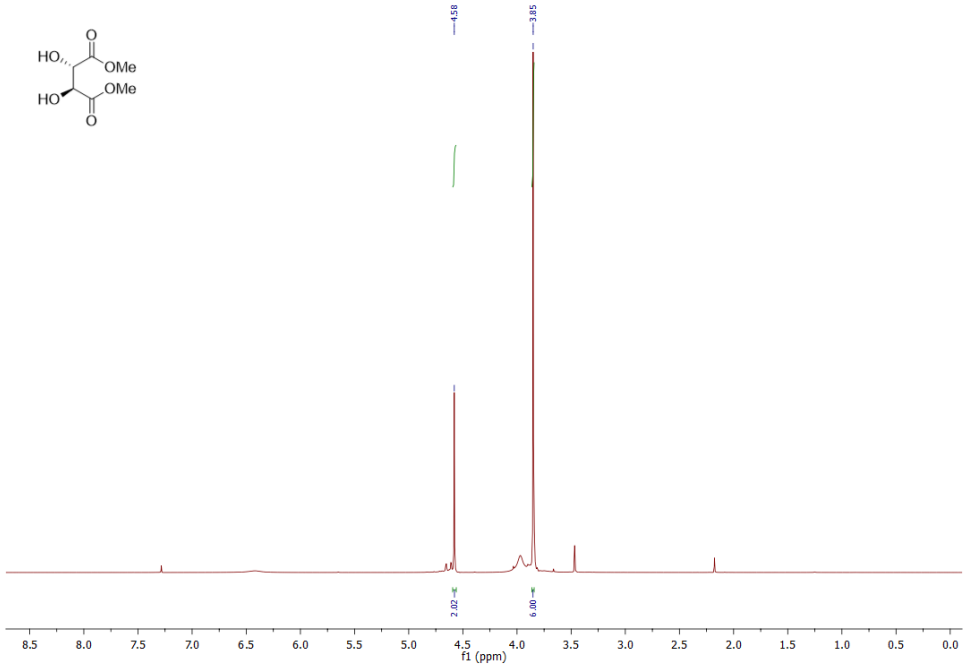

Figure A.2. ^{1}H NMR Spectrum of **TD-1**

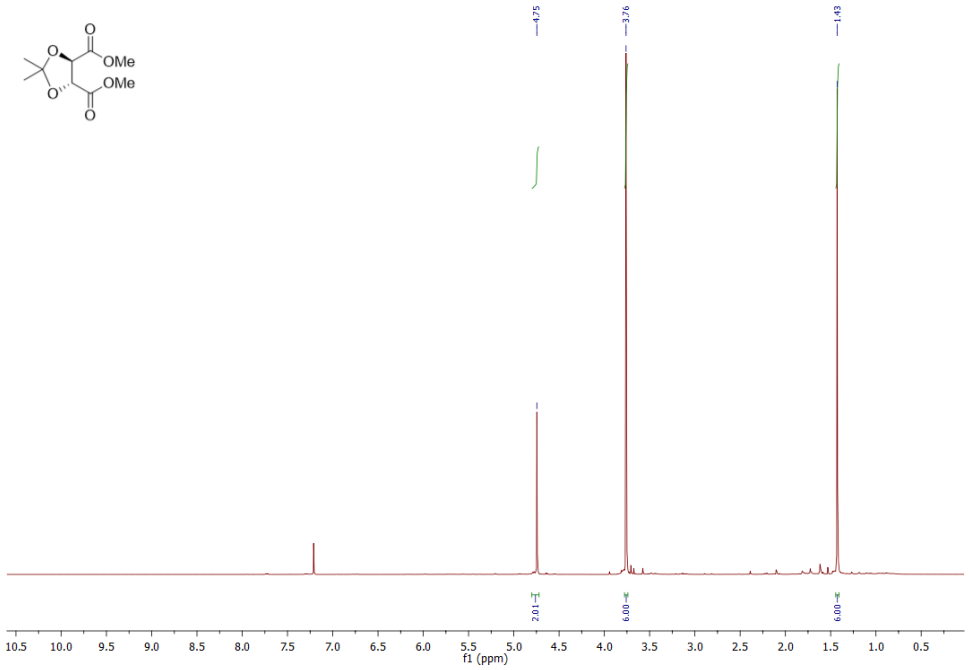

Figure A.3. ^{1}H NMR Spectrum of **TL-2**

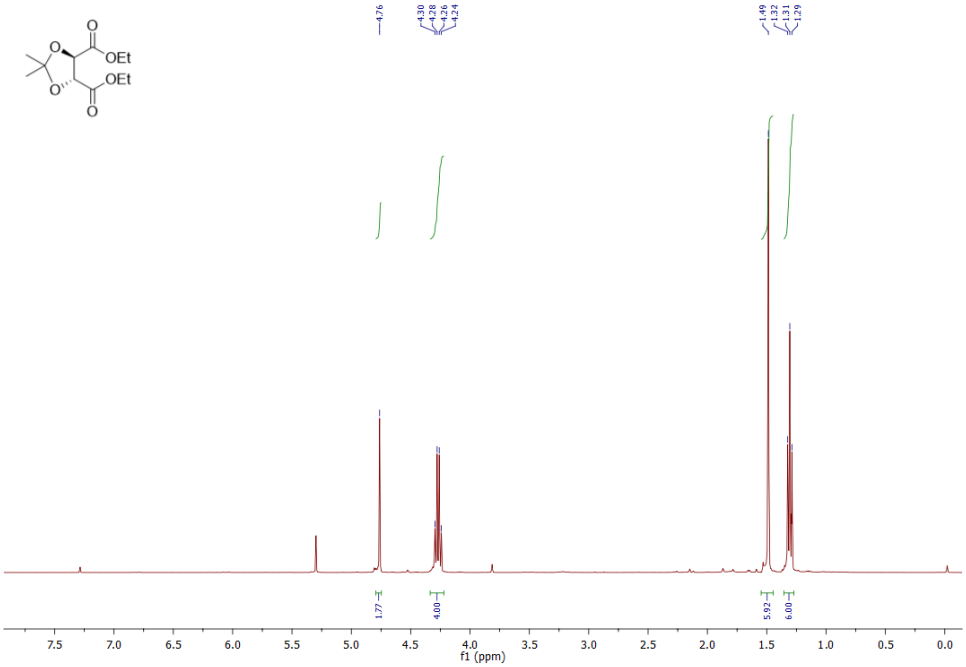

Figure A.4. ^{1}H NMR Spectrum of **TL-2a**

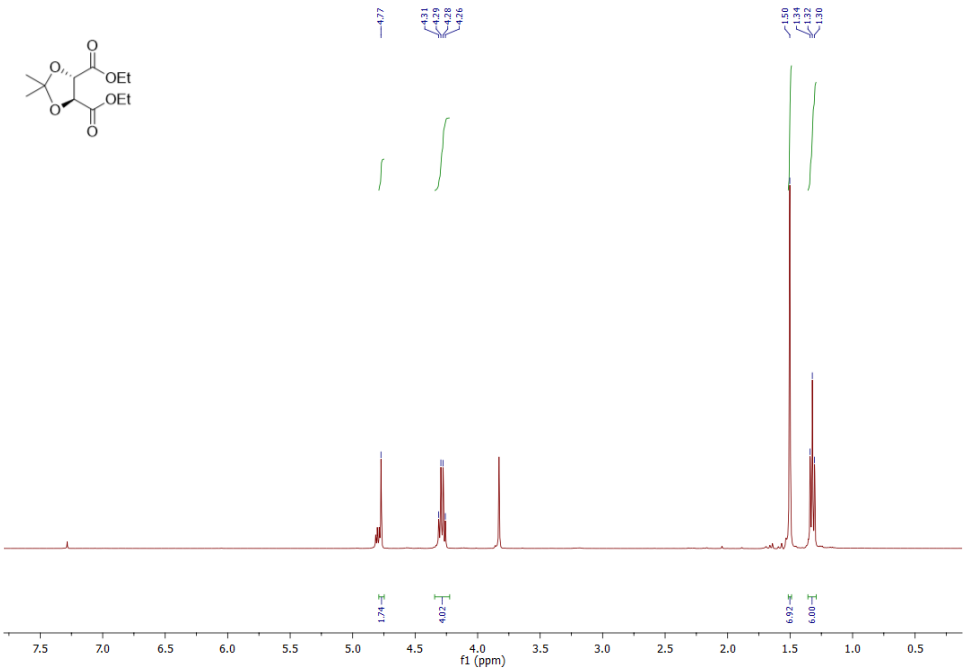

Figure A.5. ^{1}H NMR Spectrum of **TD-2a**

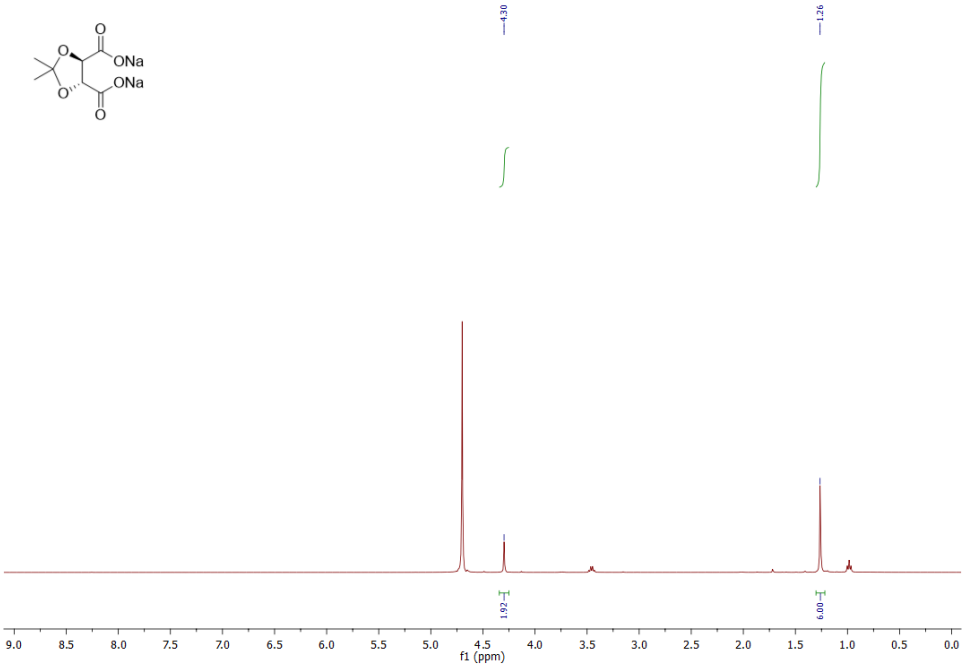

Figure A.6. ^{1}H NMR Spectrum of **TL-3**

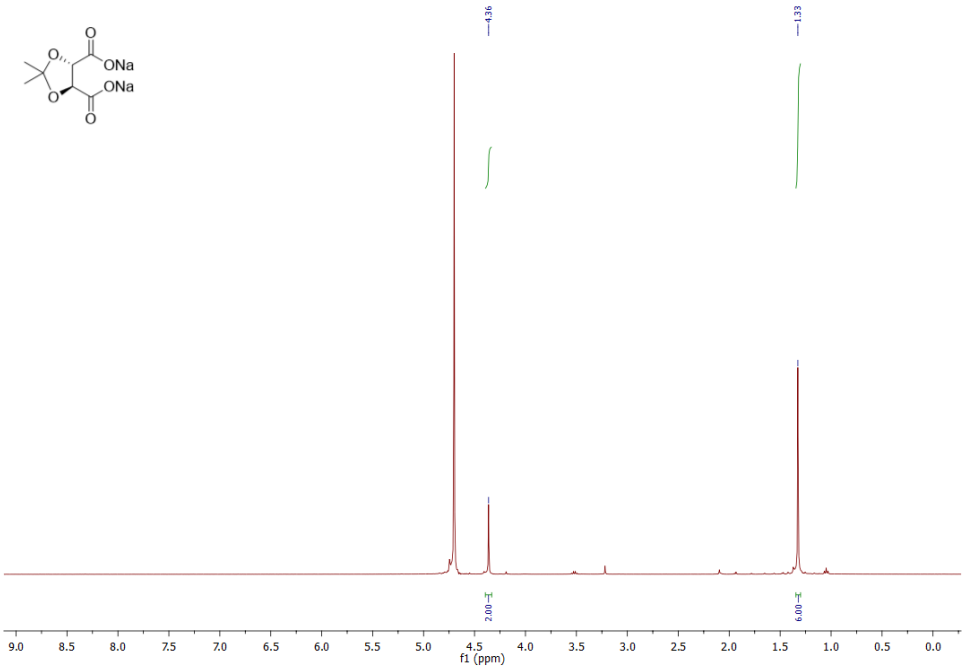

Figure A.7. ^{1}H NMR Spectrum of **TD-3**

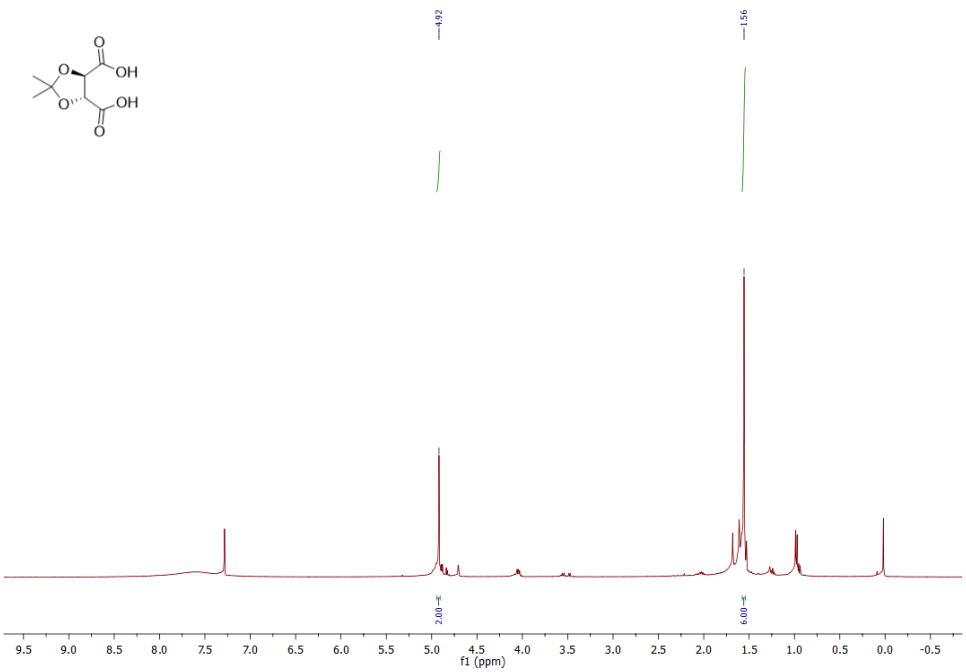

Figure A.8. ^{1}H NMR Spectrum of **TL-4**

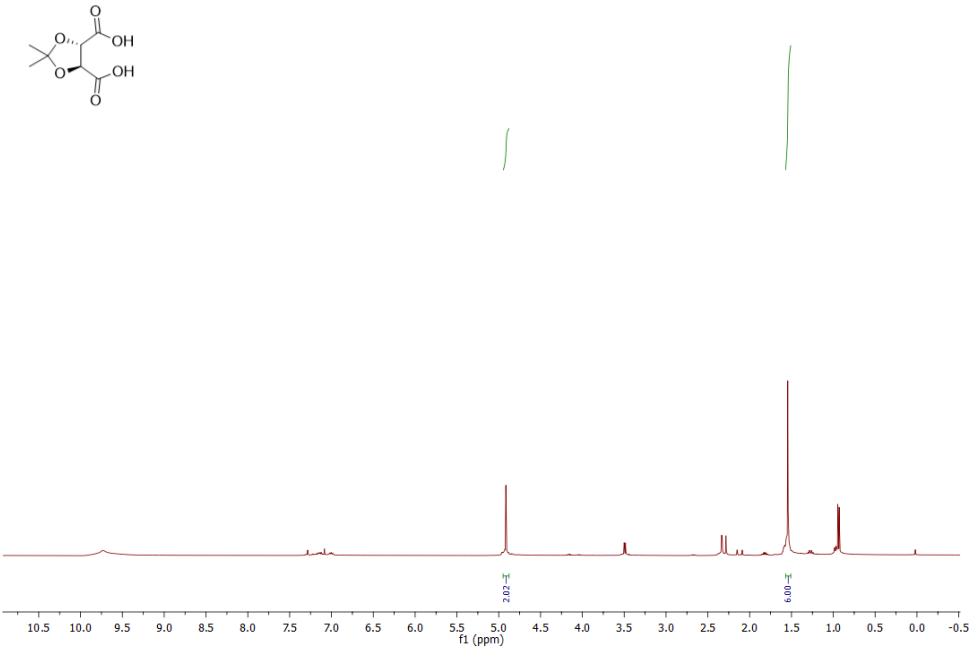

Figure A.9. ^{1}H NMR Spectrum of **TD-4**

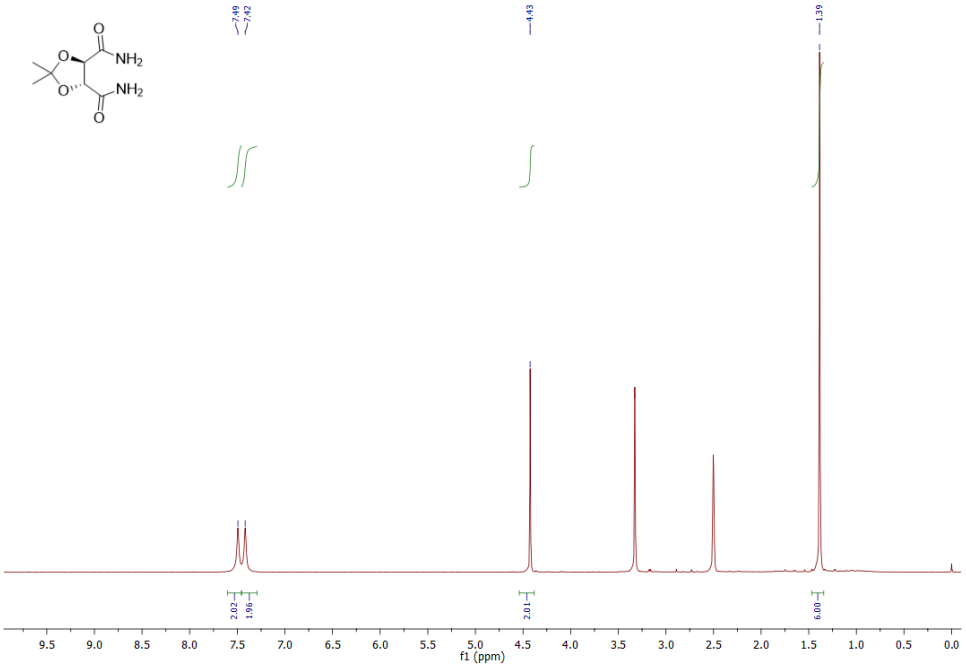

Figure A.10. ^{1}H NMR Spectrum of **TL-5**

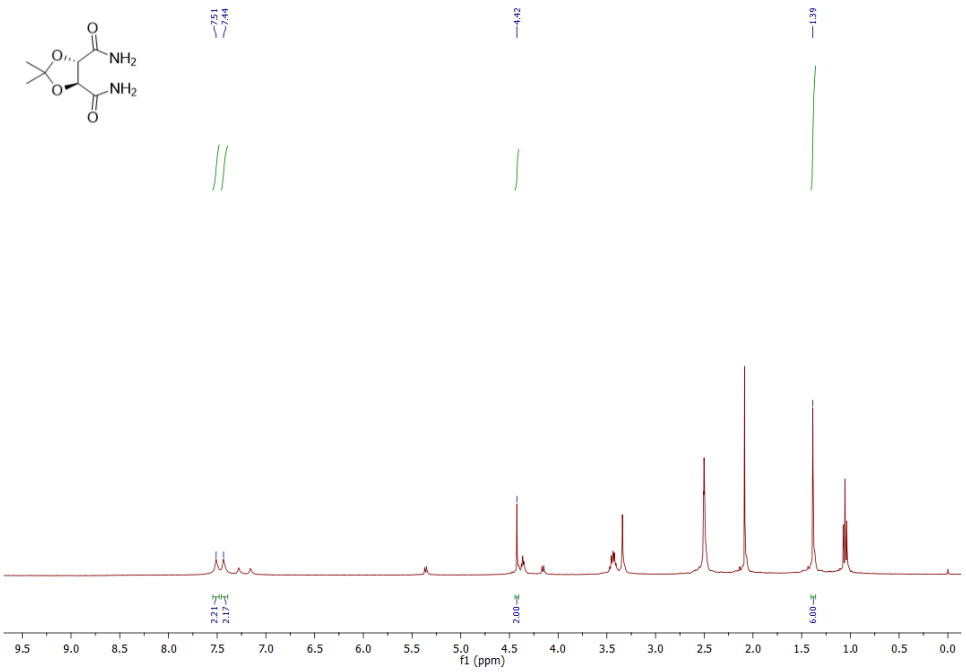

Figure A.11. ^{1}H NMR Spectrum of **TD-5**

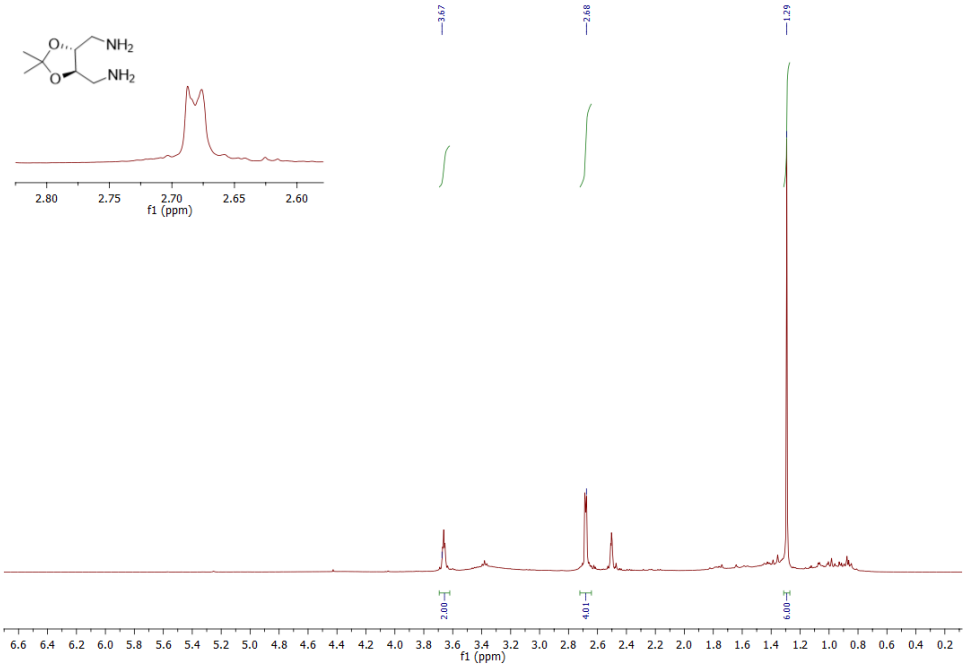

Figure A.12. ^{1}H NMR Spectrum of **TL-6**

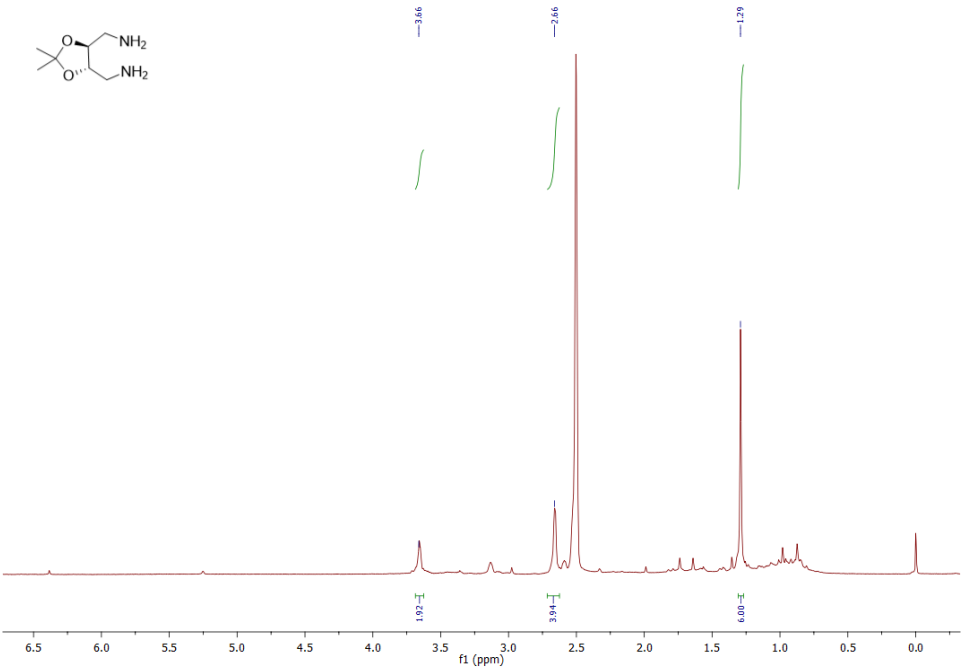

Figure A.13. ^{1}H NMR Spectrum of **TD-6**

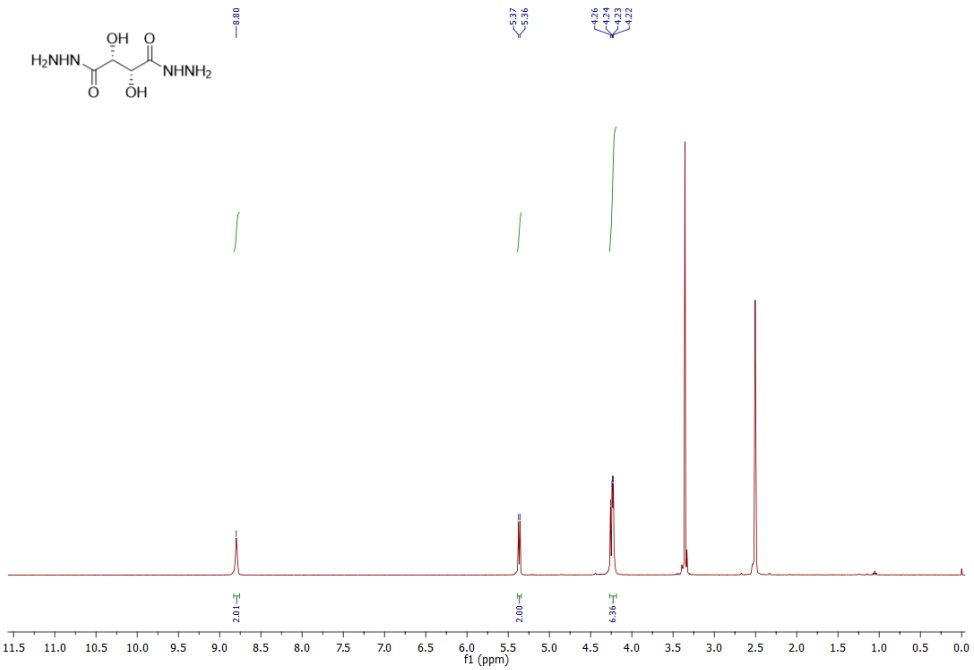

Figure A.14. ^{1}H NMR Spectrum of **TL-7**

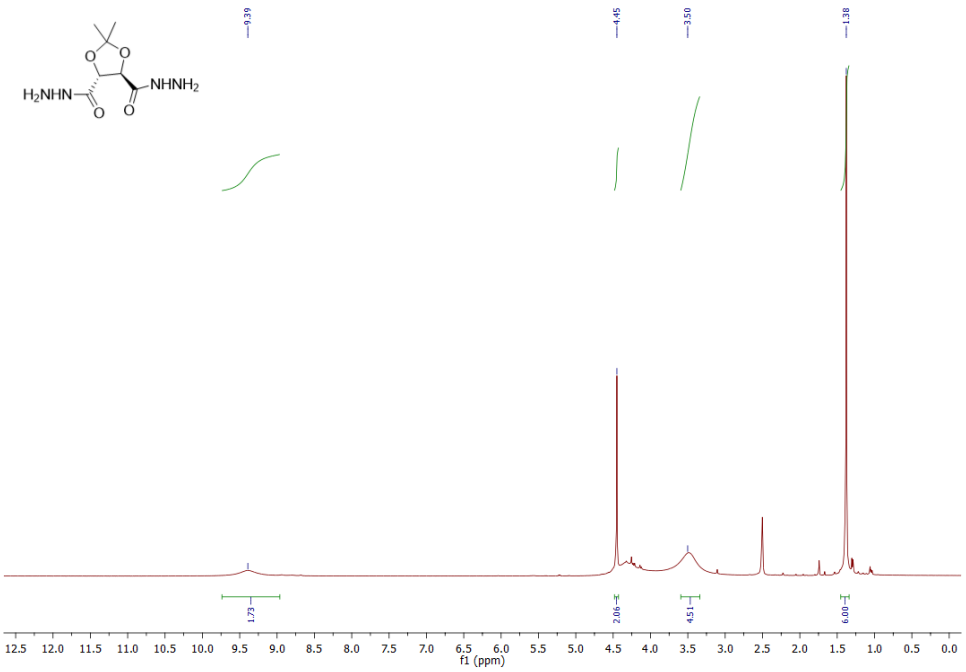

Figure A.15. ^{1}H NMR Spectrum of **TL-8**

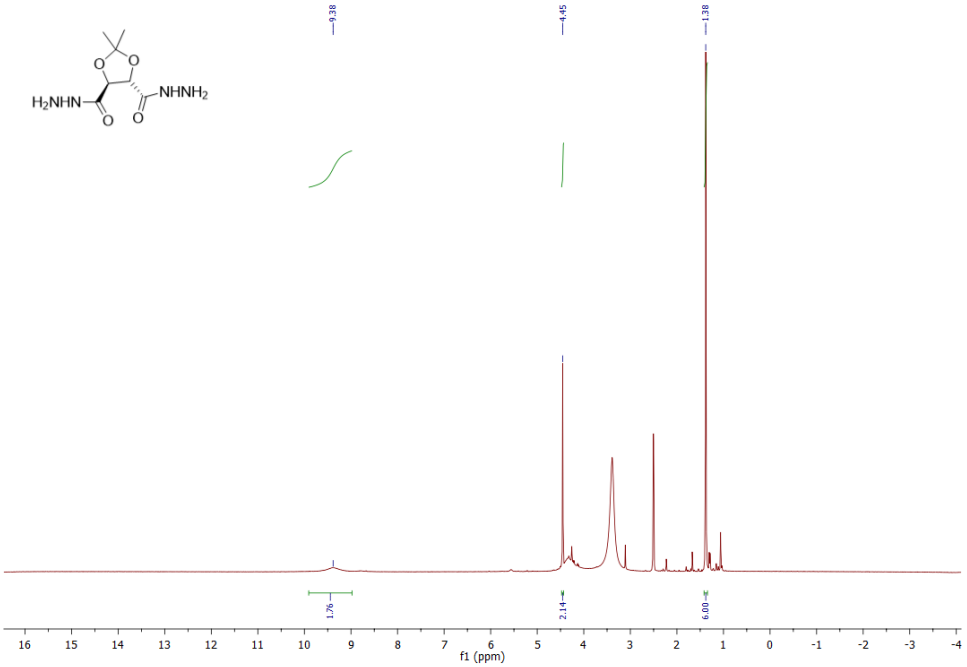

Figure A.16. ^{1}H NMR Spectrum of **TD-8**

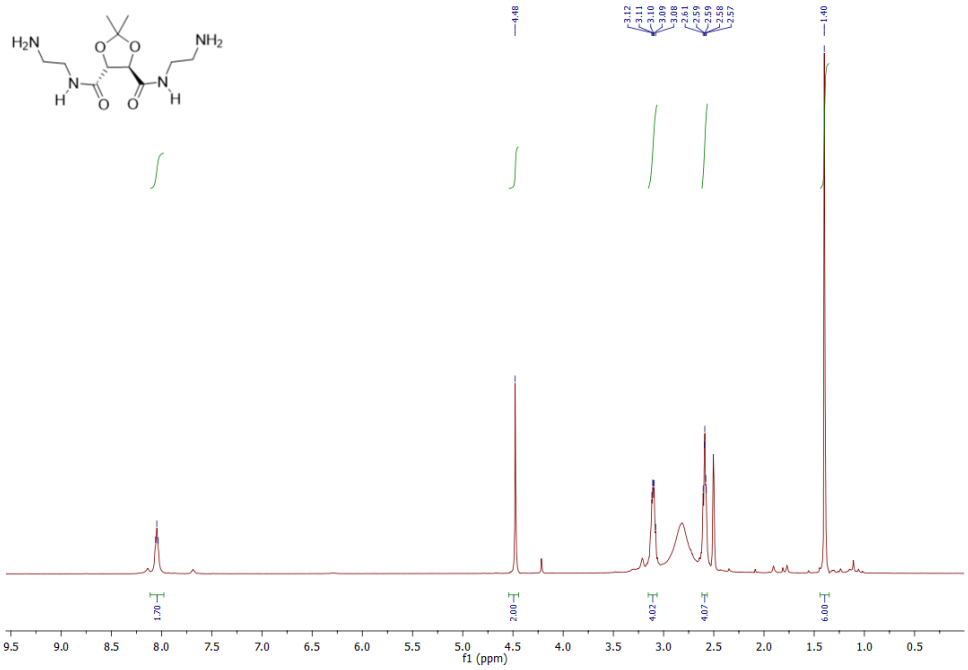

Figure A.17. ^{1}H NMR Spectrum of **TL-9**

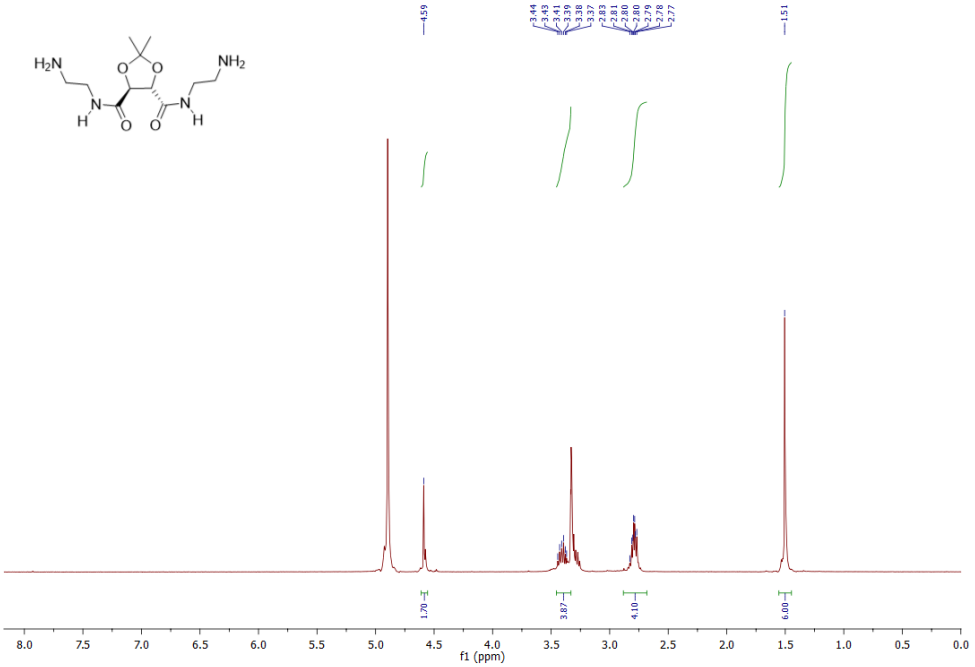

Figure A.18. ^{1}H NMR Spectrum of **TD-9**

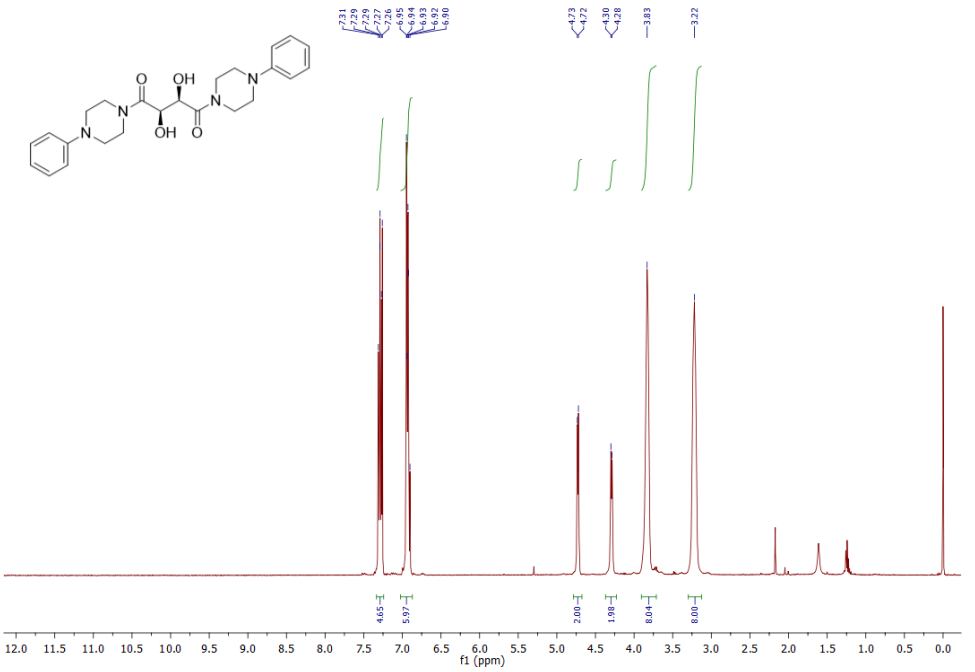

Figure A.19. ^{1}H NMR Spectrum of **TL-10**

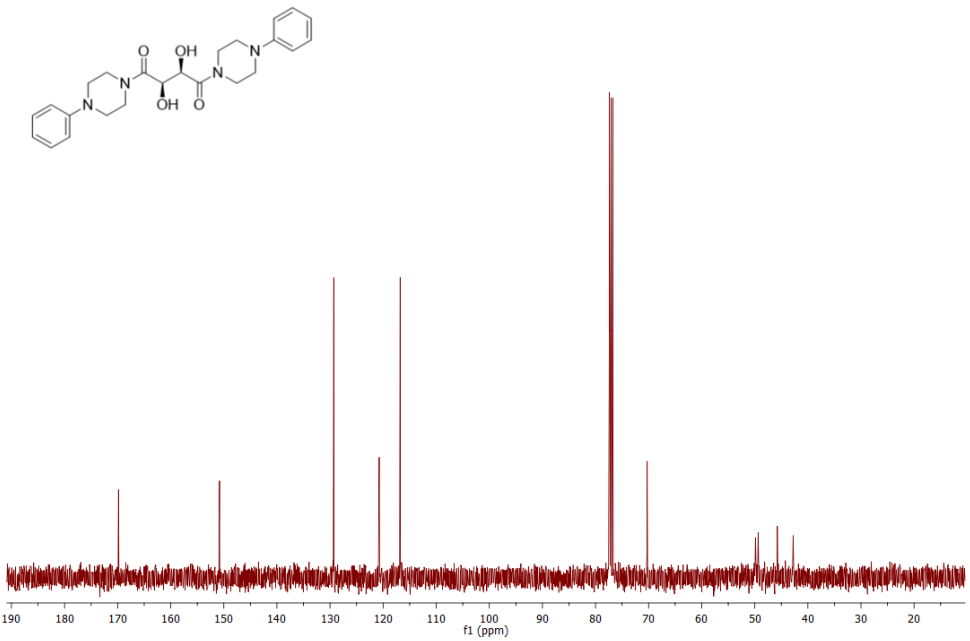

Figure A.20. ^{13}C NMR Spectrum of **TL-10**

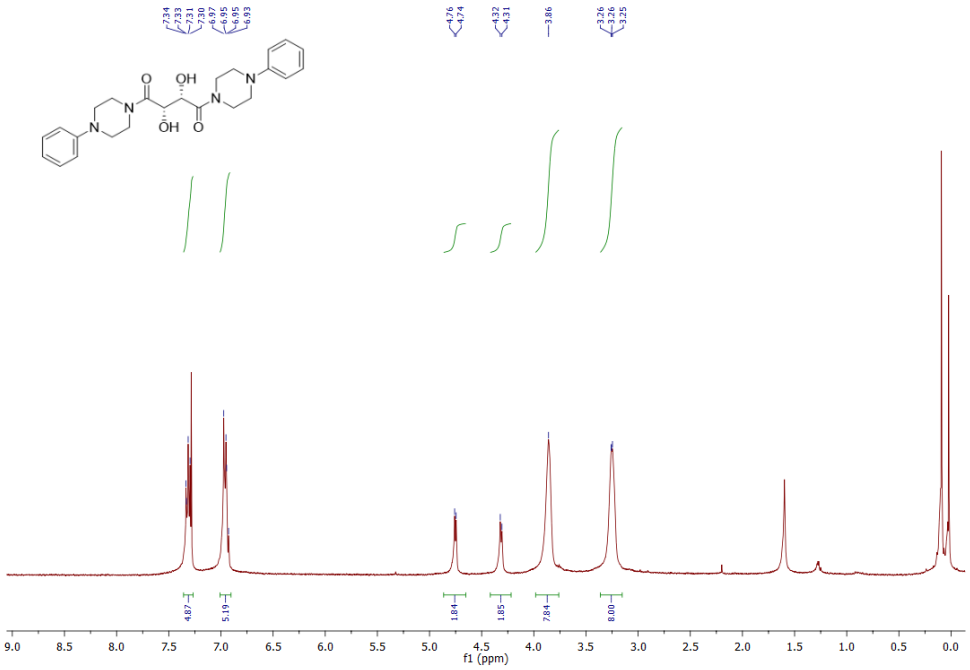

Figure A.21. ^{1}H NMR Spectrum of **TD-10**

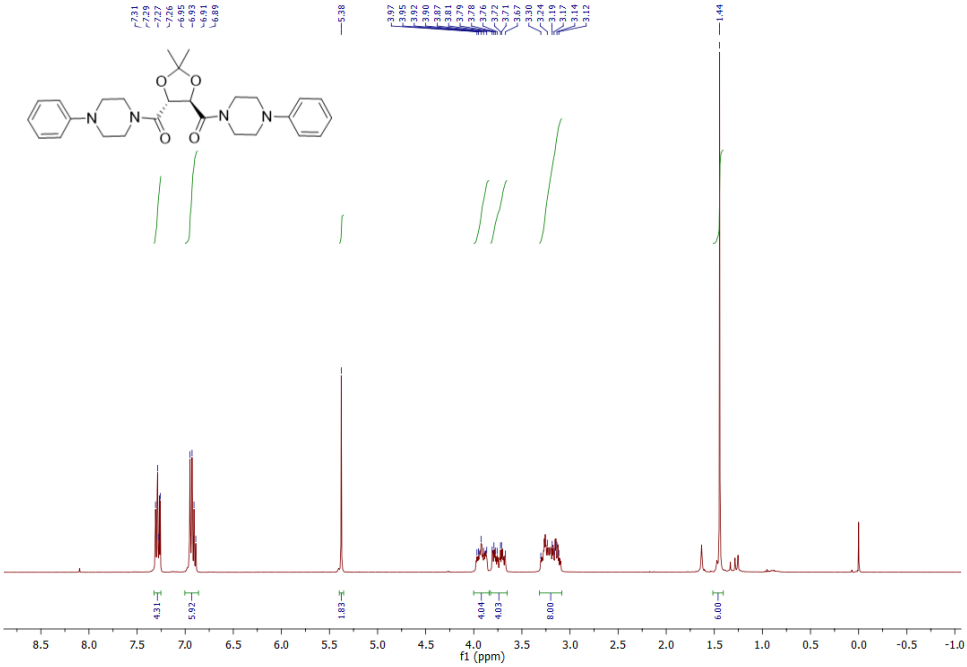

Figure A.22. ^{1}H NMR Spectrum of **TL-11**

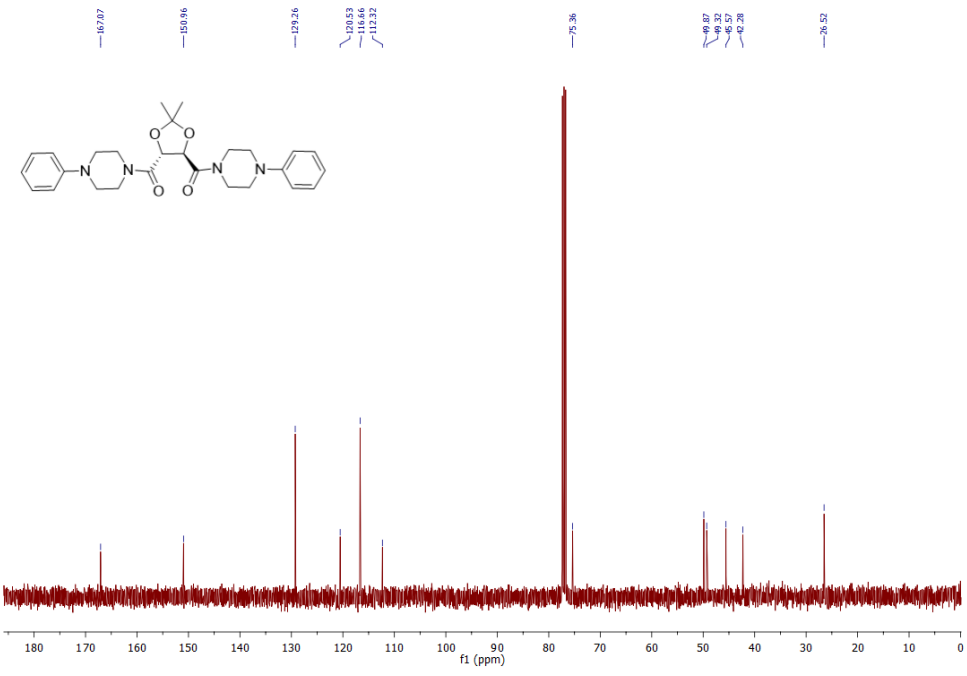

Figure A.23. ^{13}C NMR Spectrum of **TL-11**

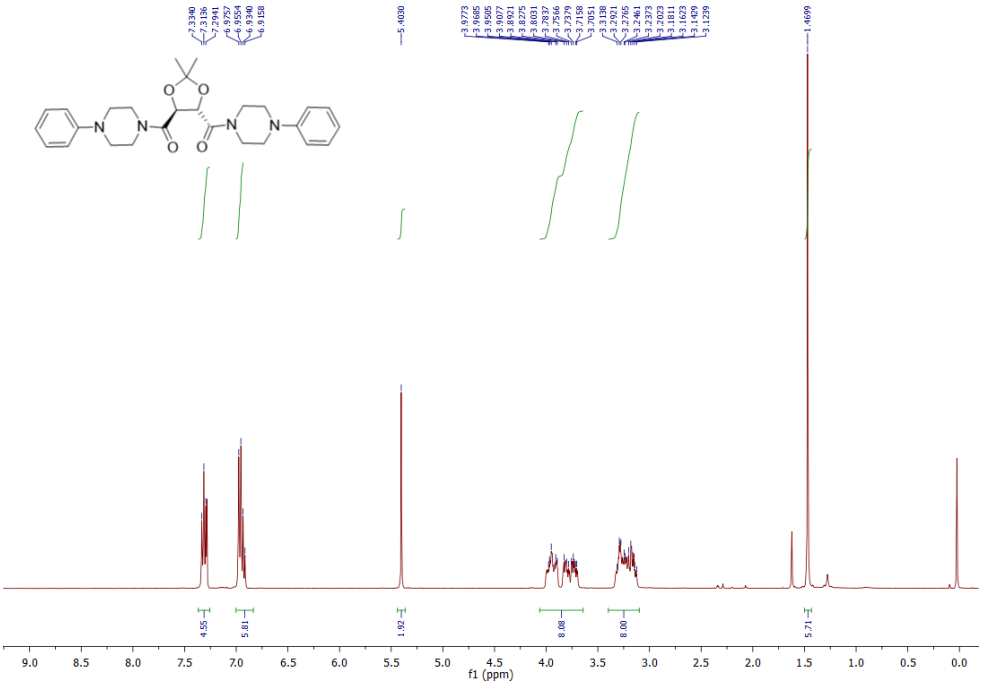

Figure A.24. ^{1}H NMR Spectrum of **TD-11**

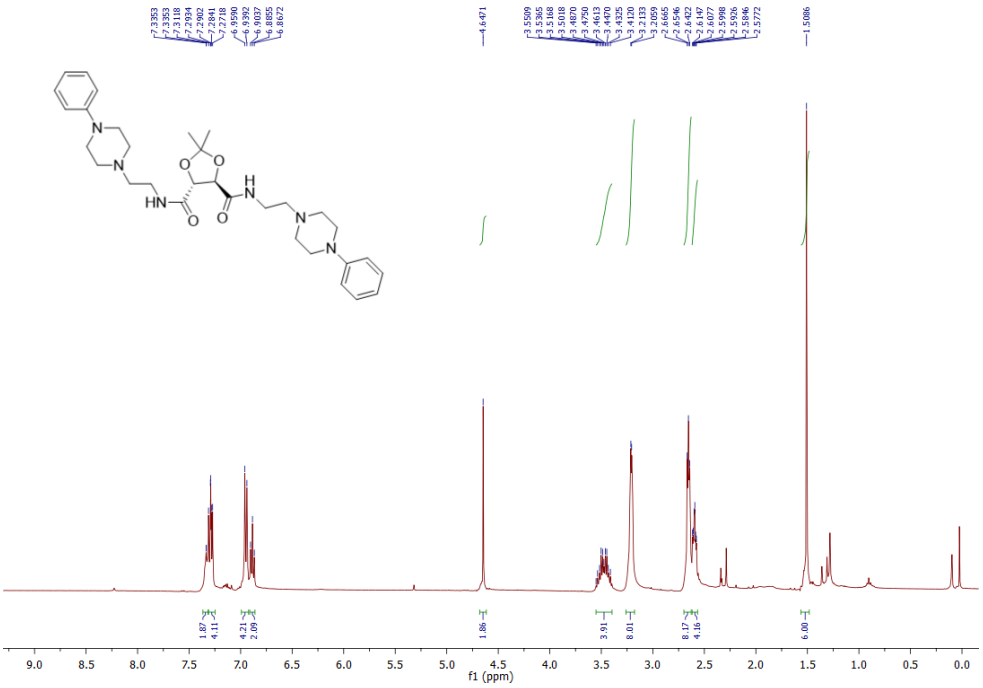

Figure A.25. ^{1}H NMR Spectrum of **TL-12** (Method A)

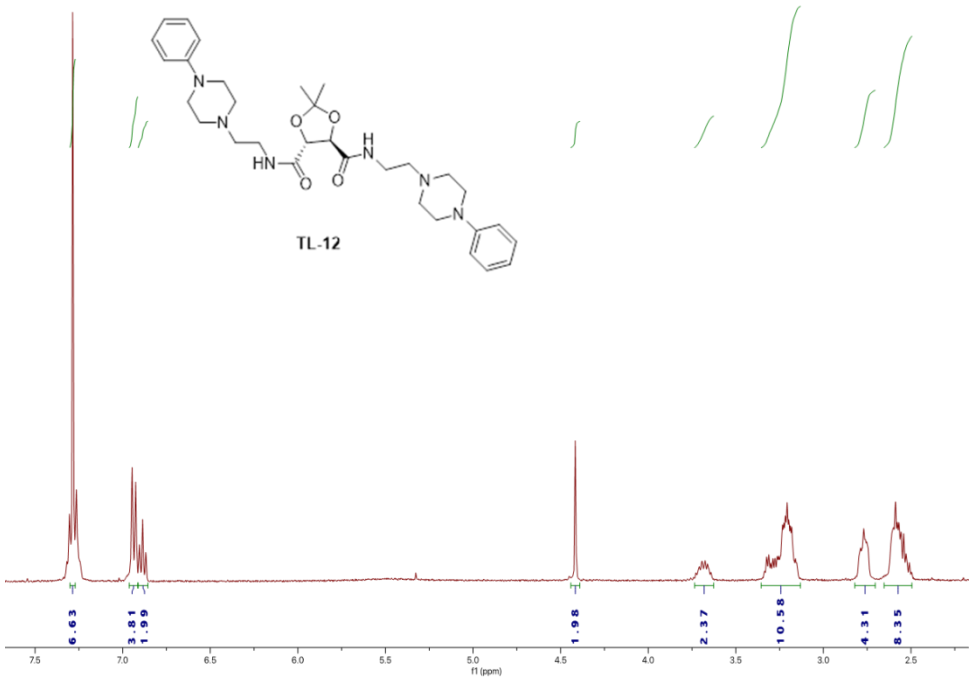

Figure A.26. ^{1}H NMR Spectrum of **TL-12** (Method B)

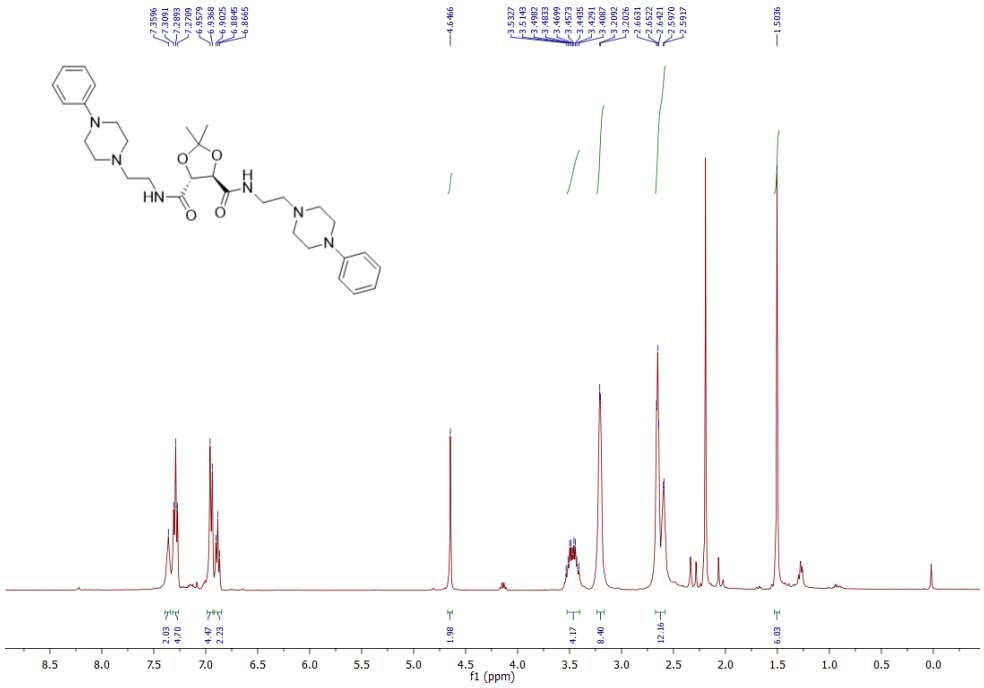

Figure A.27. ^{1}H NMR Spectrum of **TL-12** (Method C)

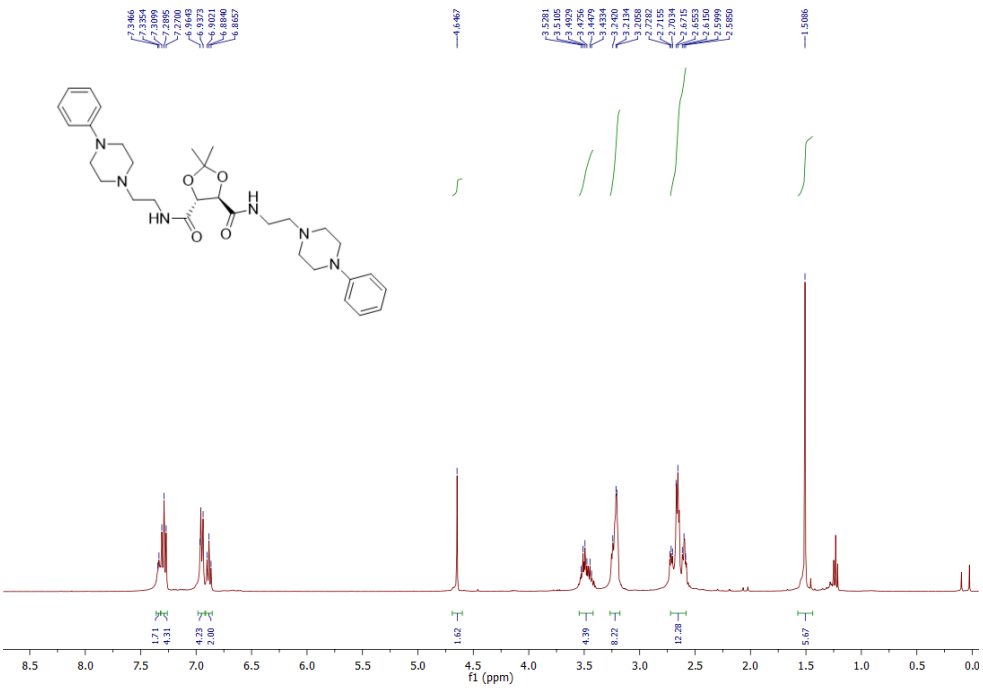

Figure A.28. ^{1}H NMR Spectrum of **TL-12** (Method D)

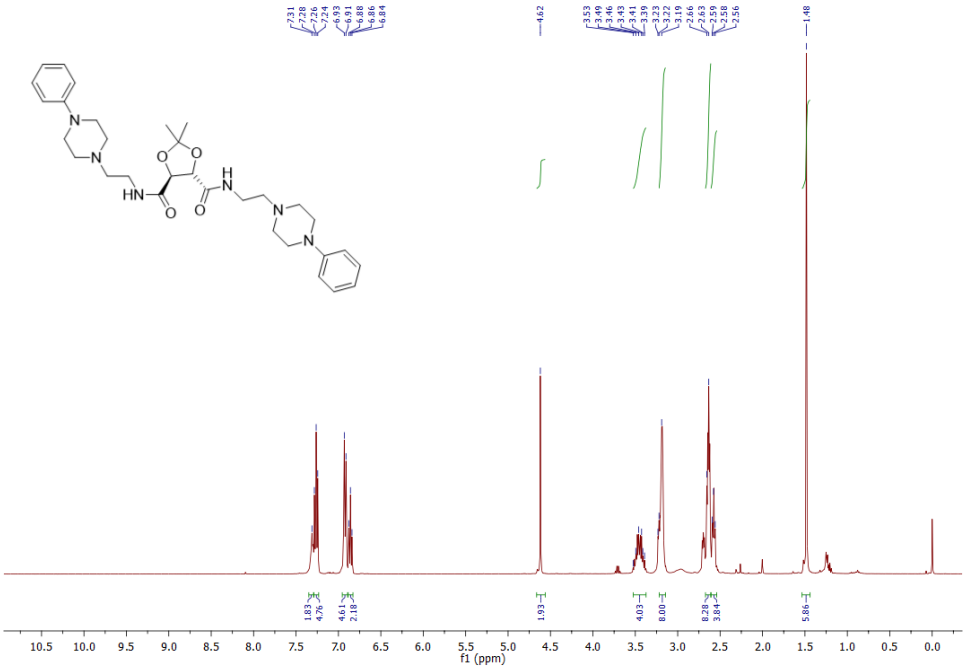

Figure A.29. ^{1}H NMR Spectrum of **TD-12** (Method D)

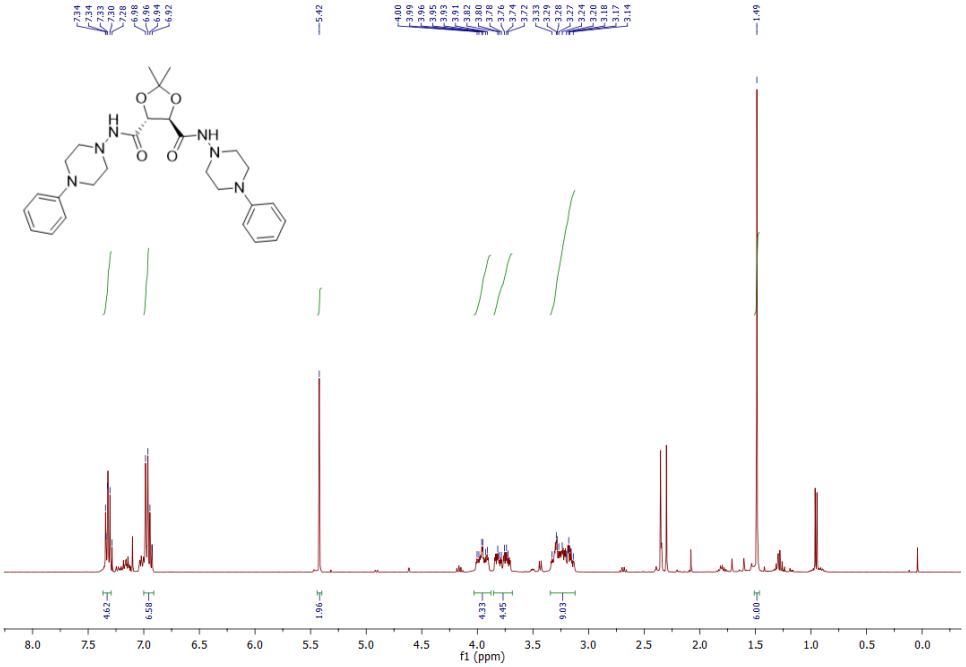

Figure A.30. ^{1}H NMR Spectrum of **TL-13**

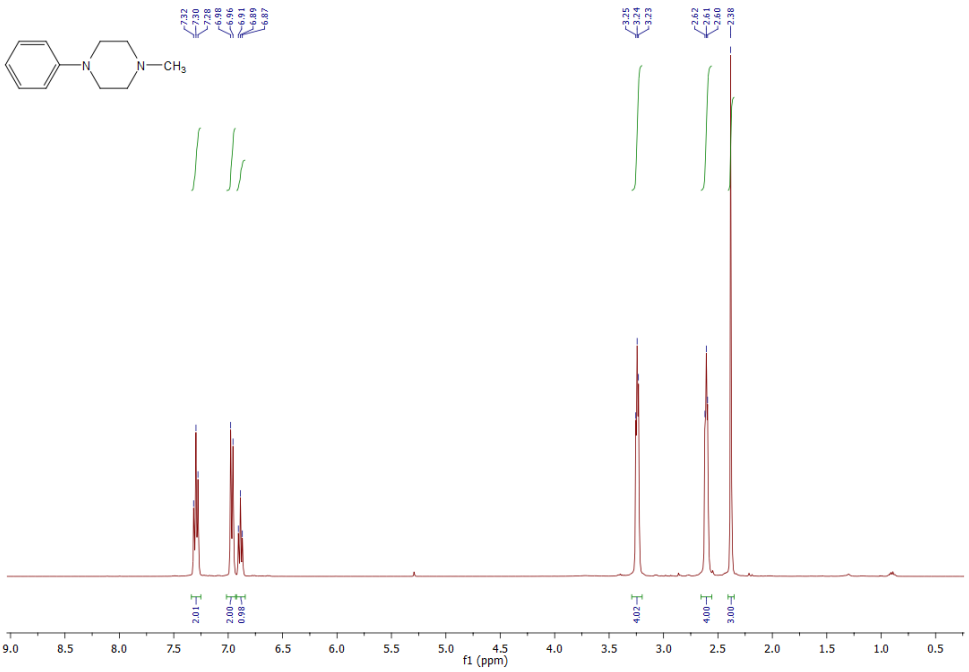

Figure A.31. ^{1}H NMR Spectrum of **P-1**

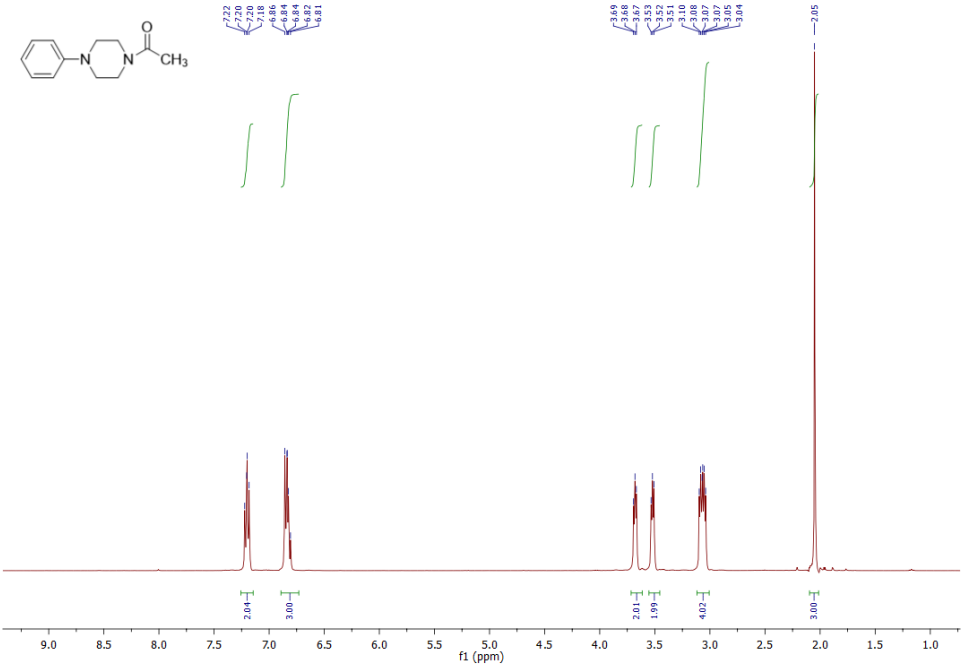

Figure A.32. ^{1}H NMR Spectrum of **P-2**

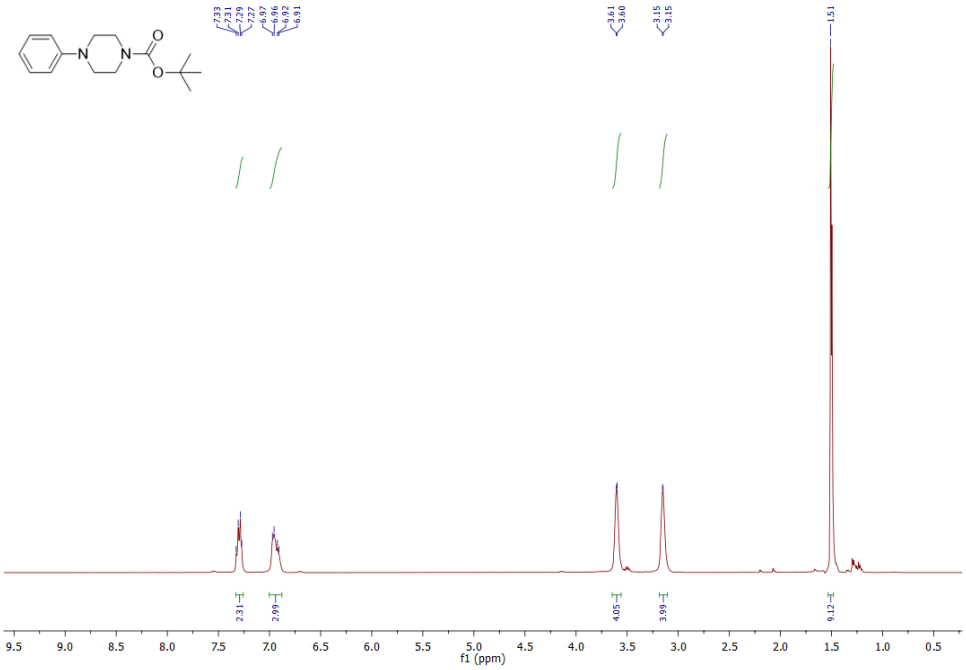

Figure A.33. ^{1}H NMR Spectrum of **P-3**

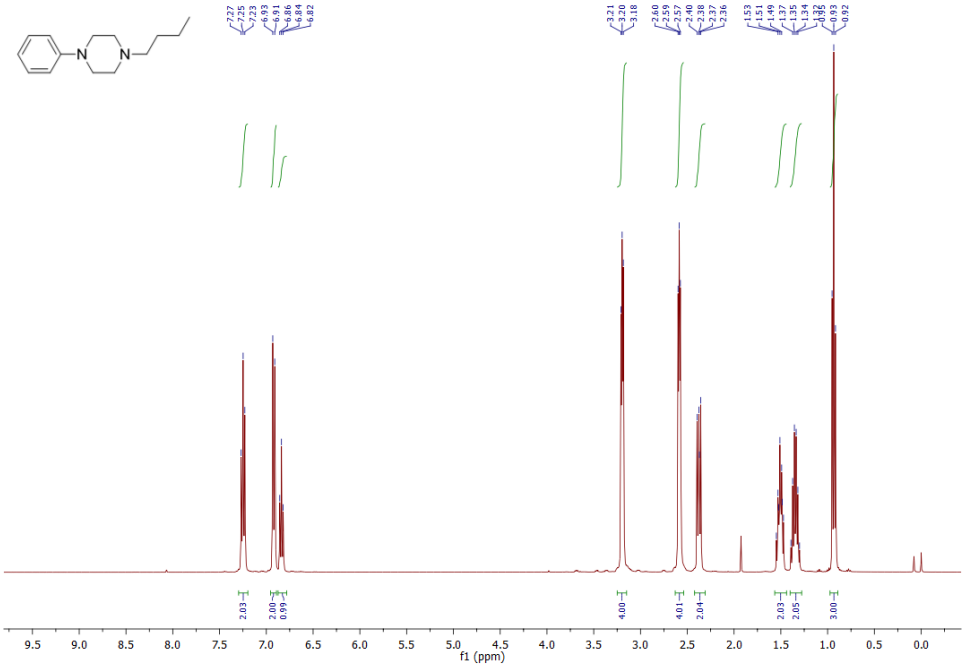

Figure A.34. ^{1}H NMR Spectrum of **P-4**

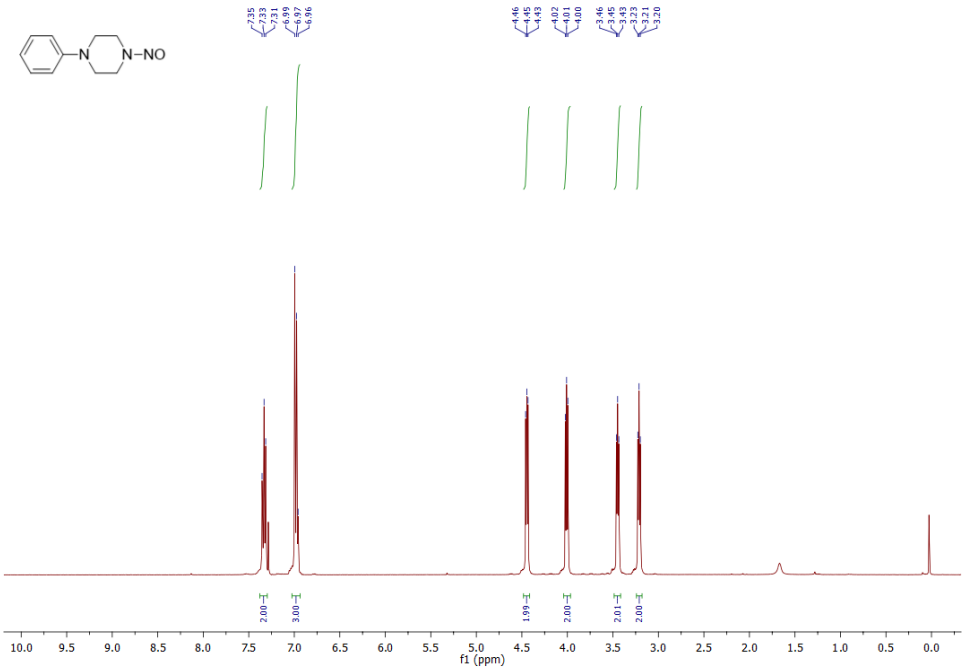

Figure A.35. ^{1}H NMR Spectrum of **P-5**

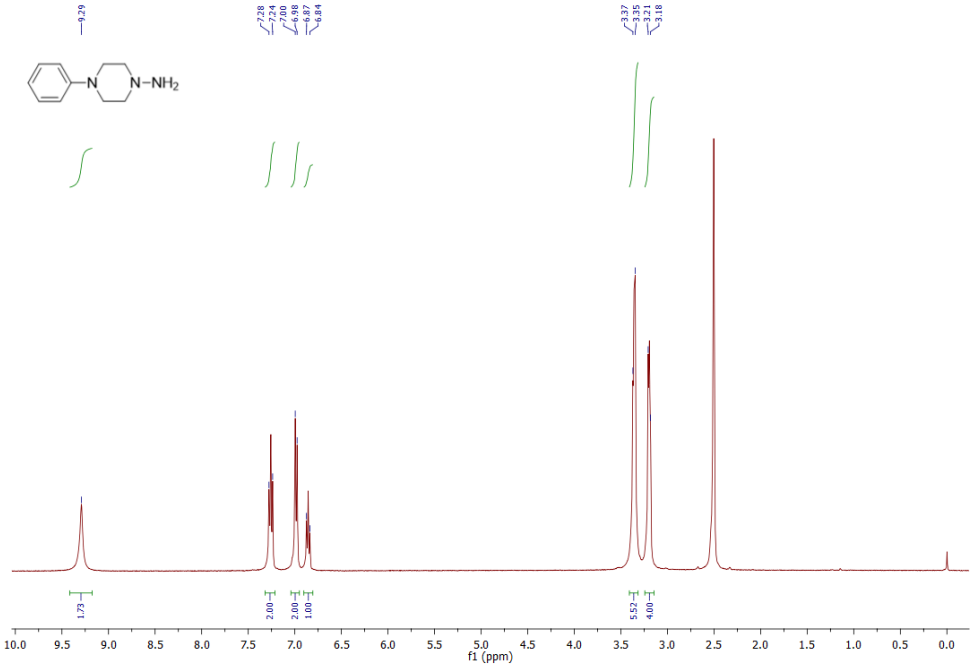

Figure A.36. ^{1}H NMR Spectrum of **P-6**

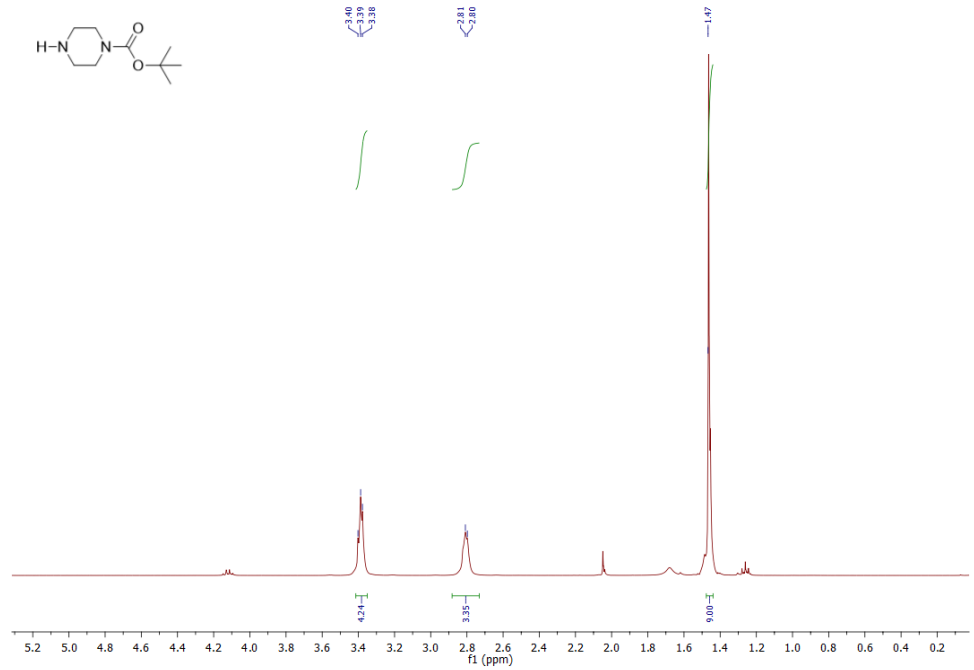

Figure A.37. ^{1}H NMR Spectrum of **P-7**

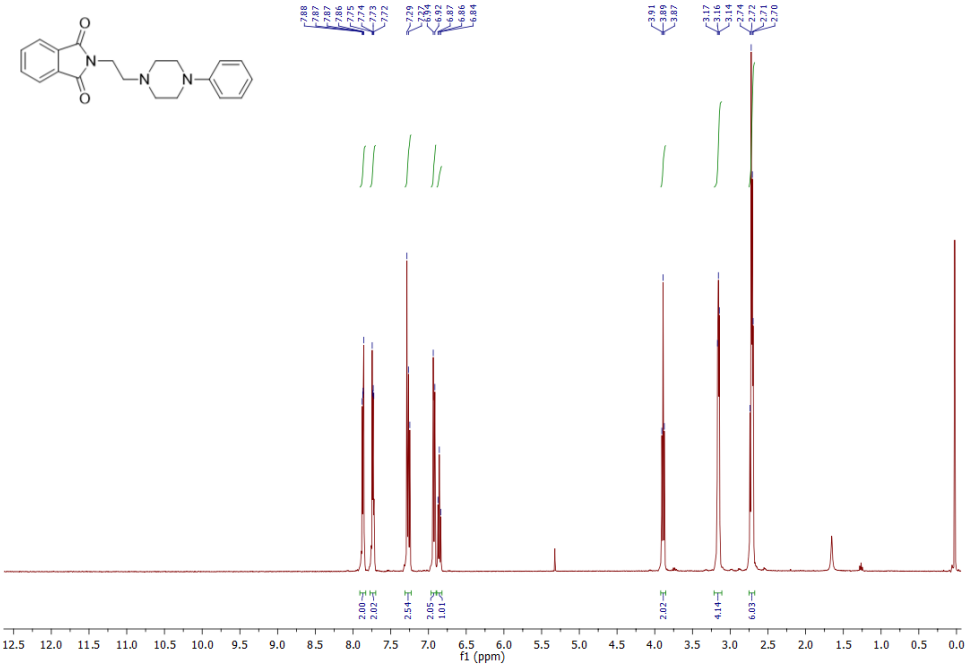

Figure A.38. ^{1}H NMR Spectrum of **P-8**

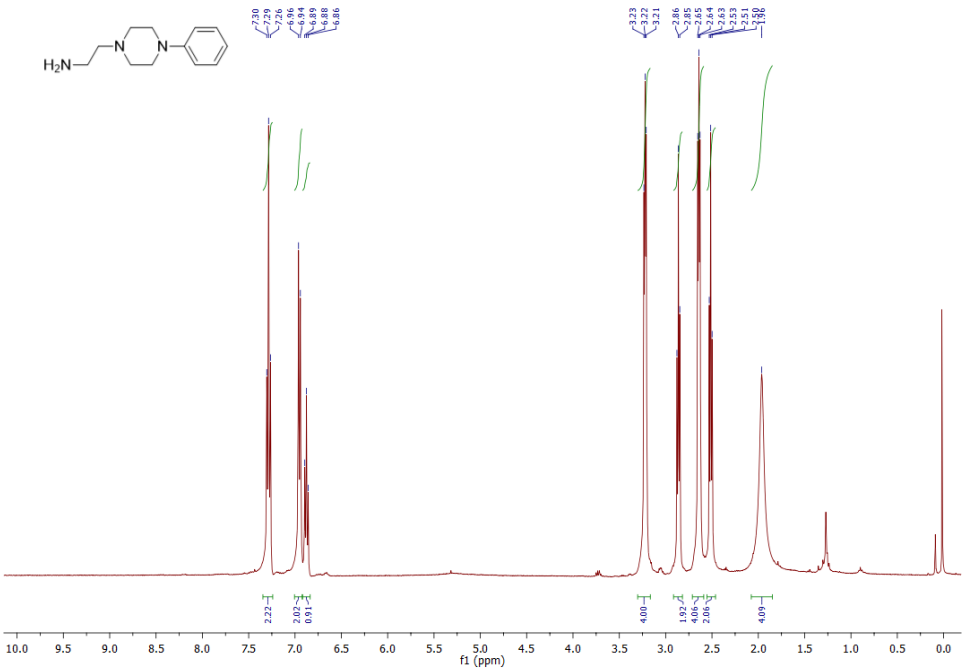

Figure A.39. ^{1}H NMR Spectrum of **P-9**

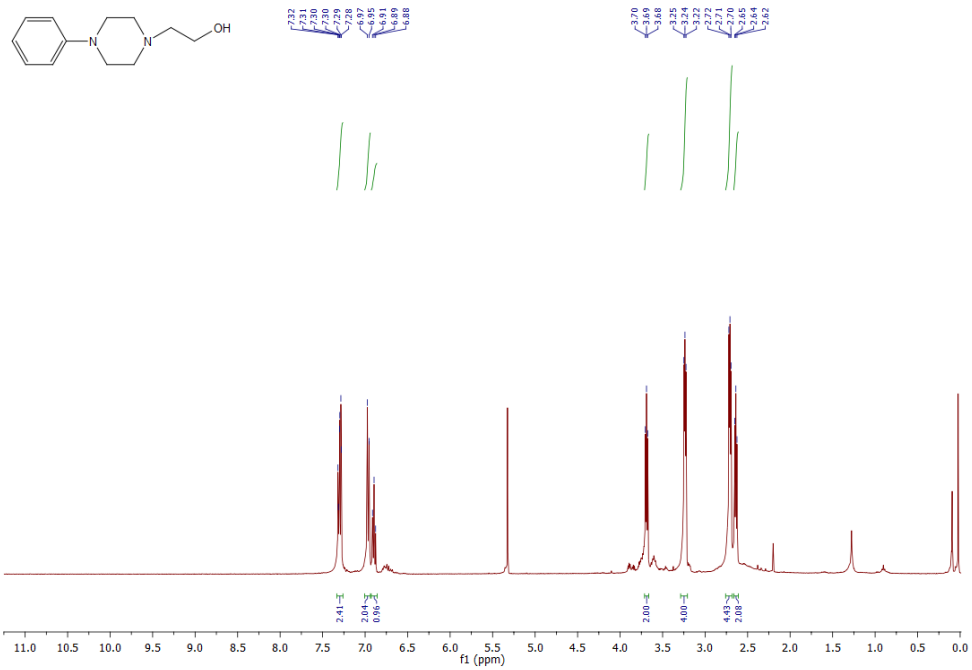

Figure A.40. ^{1}H NMR Spectrum of **P-10**

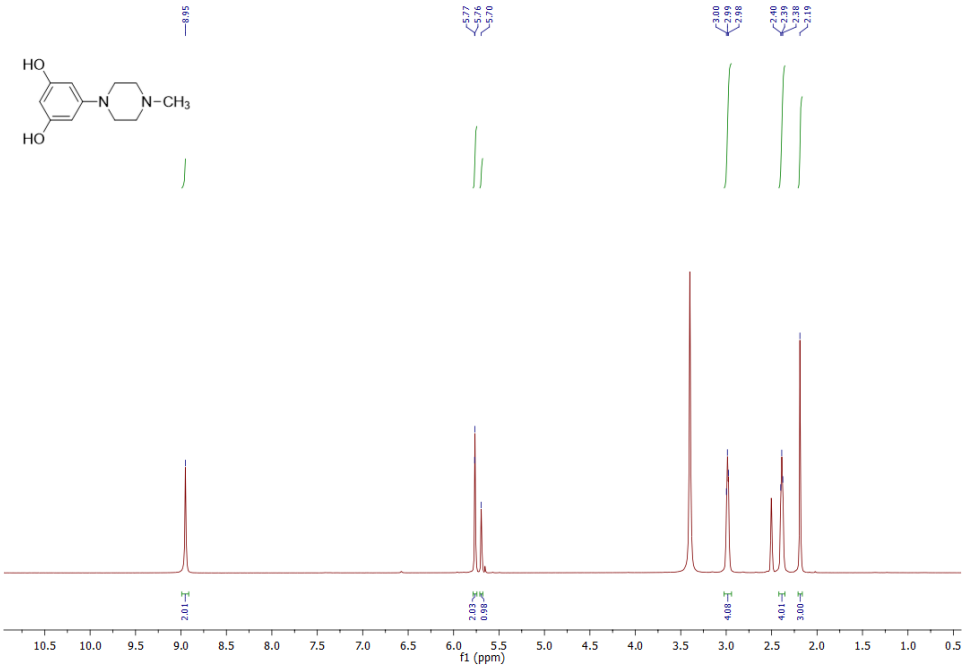

Figure A.41. ^{1}H NMR Spectrum of **P-11**

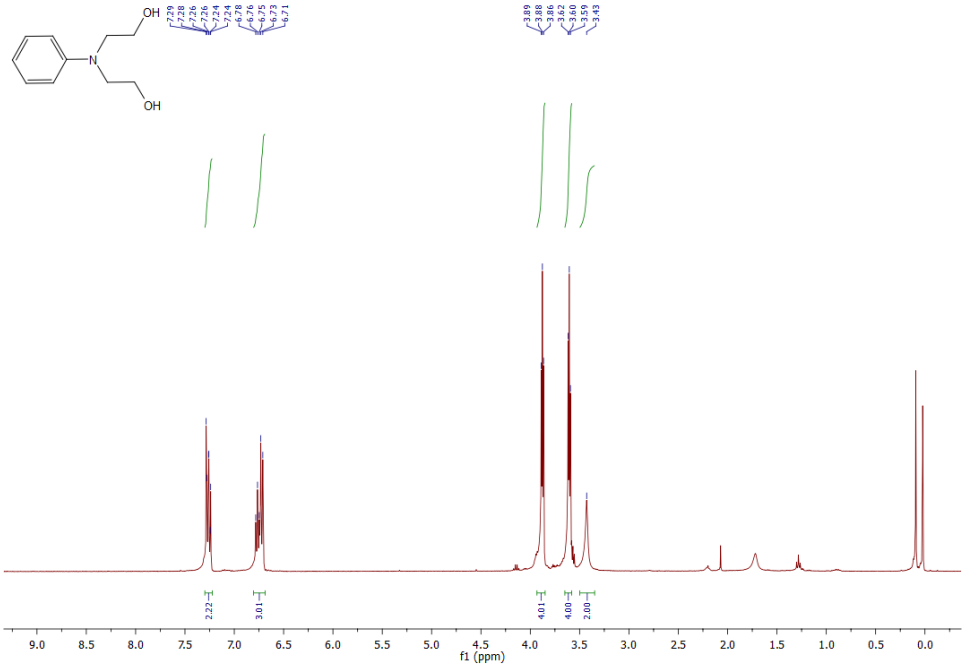

Figure A.42. ^{1}H NMR Spectrum of **R-1**

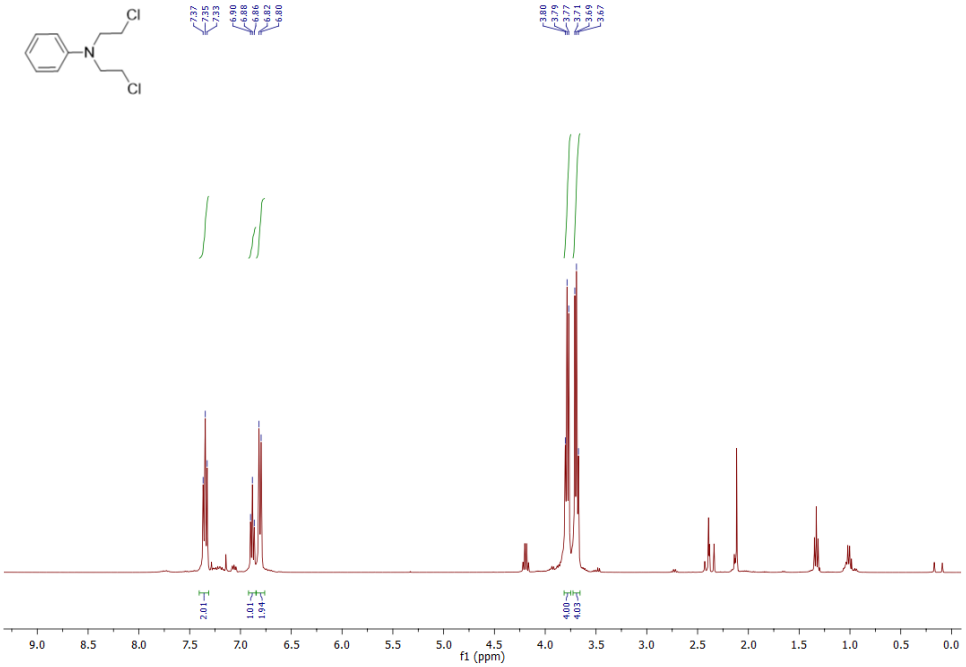

Figure A.43. ^{1}H NMR Spectrum of **R-2**

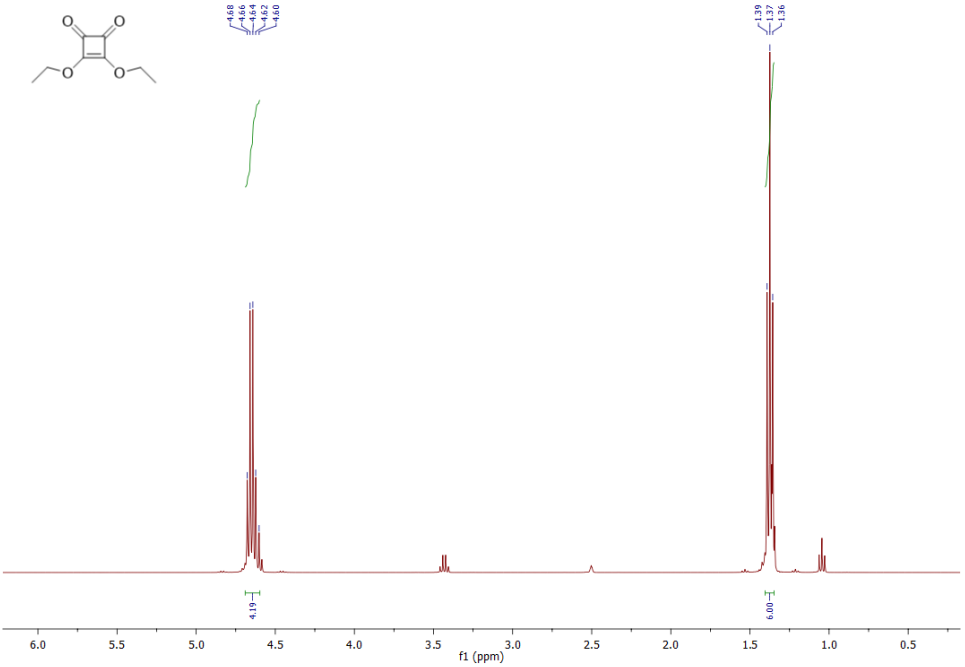

Figure A.44. ^{1}H NMR Spectrum of **S-1**

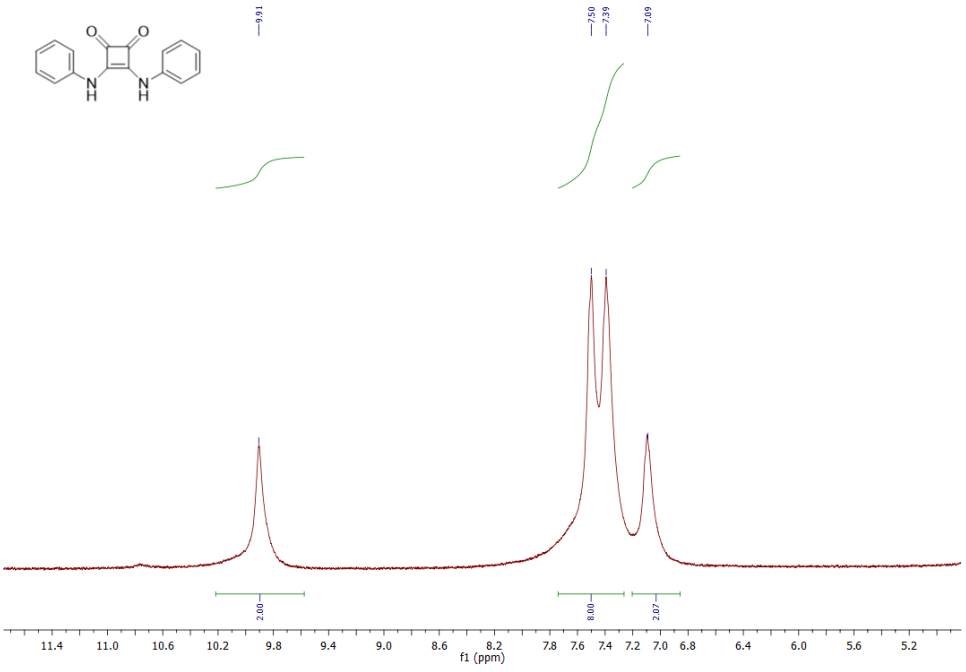

Figure A.45. ^{1}H NMR Spectrum of **S-2**

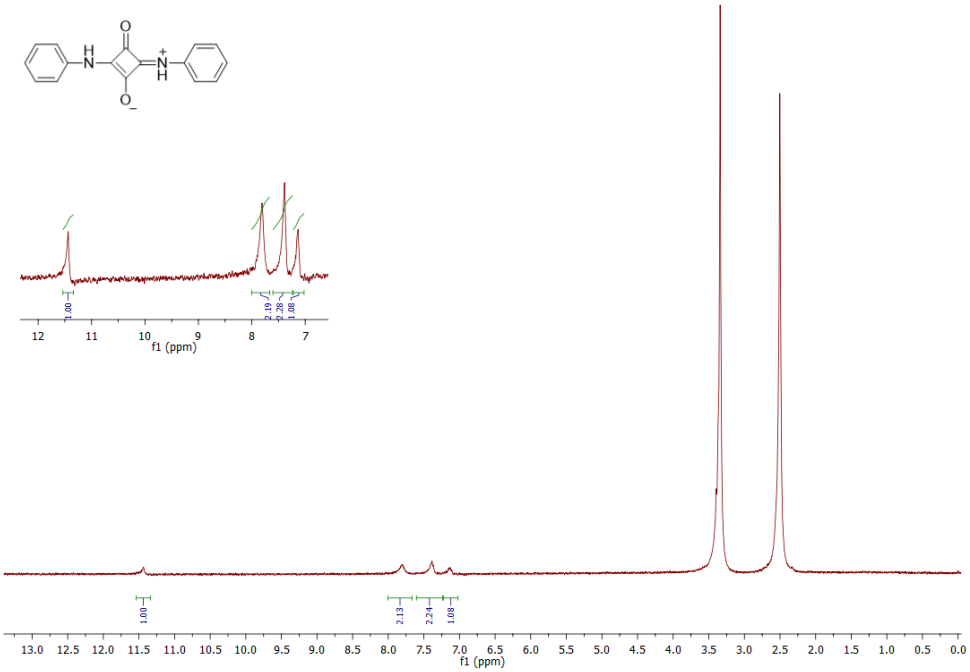

Figure A.46. ^{1}H NMR Spectrum of **SQ-1**

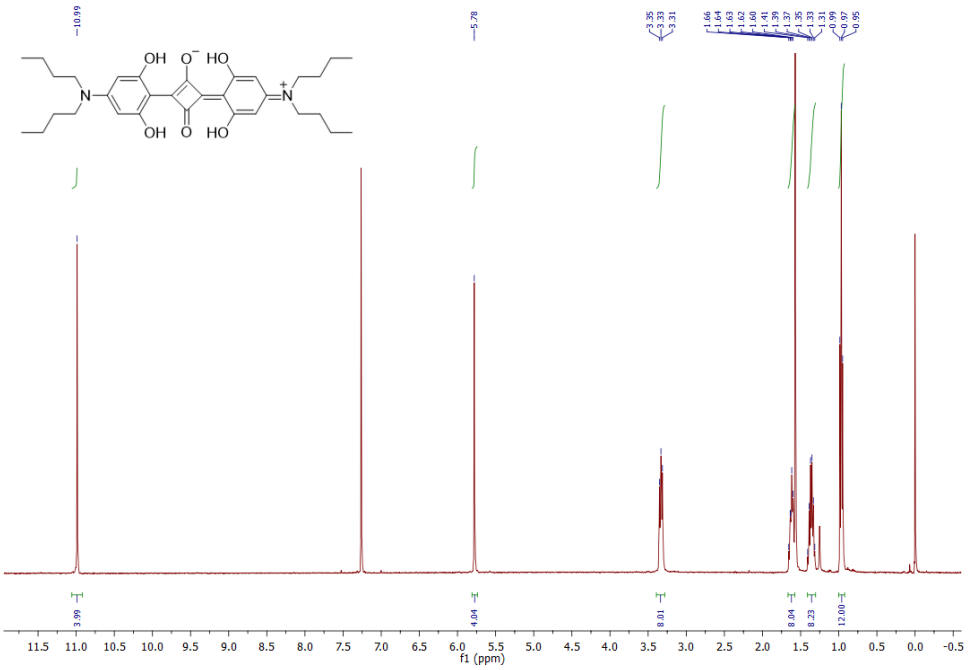

Figure A.47. ^{1}H NMR Spectrum of **SQ-3**

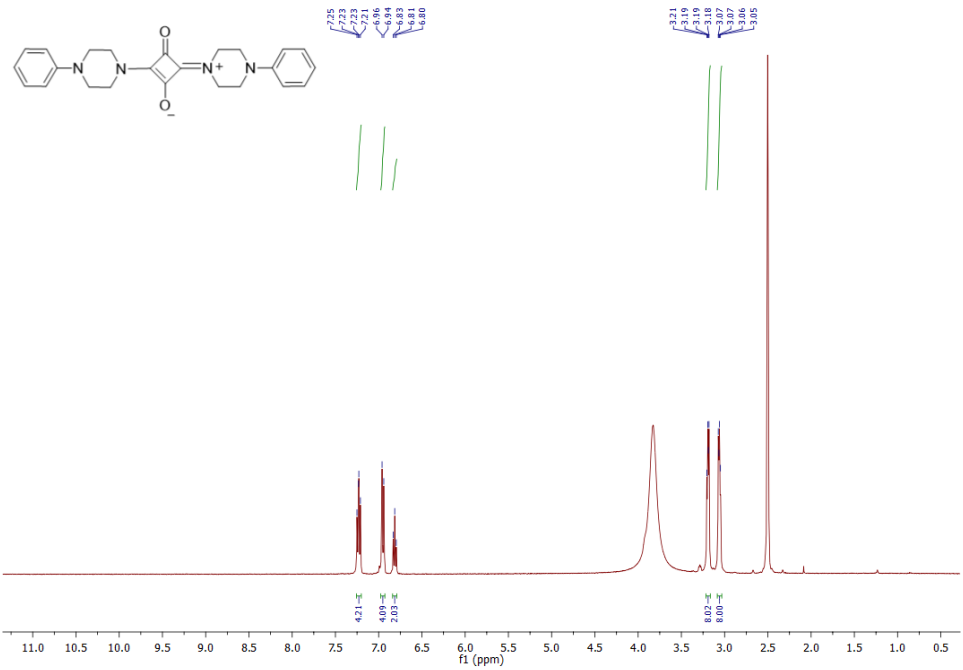

Figure A.48. ^{1}H NMR Spectrum of **SQ-4**

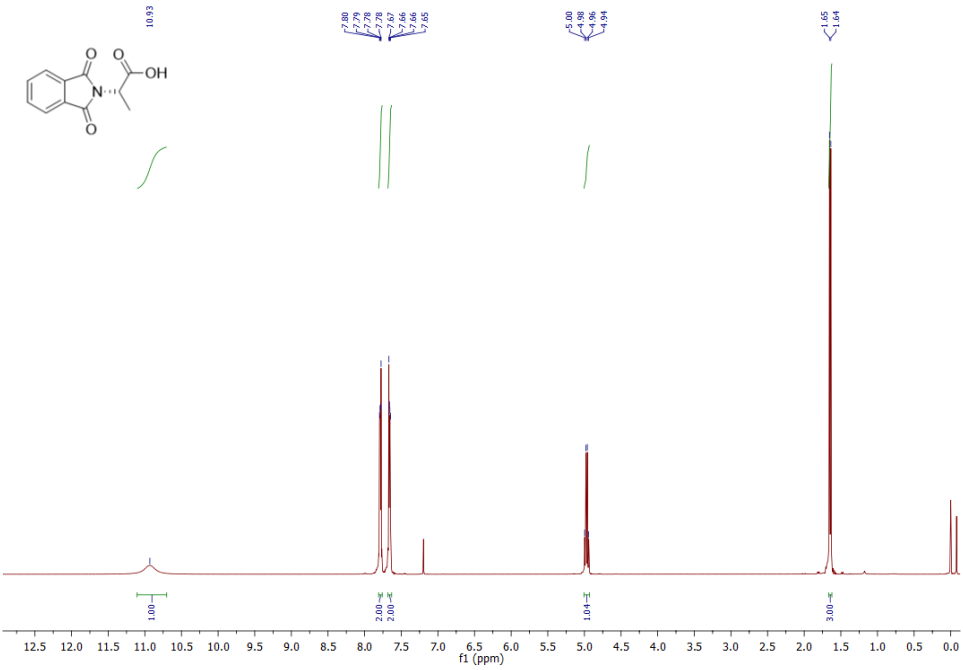

Figure A.49. ^{1}H NMR Spectrum of **L-CSA-1**

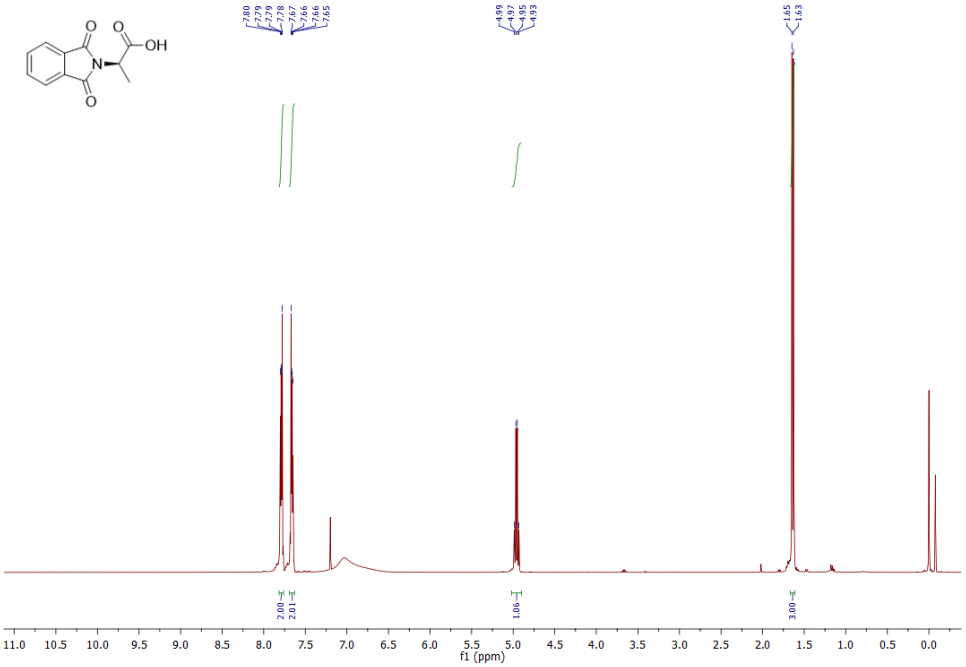

Figure A.50. ^{1}H NMR Spectrum of **D-CSA-1**

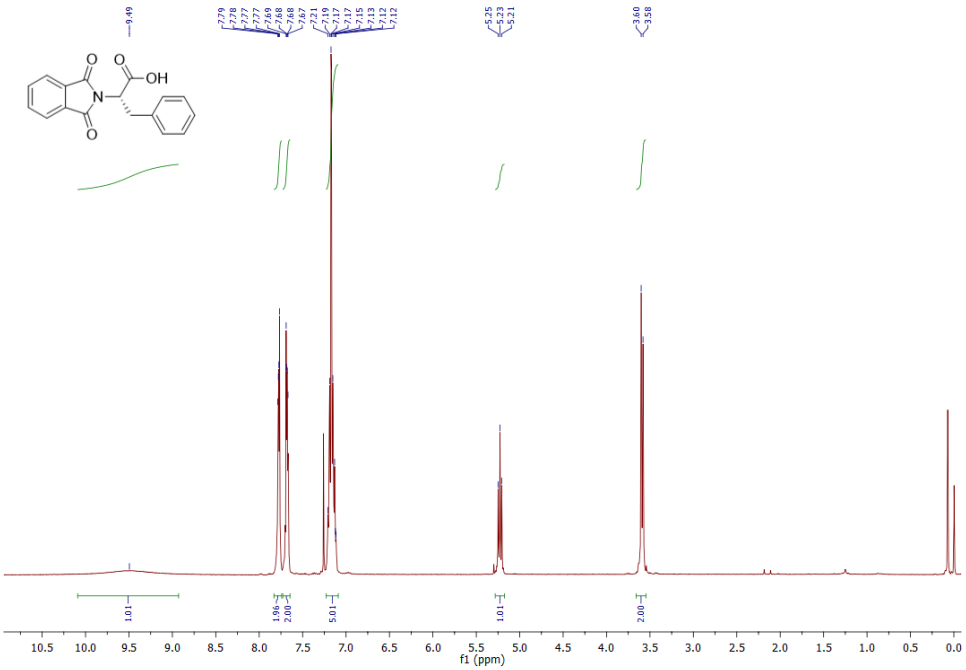

Figure A.51. ^{1}H NMR Spectrum of **L-CSP-1**

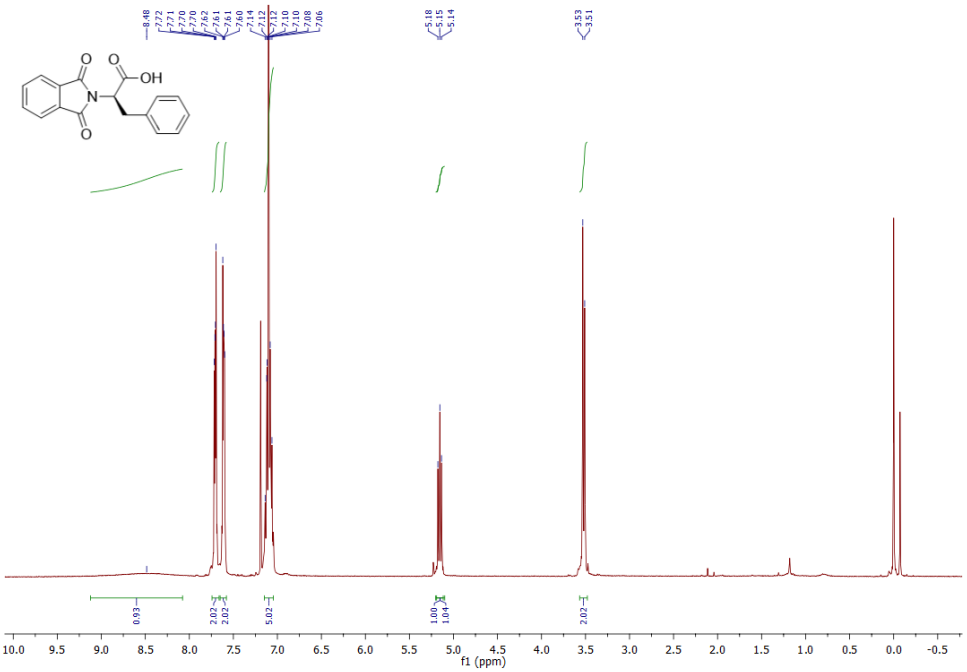

Figure A.52. ^{1}H NMR Spectrum of **D-CSP-1**

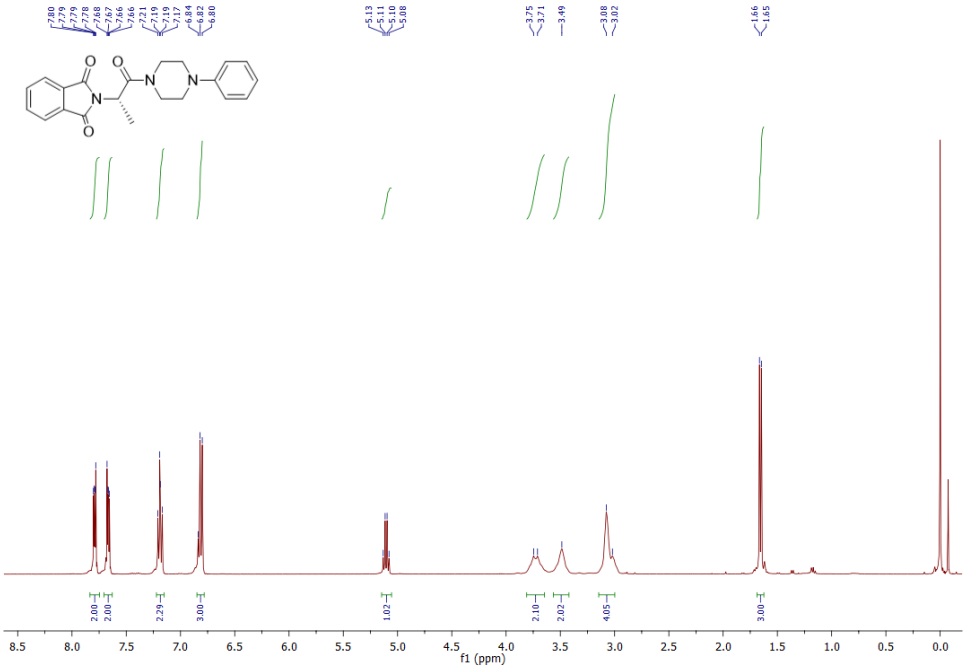

Figure A.53. ^{1}H NMR Spectrum of **L-CSA-2**

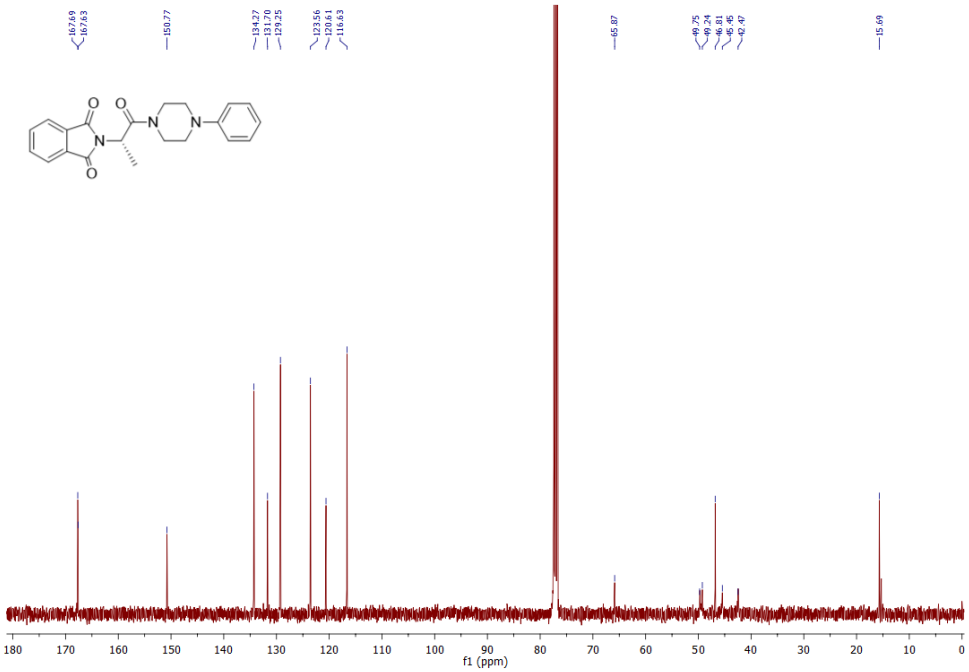

Figure A.54. ^{13}C NMR Spectrum of **L-CSA-2**

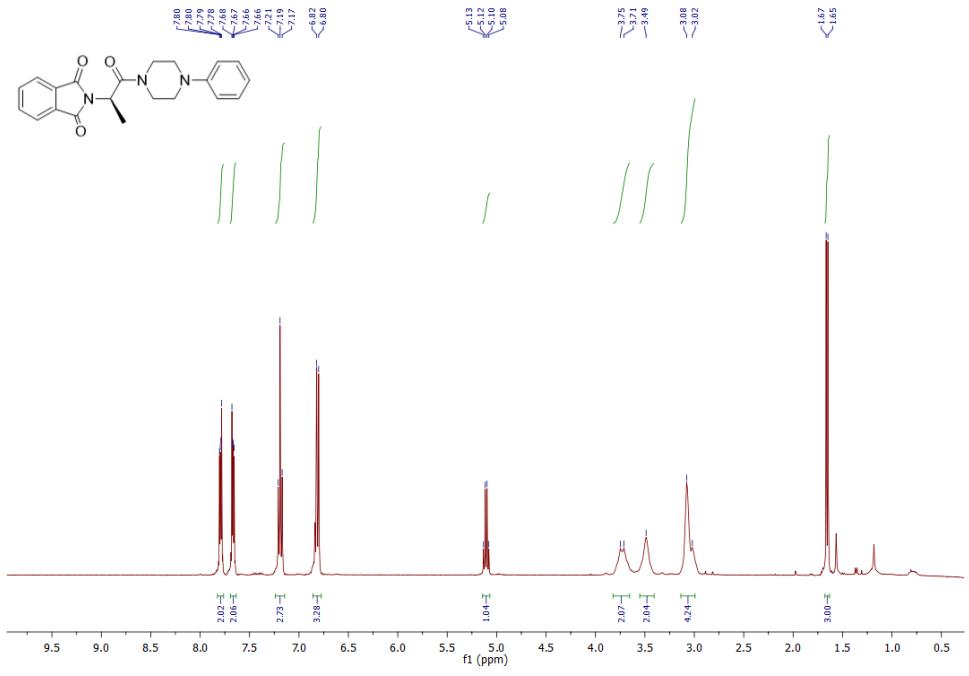

Figure A.55. ^{1}H NMR Spectrum of **D-CSA-2**

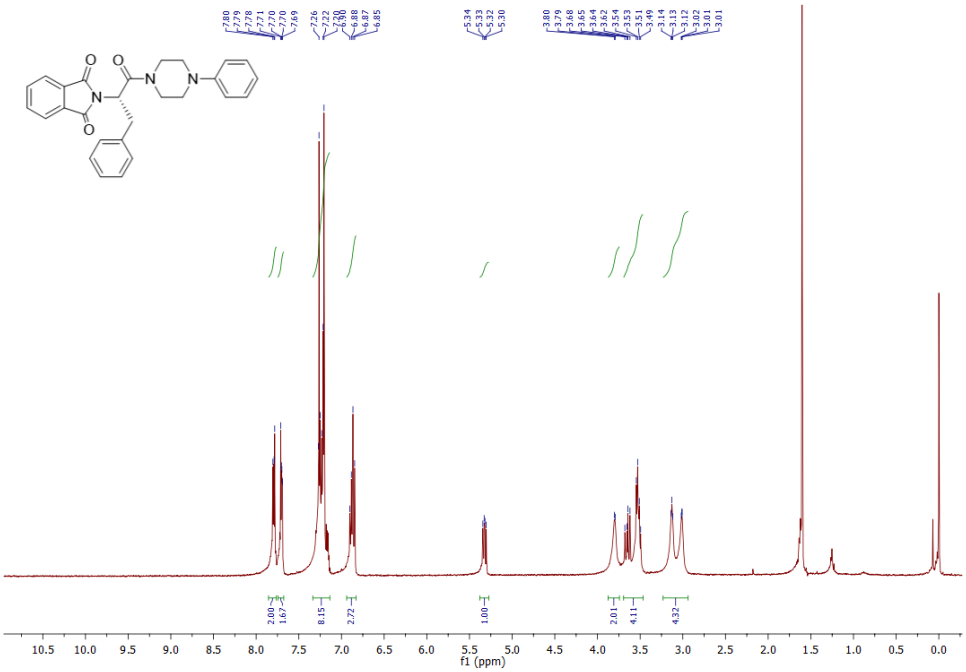

Figure A.56. ^{1}H NMR Spectrum of **L-CSP-2**

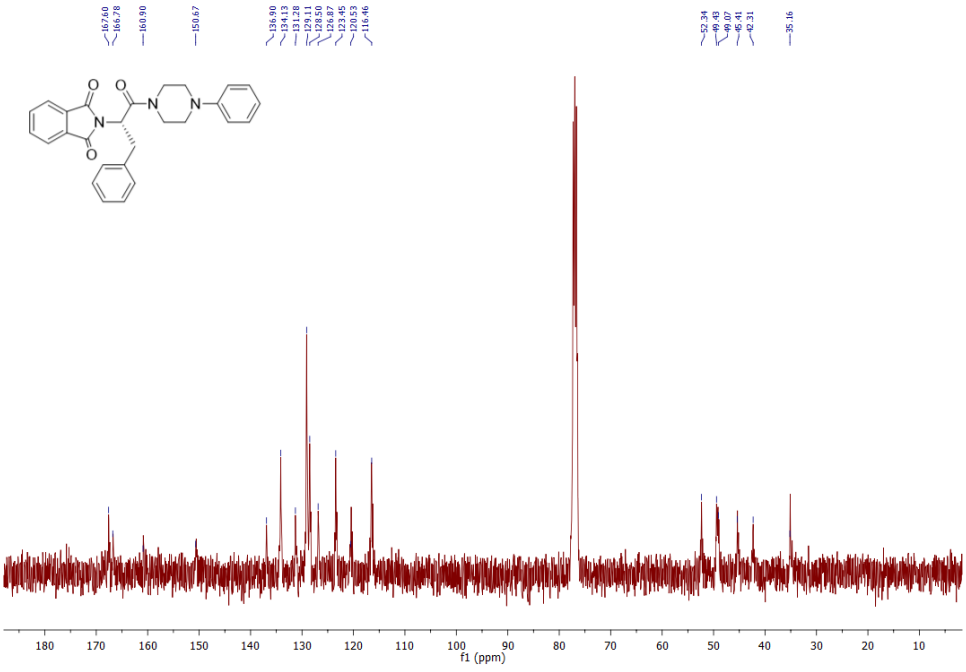

Figure A.57. ^{13}C NMR Spectrum of **L-CSP-2**

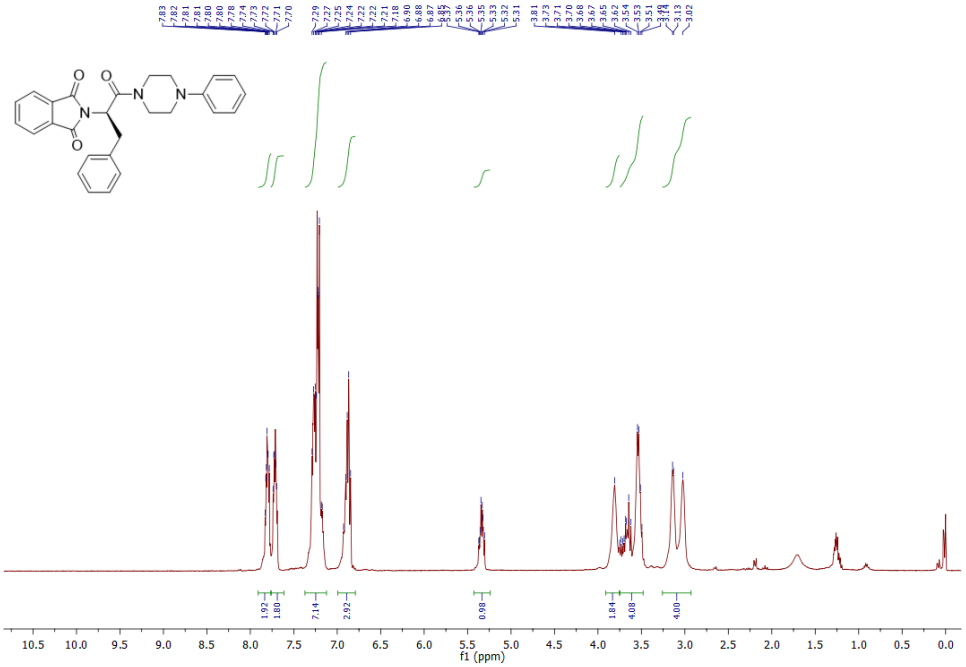

Figure A.58. ^{1}H NMR Spectrum of **D-CSP-2**

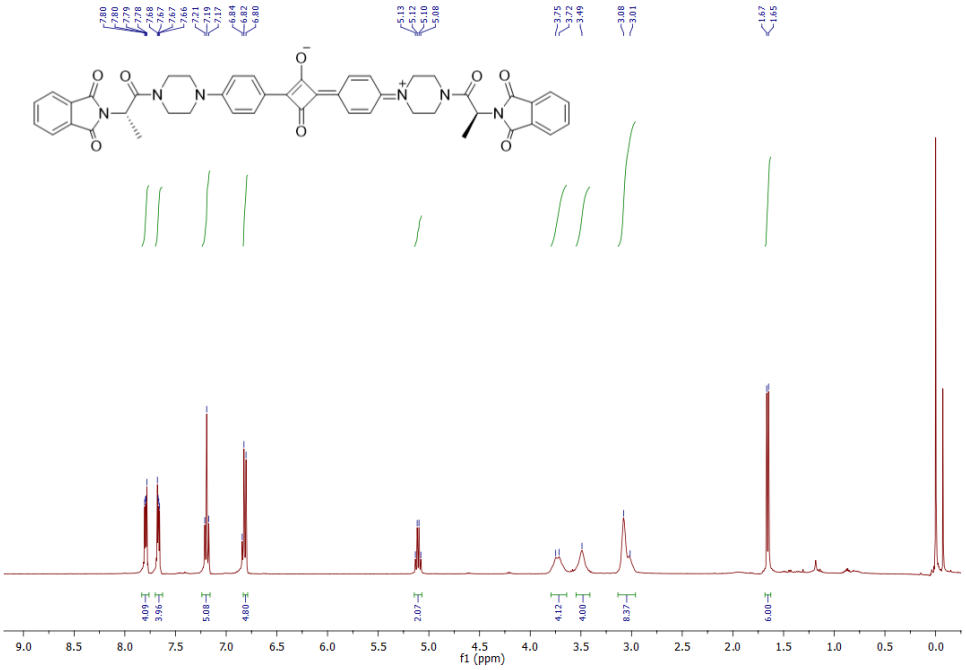

Figure A.59. ^{1}H NMR Spectrum of **L-CSA-3**

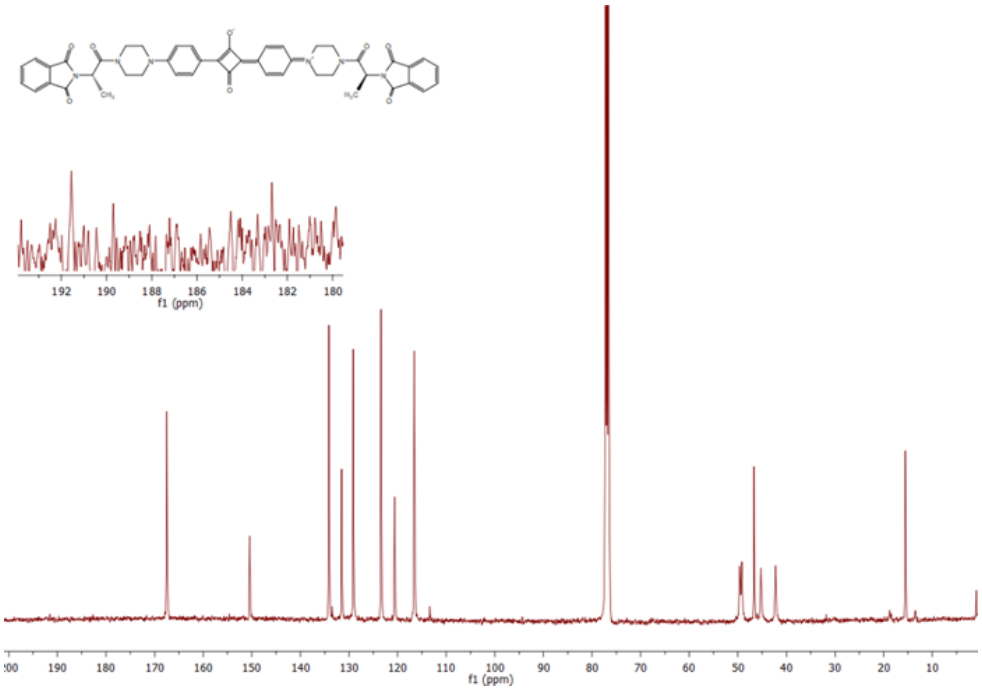

Figure A.60. ^{13}C NMR Spectrum of **L-CSA-3**

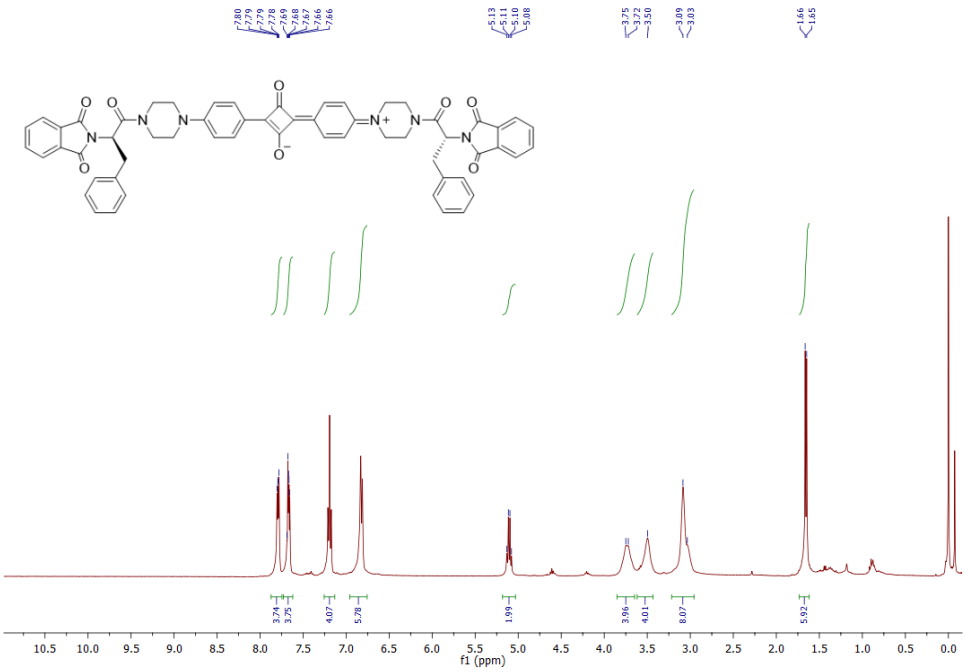

Figure A.61. ^{1}H NMR Spectrum of **D-CSA-3**

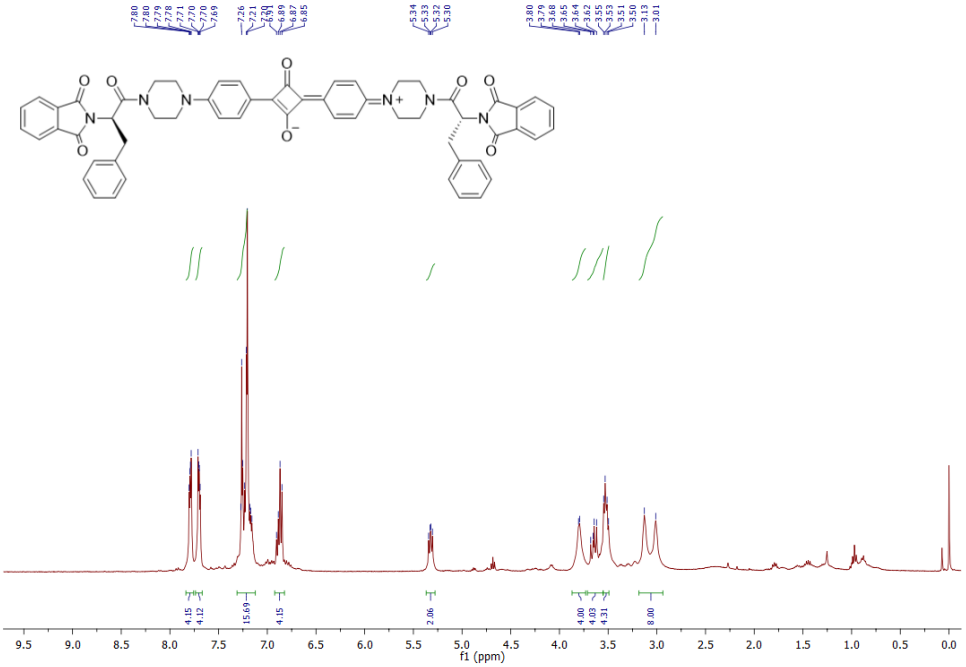

Figure A.62. ^{1}H NMR Spectrum of **L-CSP-3**

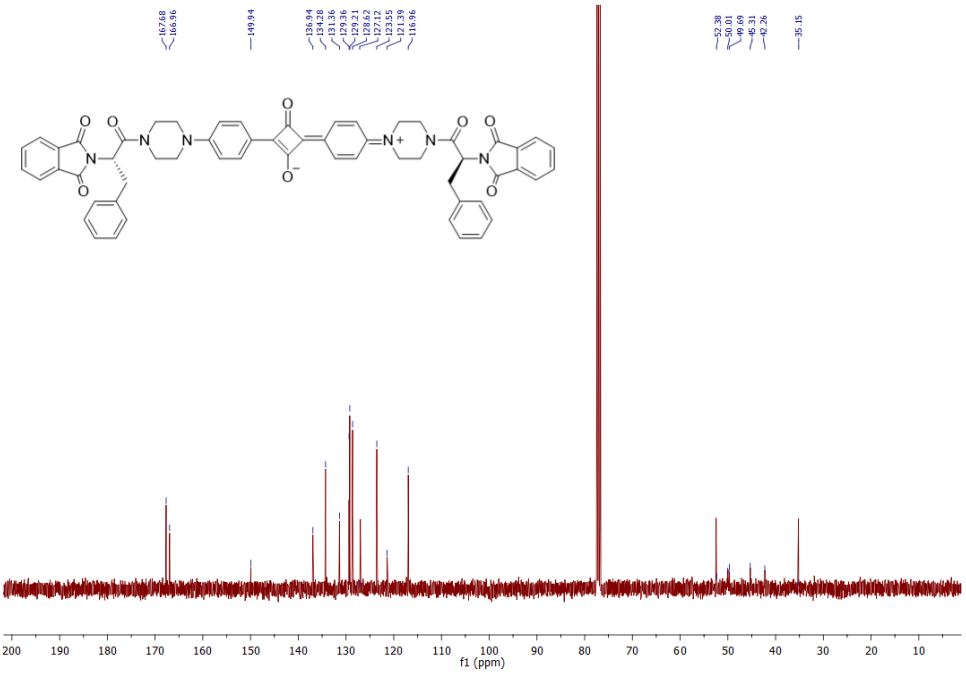

Figure A.63. ^{13}C NMR Spectrum of **L-CSP-3**

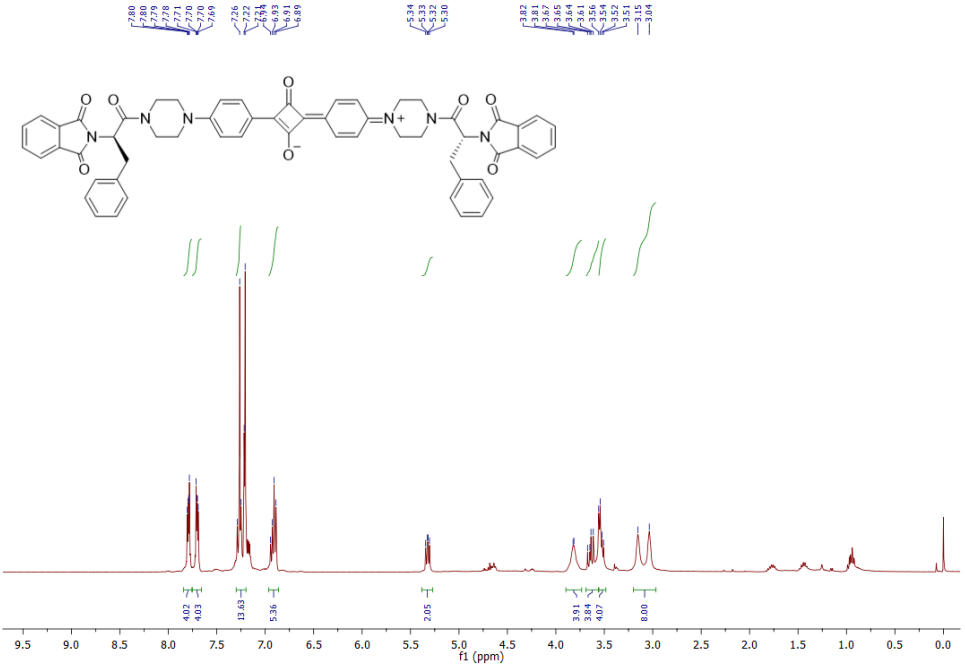

Figure A.64. ^{1}H NMR Spectrum of **D-CSP-3**

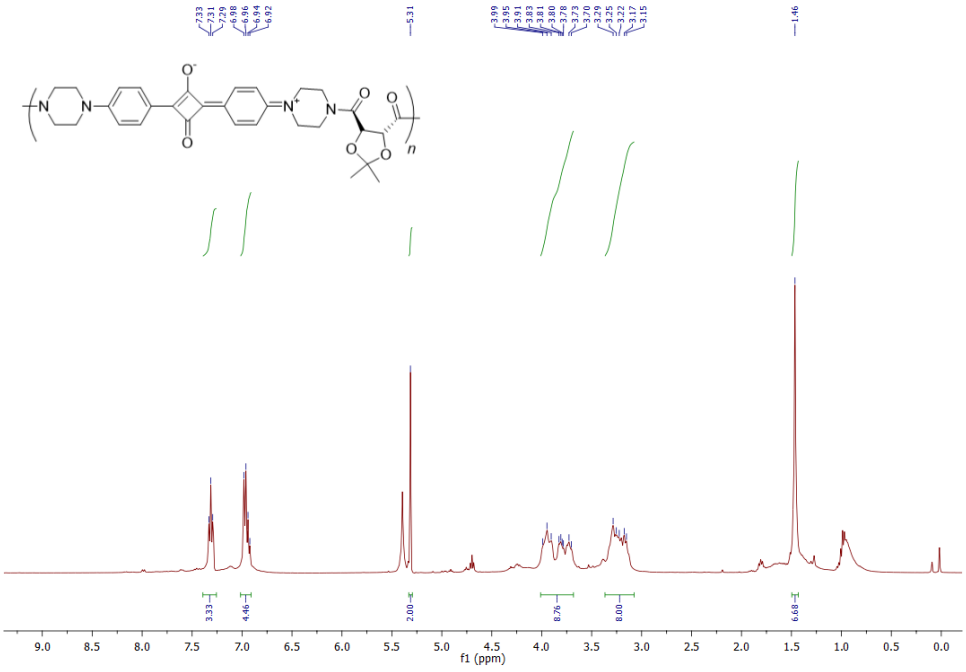

Figure A.65. ^{1}H NMR Spectrum of **SQPOL-L**

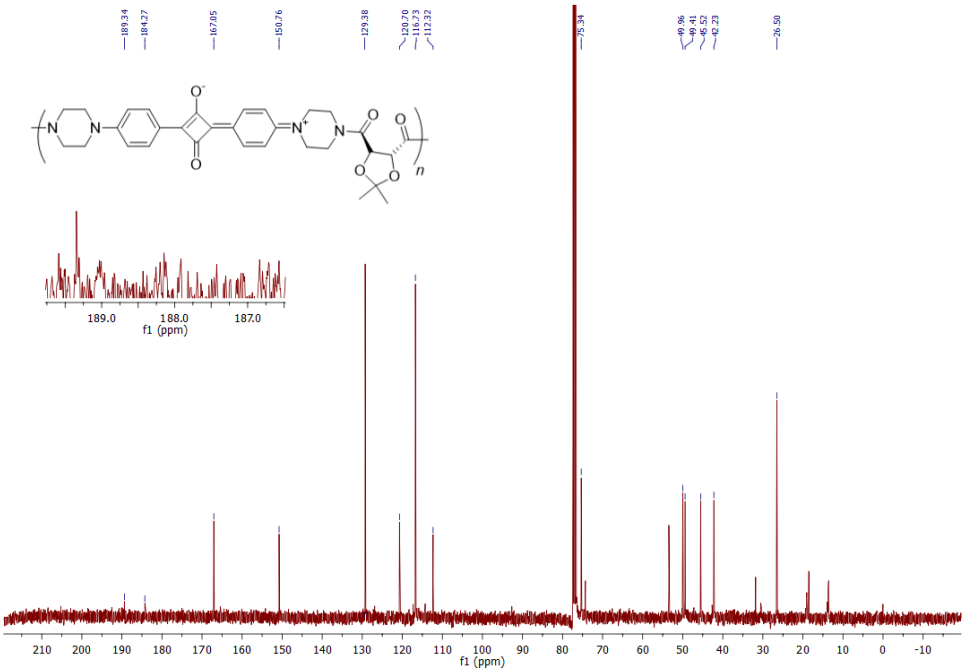

Figure A.66. ^{13}C NMR Spectrum of **SQPOL-L**

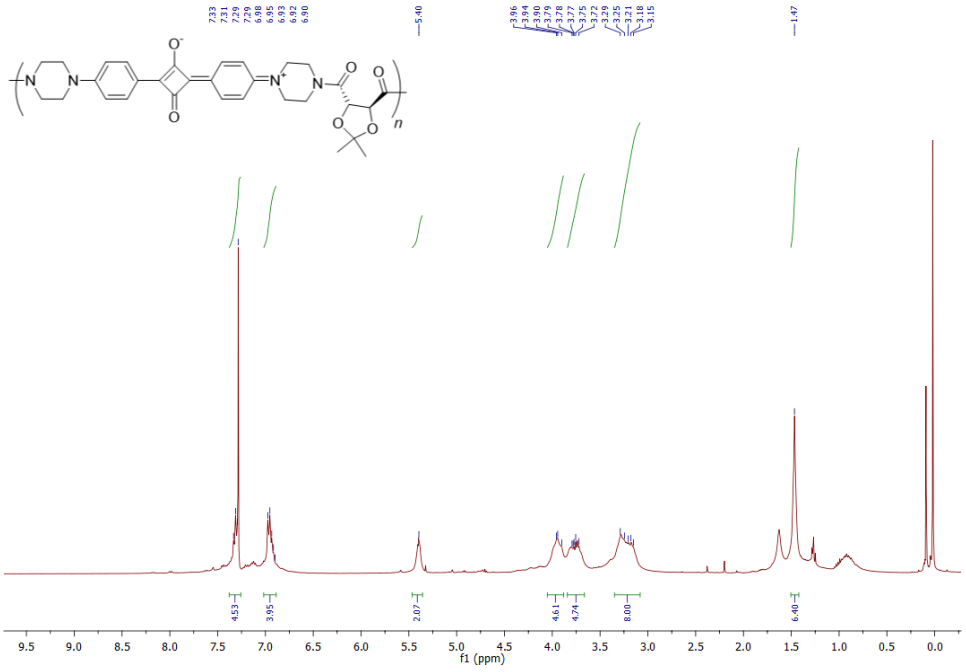

Figure A.67. ^{1}H NMR Spectrum of **SQPOL-D**

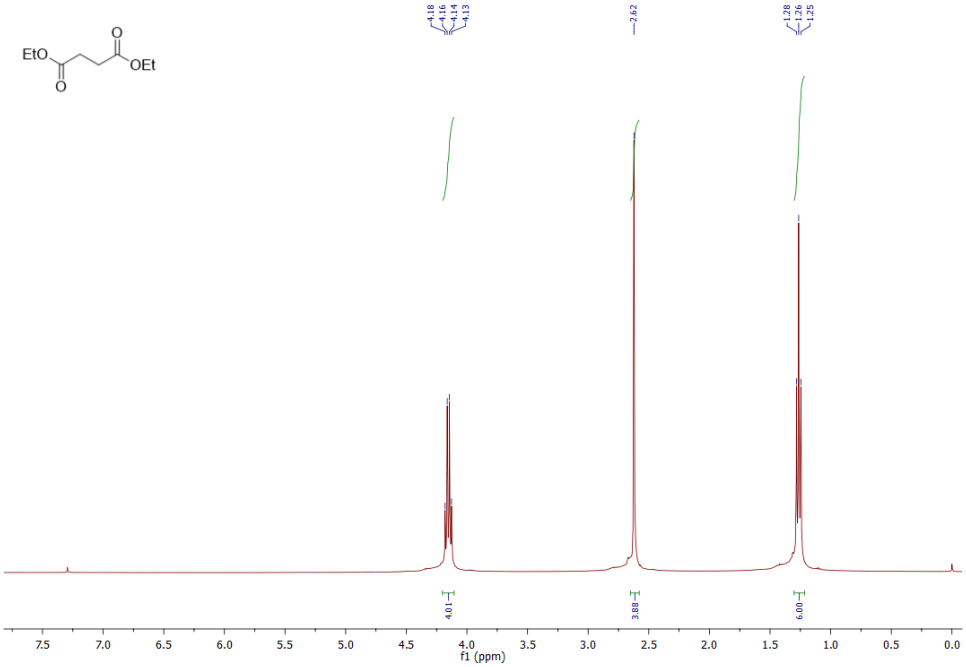

Figure A.68. ^{1}H NMR Spectrum of **S-3**

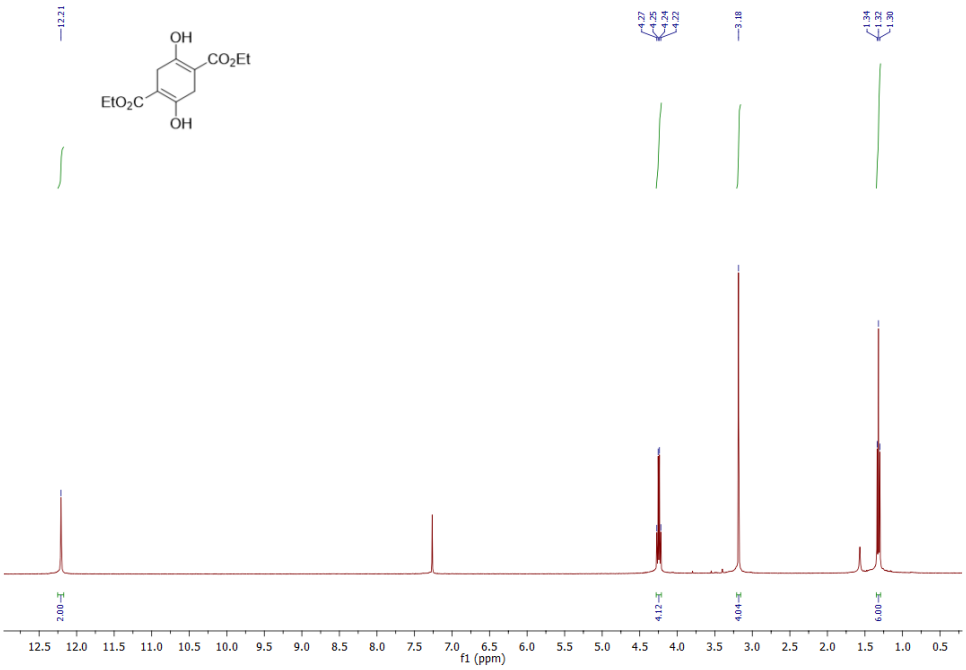

Figure A.69. ^{1}H NMR Spectrum of **S-4**

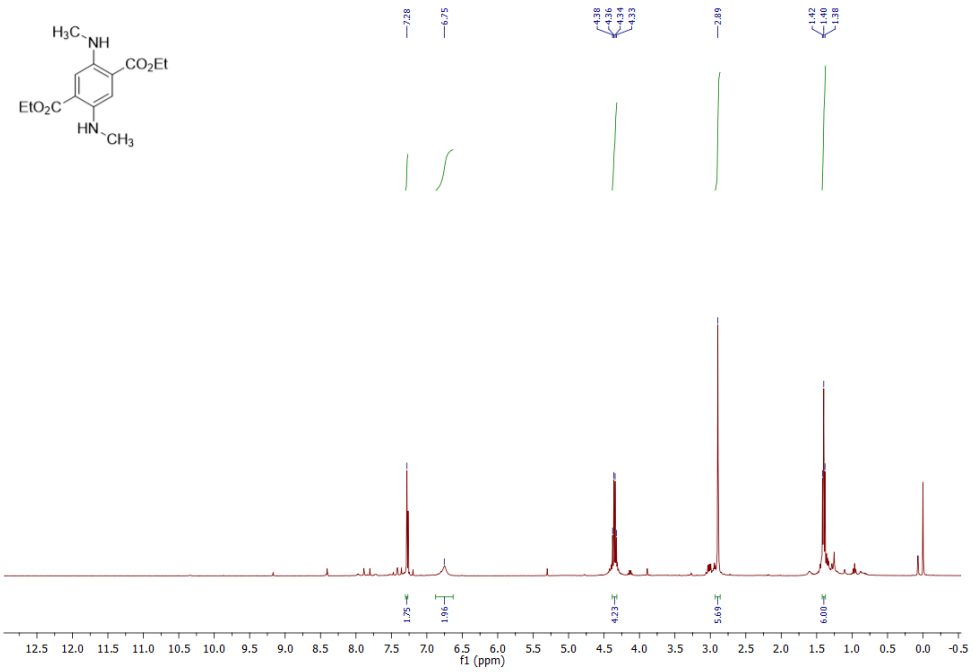

Figure A.70. ^{1}H NMR Spectrum of **S-6**

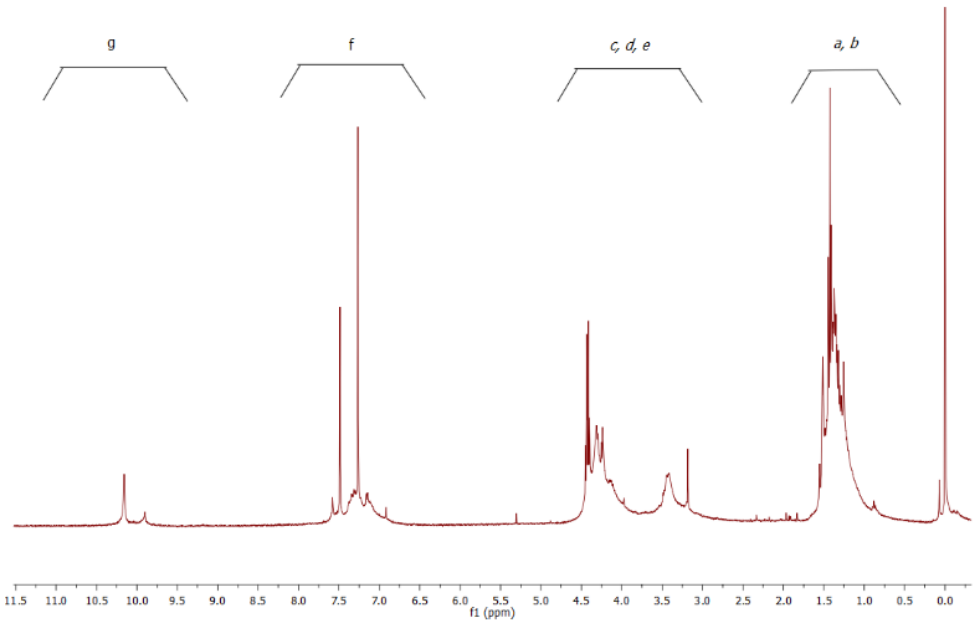

Figure 3.50. ^{1}H NMR Spectrum of **DATPOL-L**

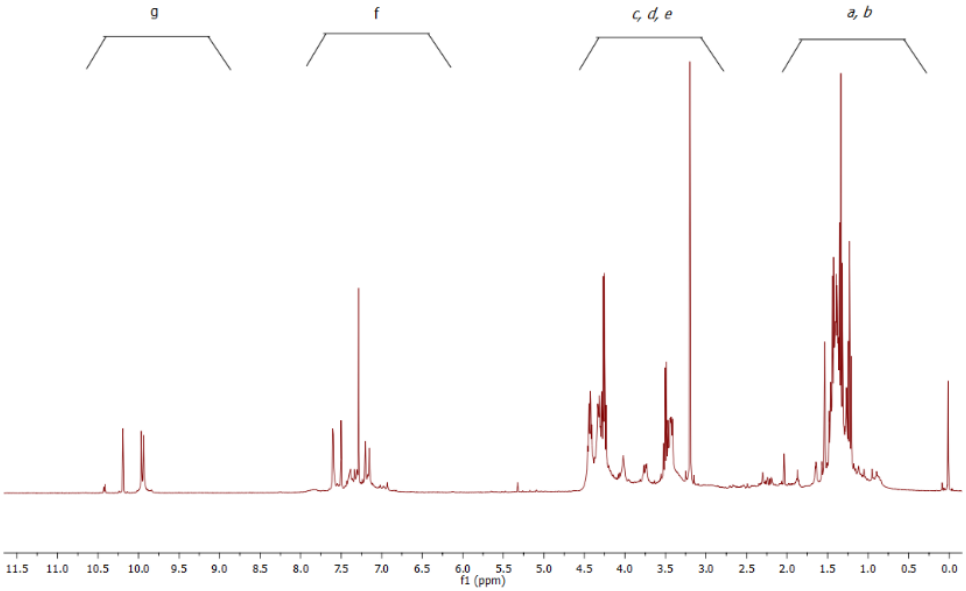

Figure 3.51. ^{1}H NMR Spectrum of **DATPOL-D**

B. IR Spectra

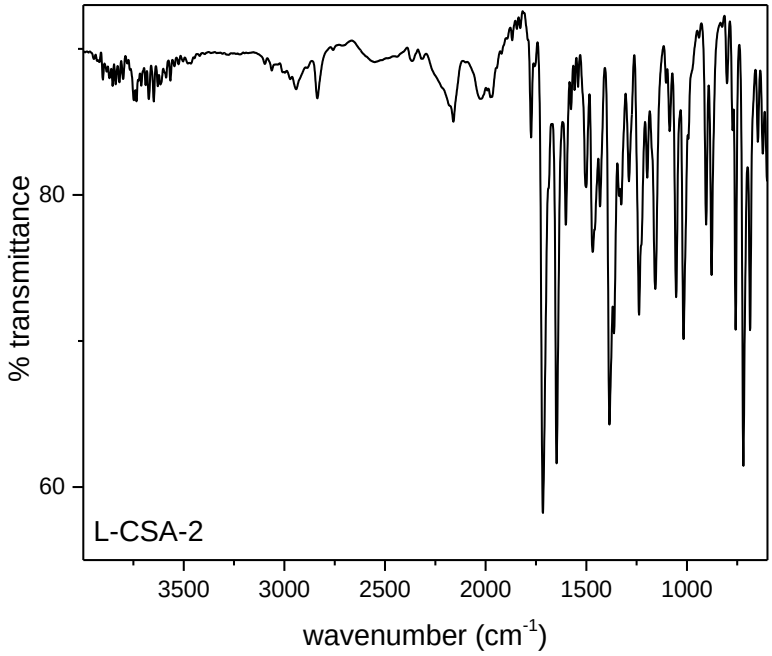

Figure B.1. IR Spectrum of **L-CSA-2**

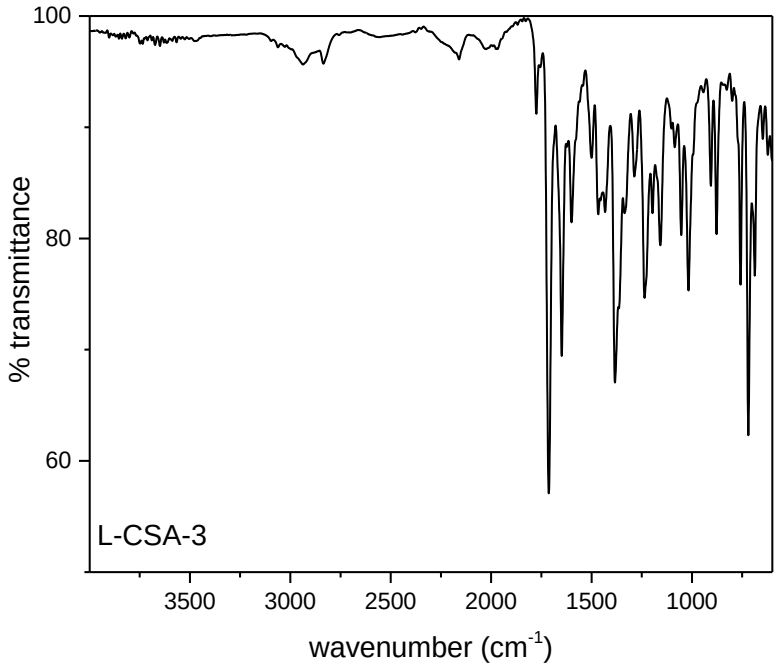

Figure B.2. IR Spectrum of **L-CSA-3**

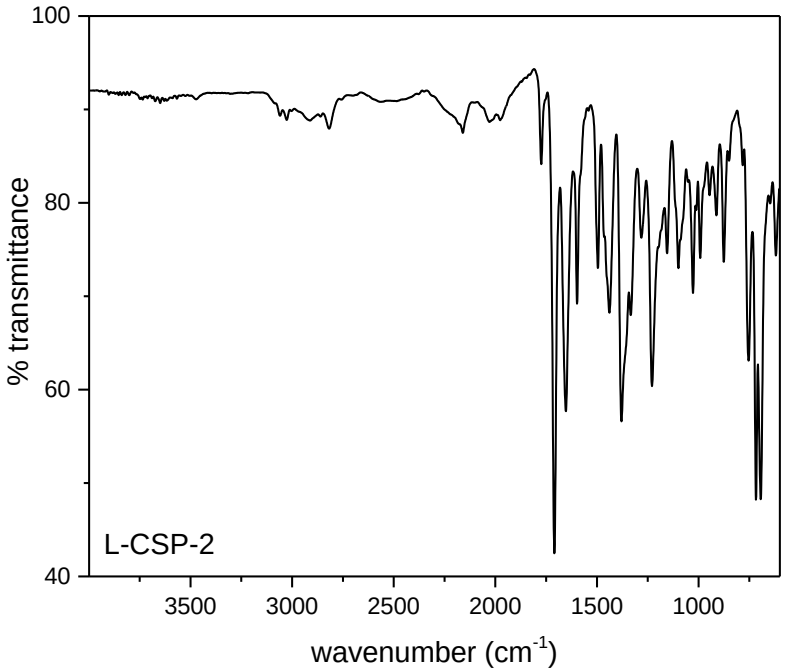

Figure B.3. IR Spectrum of **L-CSP-2**

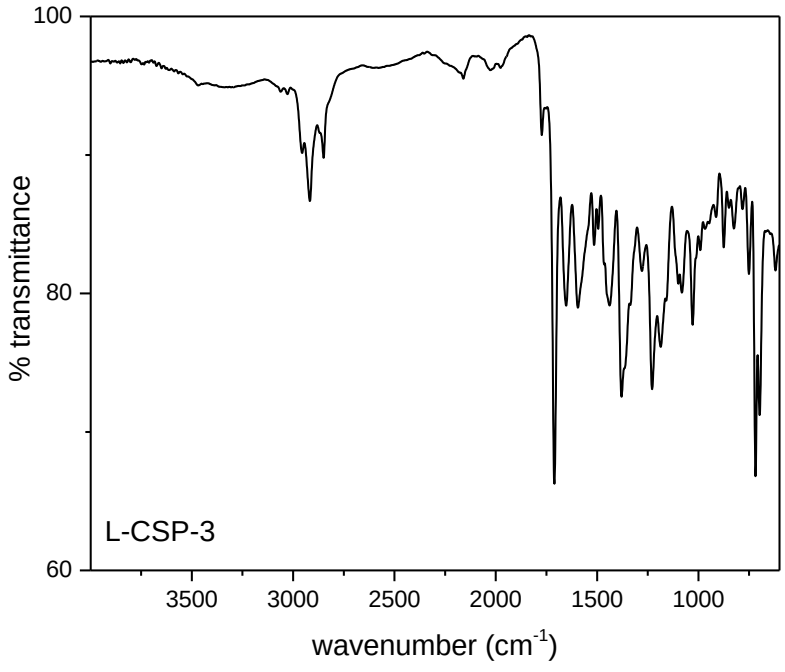

Figure B.4. IR Spectrum of **L-CSP-3**

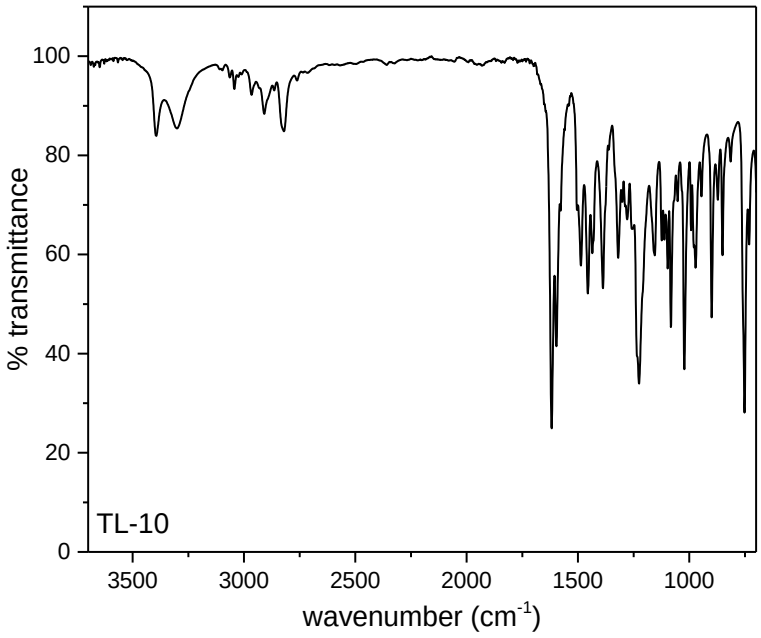

Figure B.5. IR Spectrum of **TL-10**

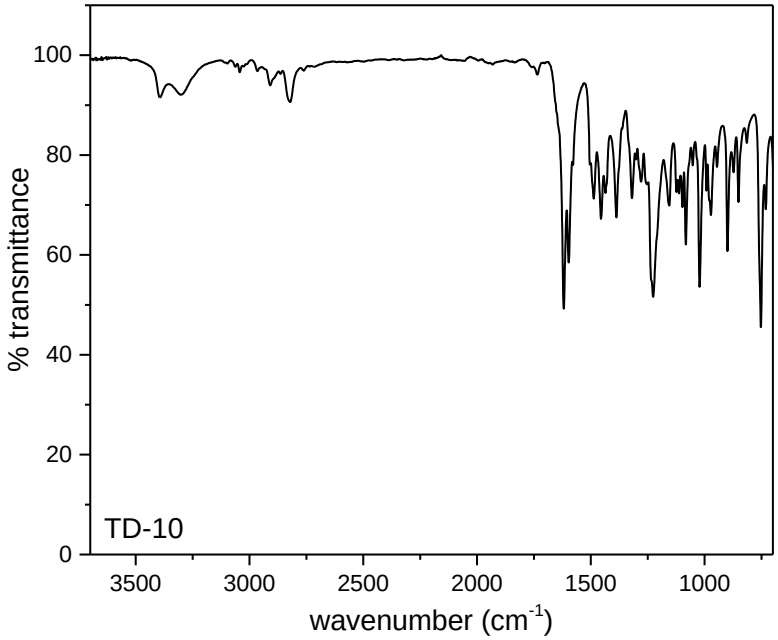

Figure B.6. IR Spectrum of **TD-10**

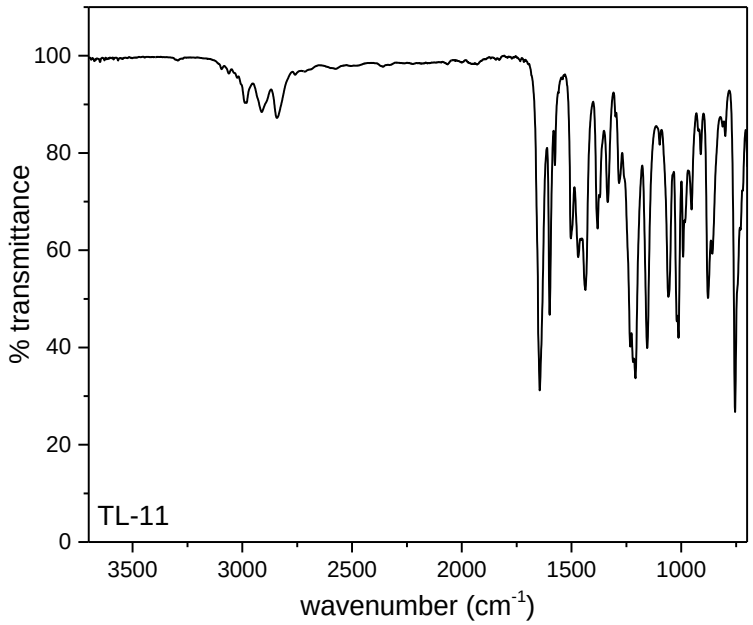

Figure B.7. IR Spectrum of **TL-11**

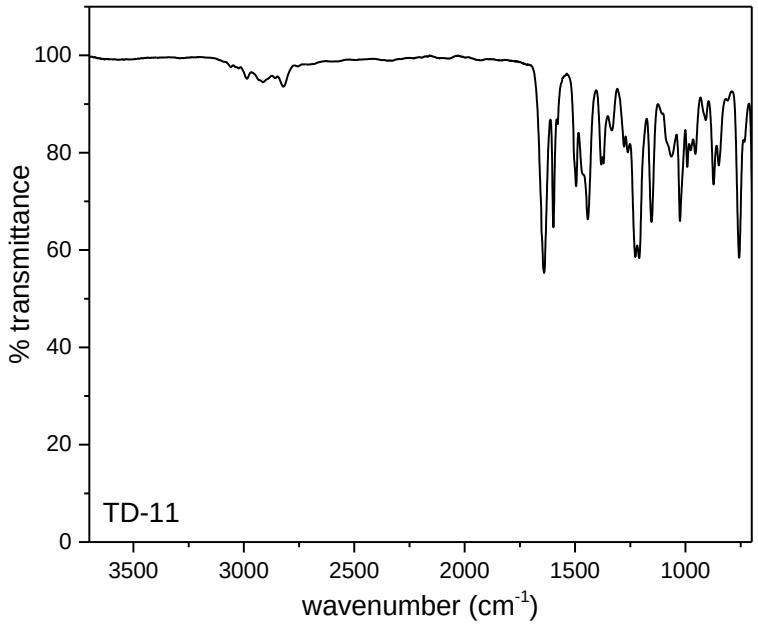

Figure B.8. IR Spectrum of **TD-11**

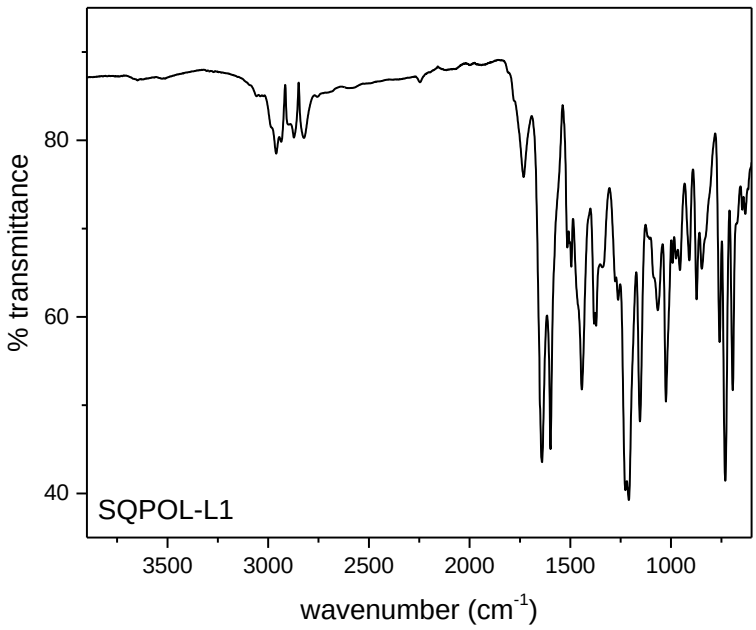

Figure B.9. IR Spectrum of **SQPOL-L1**

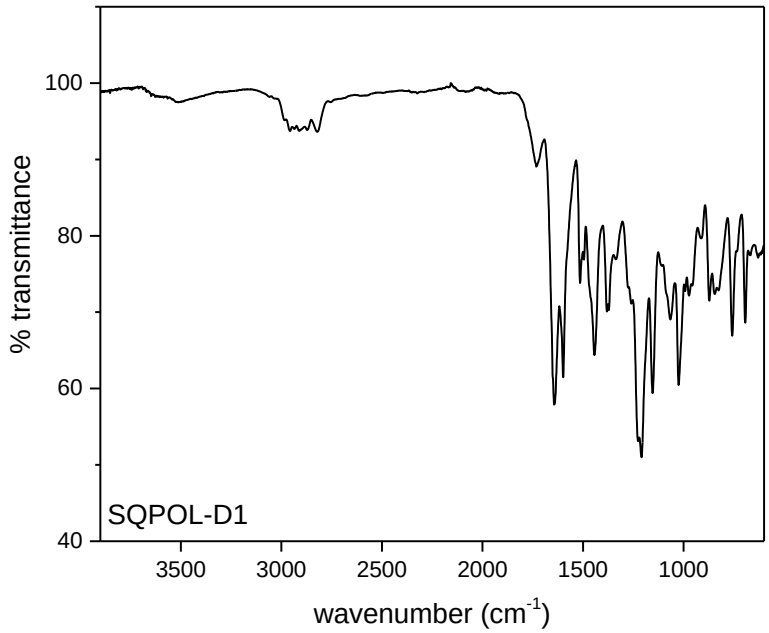

Figure B.10. IR Spectrum of **SQPOL-D1**

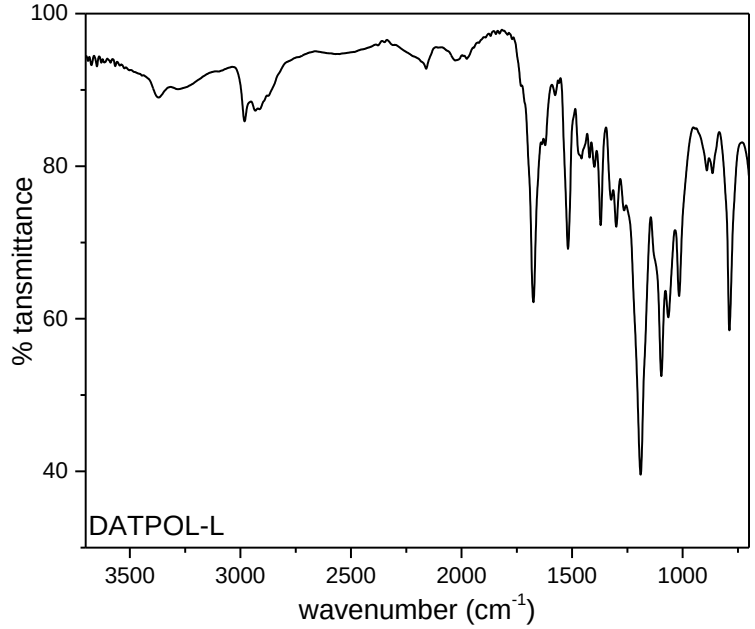

Figure B.11. IR Spectrum of **DATPOL-L**

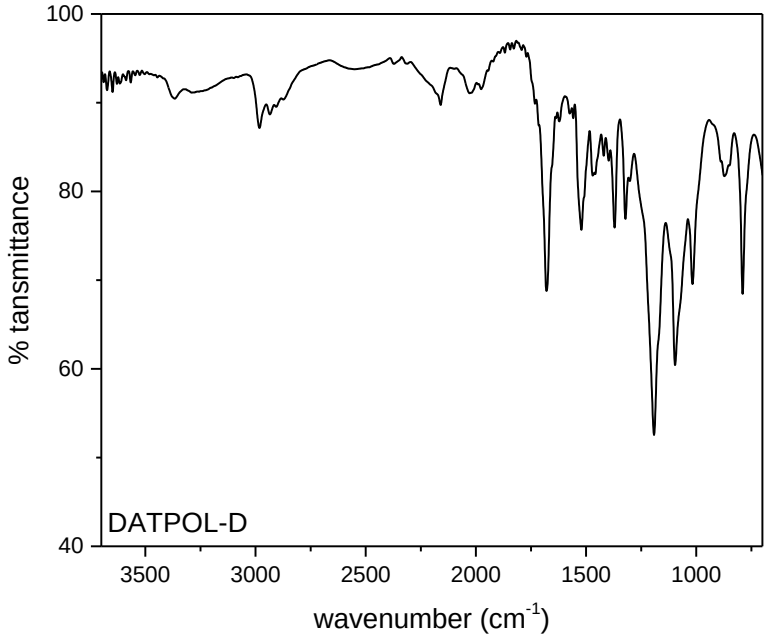

Figure B.12. IR Spectrum of **DATPOL-D**

C. HRMS Spectra

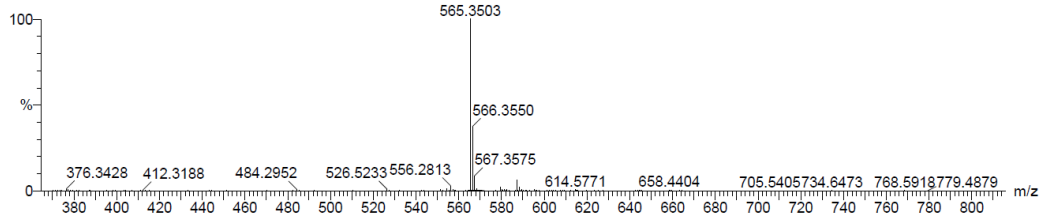

Minimum:				-5.5			
Maximum:		1000.0	1000.0	1000.0			
Mass	Calc. Mass	mDa	PPM	DBE	i-FIT	i-FIT (Norm)	Formula
565.3503	565.3502	0.1	0.2	12.5	262.2	0.0	C31 H45 N6 O4

Figure C.1. HRMS Spectrum of **TL-12**

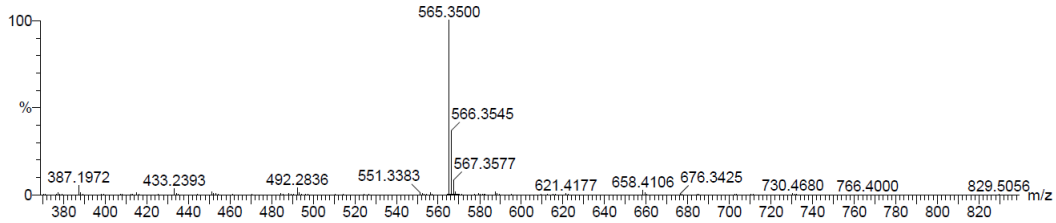

Minimum:				-5.5			
Maximum:		1000.0	1000.0	1000.0			
Mass	Calc. Mass	mDa	PPM	DBE	i-FIT	i-FIT (Norm)	Formula
565.3500	565.3502	-0.2	-0.4	12.5	279.5	0.0	C31 H45 N6 O4

Figure C.2. HRMS Spectrum of **TD-12**

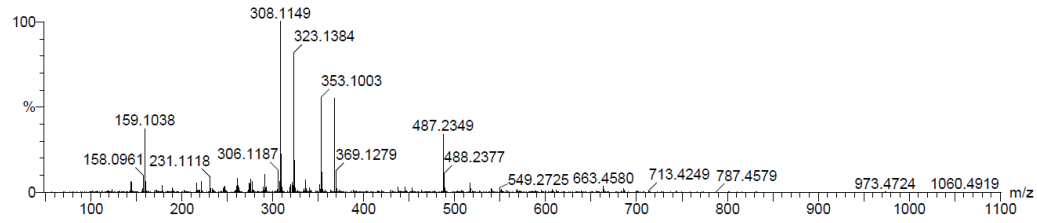

Minimum:				-5.5			
Maximum:		1000.0	5000.0	1000.0			
Mass	Calc. Mass	mDa	PPM	DBE	i-FIT	i-FIT (Norm)	Formula
487.2349	487.2345	0.4	0.8	15.5	271.1	0.0	C28 H31 N4 O4

Figure C.3. HRMS Spectrum of **SQ-5**

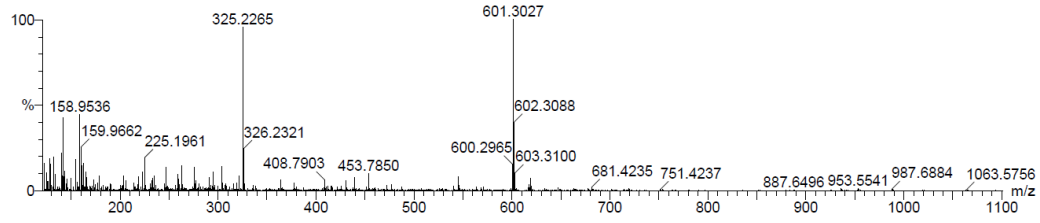

Minimum:				-5.5			
Maximum:		1000.0	5000.0	1000.0			
Mass	Calc. Mass	mDa	PPM	DBE	i-FIT	i-FIT (Norm)	Formula
601.3027	601.3026	0.1	0.2	16.5	419.6	0.0	C34 H41 N4 O6

Figure C.4. HRMS Spectrum of **SQ-6**

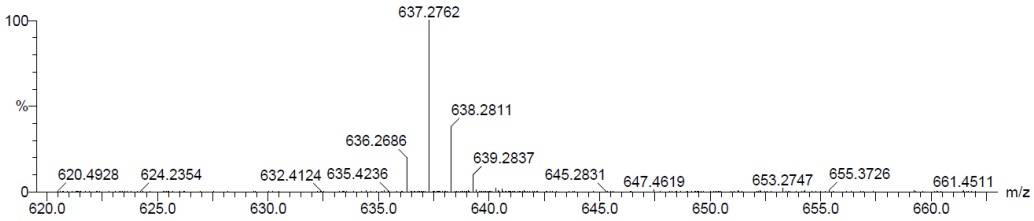

Minimum:				-5.5			
Maximum:		1000.0	5000.0	1000.0			
Mass	Calc. Mass	mDa	PPM	DBE	i-FIT	i-FIT (Norm)	Formula
637.2762	637.2761	0.1	0.2	15.5	305.4	0.0	C34 H41 N2 O10

Figure C.5. HRMS Spectrum of **L-CSPID**

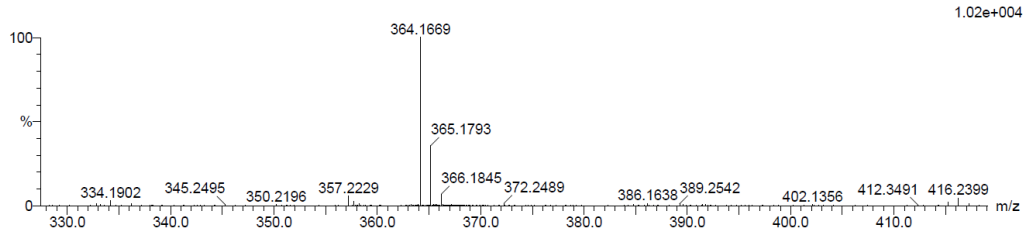

Minimum:				-5.5			
Maximum:		1000.0	1000.0	1000.0			
Mass	Calc. Mass	mDa	PPM	DBE	i-FIT	i-FIT (Norm)	Formula
364.1669	364.1661	0.8	2.2	12.5	751.4	0.0	C21 H22 N3 O3

Figure C.6. HRMS Spectrum of **L-CSA-2**

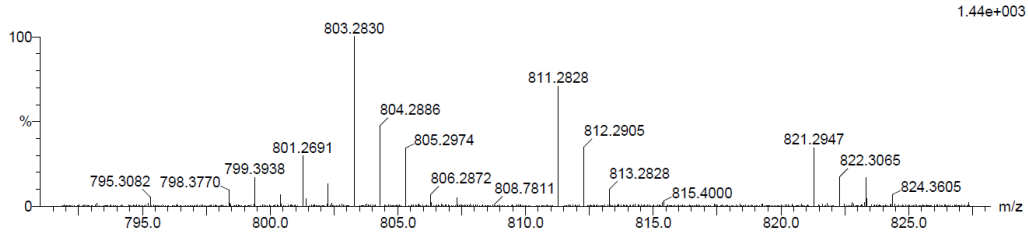

Minimum:				-5.5			
Maximum:		1000.0	5000.0	1000.0			
Mass	Calc. Mass	mDa	PPM	DBE	i-FIT	i-FIT (Norm)	Formula
803.2830	803.2829	0.1	0.1	30.5	148.8	0.0	C46 H39 N6 O8

Figure C.7 HRMS Spectrum of **L-CSA-3**

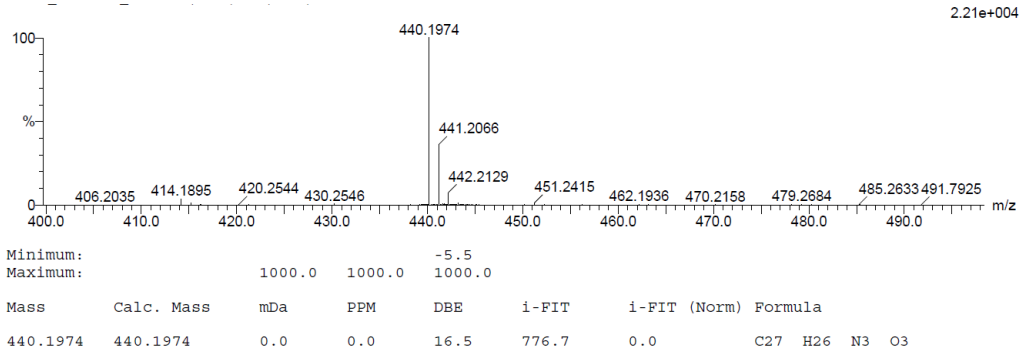

Minimum:				-5.5			
Maximum:		1000.0	1000.0	1000.0			
Mass	Calc. Mass	mDa	PPM	DBE	i-FIT	i-FIT (Norm)	Formula
440.1974	440.1974	0.0	0.0	16.5	776.7	0.0	C27 H26 N3 O3

Figure C.8. HRMS Spectrum of **L-CSP-2**

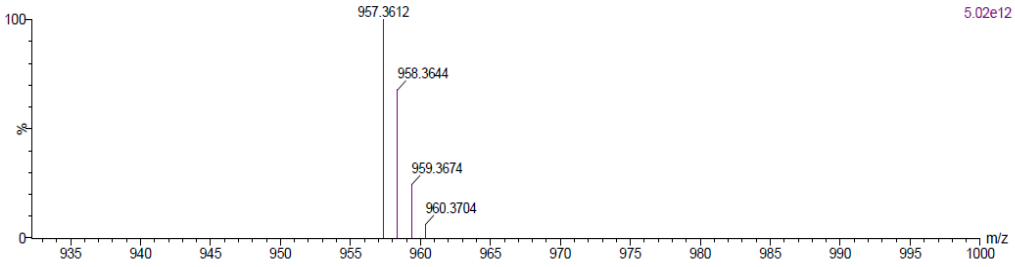

Figure C.9. HRMS Spectrum of **L-CSP-3**

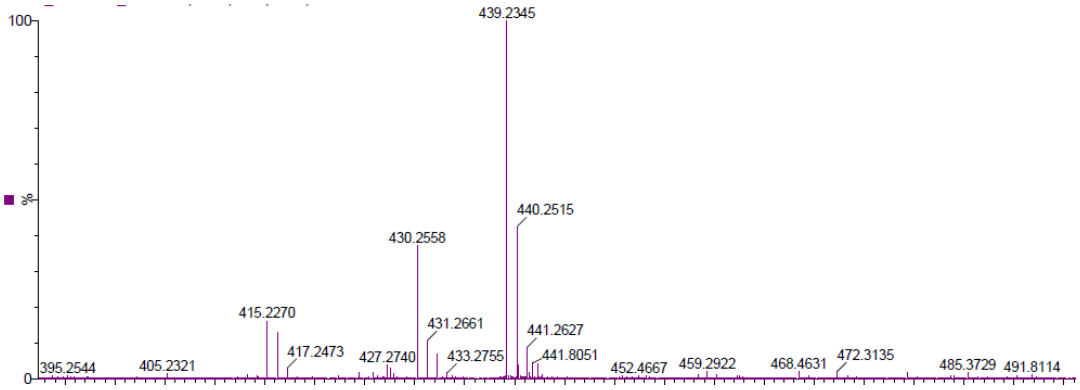

Figure C.10. HRMS Spectrum of **TD-10**

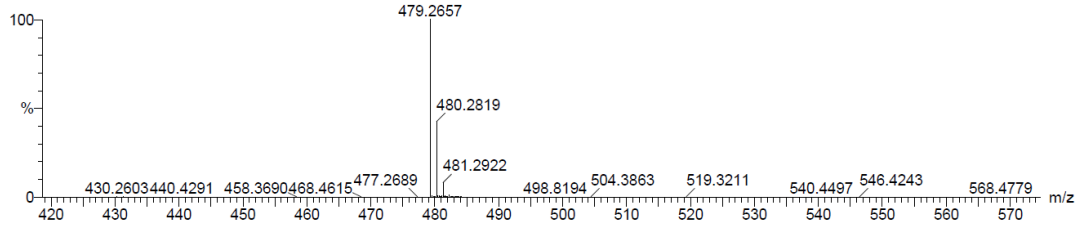

Minimum:				-5.5			
Maximum:		1000.0	1000.0	1000.0			
Mass	Calc. Mass	mDa	PPM	DBE	i-FIT	i-FIT (Norm)	Formula
479.2657	479.2658	-0.1	-0.2	12.5	1675.3	0.0	C27 H35 N4 O4

Figure C.11. HRMS Spectrum of **TD-11**

D. XY Coordinates of Optimized Structures

For S-6

TPA

N	0.045220	0.170553	0.013679
C	-0.004331	0.117270	1.392802
C	1.181876	0.104927	2.141655
C	1.221722	0.102885	3.541407
C	0.004331	0.117270	4.287198
C	-1.181876	0.104927	3.538345
C	-1.221722	0.102885	2.138593
H	2.138899	0.097447	1.636943
C	2.598583	0.070520	4.106997
N	-0.045220	0.170553	5.666321
H	-2.138899	0.097447	4.043057
C	-2.598583	0.070520	1.573003
C	-1.268731	-0.035543	6.410053
H	0.823129	-0.033364	6.135069
C	1.268731	-0.035543	-0.730053
H	-0.823129	-0.033364	-0.455069
H	1.029980	-0.018271	-1.796629
H	1.992991	0.766231	-0.538032
H	1.760427	-0.994696	-0.500051
H	-1.029980	-0.018271	7.476629
H	-1.992991	0.766231	6.218032
H	-1.760427	-0.994696	6.180051
O	2.639632	-0.007980	5.469959
O	3.616144	0.102946	3.439485
C	3.954936	-0.048819	6.076690
H	3.798705	0.348811	7.082857
C	4.507122	-1.465693	6.114187
H	4.614402	0.619816	5.519894
H	5.468241	-1.475055	6.641249
H	3.821587	-2.139719	6.638715
H	4.666867	-1.840974	5.099994
O	-2.639632	-0.007980	0.210041
O	-3.616144	0.102946	2.240515
C	-3.954936	-0.048819	-0.396690
H	-3.798705	0.348811	-1.402857
C	-4.507122	-1.465693	-0.434187
H	-4.614402	0.619816	0.160106
H	-5.468241	-1.475055	-0.961249

H	-3.821587	-2.139719	-0.958715
H	-4.666867	-1.840974	0.580006

TPB

C	-1.154079	0.000000	2.043715
C	0.091754	0.000000	1.403758
C	1.297345	0.000000	2.173305
C	1.154655	0.000000	3.570265
C	-0.091178	0.000000	4.210222
C	-1.296769	0.000000	3.440675
C	0.149083	0.000000	-0.074270
O	1.177185	0.000000	-0.745324
N	2.537413	0.000000	1.587000
C	3.776388	0.000000	2.323178
C	-0.148508	0.000000	5.688249
O	-1.176611	0.000000	6.359302
N	-2.536836	0.000000	4.026982
C	-3.775812	0.000000	3.290805
O	-1.071012	0.000000	-0.658193
O	1.071585	0.000000	6.272175
H	2.038286	0.000000	4.193196
H	-2.037710	0.000000	1.420784
C	-1.083945	0.000000	-2.101766
C	1.084515	0.000000	7.715748
H	4.603015	0.000000	1.608429
H	3.882578	0.888701	2.963982
H	3.882578	-0.888701	2.963982
H	-4.602438	0.000000	4.005554
H	-3.882002	0.888701	2.650000
H	-3.882002	-0.888701	2.650000
H	-2.544739	0.000000	5.038073
H	2.545319	0.000000	0.575909
C	2.536582	0.000000	8.155972
H	0.546060	0.882902	8.075080
H	0.546060	-0.882902	8.075080
H	2.592893	0.000000	9.250035
H	3.058442	-0.887833	7.784480
H	3.058442	0.887833	7.784480
C	-2.536013	0.000000	-2.541987
H	-0.545490	0.882902	-2.461099
H	-0.545490	-0.882902	-2.461099
H	-2.592326	0.000000	-3.636050
H	-3.057872	-0.887833	-2.170493

H	-3.057872	0.887833	-2.170493

TPB_M

C	1.368360	-0.276764	-0.168135
C	0.919432	1.080810	-0.180892
C	-0.469364	1.286361	-0.171601
C	-1.396374	0.236536	-0.169095
C	-0.947442	-1.121063	-0.178666
C	0.441352	-1.326593	-0.168528
N	1.794583	2.139064	-0.215080
C	1.386355	3.515321	-0.072256
C	-2.843123	0.545660	-0.138045
O	-3.745928	-0.284941	-0.095296
N	-1.822583	-2.179392	-0.210709
C	-1.414396	-3.555324	-0.064668
C	2.815101	-0.585818	-0.135989
O	3.717896	0.244880	-0.094897
O	-3.108757	1.871783	-0.156630
C	-4.504403	2.239322	-0.119964
C	-4.575333	3.754748	-0.145760
O	3.080742	-1.911979	-0.151547
C	4.476379	-2.279430	-0.113708
C	4.547318	-3.794911	-0.136103
H	0.827768	-2.336229	-0.159645
H	-0.855782	2.296014	-0.165101
H	-2.308443	-4.183669	-0.076835
H	-0.766614	-3.879000	-0.891613
H	-0.874958	-3.744350	0.877485
H	2.280405	4.143638	-0.085592
H	0.738801	3.837130	-0.900108
H	0.846657	3.706472	0.869320
H	2.770312	1.894756	-0.107032
H	-2.798343	-1.934842	-0.103481
H	4.983935	-1.831270	-0.973967
H	4.928820	-1.860088	0.790756
H	5.593781	-4.117787	-0.108239
H	4.031659	-4.223951	0.729133
H	4.087763	-4.195230	-1.045574
H	-5.011741	1.789243	-0.979352
H	-4.957073	1.821999	0.785317
H	-5.621802	4.077688	-0.118881
H	-4.059892	4.185717	0.718648
H	-4.115545	4.153037	-1.056005

O	3.550722	3.055864	-0.159832
H	4.467003	2.826442	-0.058368
C	3.699597	3.577179	1.130930
H	4.306645	4.480356	1.089859
H	2.719588	3.816826	1.540895
H	4.188363	2.839865	1.766065
O	-3.578739	-3.096066	-0.153877
H	-4.495047	-2.866415	-0.053182
C	-3.461111	-3.235359	1.234201
H	-2.440306	-3.519672	1.485284
H	-3.703275	-2.289131	1.715794
H	-4.148257	-4.005623	1.581253

CURRICULUM VITAE

Surname, Name: Çalışgan Ünay, Gizem

EDUCATION

Degree	Institution	Year of Graduation
MS	METU Chemistry	2016
BS	METU Chemistry	2013
High School	Dr.Rıdvan Binnaz Ege Anatolian High School	2006

FOREIGN LANGUAGES

Advanced English

PUBLICATIONS

1. Ünay, G. Ç.; Yıldırım, E.; Akdag, A. Chiral Polyurea from Tartaric Acid Derived and Lysine Backbone: A Synthetic and Computational Study. *ChemistrySelect* **2020**, *5* (42), 13358–13369. https://doi.org/10.1002/slct.202003534.